Integration of Bioreactor and Membrane Separation Processes: A Model Based Approach

Reverse Electro-Enhanced Dialysis process for lactic acid fermentation

Prado Rubio, Oscar Andres

Publication date:
2010

Document Version
Publisher's PDF, also known as Version of record

Integration of Bioreactor and Membrane Separation Processes: A model based approach

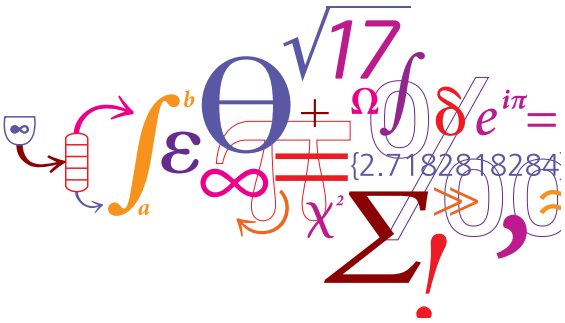

Oscar Andrés Prado-Rubio

Ph.D. Thesis

August 2010

DTU Chemical Engineering
Department of Chemical and Biochemical Engineering

Integration of Bioreactor and Membrane Separation Processes: A model based approach

Reverse Electro-Enhanced Dialysis process for lactic acid fermentation

Ph.D. thesis
Oscar Andrés Prado-Rubio

August, 2010

Computer Aided Process Engineering Center
Department of Chemical and Biochemical Engineering
Technical University of Denmark

Address: Computer Aided Process Engineering Center
Department of Chemical and
Biochemical Engineering
Technical University of Denmark
Søltofts Plads, Building 229
DK-2800 Kgs. Lyngby
Denmark
Phone: +45 4525 2800
Fax: +45 4525 2906
Web: www.capec.kt.dtu.dk

Print: J&R Frydenberg A/S
København
Marts 2011

ISBN: 978-87-92481-37-5

Preface

This dissertation was written as partial fulfillment of requirements for the degree of Doctor of Philosophy (Ph.D.) in Chemical Engineering. The project has been carried out in from Jun 2007 until August 2010. This thesis was prepared at Computer Aided Process-Product Engineering Center (CAPEC) at the Department of Chemical Engineering (KT) at the Technical University of Denmark (DTU).

This project has been financed by the Sixth framework project of the European Union: NMP2-CT-2007-O2b515 IP "BIOPRODUCTION".

Firstly, I would like to acknowledge my supervisors Associate Professor Gunnar E. Jonsson and Professor Sten Bay Jørgensen for their motivation, guidance, criticism, inspiration and patience. I am very grateful to all people that supported my work with interesting discussions, stimulating conversations and useful suggestions. I would like to specially thank to Paloma Andrade, Jakob Kjøbsted Huusom, Ricardo Morales, Merlin Alvarado, Hugo Gonzales, Ana Carvalho and Nanna Petersen. I wish to give a special thanks to Sijing Liu for the opportunity to collaborate during her Master thesis work. I am grateful to work in CAPEC and at DTU, since I believe it provides a good work environment.

It was a pleasure to work with the other members of CAPEC: Elisa, Rasmus, Sasha, Azizul, Fazly, Kamma, Martin, Axel, Alicia, Martina, Philip, Vipasha, Kavitha, Piotr and Forin. I'll remember the times we spent together, specially the seminars and conferences.

Finally, I wish to thank to my family for the unconditional support from far far away, somewhere in the Colombian mountains.

Oscar Andrés Prado-Rubio

Kgs. Lyngby, August, 2010

Abstract

This work is motivated by the need for tighter integration of industrial processes in an attempt to improve process sustainability. To this end, this work considers a interesting case study around which different systematic approaches are used or developed to achieve the above goal. The thesis is concerned with the understanding of an integrated bioreactor and electrically driven membrane separation processes for lactic acid fermentation. This is achieved through a model based investigation of the individual units and the integrated system. Development of system understanding is the key to reveal how the system should be designed and operated in accordance with different production goals.

The selected case includes a fermenter and a two stage membrane separation. In the first membrane stage the lactate is exchanged by hydroxide by means of anion exchange membranes, in a process referred to as Reverse Electro-Enhanced Dialysis (REED). Unconsumed substrate and biomass are effectively recycled to the fermenter. In the second membrane separation stage, the lactate is recovered and concentrated as lactic acid using Electrodialysis with bipolar membranes (EDBM), while sodium hydroxide is regenerated and recirculated. The novelty of the process relies in the specialized design and operation of the Reverse Electro-Enhanced Dialysis module. The REED design allows removal of the lactate from the fermentation broth and simultaneously facilitates pH control in the fermenter using hydroxide. Additionally, the periodic operation of the REED mitigates the adverse influence of the formation of a fouling layer at the membrane surface.

A first principles dynamic model is derived for the REED module to describe the transport of multiple ions through ion exchange membranes and adjacent boundary layers in a dialytic module. The unknown model parameters are regressed from experimental data for Donnan Dialysis recovery of different monoprotic carboxylic acids. Static simulation results agree with previously qualitative predictions of concentration profiles during Donnan Dialysis separation. Further static simulations under current load conditions are used to evaluate the influence of imposing an external electrical potential gradient on the ion fluxes and concentration profiles. Results demonstrate the development of asymmetric concentration profiles, the potential ion fluxes enhancement and the limiting current density constraint. Through dynamic simulations, the system behavior is investigated under current reversal conditions. Several phenomena are predicted such as preferable ion transport at the interfaces, transient flux inversion and accumulation/depletion of ions within the membranes. The combination of those phenomena can explain a loss of current efficiency, which has been experimentally demonstrated. Diverse numerical issues are encountered during the different type of simulations, and solutions are proposed.

A bioreactor model with unstructured kinetics is proposed which is suitable for integration with the Reverse Electro-Enhanced Dialysis process. An identifiable set of parameters are estimated from experimental data. The identifiability analysis is supported by mathematical and statistical tools.

In order to investigate the operability of the REED module, a methodology for

control structure design is extended to handle periodically operated systems. As case study, the pH regulation of the outlet stream of the membrane unit is addressed. Based upon the goal driven analysis, a non conventional input resetting control structure is designed. The control performance is evaluated through a set point tracking test. Satisfactory results are obtained regulating the pH and managing the input constraints.

The design and operability of the integrated bioreactor and REED module are investigated using the developed models and control structure. The study involves two different case studies: continuous lactic acid production and batch production of a starter culture. Substantial improvements are predicted in productivity and substrate utilization, while design and operability limitations are discussed.

The investigated integrated system is a clear example where a model based approach, supported by experimental evidence, can bring improvements in the system understanding, and therefore promote the development of goal driven process design and the process control discipline.

Resumé

Dette arbejde er motiveret af behovet for tættere integration af industrielle processer i et forsøg på at forbedre processens bæredygtighed. Med henblik herpå behandles et interessant proceseksempel ved hjælp af de systematiske metoder, som er udviklet for at opnå ovennævnte mål. Afhandlingen beskæftiger sig med forståelsen af en integreret bio-reaktor med elektrisk drevet membranseparation til produktion af mælkesyre. Dette opnås gennem en model baseret undersøgelse af de enkelte enheder og det integrerede system. Udvikling af system forståelse er nøglen til at forstå hvordan systemet bør udformes og drives i overensstemmelse med forskellige produktions-mål.

Den udvalgte proces omfatter en fermentering og en to-trins membranseparation. I den første membran separation bliver laktat udvekslet med hydroxid ved hjælp af en anionbytter membran. Processen kaldes Reverse Electro-Enhanced Dialyse (REED). Uomdannet substrat og biomasse bliver effektivt recirkuleret og genbrugt i fermenteringstanken. I den anden membranseparation udvindes laktat og opkoncentreres som mælkesyre ved hjælp af elektrodialyse og bipolare membraner (EDBM). I dette trin bliver natriumhydroxid regenereret og recirkuleres til det første trin. Det nye i denne proces er det specialiserede design og driften af REED modulet. Dette REED design tillader fjernelse af laktat fra gærings processen og giver mulighed for pH kontrol af fermenteringstanken ved hjælp af hydroxid. Derudover bevirker den periodiske drift af REED at den uhensigtsmæssige dannelse af et voksende lag af biologisk materiale på membranoverfladen mindskes.

En dynamisk model baseret på massebalancer er udledt for REED modulet for at beskrive transporten af ioner gennem membranerne og det tilstødende grænselag i dialysemodulet. De ukendte modelparametre er estimeret baseret på eksperimentelle data for Donnan dialytisk udvinding af en række monoprotiske kulstofsyrer. Statistiske simuleringer underbygger tidligere kvalitative forudsigelser af koncentration profiler ved separation med Donnan dialyse. Yderligere statistiske beregninger er benyttet til at undersøge indflydelsen af en ekstern elektrisk spændingsgradient på ion-strømme og koncentrations-profiler. Resultaterne viser udviklingen af asymmetriske koncentrationsprofiler, øgning af de potentielle ion-strømme og begræ ænsningen for strømtætheden. Gennem dynamiske simuleringer er systemets adfærd undersøgt for betingelser hvor det elektriske felt skifter. Flere fænomener er forudsagt såsom den dominerende ion transport i grænsefladerne, transiente ionfluks-inversioner og akkumulering/udtømning af ioner i membraner. Kombinationen af disse fænomener kan forklare det tab af effektivitet af spændingsfeltet, som er blevet eksperimentelt påvist. En række numeriske vanskeligheder har optrådt i forbindelse med disse simuleringer, og løsningsforslag er blevet præsenteret.

En bio-reaktor model med ustruktureret kinetik er blevet foreslået, som er egnet til integration med REED processen. Et identificerbart sæt af parametre er estimeret ud fra eksperimentelle data. Identificerbarhedsanalysen er understøttet af matematiske og statistiske værktøjer.

For at undersøge driften af REED-modulet, er en metode til kontrolstruktur-

design blevet udvidet til at håndtere periodiske systemer. pH regulering af produktstrømmen fra membran-enheden er blevet studeret. En ikke-konventionel input resetting kontrolstruktur er designet. Kvaliteten af styringen er vurderet efter hvor effektivt systemet følger set-punkterne for en række tests. Der er opnået tilfredsstillende resultater hvor pH er reguleret uden overtrædelse af inputbegrænsninger.

Udformningen og driften af den integrerede bio-reaktor og REED-modulet er undersøgt ved hjælp af de udviklede modeller og kontrolstrukturen. Analysen omfatter to forskellige undersøgelser: Kontinuerlig mælkesyre produktion samt batch produktion af en opstarts-kultur. Væsentlige forbedringer forudsiges for produktivitet og substrat-udnyttelse, og design og drifts-begrænsninger diskuteres.

Det undersøgte integrerede system er et klart eksempel på hvordan en modelbaseret tilgang støttet af eksperimentelt bevismateriale, kan bringe forbedringer af systemforståelsen og derfor fremme udviklingen af proces-design og procesregulering.

Contents

Appendices

1

Introduction

The product consumption due to rapidly increasing world population possess the challenge of providing necessary raw material for any industry. In particular, products obtained from non renewable sources, such as fossil fuels, are compromised since their depletion is imminent. Therefore, research has been focus to propose sustainable process alternatives that diminish our dependency on fossil feedstock.

This work is part of a bigger project for sustainable bioproduction of functional materials. The main interest is to investigate the Polylactic acid (PLA) production and its potential applications. In order to make the PLA production economically feasible, and then substitute their chemical or petrochemical based competitors, optimization of the design and operation of the existing production technologies is necessary. This project role within the macro-project is in the lactic acid bioproduction, as main feedstock for PLA production.

This work is focused on the investigation of a novel process for lactic acid production, where the fermentation and the product removal are tightly integrated. The process consists of a bioreactor and two stages of membrane based separation processes. This intensified process can be used for a variety of applications in biotechnology, where the fermentation production rate is limited by ionic species. The novelty of the intensified process lies in the first electrically driven membrane separation process employed, referred to as Reverse Electro-Enhanced Dialysis (REED). Through this technology, the bioproduction of lactic acid is intensified by the continuous removal of the biotoxic carboxylic anions from the cultivation broth and the recycling of biomass and unconsumed substrate. At the same time, the adverse influence of the membrane fouling is reduced by periodically reversing the imposed current density.

Conventional process engineering problems involve the process and control structures design for single processing units, including from single to multiple control loops. However, more realistic industrial applications include multiple processing units that usually interact with each other.

The design and operability of an integrated plant are complex mainly due to the units interaction. Therefore, it is crucial to reveal the interactions between the units. Based on that understanding, ways to mitigate or exploit those interactions can be proposed to achieve a more effective plant operation. Conventionally, the main purpose of using an integrated reactor and separation process is to have a material recycle and in that way increase the reaction conversion or yield. Although the recycle stream can significantly reduce operation cost, the integration increases the interaction between the processing units and move the degrees of freedom for control. Therefore, the control structure design becomes non trivial (Luyben, 1993).

Plantwide control deals with the selection of appropriate measured and manipu-

lated variables to achieve the defined process goals. Additionally, the implementation of the control strategy that ensure the achievement of the goals. A plantwide control methodology employs model based tools combined with heuristic approaches to design the control structure. Steady state and dynamic models are used plus an understanding of the plant behavior (Skogestad, 2000, 2004; Jørgensen, 2006).

A first characteristic for interacting systems control, specially the ones having an internal feedback of material or energy, is the so called snowball effect. The snowball effect is a static problem that arises when one output is very sensitive to small disturbances in an input variable. This problem can be attenuated by a proper system design or an appropriate control structure.

A second characteristic of a recycle system is that the plant may respond more slowly than anticipated based on the time constants of an individual units. If there are considerable differences between the units time constants, the plant is likely to have a larger time constant than the individual units. Meaning that the plant has slower dynamics than the individual units due to the positive material feedback (Kapoor and McAvoy, 1987).

The third characteristic and major concern is the propagation and recirculation of disturbances. The disturbances can be damped by surge tanks between units. However, this design solution should be avoided due to the extra capital and operating cost. New plants have little surge capacity and then unattenuated disturbances propagate around internal process flow paths. In order to control these complex systems, advanced control strategies may be required.

A model based investigation, supported by experimental evidence, can provide the system understanding which is vital for the integrated system design and operation. Due to the novelty of the Reverse Electro-Enhanced Dialysis process, it is specially interesting to reveal the process behavior under different operation modes. The modeling, operation and optimization of integrated biological reactive systems and membrane separation processes are challenging due to their complexity over the space and time which leads to a highly nonlinear behavior.

1.1 Lactic acid fermentation

Lactic acid bacteria (LAB) refer to a large group of gram-positive bacteria that have similar properties and all produce lactic acid as major or sole fermentation product. They are widespread in nature and are also found in our digestive systems. Although they are best known for their role in the preparation of fermented dairy products, they are also used for pickling of vegetables, baking, winemaking, curing fish, meats and sausages. Lactic acid bacteria are able to grow in presence or absence of oxygen and thus so called aerotolerant anaerobes (Madigan *et al.*, 2003).

Lactic acid bacteria have a limited biosynthetic ability, thus they often grow on a medium rich in aminoacids, vitamins, purines and pyrimidines. Besides, Lactic acid bacteria mainly obtain energy through the metabolism of sugars, which is considered decoupled of from growth, and therefore analyzed separately (Stephanopoulos *et al.*, 1998).

Lactic acid bacteria have been divided into two groups, homofermentative and heterofermentaive. Homofermentaive bacteria produce a single fermentation prod-

uct, lactic acid. Whereas heterofermentative bacteria produce other products such as ethanol, carbon dioxide and lactate. The difference in the fermentation patters is determined by the presence of the enzyme aldolase (Madigan *et al.*, 2003).

1.1.1 Fermentation products

Since lactic acid was discovered, it has been utilized in the leather and textile industries. Recently, it is widely used in the food industry as a pH regulator, solvent, preservative, electrolyte and precursor for lactate ester, propylene glycol, 2,3-pentanedione, propionic acid, acrylic acid, acetaldehyde, and dilactide (Varadarajan and Miller, 1999; Åkerberg and Zacchi, 2000). A detailed list of lactic acid and its salt applications is shown in Fig. 1.1. Perhaps its greatest industrial potential is for sustainable production of polymers such as Polylactic acid (PLA). Lactic acid consumption for industrial applications has surpassed the food and beverages industry as the leading market for lactic acid. This is a result of the continued high growth of PLA applications. It is expected that by 2013, industrial applications will account for more than half of global lactic acid use (SRI-Consulting, 2010). PLA is being promoted due to its environmentally friendly characteristics such as: biodegradability, composting of waste by-products from PLA production, sustainable production of the main feedstock and the potential energy saved versus conventional polymer production.

Chemical feedstock	Chemical industry	Food industry	Cosmetic industry	Pharmaceutical industry
-Propylene oxide -Acetaldehyde -Acrylic acid -Propionic acid -2,3-pentanedione -Ethyl lactate -Dilactide -Polylactic acid	-Descaling agents -pH regulator -Neutralizers -Chiral intermediates -Green solvents -Cleaning agent -Slow acid release agents -Metal complexing agents	-Acidulants -Preservatives -Flavors -pH regulators -Improving microbial quality -Mineral fortification	-Moisturizers -Skin-lightening agent -Skin-rejuvenating agents -pH regulators -Anti-acne agents -Humectants -Anti-tartar agents	-Parental/I.V. solution -Dialysis solution -Mineral preparations -Tablettings -Prostheses -Surgical sutures -Controlled drug delivery systems

Figure 1.1: List of commercial uses and applications of lactic acid and its salt. Adapted from Young-Jung *et al.* (2006)

High molecular weight PLA is obtained catalytically through the cyclic lactide ring-opening polymerization. The later cyclic component is produced in a two steps process. Lactic acid is firstly oligomerized and then catalytically dimerized to generate the required cyclic lactide. PLA have already been used in packaging, biomedical applications and textiles (Kharas *et al.*, 1996). PLA production is presently more expensive than petrochemical based polymers. Therefore, it can only substitute its competitors through optimization of its production, including the main feed stock i.e. Lactic acid. However as oil prices are expected to continue to increase, there seems to be a very good market potential for sustainable lactic acid based products.

Other application of the lactic acid fermentation is the production of biomass as probiotic culture or starter culture for food industry. Lactic acid bacteria have been used for over five thousand years in food preparations. They are employed in particular in fermented dairy products such as yoghurt, cheese and butter (Stiles and Holzapfel, 1997). The concept of the lactic acid bacteria as a group of organisms was developed at the beginning of the 1900s, and almost simultaneously their industrial exploitation. More recently, the concept of probiotic cultures has encouraged research in this area. Probiotics have been defined as "living micro-organisms, which upon ingestion in certain numbers, exert health benefits beyond inherent basic nutrition"(Guarner and Schaafsma, 1998). Several lines of evidence have established the benefits of ingestion of lactic acid bacteria on lactose digestion, some diarrheal illnesses, small bowel overgrowth associated with chronic kidney disease, and reduction of fecal enzymes that may play a role in colon cancer (Sanders, 1993). Further potential benefits are expected in fields such as modulation of blood cholesterol levels and competitive exclusion of intestinal pathogens. A number of *Lactobacillus* species, *Bifidobacterium* sp, *Saccharomyces boulardii*, and some other microbes have been proposed as and are used as probiotic strains (Ljungh and Wadström, 2006).

1.1.2 Lactic acid fermentation challenge

The bottleneck of lactic acid fermentation is that LAB are normally impaired by product inhibition, like many other fermentation processes, at a certain concentration level of the main metabolic product or one of the bi-products (Nielsen *et al.*, 2003). Hongo *et al.* (1986) studied the inhibition of *Lactobacillus delbrueckii* by the presence of different lactates with and without pH control, concluding that even neutralized lactates generate inhibition and the strongest effect is observed by lactate. The inhibitory effect generated by the presence of lactates and low pH can be potentially diminished by continuous removal of lactate from the fermenter and pH control, this will result in a higher productivity and product yield. On the other hand, continuous recycle of biomass will allow obtaining higher cell densities that minimizes the risk of a cell wash-out, thereby the continuous fermentation can be operated at high dilution rates greater than the specific growth rate of the organism.

Due to the lactic acid properties, conventional continuous separation operations such as distillation have limitations to be used. Usually, the lactate separation is done by precipitation, where the precipitated calcium lactate must be recovered employing strong acid. This procedure implies a high chemical cost and waste generation. For this reason, other options for lactate recovery have been studied such as solvent extraction, adsorption, direct distillation and membrane separation processes (Lee *et al.*, 1998a). It has been estimated that the cost of recovery and concentration of lactate from the cultivation broth can be up to 80% of the total production cost, then research has been focused developing alternatives for downstream processing (Hulse, 2004). Membrane based separation processes are attractive since they can selectively separate the lactate, are capable of being operated aseptically and basically there are no by-products generation.

1.2 Membrane based technologies for lactic acid recovery

Since 1960's, membrane separation processes have been suggested as an alternative for lactic acid extraction and biomass confinement or recycling. The application of processes as Dialysis, Donnan Dialysis, Electodialysis, Ultrafiltration, Nanofiltration and Reverse Osmosis is well documented, but only few will be quoted herein.

Probably one of the first evidences of utilizing membranes to concentrate cultures of microorganisms, including LAB, is proposed by Gerhardt and Gallup (1963). High density populations of microorganisms and their extracellular products were obtained in a dialysis flask. Since that time, it was evidenced that continuous removal of lactic acid from the fermentation broth by diffusion into a reservoir diminished the product inhibition, therefore enhanced the product yield. Few years later, Friedman and Gaden (1970) studied and modeled the growth and acid production by *L. delbrueckii* in a dialysis fermentation system using mainly ultrafiltration membranes. The results corroborate the earlier observations, where the microorganism exhibits higher production rates and cell concentrations than non-dialysis experiments. The main drawback of utilizing dialysis fermentation is the low diffusion efficiency.

In 1980's, Ohleyer *et al.* (1985) used a cell-recycle fermentation system where a bioreactor was coupled to a cross-flow filtration module. The continuous *L. delbrueckii* growth was investigated employing different substrates. Stability of long term fermentations was achieved and the maximum lactic acid concentration before complete inhibition was estimated. Electrodialysis was suggested by Hongo *et al.* (1986) as a potential *in situ* separation method since lactate can be selectively removed by ion exchange membranes. In the paper, the inhibitory effect of lactates on *L. delbrueckii* growth is studied. Besides, the advantages and potential problems of applying electrochemically pH-controlled electrodialysis fermentation are pointed out.

A combination of ultrafiltration and electrodialysis is used later by Boyaval *et al.* (1987) and Raucourt *et al.* (1989). This integrated bioreactor and purification system appears as an alternative to reduce fouling problems when only electrodialysis is used. The fouling issue is handled by the intermediate ultrafiltration stage since the cells are retained and recycled. Subsequently, lactate is recovered from the permeate by electrodialysis.

A process for producing and concentrating lactic acid is patented by Glassner and Datta (1990). The fermentation broth is fed to an electrodialysis unit to recover a lactate salt in an aqueous stream which is subjected to water-splitting electrodialysis to form base and a lactic acid product. Finally, the lactic acid product is treated with ion exchangers in different steps to remove any cations, sulfate ions or sulfuric acid.

Studies on electrodialysis were continued by Heriban *et al.* (1993), where double exchange reaction electrodialysis was employed for the isolation and concentration of lactic acid. Double exchange reaction electrodialysis uses a conventional electrodialysis module with alternating anion and cation exchange membranes plus an inorganic acid. This technology has been used to exchange ions between salts and

then obtain a higher value product. In their best scenario the lactic acid concentration was increased up to 4 times. The authors suggested the implementation of ultrafiltration module and to use bipolar membranes coupled to electrodialysis.

Despite in 1970's some drawbacks of applying reverse osmosis to lactic acid separation were mentioned, Timmer *et al.* (1994) took again the idea of recovering lactic acid from a fermentation without pH control. The low pH obtained after the fermentation enhances the selectivity of cellulose acetate membranes to lactic acid. A further concentration of lactic acid is carried out in nanofiltration module. At the same time, ultrafiltration is employed in a continuous membrane bioreactor by Zhang and Cheryan (1994) to guarantee long stable operation and high productivity of the cultivation. This is done by maintaining high cell densities, removing lactate and recirculating the substrate (starch). The bioprocess is carried out as a constant volume pH controlled fermentation.

Two step electrodialysis is investigated and modelled by Lee *et al.* (1998a), special attention was paid to the limiting current density in order to determine the switching condition from constant-current mode to constant-voltage mode in desalting electrodialysis. Predictions for lactate concentration, volume changes, switching times and energy consumption were validated experimentally. Zheleznov *et al.* (1998) were studying the transport of some carboxylic acids, usually found in fermentations, across anion exchange membranes during Donnan dialysis operation. They pointed out the benefits of this method and its potential. Therein, the influence of base concentration in the dialysate channel was correlated to the carboxylic anions flux using simple steady state relations.

Garde (2002) and Rype (2003) introduced a device referred to as Reverse Electro-Enhanced Dialysis (REED), this technology was proposed to overcome some of the drawbacks of Donnan dialysis and electrodialysis such as fouling and scaling. The REED design emerges as a method to enhance the lactate fluxes in conventional Donnan dialysis operation, this is done by imposing an external potential gradient. The REED module combines elements from electrodialysis reversal (EDR) and Donnan dialysis (DD) operations (Strathmann, 2004).

A more detailed process for lactic acid recovery from fermentation broths is described by Hábová *et al.* (2004). The entire process is composed by ultrafiltration, decolourisation, removal of multivalent ions as pretreatment of the fermentation broth and desalting electrodialysis and water splitting electrodialysis for the further lactic acid recovery and concentration.

1.3 Reverse Electro-Enhanced Dialysis process

The Reverse Electro-Enhanced Dialysis proposes itself to directly coupling with the lactic acid fermentation. The integrated system is composed of the fermenter and two electrically driven membrane separation modules (as shown in Fig. 1.2). In the first membrane separation process the lactate is separated from the fermentation broth by Reverse Electro-Enhanced Dialysis (REED). The supernatant stream is recycled to the bioreactor. In the second stage, lactic acid is recovered from the dialysate and concentrated using bipolar membranes in an Electrodialysis process with Bipolar Membranes (EDBM).

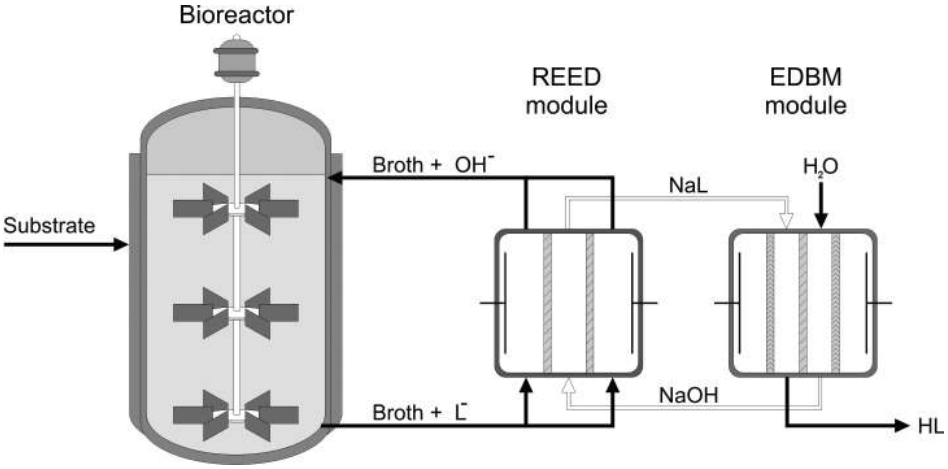

Figure 1.2: Sketch of the integrated membrane bioreactor for organic acid production. Adapted from Rype (2003)

The core and novelty of the process is the Reverse Electro-Enhanced Dialysis separation unit. The REED module is composed of several cells assembled in a plate-and-frame stack. A cell consists of feed and dialysate channels separated by anion exchange membranes. A schematic draw of REED module is depicted in Fig. 1.3.

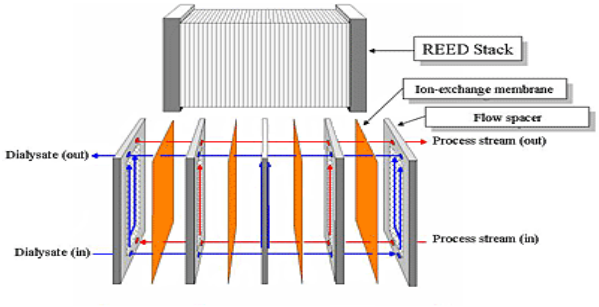

Figure 1.3: Sketch of REED module. Section in the module and flow distribution are shown. Taken from Jurag-Separation (2009)

1.3.1 Potential problems during *in situ* lactate recovery

The motivation to propose the Reverse Electro-Enhanced Dialysis is the potential problems evidenced when electrically driven membrane separation processes were proposed (Grossman and Sonin, 1973; Hongo *et al.*, 1986; Heriban *et al.*, 1993; Garde, 2002; Rype, 2003):

- Membrane fouling: this problem is probably the biggest obstacle when ion exchange membranes are used. Fouling can be generated by bacterial attachment, extracellular protein adsorption or colloidal particle deposition on the membrane surface. This is due to the fact that biomass, some proteins and colloids have local charged groups which are attracted by the ion exchange membranes.

- Scaling: certain multivalent ions such as Calcium and Magnesium contained in the feed solution are allowed to pass through cation exchange membranes. Those ions form salts that precipitate on the membrane surface.

- Bipolar membrane degradation: this kind of membrane is commonly used for the further recovery and concentration of lactic acid. The presence of Calcium, Magnesium and Iron can damage or destroy these membranes, even if they are present in small amounts.

Some solutions to the above issues have been proposed in order to reduce the adverse influence of the listed problems. Electrodialysis has been coupled with other separation processes, as pretreatments, such as activated carbon, ion exchangers, ultrafiltration, nanofiltration and reverse osmosis. In addition, the product from electrodialysis module requires further purification processes such as water splitting electrodialysis (electrodialysis with bipolar membranes), carbon adsorption, extraction, evaporation and pervaporation/distillation (Rype, 2003). From the technical point of view, it is possible to meet the product requirements by employing a different combination of processes. However, for commercial applications the process investment and operational costs must be minimized to make the process economically feasible.

1.3.2 Donnan dialysis recovery

For organic acid recovery, Donnan dialysis is a promising process where the scaling and bipolar membranes degradation problems are avoided since only anion exchange membranes (AEM) are used. Besides, the fouling problem is reduced due to high flow velocities and a destabilization mechanism generated by the hydroxide flow through the membrane in the opposite direction than fouling layer formation. Hydroxide has been used to clean fouled membranes (Zheleznov *et al.*, 1998).

Fig. 1.4 depicts the Donnan dialysis process for extraction of lactic acid from a fermentation broth. In this process, the fermentation broth is fed to every even channel in the membrane stack (feed channels). A concentrated sodium hydroxide solution is fed in the remaining channels (dialysate compartments). The feed from the fermenter has a low pH compared to the alkaline solution, therefore the hydroxide is transported through the AEM due to the large concentration gradient between the two solutions. The hydroxide flux is leading the lactate flux in the opposite direction. The fastest ion (OH^- in this case) induces a potential gradient which drives the lactate flux out of the feed channel (Mulder, 1997; Strathmann, 2004). Those fluxes are coupled since electroneutrality condition and Faraday's law must be fulfilled.

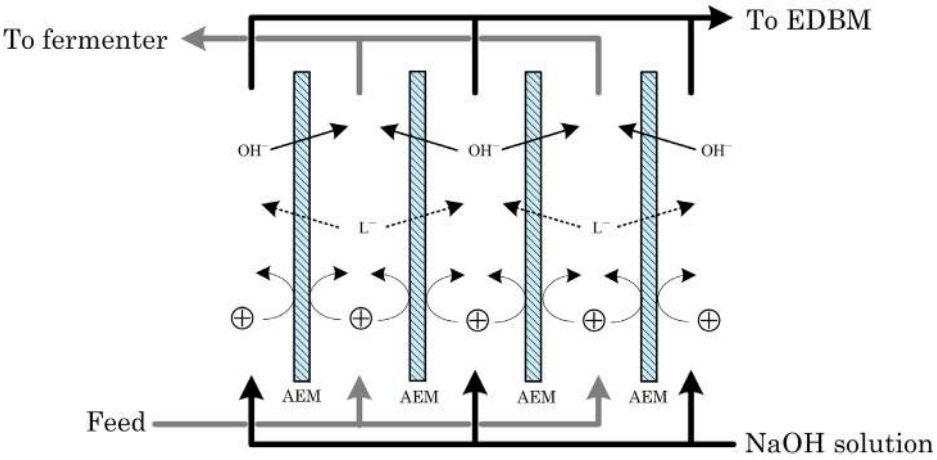

Figure 1.4: Schematic drawing illustrating lactic acid extraction by Donnan Dialysis employing only anion exchange membranes (AEM), adapted from Møllerhøj (2006)

The main disadvantage using Donnan dialysis for lactate recovery from the cultivation broth is a rather low lactate flux, since the driving force behind the lactate transport is the hydroxide concentration gradient in the opposite direction, which implies larger membrane area and concentration gradients.

1.3.3 Reverse electro-Enhanced Dialysis design

The REED design emerges as a potential method to enhance the lactate fluxes in conventional Donnan dialysis operation. This is done by imposing an electrical field, then fluxes can be potentially increased by several order of magnitude. Fig. 1.5 shows the expected ions transport through anion exchange membranes in parallel under current load conditions. Imposing an external potential gradient, the transport mechanism changes from counter ion transfer to a competitive ion transport. Rype (2003) used a simply model to show how lactate is preferably transported when the pH is below 11, meanwhile for pH higher than 12.5 hydroxide is carrying an increasing amount of current. Assuming that the solution in the feed channel stays at pH below 11, the lactate extraction from the feed stream is favored.

1.3.4 Electrodialysis with bipolar membranes

The solution containing the lactate extracted from the cultivation broth in the REED module is fed to the Electrodialysis with Bipolar Membranes (EDBM). The purposes of this operation are to recover and concentrate the lactic acid while the alkaline solution is regenerated and recycled to the REED unit.

The salt of a week acid can be converted in the corresponding acid employing a two compartment cell with bipolar membranes (BM) plus either cation or anion exchange membranes (CEM/AEM). A Bipolar membrane is composed of an anion

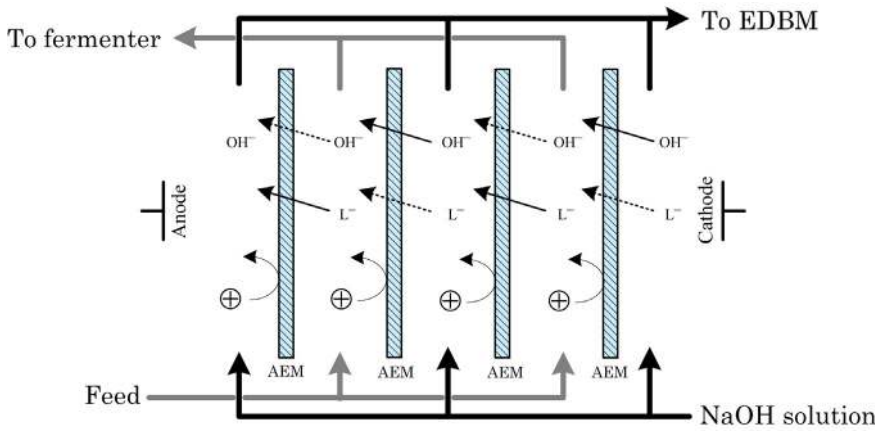

Figure 1.5: Schematic drawing illustrating the expected competitive lactate and hydroxide transport through anion exchange membrane (AEM), solid lines correspond to the favored fluxes, adapted from Møllerhøj (2006)

exchange membrane (AEM), a cation exchange membrane (CEM) and a contact region between the two ion exchange membranes. The water from outside solutions diffuses across both membranes and reaches the interface. Under an electrical field, the water is split into hydrogen ion (H^+) and hydroxide ion (OH^-). The generated hydrogen and hydroxide ions are used to combine with the anion (L^-) and the cation (Na^+) coming from the REED module. In order to separate the anion and the cation of sodium lactate, an ion exchange layer is placed in between two bipolar membranes. Schematic representation of the two compartment EDBM is depicted in Fig. 1.6. The difference between the two configurations is the separation purpose less than 100% efficient operation. Configuration (a) recovers and concentrates lactate as lactic acid in the acid chamber, while sodium hydroxide and sodium lactate remains in the base channel. Configuration (b) regenerates the sodium hydroxide in the base chamber, while lactic acid and sodium lactate remains in the acid channel.

In order to remove other inorganic acids present in the feed and purify the lactic acid, a subsequent electrodialysis unit can be used since at very low pH the lactic acid stays in its undissociated form.

1.4 Research motivation and objectives

Many biochemical products are obtained in bioprocesses where the reactions are kinetically and/or equilibrium controlled and overall process productivity depends on process conditions like pH, temperature, substrates concentration, etc. In recent years, there has been an increasing interest in fermentations processes since the main raw materials are renewable and products obtained in these processes are widely used in the fine chemical, pharmaceutical and food industry. However, a main difficulty of obtaining a high productivity in fermentation may be the product inhibition of microbial growth. Therefore, continuous removal of lactic acid from the fermenter

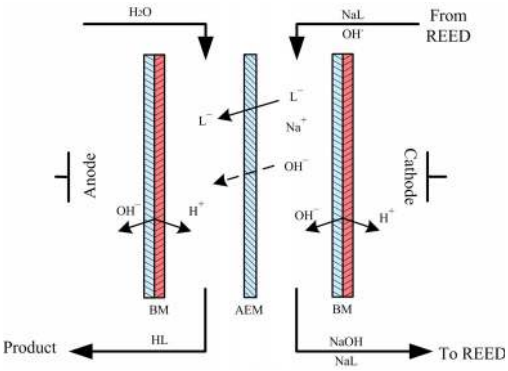

(a) BM+AEM

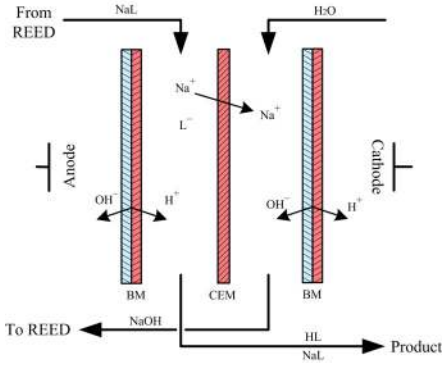

(b) BM+CEM

Figure 1.6: Ions transport in a 100% efficient two compartment cell bipolar membranes (BM) for weak acid recovery. (a) with anion exchange membrane (AEM) and (b) with cation exchange membrane (CEM).

will result in a higher productivity and product yield.

Recently, the application of an electrically driven membrane separation techniques has shown promising performance for continuous removal of lactic acid during fermentation, referred to as Reverse Electro-Enhanced Dialysis (REED) (Garde, 2002; Rype, 2003).

The key idea of this project is to use software tools in order to develop a combined knowledge-based and data-driven approach for design, operation, control and optimization of the integrated bioreactor and Reverse Electro-Enhanced Dialysis process for lactic acid fermentation. It is believed that this approach will bring new prospects for substantial improvements in production efficiency and product quality. This investigation objective is based on the following hypotheses:

- Through modeling and simulation, it is possible to contribute in the understanding: of Donnan dialysis separation, ion transport through anion exchange membranes under current load conditions (Electro-Enhanced Dialysis) and

current reversal conditions (Reverse Electro-Enhanced Dialysis).

- It is possible to extend the concepts behind a goal driven control structure design for integrated systems, which are partially operated periodically.

1.5 Thesis organization

This thesis has been organized into two main parts covering the contributions in membrane and process system engineering fields. These parts exclude this introduction chapter, final conclusions, suggestions for future work, appendices and references. This document is the compilation of journal papers, scientific conference contributions and technical reports, which have been developed/presented/submitted within the scope of this project. The content of each chapter reflects the content or extended version of the content of a contribution formatted to fit this thesis. Hence, relevant information may be repeated along the thesis since each contribution aims at being self explanatory. The title of the chapters have been adapted to give a sequence in the thesis. The references given in these papers are collected at the end of the thesis.

Part I - Modeling ion transport in a Dialytic module

This part of the thesis is aimed to provide understanding of the key electrically driven membrane separation unit in the integrated system, which is the Reverse Electro-Enhanced Dialysis. This process understanding is the pillar for the remaining parts of the thesis. This part of the work is based on two paper conference contributions, one published journal paper, two papers submitted for publication journal and a Master thesis.

In Chapter 2, a first principles dynamic model is developed to describe simultaneous ion transport in a Dialytic separation, for carboxylic anion recovery. Then, Donnan dialysis separation is studied. A detailed description of the model derivation, implementation and solution is presented. The model structure is tested using experimental data for Donnan dialysis recovery of several monoprotic carboxylic acids reported in the literature.

A static investigation of the competitive ion transport under current load conditions is performed in Chapter 3. Therefore, this chapter is focused studying why the ion fluxes are enhanced by imposing an external potential gradient to a dialytic module. The results are compared to Donnan Dialysis operation for lactate recovery. The system operating under current reversal conditions is studied in Chapter 4. The investigation aims to predict transient phenomena that are able to explain the loss of current efficiency during current reversal operation, which has been experimentally demonstrated. In the Chapters 3 and 4, an overview of the model equations and their solution is presented.

The derived dynamic model, for ion transport in the dialytic module, is modified to have a simple representation of an ideal two compartments Electrodialysis with bipolar membranes module. This is an extension to the work presented in this part of the thesis which has been carried out in collaboration

with MSc. student Sijing Liu during her master thesis. The most relevant achievements of her thesis are shown in appendix E.

Part II - Integrated system analysis

The second part of the thesis is aimed develop the necessary models and tools required to investigate the operability of the integrated system. This work is based on two conference paper contributions.

In Chapter 5, an unstructured model for lactic acid fermentation is proposed which is suitable for integration with the model for Reverse Electro-Enhanced Dialysis derived in part I. This model should be able to describe batch as well as continuous fermentations. Due to the model structure, it is particularly interesting to investigate the model parameter identifiability. A methodology is employed to estimate the kinetic parameters using experimental literature data and mathematical and statistical tools. The employed methods and tools are evaluated and discussed.

In order to facilitate the fermenter and REED models integration, a goal driven methodology for control system development is extended to deal with this particular periodically operating system in Chapter 6. A control structure in the REED module is investigated which can facilitate the pH control in the fermentation. The designed control structure is implemented and its performance evaluated.

In Chapter 7, the design and operation of the integrated fermenter and REED separation system are investigated using two different production goals. The productivity results are compared with those of a conventional fermentation. Potential problems in the design and controllability of the integrated system are discussed.

Concluding remarks and future work are presented in Chapter 8.

1.6 Contributions

The following is a list of the main contributions within this project. The following is divided into journal papers, peer reviewed conference proceedings, conference oral presentations and conference poster presentations. These contributions compile the present understanding of the Reverse Electro-Enhanced Dialysis process under no current/current/reversal current conditions. Additionally, an extended methodology for goal driven control structure design in a periodically operated system. Finally, the strategy for design of operation of the integrated system according to a fermentation objective is presented.

1.6.1 Journal papers

- Prado-Rubio, O.A., Møllerhøj, M., Jørgensen, S.B. and Jonsson, G. (2010). Modeling Donnan Dialysis Separation for Carboxylic Anion Recovery. *Computers & Chemical Engineering*, (ESCAPE 19$^{\text{th}}$ - selected paper), 34, 1567-1579.

- Prado-Rubio, O.A., Jørgensen, S.B. and Jonsson, G. (2011). Model based investigation of the potential lactate recovery using Electro-Enhanced Dialysis - Static analysis. *Separation and Purification Technology Journal*, 78, 113-124.

- Prado-Rubio, O.A., Jørgensen, S.B. and Jonsson, G. (2011). Reverse Electro-Enhanced Dialysis for lactate recovery from a fermentation broth. *Journal of Membrane Science*, 374, 2032.

1.6.2 Peer reviewed conference proceedings

- Prado-Rubio, O., Jørgensen, S., and Jonsson, G. (2010). Systematic Procedure for Integrated Process Operation: Reverse Electro-Enhanced Dialysis during Lactic Acid Fermentation. 21th European Symposium on Computer Aided Process Engineering - ESCAPE21. (*Accepted*).

- Prado-Rubio, O., Jørgensen, S., and Jonsson, G. (2010). Control System Development for Integrated Bioreactor and Membrane Separation Process. S. Pierucci and G. Buzzi Ferraris (Editors). 20th European Symposium on Computer Aided Process Engineering - ESCAPE20. Computer-Aided Chemical Engineering (ISBN: 978-0-444-53569-6), volume 28, pages 289-294. Great Britain: Elsevier.

- Prado-Rubio, O., Jørgensen, S., and Jonsson, G. (2009). Tool for Optimizing the Design and Operation of Reverse Electro-Enhanced Dialysis of Monoprotic Carboxylic Acids. Rita Maria de Brito Alves, Claudio Augusto Oller do Nascimento and Evaristo Chalbaud Biscaia Jr. (Editors). 10th International Symposium on Process Systems Engineering - PSE2009. Computer-Aided Chemical Engineering (ISSN: 1570-7946), volume 27A, pages 663-668. The Netherlands: Elsevier.

- Oscar A. Prado Rubio, Sten B. Jørgensen, Gunnar E. Jonsson. (2009). Lactic acid recovery in electro-enhanced dialysis: Modelling and validation. In Jezowski, J. and Thullie, J. (Editors). 19th European Symposium on Computer Aided Process Engineering - ESCAPE19. Computer-Aided Chemical Engineering (ISBN:978-0-444-53433-0), volume 26, pages 773-779. The Netherlands: Elsevier.

1.6.3 Conference oral presentations

- Prado-Rubio, O., Jørgensen, S., and Jonsson, G. Control System Development for Integrated Bioreactor and Membrane Separation Process. Presented at 20th European Symposium on Computer Aided Process Engineering - ESCAPE20. Jun 2010. Ischia, Naples - Italy

- Prado-Rubio, O.A., Jørgensen, S., and Jonsson, G. Lactic Acid Recovery in Electro-Enhanced Dialysis: Modelling and validation. Presented at 19th European Symposium on Computer Aided Process Engineering . Jun 2009. Krakow - Poland.

- Prado-Rubio, O.A.; Jørgensen, S.B.; Jonsson, G. Modeling Reverse Electro-Enhanced Dialysis for Integration with Lactic Acid Fermentation. Presented at Nordic Process Control Workshop '09, NPCW09. January 2009. Porsgrunn - Norway.

- Prado Rubio, O.A.; Jørgensen, S.B. ; Jonsson, G. Modelling of Ion Transport across Anion Exchange Membranes Under Current Reversal Conditions. Presented at AIChE Annual Meeting 2008, November 2008. Philadelphia, PA - USA.

- Prado-Rubio, O.A.; Jonsson, G. and Jørgensen, S.B. Modelling Electrically Driven Membrane Separation Processes for Lactic Acid Production. Presented at BEC2008. September 2008. Brâc - Croatia.

1.6.4 Conference poster presentations

- Prado-Rubio, O.A., Jørgensen, S., and Jonsson, G. Tool for Optimizing the Design and Operation of Reverse Electro-Enhanced Dialysis of Monoprotic Carboxylic Acids. Poster at 10^{th} International Symposium on Process Systems Engineering - PSE2009. August 2009. Salvador, Bahia - Brazil.

- Prado-Rubio, O.A.; Jonsson, G. and Jørgensen, S.B. Metabolic Engineering Modelling for Optimizing an Integrated Bioreactor and Membrane Separation Processes. Poster at ISGSB09. August 2008. Helsingør - Denmark.

- Prado-Rubio, O.A.; Jonsson, G. and Jørgensen, S.B. Modelling and Optimization of Integrated Bioreactor and Membrane Separation Processes - Prospective. Poster at 1^{st} Bioproduction annual Meeting. September 2007. Poros - Greece.

Part I

Modeling ion transport in a Dialytic module

2

Model development and regression

2.1 Abstract

A dynamic model for transport of multiple ions through an anion exchange membrane is derived based on the Nernst-Planck approach. This model accounts for the convective transport of the dissociated and undissociated species in the channels with diffusion and migration across the boundary layers and membranes. Donnan equilibrium, flux continuity of the transported ions, the electroneutrality condition and Faraday's law are employed to describe the electrical potential and concentration discontinuities at the interfaces. The Nernst-Planck equation is used to model the ion transport though boundary layers and membranes. The model consists of a system of partial differential equations that are solved numerically. The aim of this paper is to corroborate this general model for several monoprotic carboxylic acids reported in the literature. The model reproduces satisfactorily experimental fluxes for monoprotic ions. Additionally, previously qualitatively estimated concentration profiles within the boundary layers and membranes are predicted.

2.2 Introduction

Presently, economical and sustainability issues are the main driving forces to generate improvements in process design and operation. Bioproduction of commodity chemicals is particularly necessary in order to substitute their chemical or petrochemical based synthesis. There has been a constant interest in biotechnological production of carboxylic acids due to their well known industrial applications. Recently, there is a growing interest in lactic acid since it is the main feedstock for Polylactic acid (PLA) production. Polymers derived from PLA can substitute petrochemically based polymers in several applications and thus reduce our dependency on fossil feedstock. In order to make the PLA production economically viable, optimization of the design and operation of the developing production technologies is necessary.

Probably the main in limitation producing carboxylic acids by fermentation is that microorganisms are normally impaired by product inhibition and low pH (Nielsen *et al.*, 2003). Investigations on lactic acid bacteria cultivations without pH control have shown that the inhibition is generated by the presence of different lactates, and even neutralized lactates provoke inhibition. The strongest adverse influence has been seen in the presence of pure lactate (Hongo *et al.*, 1986). Therefore, a higher productivity and product yield can be achieved by the continuous removal of lactate from the fermenter and pH control. However, it has been seen that lac-

tate recovery from the diluted cultivation broth constitutes a challenging separation problem (Lee *et al.*, 1998a). Usually, the lactate separation is by precipitation, where the precipitated calcium lactate must be recovered by employing a strong acid. This procedure implies high chemical cost and waste generation. For this reason, alternatives for lactate recovery have been studied such as solvent extraction, adsorption, direct distillation and membrane separation processes (Lee *et al.*, 1998a). From this list of options, membrane separation processes are attractive since they can be very selective and capable of being operated aseptically without by-product generation. Additionally, if biomass can be recycled, it would allow obtaining higher cell densities to minimize the risk of cell wash-out, thereby the continuous fermentation can be operated at higher dilution rates than the specific growth rate of the organism. Thus providing even higher productivity. The potential recycling of biomass would still render membrane separation a promising alternative even if product inhibition was minimized genetically.

Electrically driven membrane separation processes have shown to be very selective for recovery of ion species. Among all alternatives, Donnan dialysis lactate recovery has experimentally shown promising performance (Narbęska and Staniszewski, 1998a; Zheleznov *et al.*, 1998). This process is attractive since the separation is driven by the electrochemical potential gradient across the membrane. Therefore, the energy consumption is only due to pumping the solutions through the module. In this separation process, only anion exchange membranes (AEMs) are employed and the stripping agent is an aqueous base. Employing this technology, conventional problems found in electrodialysis are reduced. Scaling problems are avoided due to the absence of cation exchange membranes. Besides, fouling is minimized due to high flow velocities and a destabilization mechanism, where the latter is generated by the hydroxide flux through the membrane in the opposite direction than the fouling layer formation.

Previously, mainly static models have been proposed for modeling the ion transport in Donnan dialysis. Different approaches have been used from mechanistic to first principles models in diverse geometries. The set of assumptions define the model structure in dependence of the model purpose. Most of the models were developed to investigate metal ion transport through cation exchange membranes.

In late 70's, a simple model characterized by mass transfer coefficients and Donnan equilibrium was proposed (Lake and Melsheimer, 1978). The importance of boundary layer and membrane resistances was recognized. However, this kind of model neglects the coupling between fluxes by the electrical potential gradient and osmotic flow. Therefore, it can not predict the dependence on ion type and ion concentration in the feed and dialysate channels. This situation can be overcome by employing the Nernst-Plank equation for the ion fluxes, e.g. to investigate: the transport of cations in charged pores in the membrane control regime (Cwirko and Carbonell, 1989, 1990), the neutralization of waste water considering the boundary layer resistance Starov *et al.* (1990), mono and polyvalent ion fluxes through diverse cation exchange membranes and their respective boundary layers (Miyoshi, 1997). These models are different mainly because they account for different terms in the Nernst-Plank equation, due to the system geometry and the way to model the concentration and potential discontinuities at the membrane-boundary layer interfaces. Despite the differences, these approaches account for the effect of ion bulk concen-

trations on the ion transport. After some assumptions, it has been shown that the steady state fluxes can be estimated using simple algebraic equations according to the dominant transport resistance (Starov *et al.*, 1990) and reproduce to some extent the experimental data for Donnan dialysis recovery of carboxylic anions (Zheleznov *et al.*, 1998). However, the predictive power of those models is very limited.

The objective of this contribution is to depict a general model describing the simultaneous ion transport through ion exchange membranes, when the target ion is recovered from a fermentation broth. The system is a dialysis module operating at a variable imposed potential gradient. In the presented paper, the model is adjusted to reproduce experimental data collected for monoprotic anion recovery using Donnan dialysis. This model could be used to evaluate the potential anions recovery under diverse operation modes and then provide a further understanding of the limiting transport factors.

Even though ion exchange membranes have been widely used in industry, the transport mechanism behind the separation has not yet been completely understood. Thus, it is desirable to develop models which can provide a better understanding of the transport phenomena in such electrochemical systems. Furthermore, models will potentially enable optimization of the design and operation of the modules. Our main modeling contributions are: to account for the carboxylic acid dissociation, to include a pH buffer effect in the feed channel and to develop a dynamic model. The dissociation reactions are important since the feed stream comes from a fermenter. Besides, we have developed this dynamic model since our ultimate goal is to optimize the operation of electrically driven separation processes.

The paper is structured as follows: the Donnan dialysis process for anion recovery is introduced and the dynamic model is described. The experimental data are presented and analyzed for Donnan dialysis recovery of some monoprotic carboxylic anions. The unknown parameters in the first principles model are estimated using simulations and a parameter estimation procedure. The developed model is shown to reproduce experimental fluxes for several monoprotic carboxylic acids satisfactorily. The model is used to predict concentration profiles under boundary layer and membrane controlled transport conditions. Finally, the conclusions are drawn.

2.3 Model development

2.3.1 Process description

Fig. 2.1 depicts a section of the Donnan dialysis process for extraction of lactic acid. In this process, the feed is introduced to every other channel in the membrane stack. A concentrated sodium hydroxide solution is fed in the remaining channels (dialysate compartments). The feed has a low pH compared to the alkaline solution, therefore the hydroxide ion is transported through the anion exchange membrane due to the large concentration difference between the two solutions. The hydroxide flux induces an electrical potential gradient which drives the lactate ions out of the feed channels (Mulder, 1997; Strathmann, 2004). Thus, the hydroxide flux is effectively leading the lactate flux in the opposite direction across the membrane. Those fluxes are coupled since the electroneutrality condition must be fulfilled as

well as the Faraday's law. Sodium fluxes, depicted with dashed arrows in Fig. 2.1, are considerably lower than lactate and hydroxide fluxes due to Donnan exclusion. However, the sodium flux is necessary to account for since it is coupled as well. It has been seen that Donnan exclusion becomes less effective when the base concentration in the dialysate channel increases.

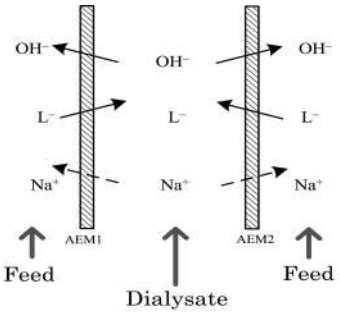

Figure 2.1: Schematic drawing illustrating lactic acid extraction by Donnan dialysis employing only anion exchange membranes (AEMs). Dominant fluxes are depicted in solid lines

2.3.2 Static black box models

The carboxylic acid fluxes in Donnan dialysis are characterized by two limiting regions, referred to as boundary layer and membrane controlled regions, according to the prevailing transport resistance. Experimentally, it has been shown that the dominant resistance depends on the concentration gradients and flow conditions (Lake and Melsheimer, 1978). Previous work has derived simple mechanistic expressions to reproduce experimental fluxes under the prevailing transport resistance. Under boundary layer control, the main resistance for mass transport is in the liquid phase adjacent to the membrane surface. In that case, the concentration gradient within the membrane becomes negligible and anion fluxes are proportional to the base concentration in dialysate channel, as it is shown in Eq. 2.1 (Starov *et al.*, 1990).

$$J_{A^-} = \frac{D_{A^-} D_{OH^-}}{\delta_{BL} \left(D_{OH^-} - D_{A^-}\right)} \left(\sqrt{\frac{D_{OH^-}}{D_{A^-}}} - 1 \right) C_{OH^-} \tag{2.1}$$

where δ_{BL} is the thickness of the boundary layer and D_k is the diffusion coefficient for anion k in the aqueous solution. It can be seen in Eq. 2.1 that the anion flux is independent of the membrane properties and acid concentration in the feed. Therefore, an increment in the base concentration generates an increase in the anion flux. When the base concentration in the dialysate channel is increased further, the mass transport resistance within the membrane becomes important until the point where the main resistance is determined by the membrane. Therefore, the so called

membrane control has been achieved. In the limit of the membrane control region, the concentration gradients inside the membrane are steep due to the high transport resistance. Besides, the concentration profiles are fully developed. The anion flux is independent of the base concentration in the dialysate channel as it is shown in Eq. 2.2 (Starov *et al.*, 1990).

$$J_{A^-} = \frac{QD_{A^-}D_{OH^-}}{\delta_m \left(D_{OH^-} - D_{A^-}\right)} \ln\left(\frac{D_{OH^-}}{D_{A^-}}\right) \tag{2.2}$$

where Q is the ion exchange capacity of the membrane, δ_m is the membrane thickness and D_k is the diffusion coefficient of anion k within the membrane. The saturation of the anion flux through the membrane is determined by the membrane thickness and the diffusion coefficient of both anions in the membrane. The overall dependency of the anion transport across the membrane, as a function of the base concentration in the dialysate channel, can be represented by a Langmuir function (Eq. 2.3) (Zheleznov *et al.*, 1998). This is analogous to a reaction-diffusion mechanism, the membrane is considered as an ideal reactive carrier and the fluxes are described by Michaelis-Menten reaction type as function of concentration in the bulk channel (Wódzki and Nowaczyk, 1999).

$$J_{A^-} = \frac{abC_{OH^-}}{1 + bC_{OH^-}} \tag{2.3}$$

where a and b are characteristic parameters that depend on the anion, membrane and experimental conditions. From the experimental data depicted in Fig. 2.4, it can be seen that experimental fluxes for lactate and propionate do not achieve a maximum value for the flux (J_{max}) as it is predicted by the reaction-diffusion model. This could be provoked by a measurement problem during the experiments or most likely the evidence of a dual transport mechanism. A dual mechanism is the combination of a reaction-diffusion and solution-diffusion mechanisms. During solution-diffusion mechanism, the transported species are dissolved in the membrane and then they can diffuse throughout it. The dual mechanism can be represented by the following expression:

$$J_{A^-} = J_{max}\left(\frac{kC_{OH^-}}{1 + kC_{OH^-}}\right) + PC_{OH^-} \tag{2.4}$$

We quantitatively confirmed that lactate and propionate fluxes are better described by the dual mechanism, while acetate transport is well represented by pure reaction-diffusion model (see Appendix B). Different contributions of both mechanisms have been seen before, when the permeation of some carboxylic acids was studied in dialysis using Neosepta-AMH (Wódzki and Nowaczyk, 1999). In that case, the contribution of solution-diffusion flux became relevant for tartaric and oxalic acids at high concentrations, while for lactic acid it is definitely dominant. On the other hand, reaction-diffusion flux was more important for propionic, acetic and citric acid. The different properties exhibited by lactic acid were explained by the fact that the transport of lactic acid is reaction rate-determined. Therefore, it is possible that

this facilitated transport is slower than the free diffusion. In contrast during Donnan dialysis, reaction-diffusion fluxes for the monoprotic acids through Neosepta-AMH are dominant with only a small influence of solution-diffusion fluxes, for lactic and propionic acids, at high base concentrations in the dialysate channel. Therefore for counter-ion diffusion, the reaction-diffusion transport is several times faster than for solution-diffusion, especially for acetate. Based on these findings, we conclude that experimental work is required to understand the transport mechanisms during dialytic recovery of carboxylic anions with a specific membrane, and is absolutely necessary if only black box models are used. However, the lack of predictive power of the depicted models is a strong motivation to work with a first principles model.

2.3.3 Model assumptions

The transport of ions through a section of the Donnan dialysis unit is modeled. The entire module can be composed by several cells in parallel assembled in a plate-and-frame stack. This electrochemical system is characterized by several simultaneous phenomena such as species dissociation and multicomponent mass transport through different solution and membrane phases. A dynamic model is derived for transport of multiple ions through anion exchange membranes and Nernst diffusion layers (adjacent to the membranes). The model is based on first principles for dissociation, diffusion, convection and migration of the main species found in a cultivation broth. The modeled module section is composed of two feed channels with one dialysate channel bounded by two anion exchange membranes. A detailed sketch is depicted in Fig. 2.2, where the section is divided into different zones and the ions present in each zone are shown. The zones are: three bulk channels, two membranes and four boundary layers. The model accounts for the convective transport of different species in the bulk channels (y-direction) and the diffusion and migration through the membranes and boundary layers (x-direction). The Nernst-Planck approach is used to describe the transport phenomena in the boundary layers and membranes. Finally, assumptions GA1, GA2, GA10 and MA4 are used to model the concentration and potential discontinuities at the interfaces (Prado-Rubio *et al.*, 2009a).

Due to the complexity of a real dialytic system, any theoretical analysis is of necessity based on a simplified model of the actual process. In order to set-up the model, the following main assumptions were made.

2.3.3.1 General assumptions (GA)

GA1. Electroneutrality condition must be fulfilled at any location in the system.

GA2. The electrical current is carried by ions (Faraday's law).

GA3. The expected influence of temperature changes due to the combined resistance of the cells is neglected.

GA4. Constant properties such as: diffusion coefficients (in the solution) and dissociation constants. Variations of physicochemical properties as function of temperature and concentration are neglected, because the expected changes are small and information available is limited.

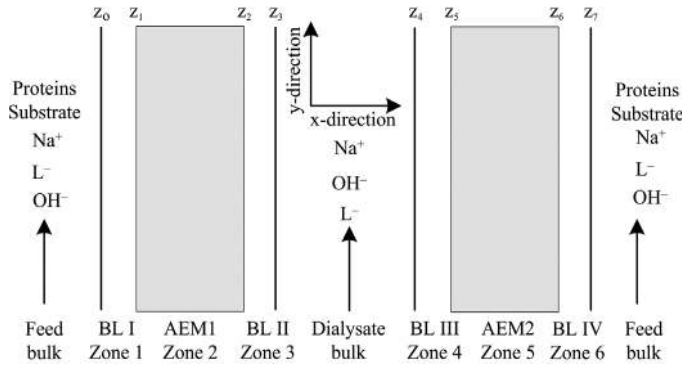

Figure 2.2: Sketch of a section of the dialysis module for lactate recovery from a fermentation broth. The zones in the section and ions present in each zone are depicted. BL: boundary layer and AEM: anion exchange membrane. $z_j \ \forall \ j$=1,...,7 are the interfaces

GA5. Ideal solution. For the sake of simplicity, the system is assumed ideal since the introduction of activity coefficients increases substantially the complexity of the model. At low carboxylic anion concentration in the aqueous system, there are small deviations from ideal behavior.

GA6. An extra pH buffer effect in the fermentation broth feed channel is modeled by the introduction of the species P^- and HP. When the separation is performed from a fermentation broth, an extra pH buffer effect which is not associated to the acid dissociation is expected. This effect is apparently caused by amino and carboxylic groups present in proteins and suspended colloidal material in the cultivation broth. In order to model the extra pH buffer, a hypothetical proton acceptor group on a protein is introduced in the model (HP and P). If the separation is performed employing a pure carboxylic acid solution, the extra buffer effect can be suppressed by fixing a negligible amount protein in the feed stream.

GA7. Constant pH of the feed solution. This is reasonable if the feed stream is coming from a fermenter, where a constant pH is required.

GA8. The transport through the membranes and boundary layers in the x-direction is defined by multicomponent diffusive and electrophoretic transport, driven by concentration and potential gradients. Ideal Nernst-Planck equation is employed, neglecting the convective transport. The pressure driven convective transport in x-direction is neglected since in ion exchange membrane separation processes the pressure differences are kept as low as possible (Wilson *et al.*, 2000).

GA9. In order to model the concentration profile in the feed and dialysate channels, tanks in series approach in the y-direction is used. It is a simplification

of the ideal plug flow model, where the concentrations are assumed to be independent of position in the x-dimension.

GA10. There is not accumulation of the transported ions at the interfaces. For the un-transported ions, the fluxes equal zero.

2.3.3.2 Membrane assumptions (MA)

MA1. The transport in the y-direction in the membranes is neglected. The concentration and electrical potential gradients in the y-direction are significantly smaller than in x-direction, then it is reasonable to neglect the transport in y-direction.

MA2. Transport of water through the membrane by osmosis is neglected due to the low pressures differences. In addition, electro-osmotic water transport facilitated by ion movement is not investigated.

MA3. There is no transport of uncharged species or large molecules through the membrane (P^-, HL, HP). Both forms of the protein can not penetrate the membrane due to their size. Besides the lactic acid (HL) is completely dissociated at the membrane surface since the pH there is very high. The transport of other low molecular weight ionic species that could be in the cultivation broth is not investigated.

MA4. The ionic solution is in equilibrium with the adjacent membrane surface, it means that electrochemical potential of each component in both phases are identical. This situation is described by the Donnan equilibrium condition.

MA5. It is expected that the membrane water content changes with different average pH, however the dimensions of the membrane are assumed constant.

2.3.3.3 Boundary layer assumptions (BLA)

BLA1. Convective transport in the y-direction in boundary layer is neglected. The assumption of a stagnant liquid film adjacent to the membrane surface is widely accepted in modeling of chemical systems.

BLA2. There are correlations in the literature to estimate the thickness of the boundary layer in electrodialysis based on dimensionless numbers: Reynolds, Schmidt and Sherwood (Moon *et al.*, 2004). However, for a given flow condition the thickness of the boundary layer is assumed constant.

2.3.4 Mass balances

In the model, the species and the zones are denoted by the subscripts k and p, respectively. The zones are boundary layers and membranes.

2.3.4.1 Transport through boundary layers and membranes

A dynamic mass balance for each species in the mentioned phases can be written as follows (Taylor and Krishna, 1996):

$$\frac{\partial C_{k,p}}{\partial t} + \nabla J_{k,p} - R_k = 0 \tag{2.5}$$

where the component flux $J_{k,p}$ is estimated using Nernst-Planck approach. From the generalized Maxwell-Stefan formulation, the Nernst-Planck equation can be derived for a multicomponent electrochemical system. This approach accounts for diffusion, migration and convection of species (Taylor and Krishna, 1996). The general Nernst-Planck equation is simplified for an ideal solution and neglecting convective transport (Lakshminarayanaiah, 1969; Strathmann, 2004):

$$J_{k,p} = -D_{k,p}\left(\frac{\partial C_{k,p}}{\partial x} + \frac{z_k F C_{k,p}}{RT}\frac{\partial \psi_p}{\partial x}\right) \tag{2.6}$$

The reaction term R_k in Eq. 2.5 is used to introduce the carboxylic acid dissociation into the model and the pH buffer effect. In general, proteins are large molecules that can contain several charged groups. If the protein dissociation is modeled as a polyprotic acid reaction, the stiffness of the system of equations could increase considerably. To overcome this situation, the proton acceptor groups in the protein are considered in terms of equivalents, i.e. the protein concentration is defined as moles acid equivalents per volume. Therefore, the dissociation of a polyprotic species is simplified to a monoprotic acid reaction. The protein species represents a wide range of components in the fermentation broth from low molecular weight proteins to colloidal material. The reaction system is given by the following equilibrium expressions involving the dissociation of the carboxylic acid and the protein:

$$HA + OH^- \underset{k_2}{\overset{k_1}{\rightleftharpoons}} A^- + H_2O$$
$$HP + OH^- \underset{k_4}{\overset{k_3}{\rightleftharpoons}} P^- + H_2O$$

It can be demonstrated that the dissociation constants for each reaction in this representation is related to the conventional K_a by the following expression:

$$K_d = \frac{K_a}{K_w} \tag{2.7}$$

Introducing the Nernst-Planck equation and dimensionless time and position parameters (see section 2.7) into Eq. 2.5, the general mass balance equation can be rewritten as Eq. 2.8.

$$\frac{\partial C_{k,p}}{\partial \tau} = \frac{\tau_n}{\tau_{diff}}\left(\frac{\partial^2 C_{k,p}}{\partial z^2} + z_k\left(\frac{\partial C_{k,p}}{\partial z}\frac{\partial \varphi_p}{\partial z} + C_{k,p}\frac{\partial^2 \varphi_p}{\partial z^2}\right)\right) + \tau_n R_k \tag{2.8}$$

The above equation is a general expression for all species. However, the migration terms, i.e. the terms involving the electrical potential gradient, apply only for dissociated species. The electrical potential gradient required in Eq. 2.8 is estimated assuming that all the electrical current is carried by ions (Faraday's law, GA2). This assumption is represented by Eq. 2.9. In this way, the electric potential can be eliminated from the mass balances (Starov *et al.*, 1990).

$$I_d = F \sum_k z_k J_{k,p} \tag{2.9}$$

Substituting the fluxes for each ion (Eq. 2.6) into Eq. 2.9, the potential gradient can be estimated. Notice that k in this case refers only to the ionic species and that not all species are present in every phase p.

$$\frac{\partial \varphi_p}{\partial z} = \frac{-I_d \delta_m / F - \sum_k z_k D_{k,p} \partial C_{k,p}/\partial z}{\sum_k z_k^2 D_{k,p} C_{k,p}} \tag{2.10}$$

The second derivative of the potential is found from the potential gradient equation (Eq. 2.10).

$$\begin{aligned} \frac{\partial^2 \varphi_p}{\partial z^2} =& \frac{-\sum_k z_k D_{k,p} \partial^2 C_{k,p}/\partial z^2}{\sum_k z_k^2 D_{k,p} C_{k,p}} + \\ & \frac{I_d \delta_m / F + \sum_k z_k D_{k,p} \partial C_{k,p}/\partial z}{\left(\sum_k z_k^2 D_{k,p} C_{k,p}\right)^2} \left(\sum_k z_k^2 D_{k,p} \frac{\partial C_{k,p}}{\partial z} \right) \end{aligned} \tag{2.11}$$

How the boundary conditions of potential gradients and concentrations can be estimated is explained in the following subsections. The schematic sketch of one membrane and the corresponding type of equations used in each section are depicted in Fig. 2.3. The boundary conditions for the mass balances are developed according to the relations depicted in section 2.3.4.3. The number of relations required to solve the model was determined using a degree of freedom analysis.

2.3.4.2 Bulk channel model

The concentration boundary conditions at the solution-boundary layer interfaces, in the x-direction, are estimated using tanks in series approach. A system of differential algebraic equations describe the convective transport along the bulk channels (y-direction). In each tank there is mass exchange with the adjacent boundary layers and the dissociation reactions are present. The dimensionless mass balances for each tank in the feed and dialysate channels are depicted below:

$$\begin{aligned} \frac{dC_k^{fb}}{d\tau} =& \frac{\tau_n}{\tau_{feed}} \left(C_k^{fbin} - C_k^{fb} \right) + \\ & \frac{\tau_n}{h_{feed}} \left(J_k|_{z=z_7} - J_k|_{z=z_0} \right) + \tau_n R_k \end{aligned} \tag{2.12}$$

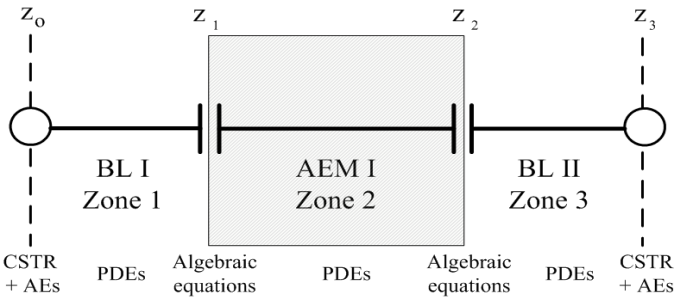

Figure 2.3: Schematic sketch of one membrane with associated boundary layers. The symbols: ‖ at the membrane surface indicates the concentration and potential discontinuities at the interfaces, ◯ represents the bulk concentration. The model employed within each zone is depicted. AE's stands for Algebraic equations and PDEs for partial differential equations.

$$\frac{dC_k^{db}}{d\tau} = \frac{\tau_n}{\tau_{dia}}\left(C_k^{dbin} - C_k^{db}\right) + \frac{\tau_n}{h_{dia}}\Big(J_k|_{z=z_3} - J_k|_{z=z_4}\Big) \tag{2.13}$$

In the dialysate channel the reaction term can be neglected. The reason is that the species are completely dissociated due to the high pH.

2.3.4.3 Algebraic relations at the interfaces

Algebraic expressions are employed to model the potential gradients and concentrations discontinuities at the membrane-boundary layer interfaces (z_1, z_2, z_5 and z_6 in Fig. 2.2). Additionally, the potential gradients in the bulk solution-boundary layer interfaces. Donnan potential gives the potential build-up at membrane-solution interfaces, which is determined by the ionic distribution of the transported ions.

$$\left(\frac{C_k^s}{C_k^m}\right)^{\frac{1}{z_k}} = \left(\frac{C_i^s}{C_i^m}\right)^{\frac{1}{z_i}} = \ldots \quad k \neq i \tag{2.14}$$

The Faraday's law states that all the electrical current is carried by ions. Since there is no current imposed on the system, the equation is reduced to:

$$F\sum_k z_k J_{k,p} = 0$$

The fluxes at the interfaces solution-boundary layer and boundary layer-membrane are continuous for the transported ions, that means that there is no accumulation at the interfaces (Eq. 2.15). Points z_j^- and z_j^+ correspond to the left and right side respectively of the interface located at z_j. For the un-transported ions the flux equals zero.

$$J_k|_{z=z_j^-} = J_k|_{z=z_j^+} \tag{2.15}$$

The electroneutrality condition affects the concentration distribution in both the solution and the membrane:

$$\sum_k z_k C_k^s = 0 \tag{2.16}$$

$$\sum_k z_k C_k^m + z_{fix} C_{fix}^m = 0 \tag{2.17}$$

2.3.5 Diffusion model development

In Donnan dialysis, where polymeric membranes with fixed charged groups are used, the transport mechanism is denoted as exchange-diffusion and the diffusion coefficients in the membrane are referred to as interdiffusion coefficients.

In the literature it has been suggested that the transport of carboxylic acids through anion exchange membranes, during dialysis conditions, is facilitated by: small size, high dissociation constant and high diffusion coefficient inside the membrane (Palatý *et al.*, 2006, 2007, 2009). When the stripping solution is water, the mechanism of transport of carboxylic ions in Neosepta-AMH is assumed to be solution-diffusion (Palatý *et al.*, 2006, 2007). Nevertheless, there is evidence of reaction-diffusion or dual mechanisms for the ion transport across the same membrane in dependence of the base concentration, when the stripping solution is sodium hydroxide (Zheleznov *et al.*, 1998). Until now, it is known that the transport characteristics depend largely on the interaction between carboxylic anion and anion exchange membrane. Therefore, a general statement can not be formulated. According to experimental Donnan dialysis results, the monoprotic anion fluxes through the membrane follow this order $J_{Ac^-} > J_{L^-} > J_{Pr^-}$, which can be compared to the diffusion coefficients in solution $D_{Ac^-} > D_{L^-} > D_{Pr^-}$ (Zheleznov *et al.*, 1998). The correlation is evident and suggests that the diffusion coefficient in the membrane can be related to the value in solution by a tortuosity factor. This fact has been seen when the permeation of some carboxylic acid through Neosepta AFN-7 was investigated (Wódzki and Nowaczyk, 1999). The agreement between an increase in J_k with D_k confirms that the transport rates in Neosepta-AMH, for those ions, are limited by diffusion phenomena. A similar analysis was done for dissociation constants (pK_a) and molecular weight (MW). However, there is not a monotonous correlation between the fluxes and those properties.

One of the most successfully used empirical correlation for tortuosity factor as a function of porosity of the membrane was developed by Mackie and Meares (Eq. 2.18, cited by (Jonsson, 1980)). Despite the physical meaning of the tortuosity factor, it has been used as a tunable parameter to correct model deficiencies (Iversen *et al.*, 1997). The smaller diffusion coefficient inside the membrane than in solution is explained by the fact that the membrane has an structural resistance to the transport. Besides, that relation accounts for the increasing diffusivity of the ion when free volume in the membrane increases. However, it neglects the coupling effect

due to interactions between molecules, which means, that diffusion coefficients of all ions passing through the membrane are affected by the same factor.

$$D_k^m = D_k^s \left(\frac{E}{\tau_f}\right) = D_k^s \left(\frac{E}{2-E}\right)^2 \tag{2.18}$$

where D_k^m and D_k^s are the diffusion coefficients of ion i in the membrane and solution, respectively, τ_f is the tortuosity factor and E is equals the fractional water content of the membrane. From Eq. 2.18 the influence of the membrane water content on the ion diffusion inside the membrane is clear.

The diffusion coefficients of some cations with the same valency have been studied under Donnan dialysis conditions (Miyoshi, 1997). The most important conclusion is that the ratio D_k^s/D_k^m equals a constant value for ions of the same valency. The resistance factor changes when different membranes are used, however all values are of the same order of magnitude for monovalent cations. Using the same order of magnitude of the resistance factors for monovalent ions reported by in the literature, we found the Mackie and Meares expression provides reasonably good agreement with the range of water content reported for Neosepta-AMH (see Table 2.2). Another proposed model in the literature is based on free volume theory (FVT) (Abdekhodaie and Wu, 2005). However, the agreement between the Mackie and Meares equation and experimental evidence was considered satisfactory to employ that approximation.

The water content of a membrane, referred to as membrane swelling as well, is a variable. This process is defined as the dissolution of a polymer in a solvent. The membrane swelling depends on conditions such as: Ion exchange capacity, pH, temperature and intrinsic properties of the membrane (i.e. ion exchange groups, species of reinforcing fabric, degree of cross-linkage, ionic form, membrane pretreatment and solvents). Swelling phenomena can be isotropic (i.e. membrane swells in the same ratio in all directions) or anisotropic. There are different models to predict the swelling process in membranes. In Two-phase and Core-shell models the water absorption is assumed to be spherical, where the expansion in one dimension is proportional to the cube root of the volume fraction of absorbed water. Besides, the lamellar model treats the swelling in one dimension, then the lateral swelling is proportional to volume fraction of the absorbed water. The cluster-network model proposes a large scale cluster organization which is formed when water is absorbed (James *et al.*, 2000). To understand the swelling process, is it required to know membrane structural organization during rehydration and how that structure regulates the solvent penetration and solvation (Mauritz and Moore, 2004). Unfortunately, this information is not available for Neosepta-AMH. Therefore, the membrane dimensions are assumed constant even though the water content of the membrane could change as function of the factors listed above. In this study, a mathematical black box model is proposed for the membrane water content as function of the concentration of hydroxide ions at the inlet of dialysate channel. In that way, the diffusion coefficient model accounts for changes in water content due to variations in average pH across the membrane.

2.3.6 Model input parameters

The first principles model was derived for a situation where the feed stream is a cultivation broth. Species included in the model are: target carboxylic anion (A^-), hydroxide (OH^-), sodium (Na^+), dissociated protein (P^-), carboxylic acid (HA) and undissociated protein (HP). In the experiments used for the model regression, solutions of the carboxylic acids were investigated (see details in section 2.4.1) (Zheleznov *et al.*, 1998). The buffer effect is eliminated by fixing a negligible concentration of the protein in the inlet stream to the feed channel. The physicochemical properties required to solve the model are listed in Table 2.1. The availability of experimental diffusion coefficients as a function of concentration and temperature is limited. The values found were estimated at normal temperature and at concentrations close to the values used in the Donnan dialysis experiments. The diffusion coefficient of the hypothetical protein was considered equal to that of Bovine Serum Albumin (BSA), which is a large protein (MW≈66500 g/mole). Besides, the protein dissociation constant was fitted based on a previous attempt to validate the model (Møllerhøj, 2006).

Table 2.1: Species properties included in the implementation of the model

Parameter	Value	Units	Source
pK_a for HL	3.860	-	(Lide, 2008)
pK_a for HAc	4.756	-	(Lide, 2008)
pK_a for HPr	4.870	-	(Lide, 2008)
pK_a for HP	5.000	-	(Møllerhøj, 2006)
D_{L^-} in solution	$1.033x10^{-9}$	m^2/s	(Lide, 2008)
D_{Ac^-} in solution	$1.089x10^{-9}$	m^2/s	(Lide, 2008)
D_{Pr^-} in solution	$0.953x10^{-9}$	m^2/s	(Lide, 2008)
D_{OH^-} in solution	$5.273x10^{-9}$	m^2/s	(Lide, 2008)
D_{Na^+} in solution	$1.334x10^{-9}$	m^2/s	(Lide, 2008)
D_{P^-} in solution	$0.09\ x10^{-9}$	m^2/s	(Bowen *et al.*, 2000)
D_{HL} in solution	$0.848x10^{-9}$	m^2/s	(Ribeiro *et al.*, 2005)
D_{HAc} in solution	$1.200x10^{-9}$	m^2/s	(Leaist and Lyons, 1984)
D_{HPr} in solution	$1.060x10^{-9}$	m^2/s	(Cussler, 1984)
D_{HP} in solution	$0.09\ x10^{-9}$	m^2/s	(Bowen *et al.*, 2000)
ρ_{HL} 0.1 M	1000.2	kg/m^3	(Lide, 2008)
ρ_{NaOH} 1 M	1042.8	kg/m^3	(Lide, 2008)
μ_{HL} 0.1 M	$1.027x10^{-3}$	kg/m/s	(Lide, 2008)
μ_{NaOH} 1 M	$1.248x10^{-3}$	kg/m/s	(Lide, 2008)
MW_{HP}	≈66500	g/mol	(Bowen *et al.*, 2000)
MW_{HL}	90.08	g/mol	-
MW_{HAc}	60.05	g/mol	-
MW_{HPr}	74.08	g/mol	-

The anion exchange membrane used in the experiments is Neosepta-AMH produced by Tokuyama Soda (Tokyo Japan). This is a strongly basic membrane with $-NC_7H_7^+$ as active groups (Ayyildiz and Kara, 2005). The characteristic properties are presented in Table 2.2.

Table 2.2: Properties of the Neosepta-AMH membrane (Ayyildiz and Kara, 2005; Palatý *et al.*, 2006)

Parameter	Range	Value	Units
Thickness	0.25-0.28	0.27	mm
Water content	17-22	estimated	%
Ion exchange capacity	1.30-1.50	estimated	meq/g

The operational conditions required to regress the model according to the experiments are shown in the Table 2.3. The temperature, flow rates and concentration of carboxylic acid and sodium hydroxide were taken from the Donnan dialysis experimental data (Zheleznov *et al.*, 1998). The membrane separation unit employed in the publication is a two compartment cell for cross flow dialysis. Keeping the same flow conditions, the model is solved using the dimensions of a rectangular dialysis module, according to the proposed geometry (Møllerhøj, 2006).

2.3.7 Model solution

The dynamic model described above consists of a system of stiff partial differential and algebraic equations that must be solved simultaneously. The method of lines is used to discretize the partial differential equations in the x-direction. In order to diminish the simulation time a sixth order Taylor expansion with asymmetric centered differences is used, thereby reducing the number of spatial discretization steps required to achieve a desired accuracy. The resulting index-1 differential algebraic equations are integrated employing a variable order multistep solver based on the numerical differentiation formulas (NDFs) (Shampine *et al.*, 1999). Due to the complexity of the model, an inconsistent set of initial conditions leads to numerical problems. Therefore, an initialization procedure was used in order to guarantee convergence in all evaluated scenarios. The concentrations in the bulk channels are initially assumed to be equal to the inlet values, which fulfill the electroneutrality condition. Experimental data are used for the procedure with a high pH value of the feed solution (pH=10). The concentration inside the membrane is assumed constant and almost evenly distributed between hydroxide and the target anion, a negligible concentration of sodium is fixed. The electroneutrality condition is fulfilled inside the membrane as well. A first simulation is performed and when the steady state is achieved, the pH value is reduced to 5.75, corresponding to an experimental data for a fermentation broth. After this step change, there is a fast change in pH. This transient period is the most time consuming part of the initialization procedure. Reasonable changes in parameters such as input concentrations, liquid flow rates, boundary layer thickness and membrane water content do not require a new initialization. However, changes in the dissociation constants or fixed charge concentration

Table 2.3: Operational parameters for Donnan dialysis operation mode

Parameter	Value	Units
Channels length	0.373	m
Channels width	0.15	m
Channels height	$6x10^{-4}$	m
Temperature	308	K
Current density	0	A/m^2
q_{feed}	120	l/h
q_{dia}	120	l/h
$C_{HA}^{fbin} + C_{A^-}^{fbin}$	100	mol/m^3
C_{NaOH}^{dbin}	≈0-2000	mol/m^3
$C_{A^-}^{dbin}$	0	mol/m^3
$C_{HP}^{fbin} + C_{P^-}^{fbin}$	$1x10^{-7}$	mol/m^3
pH_{in} feed	5.75	-

of the membrane demand the estimation of a new initial concentration profile. The dynamic nature of the model facilitates obtaining static solutions, thereby avoiding convergence issues associated to the solution of steady state models.

2.4 Results and Discussion

The model is solved and regressed to reproduce experimental ion fluxes for Donnan Dialysis recovery of some monoprotic carboxylic acids. This is done through a sensitivity analysis and parameter estimation procedure.

2.4.1 Experimental data

Data are reported for the transport of carboxylic anions through an anion exchange membrane (Zheleznov *et al.*, 1998). In that publication, the fluxes of carboxylic acids are investigated and modeled for Donnan dialysis operation. The anion exchange membrane studied is Neosepta-AMH produced by Tokuyama Soda. This membrane was selected using a preliminary test for stability toward alkaline solutions, since the pH in the dialysate channel can change over a wide range. Transport of acids was investigated using a two compartment cross flow dialysis cell with 100 cm^2 of membrane area. Feed and dialysate solutions were circulated at equal flow rates and the temperature was controlled at 50°C. The experiment is carried out employing different NaOH concentrations in the dialysate channel, from 0 to 2 M. The carboxylic acids studied were: acetic, propionic, lactic, oxalic and citric.

2.4.2 First principles model approach

In this regression, only one tank in the y-dimension was used. This is a reasonable approach since the concentration gradients in the bulk channels are not very large,

due to the small membrane area. If a larger separation module is used, then more sections in the y-dimension are required. The module section was divided into nine zones as depicted in Fig. 2.2. Those zones correspond to: three bulk channels, four boundary layers and 2 anion exchange membranes. In total, there are six zones in the REED cell where numerical approximation is required corresponding to the boundary layers and membranes, they are organized as follow: boundary layer 1 (BL1), anion exchange membrane 1 (AEM1), boundary layer 2 (BL2), boundary layer 3 (BL3), anion exchange membrane 2 (AEM2) and boundary layer 4 (BL4). The number of discretization points used in each zone are [12 30 8 8 30 12], respectively. It can be seen that the highest number of discretization points are employed for the membranes, since the largest concentration gradients are expected there. Besides, the boundary layers in the feed channels have slightly higher number of discretization points than the stagnant layers in the dialysate channel. During simulations, it was noticed that the deviation from electroneutrality condition in the feed boundary layers is larger than in other sections. Therefore, a higher number of nodes where used. The selection of the number of nodes is a trade off between accuracy and computational time since the simulation time increases exponentially with the number of discretization points (Møllerhøj, 2006).

A sensitivity analysis was performed in order to evaluate the influence of several unknown parameters on the carboxylic ion fluxes. Those parameters are: anion exchange capacity, the boundary layers thickness and the water content of the membrane. The concentration of fixed ions in the membrane needs to be expressed per volumetric aqueous phase in the porous membrane, instead of using the fixed charge concentration per membrane weight as reported in the literature (Table 2.2). However, the units conversion can not be performed if the membrane density is unknown. Therefore, the concentration of fixed ions in Neosepta-AMH is assumed to be close to that of the membrane Neosepta-ASM also produced by Tokuyama Soda. Neosepta-ASM fixed ions concentration is $C^m_{fix} = 6$ mmol/ml (Møllerhøj, 2006), this value is taken as initial guess for the investigated membrane. Through simulations, it was observed that increments in C^m_{fix} lead mainly to higher fluxes. Significant increments were evident in the membrane control region.

On the other hand, according to boundary layer theory, the film thickness is mainly determined by hydrodynamics of the system, characterized by parameters such as structure of the surface, flow velocity, solution properties and module shape and dimensions. In concentration polarization phenomena, where there is a concentration gradient in an stagnant layer adjacent to the membrane surface, the mass transfer coefficient has been defined as the ratio between the diffusion coefficient D and the thickness of the boundary layer δ_{BL} (Mulder, 1997).

$$\delta_{BL} = \frac{D}{k_l} \tag{2.19}$$

Estimating the mass transfer coefficient, the thickness of the boundary layer can be calculated. The mass transfer coefficient depends strongly of the hydrodynamics of the system, a correlation to estimate it in a electrodialysis stack, with a spacer for flow distribution, is given by Goodrige and Scott (cited by Moon *et al.* (2004)):

$$k_l = 1.25\mathrm{Re}^{0.46}\mathrm{Sc}^{1/3}\left(\frac{D_s}{d_h}\right) \quad (150 < \mathrm{Re} < 1500) \tag{2.20}$$

where D_s is the salt solution diffusion coefficient and d_h is the hydraulic diameter. The hydraulic diameter in a rectangular slit (plate and frame) can be calculated by the following equation (Mulder, 1997):

$$d_h = \frac{2Wh}{W+h} \tag{2.21}$$

where W and h are the channel width and height, respectively. Employing the module dimensions, the experimental flow conditions and the species properties, an estimation of the boundary layer thickness was performed. The thickness of the boundary layers in feed channel is $\delta_{BL1} = \delta_{BL4} = 0.8612\text{x}10^{-5}$ m; while the boundary layers in dialysate channel $\delta_{BL2} = \delta_{BL3} = 0.7795\text{x}10^{-5}$ m. The obtained boundary layer thicknesses are very similar since the flow rates in both channels are the same. In addition, the differences in rheological properties such as density and viscosity of both solutions can be considered negligible. The estimated values were used as initial values for the parameter tuning. The thicknesses are assumed to be the same in both channels. Through simulations, it was observed that the thickness of the boundary layer influences the magnitude of the fluxes as well as the size of the boundary layer and membrane control regions. It means that the flux magnitude as well as the shape of the flux profile were modified. A grid of the concentration of fixed ions in the membrane and the boundary layer thickness was evaluated. The most satisfactory representation of the experimental data was selected. The selected values are $\delta_{BL} = 7\text{x}10^{-5}$ m and $C^m_{fix} = 7.5$ mmol/ml.

The previous simulations were preformed employing a constant membrane water content. However, it was observed that this parameter has a significant influence on the fluxes. The reason is that the diffusion coefficients within the membrane are estimated using Eq. 2.18. By using a constant water content of the membrane, the anion fluxes predicted by the model, as a function of the base concentration in the dialysate channel, follow a Langmuir dependency. However, as discussed above for lactate and propionate recovery, most likely there is a small contribution of solution-diffusion mechanism at high sodium hydroxide concentrations. For that reason, several black box functions for the membrane water content were tested to reproduce the experimental data reported in the literature. The criteria to select a black box function was to minimize the number of parameters. The independent variable is the inlet base concentration of the dialysate channel, since average pH is the main variable that could affect the membrane water content. Experimentally, differences in the lactate fluxes through Neosepta AFN-7 have been found as a function of the pH in the dialysate channel. These differences have been attributed to the membrane capabilities and the water content (Narbęska and Staniszewski, 1998a). When pH increases it is expected that water concentration in the membrane increases as well following a non linear behavior. However, it is not a general statement since membrane dehydration could happen if the hydroxide concentration is very high. That behavior has been seen in Nafion membranes, where there

is a maximum swelling at an intermediate solute concentration (Izák *et al.*, 2007). Despite the fact that the hydroxide concentration in the dialysate channel is changing over a large range in the experiments, the dehydration effect is neglected. This means the water content of the membrane is assumed to increase at higher hydroxide concentrations. The selected back box model for water content of the membrane (E) is depicted in Eq. 2.22. The membrane water content is related to the membrane free volume by assuming that all the empty space in the membrane is filled.

$$E = \gamma \left(C_{OH}\right)^{\sigma} \tag{2.22}$$

The methodology used for the parameter regression is a numerical method for large scale optimization. This algorithm is referred to as interior reflective Newton method for a constrained non linear minimization (Coleman and Li, 1994; Mathworks, 2006).

After time consuming simulations, the parameters γ and σ in the Eq. 2.22 were estimated by minimizing the residual fluxes. The predicted fluxes for lactate, propionate and acetate through the anion exchange membrane are shown in Fig. 2.4. The estimated parameters are depicted in Table 2.4.

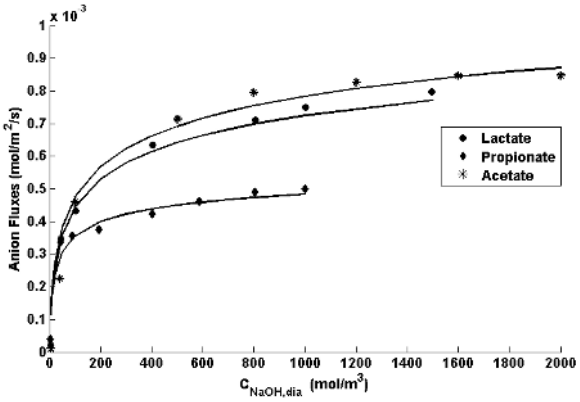

Figure 2.4: Experimental data for anion fluxes through Neosepta-AMH membrane as a function of the inlet base concentration in the dialysate channel (Zheleznov *et al.*, 1998). Solid lines correspond to the predicted fluxes using first principles model with optimal parameters for the membrane water absorption model in Table 2.4

Table 2.4: Estimated parameters for the water content model (the base concentration must be introduced in mol/l)

Carboxylic ion	γ	σ
Lactate	0.240	0.1000
Acetate	0.240	0.1004
Propionate	0.185	0.0503

The simulation results, display agreement between experimental data and the predicted fluxes. The largest deviations are evident at very low base concentrations in the dialysate channel, when the process is towards dialysis conditions. It was found that there is not a significant difference between the resistance factors for lactate and acetate recovery. This finding means, that lactate and acetate fluxes through the membrane can be described by differences in the diffusion coefficients in the solution with the same membrane water content model. However, this model could not predict the propionate fluxes since the obtained fluxes were higher than the experimental data. For that reason, it was required to estimate a particular water content model for propionate transport. Differences in the membrane affinity towards propionate could be explained by the hydrophobic properties of the anions. The hydrophobicity is quantified using the partition coefficient in the mixture 1-octanol/water, displayed in Table 2.5. There is not a significant difference between lactate and acetate. However, propionate is considerably more hydrophobic than the other anions. It means that propionate ions would not be evenly distributed in the membrane aqueous phase inside the membrane. A higher concentration will be evident towards the internal liquid-membrane interface, where there is a larger frictional transport resistance. This fact can explain why propionate has lower diffusion coefficients inside the membrane than initially predicted.

Table 2.5: Partition coefficients in mixture 1-octanol/water of the investigated anions (INCHEM, 2009)

Carboxylic ion	log P_{ow}	P_{ow}
Lactate	-0.60	0.25
Acetate	-0.31	0.49
Propionate	0.33	2.14

According to the estimated water content model, higher inlet base concentration in the dialysate channel implies higher pH gradient across the membrane and therefore, a higher water content of the membrane. Introducing that variable into Eq. 2.18, the diffusion coefficients inside the membrane will change depending on the hydroxide concentration at the inlet of the dialysate channel. The calculated values are shown in Fig. 2.5. The diffusion coefficients inside the membrane are two orders of magnitude lower than in solution. During dialytic recovery of carboxylic ions using Neosepta-AMH the same difference has been shown (Palatý *et al.*, 2009). The apparent diffusion coefficients of lactate during dialytic recovery in Neosepta AFN-7 and Selemion DSV were estimated being of the order of $\sim 10^{-11}$ m^2/s (Narbęska and Staniszewski, 1997). The diffusion coefficients for those membranes are higher than the estimated for Neosepta-AMH. However, those membranes possess higher ion exchange capacity and swelling than the Neosepta-AMH, so these results are not surprising. In Table 2.6 the average diffusion coefficients estimated for the investigated system (Zheleznov *et al.*, 1998) and those calculated using the first principle model are depicted. There is an excellent agreement for lactate and an acceptable result for acetate and propionate.

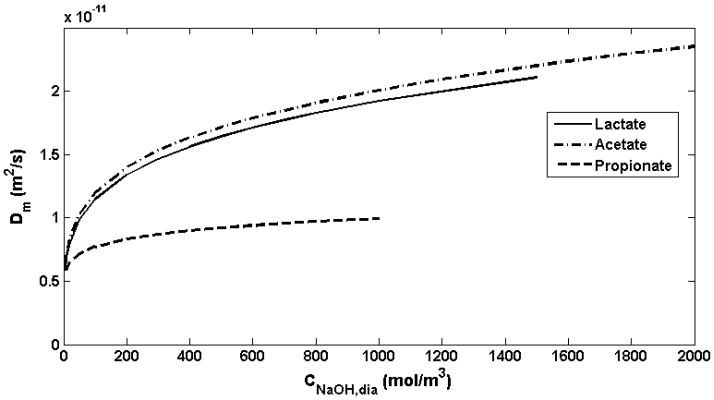

Figure 2.5: Estimated diffusion coefficients inside the Neosepta-AMH for lactate, acetate and propionate

Table 2.6: Average diffusion coefficient for the monoprotic carboxylic anions reported in the literature (Zheleznov *et al.*, 1998) and the calculated using the herein presented model, for Neosepta-AMH

Carboxylic ion	Reported D_k^m m^2/s	Calculated D_k^m m^2/s
Lactate	$1.70x10^{-11}$	$1.70x10^{-11}$
Acetate	$1.77x10^{-11}$	$1.90x10^{-11}$
Propionate	$0.98x10^{-11}$	$0.89x10^{-11}$

2.4.3 Simulation results

A qualitative visualization of the concentration profiles for both boundary layer and membrane control regions has been predicted (Zheleznov *et al.*, 1998). Under boundary layer control, it is predicted that the hydroxide concentration inside the membrane is considerably lower than lactate concentration. Besides, the concentration gradients are nearly linear since the major resistance for mass transport is in the boundary layer. During membrane control, the concentration profiles inside the membrane are steep, indicating a high transport resistance inside the membrane. Simulations were performed for low and high inlet concentrations of sodium hydroxide in the dialysate channel. The steady state profiles are depicted in Fig. 2.6 and 2.7.

Simulating the first principles model, the lactate and hydroxide concentration profiles in the membrane are nearly linear as it was predicted under boundary control conditions. Moreover, it is known that Donnan exclusion works very well at low hydroxide concentrations in the dialysate channel, it was confirmed by simulations since sodium ions were rejected, indicated by the negligible sodium concentration inside the membrane. The effectiveness of the Donnan exclusion can be also seen

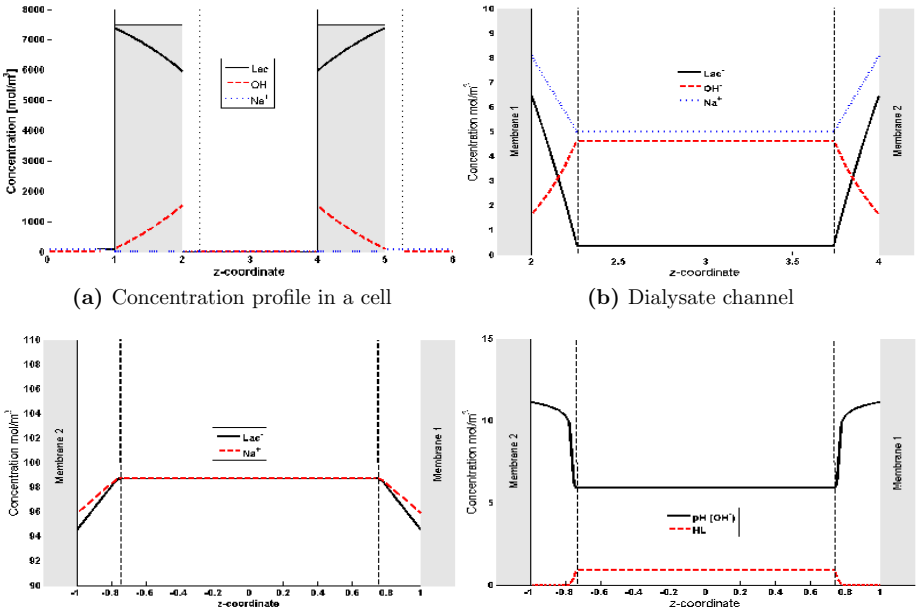

(a) Concentration profile in a cell

(b) Dialysate channel

(c) Feed channel ions

(d) Feed channel pH

Figure 2.6: Steady state concentration profiles for $C_{OH^-}^{dbin}$=5 mol/m^3 (Boundary layer control). Enlargement of the concentrations in the dialysate (b) and feed channels (c,d)

in Fig. 2.8, where the sodium flux is negligible. It starts rising when the hydroxide concentration gradient increases, but still the sodium fluxes are several orders of magnitude smaller even at high inlet base concentrations. On the other hand, neither the concentration gradients inside the membrane nor the hydroxide concentration inside the membrane are as small as predicted. Unfortunately, a numerical comparison can not be done since the results depicted in the literature are qualitative. Through simulations, it was corroborated that concentration gradients and hydroxide concentration inside the membrane can be diminished, under boundary layer control conditions, by increasing the thickness of the boundary layers. Nevertheless, the thickness of the boundary layers used in the simulations performed in the literature is unknown (Zheleznov *et al.*, 1998).

Under boundary layer control, the low hydroxide concentration gradient between the dialysate and feed channel generates a relative low driving force for lactate extraction. The consequence of the low fluxes can be seen in the ion concentration profiles in the boundary layer (see Fig. 2.6(b) and (c)). Besides, the pH value in the feed channel is similar to the inlet value due to the low hydroxide flux. Therefore, a portion of the lactate is undissociated.

It can be seen in Fig. 2.7 under membrane control, large non linear concentration profiles inside the membrane were reproduced. In the boundary layers, larger concentration gradients can be seen since the hydroxide concentration gradient is

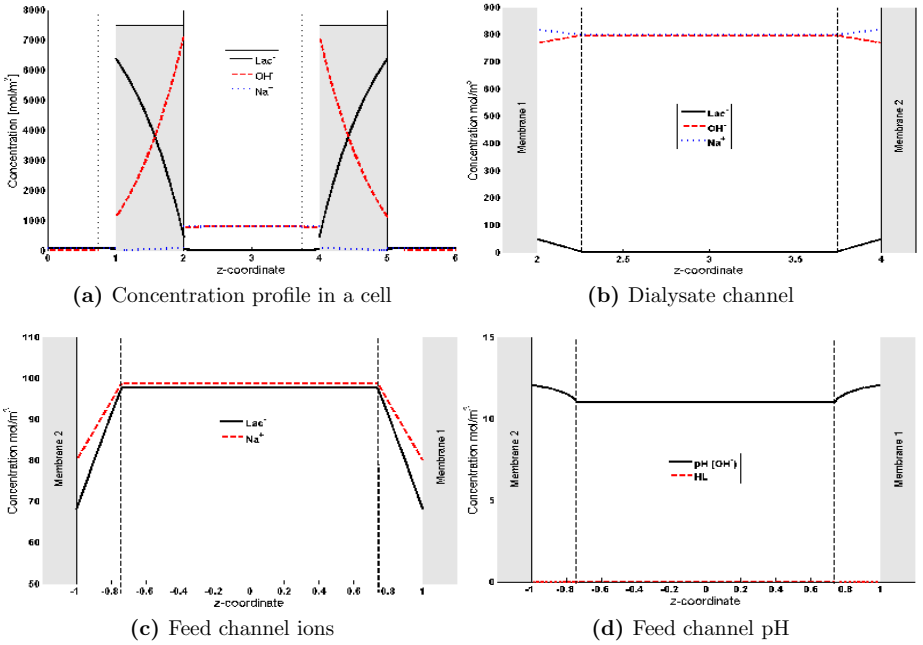

(a) Concentration profile in a cell

(b) Dialysate channel

(c) Feed channel ions

(d) Feed channel pH

Figure 2.7: Steady state concentration profiles for $C_{OH^-}^{dbin}$=800 mol/m^3 (Membrane control). Enlargement of the concentrations in the dialysate (b) and feed channels (c,d)

considerably larger than under boundary layer control. The pH in the feed channel is very high since the hydroxide flux is larger, therefore all the lactate in the channel remains dissociated. Besides, the efficiency reduction of Donnan exclusion at high hydroxide concentrations was evidenced since there is an increasing amount of sodium inside the membrane.

In both above cases the pH value within the membranes is very high as expected, confirming the validity of the assumption MA3. As a final remark, in all simulations performed the symmetry around the dialysate channel of the concentration profiles is evident. It means, the concentration profiles in the second anion exchange membrane (AEM2) are mirroring of the concentrations in the first membrane (AEM1).

2.4.4 Numerical implementation

The derived dynamic model was regressed to reproduce the transport of some carboxylic anions through Neosepta-AMH during Donnan dialysis conditions, and the obtained results were satisfactory. Nevertheless, the numerical implementation was investigated. The electroneutrality condition was evaluated at locations of the modeled section. The steady state relative deviation from the electroneutrality condition is depicted in Fig. 2.9. These values correspond to the simulation performed for lactate using a inlet hydroxide concentration in the dialysate channel of 800 mol/m^3.

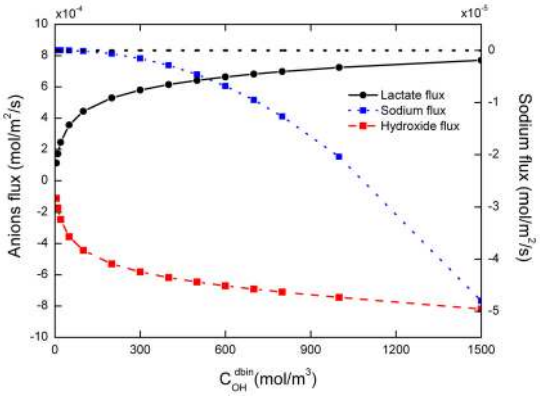

Figure 2.8: Simulated steady state ion fluxes through the anion exchange membrane as a function of the inlet base concentration in the dialysate channel, during lactate recovery. The sign of the fluxes indicates the direction of the ion transport (Anions: lactate and hydroxide)

The other input parameters remain constant and equal to the values used during the model regression. From the results, a negligible deviation is observed in the membranes, bulk channels and boundary layers adjacent to the dialysate channel. The higher deviations are observed in the boundary layers in the feed channel. This deviation was reduced by using more discretization points in that zone as mentioned before, however the number of nodes can not be increased unlimited since the simulation time increases exponentially.

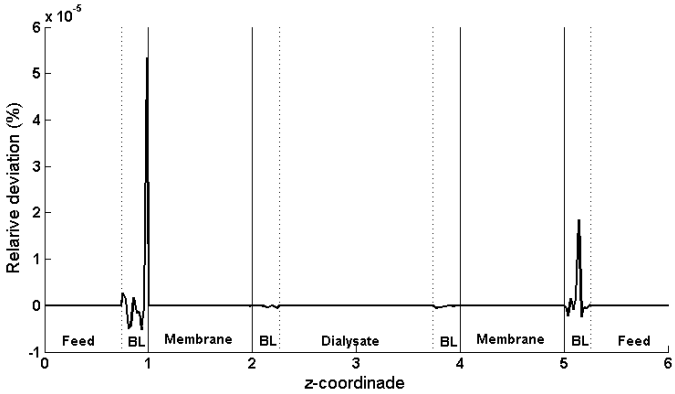

Figure 2.9: Fulfillment of the electroneutrality condition under steady-state Donnan dialysis recovery of lactate at $C_{OH^-}^{dbin}$=800 mol/m^3. The deviation is relative to the lactate concentration at each discretization point

2.5 Conclusions

A dynamic model for simultaneous transport of ions across ion exchange membranes was derived from first principles based on dissociation, diffusion, convection and migration of species. This model accounts the effects of concentration and electrical potential as driving forces for ion transport through boundary layers and membranes. From experimental data, a qualitative agreement between the flux magnitude and the aqueous diffusion coefficient was found. On the other hand, there is no qualitative agreement with other important properties such as pK_a and molecular weight.

The developed model was regressed to describe the recovery of monoprotic carboxylic under steady state Donnan dialysis conditions. A black box model was proposed to describe the membrane water content as a function of the inlet base concentration in the dialysate channel. The complete model satisfactorily reproduces steady state experimental data for several monoprotic carboxylic anions, despite the rather crude estimates of the boundary layer thickness and fixed ion concentration of the membrane. These results indicate that the changes in the ion flux as a function of the base concentration in the dialysate channel can be reproduced by this model structure for each carboxylic acid and membrane. In addition, the estimated average diffusion coefficients showed good agreement with the experimentally determined values in the literature. Besides, the simulated concentration profiles did match the previously predicted profiles in the literature, both under boundary layer and membrane control. Additionally, the effectiveness of the Donnan exclusion was evaluated. The symmetry around the dialysate channel could be exploited to reduce the computational requirements of the performed simulations. Nevertheless, our intention was not to derive a specific model for Donnan dialysis, it is to have a general model for ion transport through anion exchange membranes that can be used even under conditions that generate asymmetric profiles.

2.6 Acknowledgment

The authors acknowledge the support from the Sixth framework project of the European Union: NMP2-CT-2007-O2b515 IP “BIOPRODUCTION”.

2.7 Nomenclature

C	Concentration (mole m^{-3})
D	Diffusion coefficient (m^2 s^{-1})
E	Fractional membrane water content (-)
F	Faraday constant (C $mole^{-1}$)
I_d	Current density (A m^{-2})
J	Flux (mole m^{-2} s^{-1})
h_i	Channel i height (m)
k	Kinetic parameter (-)
k_l	Mass transfer coefficient (m s^{-1})
K_a	Acid dissociation constant (mol m^{-3})

K_d	Dissociation constant (mol m^{-3})
K_w	Ionic product for water (mol^2 m^{-6})
L	Channel length (m)
P	Effective permeability coefficient (m s^{-1})
P_{ow}	Partition coefficient in 1-octanol/water
Q	Ion exchange capacity (meq g^{-1})
q	Flow rate (m^3 s^{-1})
R_k	Total reaction rate of k (mol m^{-3} s^{-1})
R	Universal gas constant (J mol^{-1} K^{-1})
t	Time (s)
T	Absolute temperature (K)
x	Spatial direction (m)
y	Spatial direction (m)
W	Channel width (m)
z	Dimensionless distance $z = x/\delta_m$ (-)
z_k	Valence of k (-)

Greek letters

δ_{BL}	Boundary layer thickness (m)
δ_m	Membrane thickness (m)
γ	Parameter in the WC model (-)
ψ	Electrical potential (V)
ψ_n	Nominal potential ($\psi_n = RT/F$) (V)
σ	Parameter in the WC model (-)
τ	Dimensionless time ($\tau = t/\tau_n$) (-)
τ_{dia}	Residence time in dialysate channel ($\tau_{dia} = h_{dia}WL/q_{dia}$) (s)
τ_{diff}	Diffusion time ($\tau_{diff} = \delta_m^2/D_{k,p}$) (s)
τ_f	Tortuosity factor (-)
τ_{feed}	Residence time in feed channel ($\tau_{feed} = h_{feed}WL/q_{feed}$) (s)
τ_n	Nominal time ($\tau_n = 1$ (s))
φ	Dimensionless potential ($\varphi = \psi/\psi_n$) (-)

Subscripts

A^-	Anion
Ac^-	Acetate ion
BL	Boundary layer
dia	Dialysate channel
$feed$	Feed channel
fix	Fixed charges in the membrane
HAc	Acetic acid

HL	Lactic acid
HP	Undissociated protein
HPr	Propanoic acid
in	inlet
i	Specie
j	Discretization point
k	Specie
L^-	Lactate ion
max	Maximum
Na^+	Sodium ion
OH^-	hydroxide ion
P^-	Dissociated protein
p	Zone (phase)
Pr^-	Propionate ion
z	specific location

Superscripts

db	Dialysate bulk
$dbin$	Dialysate bulk inlet
fb	Feed bulk
$fbin$	Feed bulk inlet
m	Membrane
s	Solution
$-/+$	Left/Right side of a section

3

Electro-Enhanced Dialysis for Lactate Recovery

3.1 Abstract

The competitive ion transport through anion exchange membranes under current load conditions, referred to as the electro-enhanced dialysis process, is modeled and investigated through simulations. A dynamic model has been developed for simultaneous transport of multiple ions based on the Nernst-Plank equation. This model accounts for the convective transport of the dissociated and undissociated species in the module channels, and the diffusion and migration across the boundary layers and membranes. The potential static flux enhancement is evaluated and compared to Donnan dialysis operation for lactate recovery, where lactate fluxes were increased up to 230%. The effect of the imposed current on the concentration profiles is analyzed. Furthermore, the current saturation condition is investigated for the proposed electro-enhanced dialysis system. Thus, the operating window for current density and inlet hydroxide concentration was defined.

3.2 Introduction

Lactic acid is an interesting product which is increasingly used in industry. This product has in addition significant industrial potential as a main feedstock for polylactic acid (PLA) production. PLA is a biopolymer, which can substitute petrochemical derived polymers in several applications (Kharas *et al.*, 1996). A sustainable and economic lactic acid bioproduction will definitely make PLA production feasible to substitute its petrochemical based competitors. When lactic acid is produced by fermentation of carbohydrates, the production rate is adversely influenced by lactates present in the cultivation broth (Hongo *et al.*, 1986; Nielsen *et al.*, 2003). Extensive work has been carried out in metabolic engineering, since lactic acid bacteria are one of the most studied group of microorganisms, trying to understand the metabolic pathways and genetically design improved bacterial strains tolerant to inhibiting conditions. Nevertheless, the expected productivity amendment of the genetically modified microorganisms is limited. Thus, the *in situ* removal of lactates from the fermentation broth raises as the most promising alternative, since the productivity of the bacteria can be significantly increased. Membrane separation processes, especially electrically driven processes, have been studied to separate the biotoxic lactate.

In the early 1970's, the growth and acid production by *Lactobacillus delbrueckii*

in a dialysis fermentation system was studied and modeled (Friedman and Gaden, 1970). The dialysis fermentation technique using mainly ultrafiltration membranes, was previously developed and investigated (Gerhardt and Gallup, 1963; Herold *et al.*, 1967). The results corroborate the earlier observations, where the microorganism exhibits higher production rates and cell concentrations than non-dialysis experiments. The main drawback of utilizing dialysis fermentation is the low diffusion efficiency. Later on, electrodialysis was suggested as a potential *in situ* separation method (Hongo *et al.*, 1986). This process showed potential since lactate can be selectively removed by ion exchange membranes. Subsequently, a sequence of ultrafiltration and electrodialysis was proposed as an alternative to reduce fouling problems in conventional electrodialysis (Boyaval *et al.*, 1987; Raucourt *et al.*, 1989). Studies on electrodialysis were continued applying double exchange reaction electrodialysis for the isolation and concentration of lactic acid (Heriban *et al.*, 1993). Double exchange reaction electrodialysis is a special configuration for electrodialysis. The conventional module with alternating anion and cation exchange membranes plus an inorganic acid are used to produce two concentrate and diluate streams (only one concentrate stream contains lactic acid). It can be considered analogous to electrodialysis with bipolar membranes. In their best scenario the lactic acid concentration was increased up to 4 times.

Even though, electrodialysis is one of the most successful membrane based separation processes for lactic acid production, potential problems of applying electrochemically pH-controlled electrodialysis fermentation have been pointed out (Hongo *et al.*, 1986; Heriban *et al.*, 1993; Grossman and Sonin, 1973; Garde, 2002; Rype, 2003):

- Membrane fouling: this problem is probably the most significant obstacle when membranes are used. Fouling can be caused by the biomaterial present in the fermentation broth.

- Scaling: multivalent cations in the feed solution such as calcium and magnesium pass through cation exchange membranes, and their salts precipitate on the membrane surface.

- Bipolar membrane degradation: this kind of membrane is commonly used for the further recovery and concentration of lactic acid. The presence of calcium, magnesium and iron can damage or destroy these membranes, even if they are present in small amounts.

Donnan dialysis process was proposed as a method which ideally eliminate scaling and bipolar membrane degradation since only anion exchange membranes are used (Zheleznov *et al.*, 1998). Additionally, fouling issues are reduced using high flow velocities combined with the membrane cleaning effect by the hydroxide flux toward the feed channel. This separation has shown promising performance experimentally and is applicable for recovery of other bioproduced carboxylic acids. Previously, a first principles model that describes the simultaneous anion transport through ion exchange membranes and adjacent boundary layers under current load conditions has been developed. This model suitable describes Donnan dialysis recovery of monoprotic carboxylic anions (Prado-Rubio *et al.*, 2010b). There, the model was regressed to reproduce experimental fluxes of acetate, propionate and lactate through

Neosepta-AMH membranes. Besides, the concentration profiles within the modeled zones were analyzed for two different limiting transport conditions referred to as boundary layer and membrane controlled transport.

The main limitation during Donnan dialysis recovery is a rather low flux, since the driving force behind the lactate transport is the OH^- concentration gradient, which implies larger membrane area and concentration gradients (Strathmann, 2004). In this contribution, we want to exploit the derived first principles model to investigate an alternative operation mode of the Donnan dialysis module by imposing an electrical potential gradient. This method has been denoted as electro-enhanced dialysis (EED) (Garde, 2002; Rype, 2003; Prado-Rubio *et al.*, 2009a). EED proposes to increase the lactate flux in conventional Donnan dialysis operation by the imposed external electrical field. The purpose of this paper is to contribute to the understanding of simultaneous ion transport through anion exchange membranes under current load conditions. Besides, to evaluate the potential ion flux enhancement using Donnan dialysis process, operating with an imposed electrical potential gradient.

The paper is structured as follows: Donnan and electro-enhanced dialysis processes for lactate recovery are introduced. The previously derived model is briefly summarized. Simulations are performed to investigate the competitive ion transport taking place under current load conditions. The concentration profiles under boundary layer and membrane controlled transport are estimated for Donnan and electro-enhanced dialysis. The total ion flux enhancements are calculated as a function of the imposed current density and inlet hydroxide concentration in the dialysate channel. The current saturation condition is determined for the system and the involved numerical issues are addressed. Finally, the conclusions are drawn.

3.3 Process description

The module setup for electro-enhanced dialysis is obtained from that of Donnan dialysis, by adding electrode chambers at the left and right sides of the module stack. The Donnan dialysis process for extraction of lactic acid from a dilute solution is depicted in Fig 3.1. In this process, the fermentation broth with a low pH is fed to every feed channel in the membrane stack. The remaining channels are fed with a strong alkaline solution, so-called dialysate channels. Due to the large hydroxide concentration gradient between the two solutions, the hydroxide is transported through the anion exchange membrane. The hydroxide flux induces an electrical potential gradient which forces a lactate flux in the opposite direction. The ion fluxes are coupled through the electroneutrality condition and Faraday's law (Prado-Rubio *et al.*, 2010b; Strathmann, 2004; Mulder, 1997).

Fig. 3.2 shows the expected ion transport through the electro-enhanced dialysis module under current load conditions. Imposing an external electrical potential gradient, the transport mechanism changes from counter ion transfer to a competitive ion transport. Under competitive ion transport, the electrical current is distributed between the ions present to fulfill Faraday's law. When a constant current density is applied, it is expected that anions and cations will move toward the electrode with the opposite charge. This situation implies that lactate is transported from

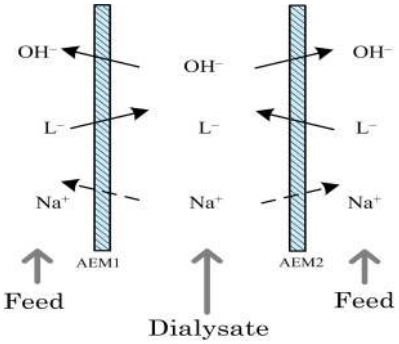

Figure 3.1: Schematic drawing illustrating the lactic acid extraction by Donnan dialysis. Dominant fluxes are depicted in solid lines (Prado-Rubio *et al.*, 2010b)

the feed channel to the adjacent dialysate channel, however it could be extracted through the next membrane and returned to the feed channel just right after. A simple model has been used to show how lactate is preferably transported when the pH is below 11, while for pH higher than 12.5 hydroxide is carrying an increasing amount of current (Rype, 2003). Assuming that the solution in the feed channel maintains a pH below 11, the lactate extraction from the feed stream is favored. This condition can be fulfilled in a fermentation broth due to the presence of pH buffer components.

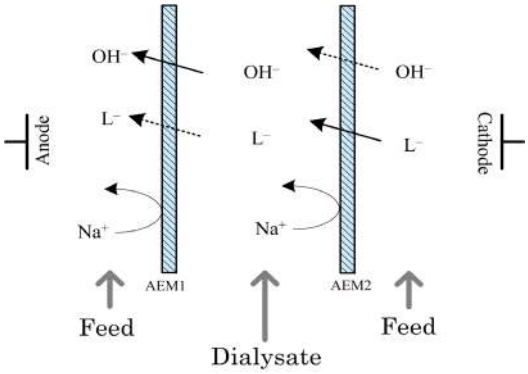

Figure 3.2: Schematic drawing illustrating lactic acid extraction by electro-enhanced dialysis under completely effective Donnan exclusion. Dominant fluxes are depicted in solid lines

3.4 Model description

A detailed sketch of the modeled section of the dialysis module is depicted in Fig. 3.3. The section is composed of two feed channels with a dialysate channel in

between, separated by anion exchange membranes. The model describes the ion transport across anion exchange membranes with corresponding boundary layers. A detailed description of the model equations, assumptions and solution is presented in a previous contribution (Prado-Rubio *et al.*, 2010b). The main assumptions are:

1. General: electroneutrality at any location in the system, the current is carried by ions in ideal solution. The species included in the model are: Lactate (L^-), hydroxide (OH^-), sodium (Na^+), dissociated protein (P^-), lactic acid (HL) and undissociated protein (HP).

2. Membrane: convective transport is not investigated, transport of water by osmosis and electro-osmosis is neglected, there is transport of neither uncharged nor large molecules through the membrane, equilibrium at the membrane surface and constant membrane dimensions.

3. Boundary layer: convective transport is neglected and the thickness of the boundary layers is constant for a given flow condition.

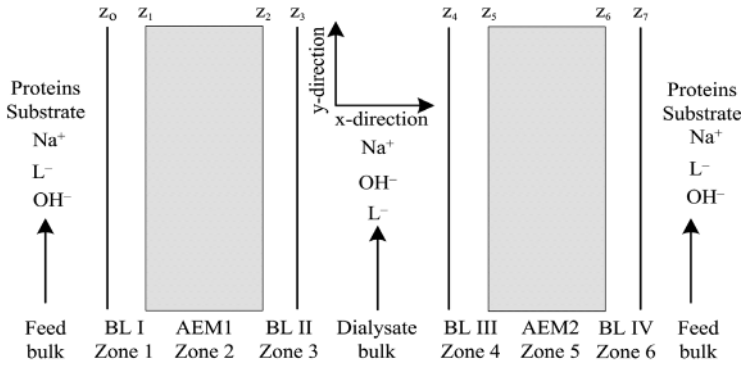

Figure 3.3: Sketch of a section of the dialysis module for lactate recovery from a fermentation broth. The zones in the section and ions present in each zone are depicted. BL: boundary layer and AEM: anion exchange membrane. The positions $z_j \ \forall \ j$=0,...,7 denote the dimensionless interface locations (Prado-Rubio *et al.*, 2010b). In EED, the electrodes are located at the left and right sides on the section

The most relevant model equations are depicted in Tables 3.1 and 3.2. The substances and the phases are denoted by the subscripts k and p, respectively. For the sake of simplicity, the mass balances are derived for one tank in the y-direction. Therefore, the index in that dimension is not shown. The flux $J_{k,p}$ is defined by the Nernst-Planck equation for ideal solutions (Eq. 3.2), neglecting convective transport (Strathmann, 2004). Relevant deviations from ideal behavior might occur within the membrane (van der Stegen *et al.*, 1999), but this is neglected in the present paper. This is due to the considerable increase in model complexity and in the required procedure to estimate the additional model parameters. Introducing the Nernst-Planck equation and dimensionless parameters (see nomenclature) into Eq. 3.1, the

mass balance can be rewritten as Eq. 3.3. Substituting the fluxes for each ion (Eq. 3.2) into Faraday's law (Eq. 3.9), the electrical potential gradient can be estimated (Eqs. 3.4 and 3.5). The model for bulk channels is formulated using a tank in series model to handle gradients in the y-direction. In each tank there is mass exchange over the adjacent boundary layers, and the dissociation reactions are present as well. The mass balance for each tank in the feed and dialysate channels are depicted in Eqs. 3.6 and 3.7. The reaction term was suppressed from the dialysate mass balance since the ions are completely dissociated due to the high pH (Eq. 3.7).

Algebraic expressions are employed to describe the electrical potential gradient and concentration discontinuities at the membrane-boundary layer interfaces (z_1, z_2, z_5 and z_6 in Fig. 3.3) and the electrical potential gradient at the bulk solution-boundary layer interfaces (z_0, z_3, z_4 and z_7). For sorption equilibrium at the membrane surface, the electrochemical potential in the ionic solution and the membrane surface must be the same, referred to as the Donnan potential. The Donnan potential gives the potential build-up at membrane-solution interfaces, which is determined by the ionic distribution of the transported ions (Eq. 3.8). Faraday's law states that all the electrical current is carried by ions (Eq. 3.9). Fluxes at the membrane-solution interfaces are continuous for the transported ions (Eq. 3.10), while for the non-transported ions the flux equals zero.

The electroneutrality condition affects the concentration distribution in both the membrane and the solution (Eqs. 3.11 and 3.12). The Mackie and Meares' expression (Eq. 3.15, (Jonsson, 1980)) has been employed to correlate the ion diffusion coefficient in solution and its value within the membrane, as a function of the free volume in the membrane. A power function has been regressed to describe the increasing membrane free volume by increasing the inlet hydroxide concentration to the dialysate channel (Eq. 3.16) (Prado-Rubio *et al.*, 2010b).

3.4.1 Model solution

The developed model includes a pH model that accounts for a pH buffer effect in the feed channel, this is used when the lactate recovery is carried out from a fermentation broth. The buffer effect is suppressed by fixing a negligible concentration of the protein in the inlet stream to the feed channel. The physicochemical properties required to solve the model are listed in Table 3.3.

The anion exchange membrane used is Neosepta-AMH which has been produced by ASTOM Corporation (Tokyo, Japan), earlier Tokuyama Soda Company, Inc. This is a strongly basic membrane with -$NC_7H_7^+$ as fixed charge groups (Ayyildiz and Kara, 2005). The characteristic properties are presented in Table 3.4.

The operational conditions employed for the simulations according to previous work are shown in Table 3.5 (Prado-Rubio *et al.*, 2010b). The temperature, flow rates and concentration of carboxylic acid and sodium hydroxide were taken from the Donnan dialysis experimental data (Zheleznov *et al.*, 1998). The model uses dimensions of a rectangular dialysis module, according to the proposed module geometry. The thickness of the boundary layer has been regressed from Donnan dialysis experimental data in a previous work (Prado-Rubio *et al.*, 2010b). Based on a numerical analysis of the model solution, there has been found no significant differences (i.e. less than 2% for five tanks) in mean ion fluxes and outlet concentrations

Table 3.1: Interfacial boundary conditions to describe the ion concentrations and electrical potential gradients, reaction and model parameter expressions

Transport in boundary layers and membranes

$$\frac{\partial C_{k,p}}{\partial t} + \nabla J_{k,p} - R_k = 0 \tag{3.1}$$

$$J_{k,p} = -D_{k,p}\left(\frac{\partial C_{k,p}}{\partial x} + \frac{z_k F C_{k,p}}{RT}\frac{\partial \psi_p}{\partial x}\right) \tag{3.2}$$

$$\frac{\partial C_{k,p}}{\partial \tau} = \frac{\tau_n}{\tau_{diff}}\left(\frac{\partial^2 C_{k,p}}{\partial z^2} + z_k\left(\frac{\partial C_{k,p}}{\partial z}\frac{\partial \varphi_p}{\partial z} + C_{k,p}\frac{\partial^2 \varphi_p}{\partial z^2}\right)\right) + \tau_n R_k \tag{3.3}$$

$$\frac{\partial \varphi_p}{\partial z} = \frac{-I_d\delta_m/F - \sum_k z_k D_{k,p}\partial C_{k,p}/\partial z}{\sum_k z_k^2 D_{k,p} C_{k,p}} \tag{3.4}$$

$$\frac{\partial^2 \varphi_p}{\partial z^2} = \frac{-\sum_k z_k D_{k,p}\partial^2 C_{k,p}/\partial z^2}{\sum_k z_k^2 D_{k,p} C_{k,p}} \cdots + \frac{I_d\delta_m/F + \sum_k z_k D_{k,p}\partial C_{k,p}/\partial z}{\left(\sum_k z_k^2 D_{k,p} C_{k,p}\right)^2}\left(\sum_k z_k^2 D_{k,p}\frac{\partial C_{k,p}}{\partial z}\right) \tag{3.5}$$

Bulk channel model

$$\frac{dC_k^{fb}}{d\tau} = \frac{\tau_n}{\tau_{feed}}\left(C_k^{fbin} - C_k^{fb}\right) + \frac{\tau_n}{h_{feed}}\left(J_k|_{z=z_7} - J_k|_{z=z_0}\right) + \tau_n R_k \tag{3.6}$$

$$\frac{dC_k^{db}}{d\tau} = \frac{\tau_n}{\tau_{dia}}\left(C_k^{dbin} - C_k^{db}\right) + \frac{\tau_n}{h_{dia}}\left(J_k|_{z=z_3} - J_k|_{z=z_4}\right) \tag{3.7}$$

by increasing the number of tanks in series. However, the simulation time increased exponentially. Therefore, only one tank is employed in the presented simulations.

The dynamic model consists of a system of stiff partial differential and algebraic equations. The spatial dimension in the partial differential equations (x-direction) is discretized using a sixth order Taylor expansion with asymmetric centered differences. The resulting index-1 system of differential and algebraic equations is integrated employing a variable order multistep solver based on the numerical differentiation formulas in Matlab2007a (Shampine *et al.*, 1999). Due to the complexity of the model, an inconsistent set of initial conditions leads to numerical problems. Therefore, an initialization procedure was used in order to guarantee convergence in all evaluated scenarios. The dynamic nature of the model facilitates obtaining static solutions, thereby avoiding convergence issues associated with solution of steady state models.

Table 3.2: Summary of the differential equations employed in the first principles model for simultaneous ion transport through an Electro-Enhanced Dialytic module. The index for the tank in series description in the y-direction is not shown

Equations at the interfaces

$$\left(\frac{C_k^s}{C_k^m}\right)^{\frac{1}{z_k}} = \left(\frac{C_i^s}{C_i^m}\right)^{\frac{1}{z_i}} = \ldots \quad k \neq i \tag{3.8}$$

$$I_d = F\sum_k z_k J_{k,p} \tag{3.9}$$

$$J_k|_{z=z_j^-} = J_k|_{z=z_j^+} \tag{3.10}$$

$$\sum_k z_k C_k^s = 0 \tag{3.11}$$

$$\sum_k z_k C_k^m + z_{fix} C_{fix}^m = 0 \tag{3.12}$$

Reactions

$$\mathrm{HL}+\mathrm{OH}^- \underset{k_2}{\overset{k_1}{\rightleftharpoons}} \mathrm{L}^- + \mathrm{H_2O} \tag{3.13}$$

$$\mathrm{HP}+\mathrm{OH}^- \underset{k_4}{\overset{k_3}{\rightleftharpoons}} \mathrm{P}^- + \mathrm{H_2O} \tag{3.14}$$

Diffusion model

$$D_k^m = D_k^s \left(\frac{E}{2-E}\right)^2 \tag{3.15}$$

$$E = \gamma (C_{OH}^{dbin})^{\sigma} \tag{3.16}$$

3.5 Results and discussion

As mentioned above, a disadvantage of Donnan dialysis operation is the rather low flux obtained through the membrane. The carboxylic anion is recovered from the feed stream due to the induced electrical potential gradient that the hydroxide flux generates. Therefore, imposing an external electrical field in the system can potentially enhance the lactate flux. Thus the main motivation for the present work is to elucidate the ion transport under current load conditions, and then to investigate to which extent fluxes can be increased.

3.5.1 Competitive ion transport

Under Donnan dialysis conditions, the transport mechanism has been called counter ion transfer since the lactate transport is driven by hydroxide ions flowing in the opposite direction. However, in electro-enhanced dialysis the external electrical po-

Table 3.3: Species properties in the numerical model implementation

Parameter	Value	Units	Source
pK_a for HL	3.860	-	(Lide, 2008)
pK_a for HP	5.000	-	(Møllerhøj, 2006)
D_{L^-} in solution	$1.033x10^{-9}$	m^2/s	(Lide, 2008)
D_{OH^-} in solution	$5.273x10^{-9}$	m^2/s	(Lide, 2008)
D_{Na^+} in solution	$1.334x10^{-9}$	m^2/s	(Lide, 2008)
D_{P^-} in solution	$0.090x10^{-9}$	m^2/s	(Bowen *et al.*, 2000)
D_{HP} in solution	$0.090x10^{-9}$	m^2/s	(Bowen *et al.*, 2000)
D_{HL} in solution	$0.848x10^{-9}$	m^2/s	(Ribeiro *et al.*, 2005)
ρ_{HL} 0.1 M	1000.2	kg/m^3	(Lide, 2008)
ρ_{NaOH} 1 M	1042.8	kg/m^3	(Lide, 2008)
μ_{HL} 0.1 M	$1.027x10^{-3}$	kg/m/s	(Lide, 2008)
μ_{NaOH} 1 M	$1.248x10^{-3}$	kg/m/s	(Lide, 2008)
MW_{HP}	≈66500	g/mol	(Bowen *et al.*, 2000)
MW_{HL}	90.08	g/mol	-
γ	0.24	-	(Prado-Rubio *et al.*, 2010b)
σ	0.10	-	(Prado-Rubio *et al.*, 2010b)

tential gradient plays an important role as well as the mentioned driving forces in Donnan dialysis. The imposed electrical potential gradient makes the ions competitively transport the current since Faraday's law must be fulfilled. Therefore, under current load conditions the transport mechanism has been denoted as competitive ion transport (Rype, 2003).

In Section 3.3, the qualitatively expected ion transport mechanism under current load conditions was depicted in Fig. 3.2 and explained in accordance with previous work (Rype, 2003). The average ion fluxes are investigated as a function of the current density at high and low inlet hydroxide concentration to the dialysate channel employing the derived model.

3.5.1.1 Transport at high base concentration gradient

The steady state fluxes of lactate, hydroxide and sodium through each anion exchange membrane in the modeled section are depicted in Fig. 3.4, as function of the imposed current density. The maximum applied current density is defined by the current saturation point. This issue is further investigated in Section 3.5.3. The initial state is Donnan dialysis conditions and the current density is increased stepwise until the next steady state is achieved. The fluxes are evaluated for an inlet base concentration in the dialysate channel of 800 mol/m^3.

When no current is applied, the flux magnitude across both membranes are the

Table 3.4: Properties of the Neosepta-AMH membrane (Ayyildiz and Kara, 2005; Palatý *et al.*, 2006). The water content and fixed charges concentration in the membrane were regressed (Prado-Rubio *et al.*, 2010b). The fixed charges concentration is referred to the free membrane volume

Parameter	Range	Value	Units
Thickness	0.25-0.28	0.27	mm
Water content	17-22	variable	%
Ion exchange capacity	1.30-1.50	-	meq/g
C_{fix}	-	7.5x10^3	mol/m^3

Table 3.5: Operational parameters for electro-enhanced dialysis operation mode. Feed and dialysate channels have the same dimensions

Parameter	Value	Units
Channel length	0.373	m
Channel width	0.15	m
Channel height	0.6x10^{-3}	m
Temperature	308	K
Current density	0-260	A/m^2
q$_{feed}$	120	l/h
q$_{dia}$	120	l/h
δ_{BL}	70x10^{-6}	m
C$_{HL}^{fbin}$ + C$_{L^-}^{fbin}$	100	mol/m^3
C$_{NaOH}^{dbin}$	≈0-1500	mol/m^3
C$_{L^-}^{dbin}$	0	mol/m^3
C$_{HP}^{fbin}$ + C$_{P^-}^{fbin}$	1x10^{-7}	mol/m^3
pH$_{in}$ feed	5.75	-

same for each type of ion. Notice that negative values correspond to fluxes going from right to left in the x-direction in Fig. 3.3. After a small positive current density is imposed, the external electrical potential gradient promotes the anion fluxes toward the anode and the cation flux toward the cathode. Therefore in AEM1, the hydroxide flux is enhanced but lactate and sodium fluxes are diminished. On the other hand, in AEM2 the lactate and sodium fluxes are increased but hydroxide flux is reduced. At low current densities, the flux enhancement in one membrane almost equals the decrement in the other one for lactate and hydroxide ions. However by increasing the current density, the flux enhancement in one membrane becomes higher than the reduction in the other membrane.

Another interesting behavior is shown at high imposed current densities, since the hydroxide flux gradually changes into the opposite direction in AEM2 at approximately 140 A/m^2. This behavior means, that at low current densities hydroxide goes from dialysate to feed channel across AEM2, but at high current densities

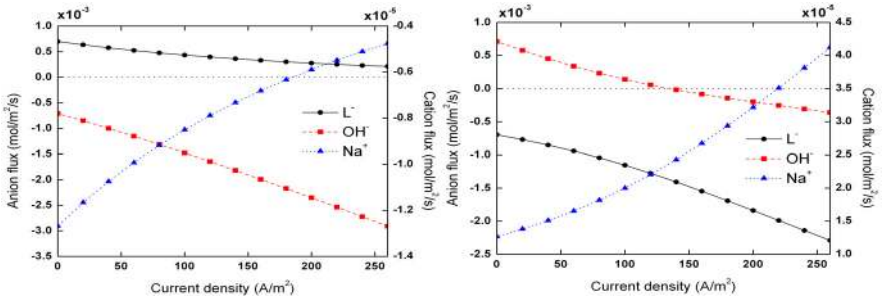

(a) Ion fluxes through AEM1 **(b)** Ion fluxes through AEM2

Figure 3.4: Steady state lactate, hydroxide and sodium fluxes at different imposed current densities for $C_{OH^-}^{dbin}$=800 mol/m^3. AEM1: anion exchange membrane between feed and dialysate channels. AEM2: anion exchange membrane between dialysate and feed channels, according to the cell sketch depicted in Fig. 3.3

the hydroxide migration toward the anode is higher than diffusive transport in the opposite direction. Moreover, there is a current density where the hydroxide flux equals zero; thus there is no net ion transport through the respective membrane. A schematic representation of flux directions in this scenario is depicted in Fig. 3.5. At high base concentration in the dialysate channel, only hydroxide flux inversion is observed. The occurrence of flux inversion has been predicted before in other electrochemical system, where the transport of multiple ions was investigated in a chlor-alkali reactor (Fila and Bouzek, 2003). In that case, Sodium (Na^+), Chlor (Cl^-), hydroxide (OH^-), Hydrogen ion (H^+) and Calcium (Ca^{2+}) fluxes were calculated as function of the imposed current density. It was observed that by increasing the strength of the electric field the sodium fluxes can be inverted.

Investigations of Donnan dialysis have shown that Donnan exclusion is very effective for this system. However, its effectiveness is reduced by increasing the hydroxide concentration in the dialysate channel (Prado-Rubio *et al.*, 2010b). The above simulation results indicate that by increasing the current density, the effectiveness of the exclusion decreases since sodium ions can carry a significant current. When no current is applied, sodium fluxes are two orders of magnitude lower than the lactate and hydroxide fluxes. At high current densities this difference is reduced to one order of magnitude.

3.5.1.2 Transport at low base concentration gradient

At low inlet base concentration in the dialysate channel, the simulations done previously are performed using $C_{OH^-}^{dbin}$=50 mol/m^3. These simulation results are depicted in Fig. 3.6. Once again, when no current is applied the flux magnitude across both membranes are nearly the same for each ion. Just for sodium there is a small difference, but accounting for the small order of magnitude, it could be a numerical inaccuracy ($\mathcal{O}(\times 10^{-8})$). In this case the fluxes are clearly lower than the situation using high base concentration in the dialysate channel due to the lower base con-

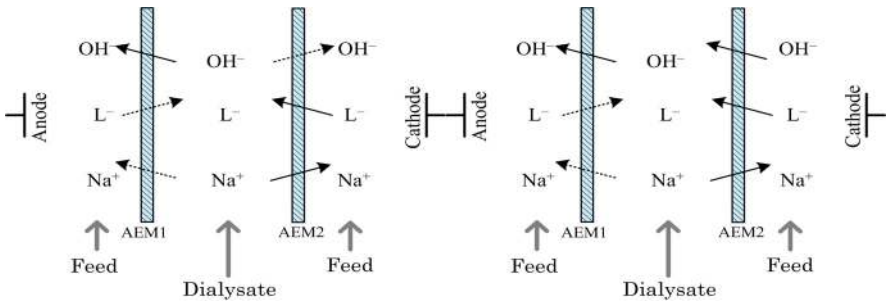

(a) Ion fluxes at low current densities **(b)** Ion fluxes at high current densities

Figure 3.5: Schematic representation of competitive transport under current load conditions at high base concentrations in the dialysate channel ($C^{dbin}_{OH^-}$=800 mol/m^3). Dashed and solid lines correspond to diminished and enhanced fluxes compared to Donnan dialysis, respectively

centration gradient. Imposing a small current density, the flux increment through one membrane almost equal the flux reduction in the next membrane resulting in a negligible lactate recovery enhancement.

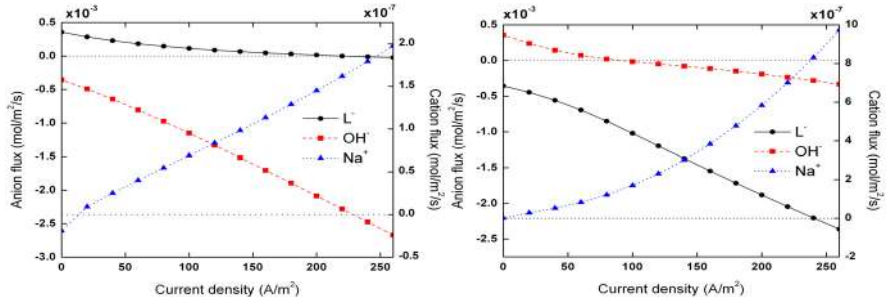

(a) Ion fluxes through AEM1 **(b)** Ion fluxes through AEM2

Figure 3.6: Steady state lactate, hydroxide and sodium fluxes at different imposed current densities for $C^{dbin}_{OH^-}$=50 mol/m^3. AEM1: anion exchange membrane between feed and dialysate channels. AEM2: anion exchange membrane between dialysate and feed channels, according to the cell sketch depicted in Fig. 3.3

In contrast to transport under high base concentration gradient, in the low base concentration scenario there is flux inversion for all ions under current load conditions. When the current density is increased, the sodium flux is inverted in AEM1. By further increasing the current density, the hydroxide flux turns in the opposite direction in AME2. Meanwhile the sodium flux is enhanced toward the cathode, the lactate flux is increased in AEM2 and reduced in AEM1. Finally, at high applied current densities, the lactate migration toward the anode overcomes the diffusive transport in the opposite direction in AEM1. Sodium flux inversion occurs at ap-

proximately 15 A/m^2 in AEM1, for hydroxide it happens at approx. 90 A/m^2 in AEM2 while lactate flux inversion appears at approx. 220 A/m^2 in AEM1.

The sodium flux inversion occurs since the Donnan exclusion is more effective at low hydroxide concentrations in the dialysate channel (Prado-Rubio *et al.*, 2010b). Besides, it is expected that hydroxide flux inversion occurs at lower current density since its concentration gradient is smaller and can be overcome more easily than under high base concentration scenario. A sketch of all situations described in this scenario is depicted in Fig. 3.7, where the initial condition is the same as shown in Fig. 3.5(a). In the figure, the last plot (c) represents the expected competitive ion transport under current load conditions shown in previous work (Rype, 2003). Clearly the presented investigations illustrate that the required current density for flux inversion depends strongly on the base concentration in the dialysate channel.

From the simulation results depicted in Fig. 3.6, the efficiency of Donnan exclusion was corroborated. At low inlet hydroxide concentration in the dialysate channel, the sodium flux through the membranes is four orders of magnitude lower than lactate and hydroxide fluxes. At high current densities, sodium fluxes increase by one order of magnitude.

The existence of the predicted transport scenarios means that the ion fluxes, and therefore the lactate recovery, strongly depend on the actual operating conditions. Due to the coupling between variables, it is difficult to predict the actual transport scenario for a given set of inputs. Thus, the derived model is very useful to evaluate the operating window for this electrochemical system.

3.5.1.3 Concentration profiles at limited transport conditions

Investigations of lactate recovery using Donnan dialysis have illustrated the concentration gradients within boundary layers and membranes under two different transport controlled cases, referred to as: boundary layer control and membrane control (Zheleznov *et al.*, 1998; Prado-Rubio *et al.*, 2010b). The hydroxide concentration in the dialysate channel defines the transport control regime. A similar set of simulations are performed for electro-enhanced dialysis in order to study the effect of the imposed electrical potential. The average static concentration profiles within the membranes at low and high hydroxide concentration in the dialysate channel are shown in Figs. 3.8 and 3.10, respectively. Analogously, the concentration profiles within the boundary layers and channels are depicted in Figs. 3.9 and 3.11.

Under Donnan dialysis conditions, the concentration profiles are symmetric around the dialysate channel (Figs. 3.8-3.11). However under current load conditions, the concentration profiles become asymmetric.

At low base concentration in the dialysate channel, the ion concentration gradients in AEM1 increase with the strength of the imposed electrical potential (Fig. 3.8(a)). The lactate content in the membrane is reduced while hydroxide concentration is augmented. The reason is the reduction and enhancement of the lactate and hydroxide fluxes, respectively in AEM1.

In AEM2, lactate flux is enhanced while hydroxide flux is diminished by increasing the current density. The membrane is almost saturated with lactate and depleted of hydroxide ions (Fig. 3.8(b)). It can be noticed that the ion concentrations at the membrane surface in the feed channel do not change as much as in the interface

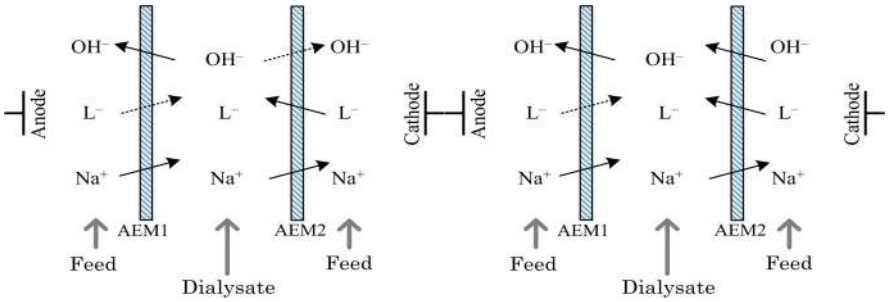

(a) Ion fluxes after Na^+ flux inversion

(b) Ion fluxes after OH^- flux inversion

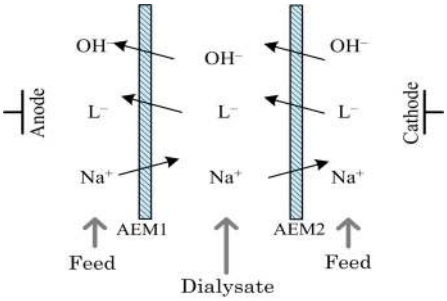

(c) Ion fluxes after L^- flux inversion

Figure 3.7: Schematic representation of competitive transport of lactate, hydroxide and sodium under current load conditions at low base concentrations in the dialysate channel ($C_{OH^-}^{dbin}$=50 mol/m^3). Dashed lines correspond to diminished fluxes and solid lines represent the enhanced fluxes

facing the dialysate channel. This might be related to the lactate concentration change in the channels and therefore in the adjacent boundary layers, since larger variations are predicted in the dialysate channel as seen in Figs. 3.9(a) and (c).

In electro-enhanced dialysis, the preferential lactate transport from the feed to dialysate channel across AEM2 can be seen in the concentration profiles depicted in Fig. 3.9. Larger concentration gradients in the boundary layers around AEM2 appear as a consequence of higher lactate flux. A reduction in pH values is predicted in BL IV (in the feed channel adjacent to AEM2) due to the lower hydroxide flux through that section, as seen in Fig. 3.9(b). The enhanced hydroxide total flux toward the feed channel, implies a higher pH in that channel and therefore the amount of lactic acid is reduced. Any increment of negative ions in the boundary layers is accompanied by a rise in sodium concentration (Fig. 3.9(c)). In this simulated scenario, there is no appreciable change in the lactate concentration in the feed channel by the imposed current density.

The simulated concentration profiles of lactate and hydroxide within the membranes at high hydroxide concentration in the dialysate channel are shown in Fig. 3.10. High concentration gradients are predicted within the membranes when no current is applied. In the AEM1, the amount of hydroxide is increased since hy-

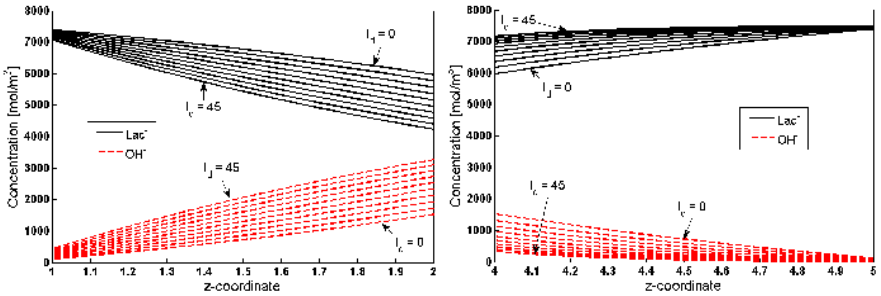

(a) Anion Exchange Membrane 1 (AEM1) **(b)** Anion Exchange Membrane 2 (AEM2)

Figure 3.8: Steady state ion concentration profiles within the membranes under current load conditions, during boundary layer controlled transport ($C_{OH^-}^{dbin}$=5 mol/m^3). The current density is increased stepwise with an amplitude of 5 A/m^2, from 0 to 45 A/m^2. z=1 and z=5 correspond to the membrane side facing the feed channel. z=2 and z=4 correspond to the membrane side facing the dialysate channel

droxide is preferably transported from the dialysate to the feed channel while lactate is depleted (Fig. 3.10(a)).

In AEM2, the amount of lactate tends to increase but the high transport resistance inside the membrane limits the transport (Fig. 3.10(b)). Additionally, the concentration profiles become highly non linear under increasing current load conditions.

The concentration profiles within the boundary layers and bulk channels are shown in Fig. 3.11. At high hydroxide concentration in the dialysate channel, the concentration gradients at the boundary layers are larger than at low hydroxide concentrations (compare Figs. 3.9(a) and 3.11(a)). In this case, the pH in the feed channel is very high even at Donnan dialysis conditions. Thus, there is no lactic acid. The hydroxide concentration profile is inverted in the feed boundary layer adjacent to AEM2. Therefore, the bulk concentration is slightly higher than at the AEM2 surface at high current densities (due to the scale, it is hardly visible in Fig. 3.11(b)).

Using both limited transport scenarios in the dialysate channel, Donnan exclusion provokes that hydroxide concentration in the membrane almost complements the lactate concentration to fulfill the electroneutrality condition. This implies that lactate concentration is a mirror image of the hydroxide concentration around $C_{fix}/2$, as seen in Figs. 3.8 and 3.10.

3.5.2 Flux enhancements

As predicted above under current load condition, the imposed potential gradient will enhance the fluxes in one membrane but diminish them in the other. In order to quantify the total fluxes toward each channel, the fluxes through both anion exchange membranes in the modeled section have to be accounted for. The total ion fluxes at steady state are calculated as follows. Note that fluxes going from right to left in the modeled section are negative.

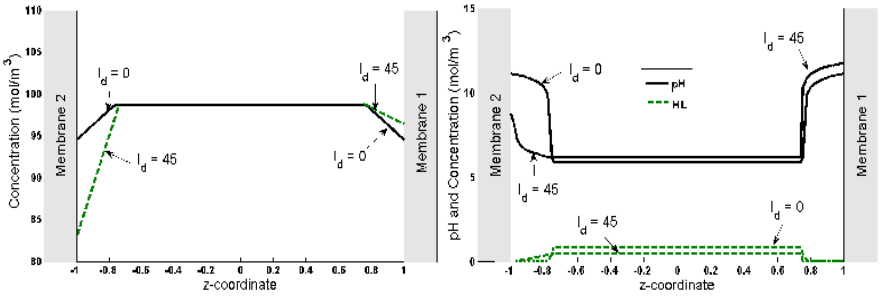

(a) Lactate in feed channel **(b)** pH in the feed channel

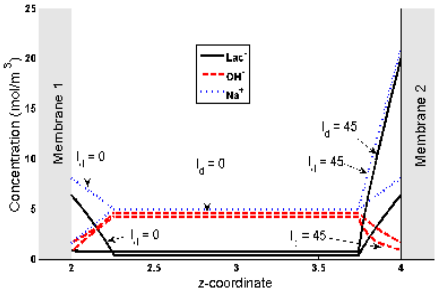

(c) Ions in the dialysate channel

Figure 3.9: Steady state ion concentration profiles in the channels and boundary layers under current load conditions, during boundary layer controlled transport ($C^{dbin}_{OH^-}$=5 mol/m^3). Concentration profiles during Donnan dialysis (I_d=0 A/m^2) and current density of I_d=45 A/m^2 are depicted. The channel widths have been scaled for illustration purposes

- Lactate flux toward dialysate channel:

$$J_{L^-,tot} = \frac{1}{2}\left(J_{L^-,AEM1} - J_{L^-,AEM2}\right) \tag{3.17}$$

- Hydroxide flux toward the feed channel:

$$J_{OH^-,tot} = \frac{1}{2}\left(J_{OH^-,AEM2} - J_{OH^-,AEM1}\right) \tag{3.18}$$

- Sodium flux toward the feed channel:

$$J_{Na^+,tot} = \frac{1}{2}\left(J_{Na^+,AEM2} - J_{Na^+,AEM1}\right) \tag{3.19}$$

Ion fluxes are calculated for a range of current densities from zero to 260 A/m^2. The relative lactate and hydroxide flux enhancements are depicted in Fig. 3.12. Donnan dialysis flux, for all range of inlet hydroxide concentrations in dialysate channel, are represented by zero relative enhancement.

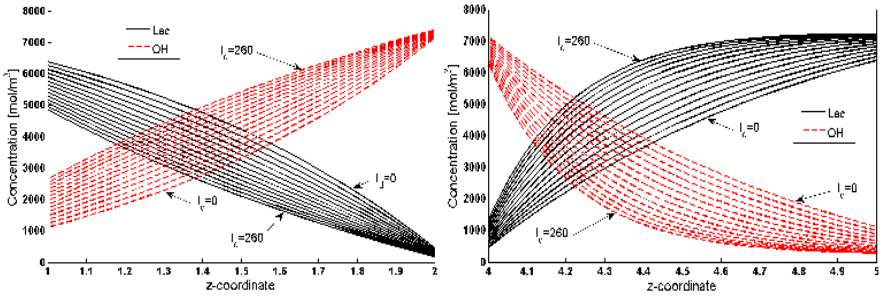

(a) Anion Exchange Membrane 1 (AEM1) **(b)** Anion Exchange Membrane 2 (AEM2)

Figure 3.10: Steady state ion concentration profiles within the membranes under current load conditions, during membrane controlled transport ($C^{dbin}_{OH^-}$=800 mol/m^3). The current density is increased stepwise with an amplitude of 20 A/m^2, from 0 to 260 A/m^2. z=1 and z=5 correspond to the membrane side facing the feed channel. z=2 and z=4 correspond to the membrane side facing the dialysate channel

From Fig. 3.12, it can be seen that for both lactate and hydroxide fluxes, the relative enhancement is non linear at low hydroxide concentration in the dialysate channel. When a low current density is imposed on the system there is no apparent flux enhancement. The reason is that the ion fluxes are increased in one membrane but diminished in the other one at nearly the same rate (see Figs 3.4 and 3.6). Consequently, the total flux is almost constant. An important fact is that none of the total fluxes calculated under current load conditions are lower than during Donnan dialysis. The total relative ion flux is larger than zero when the ion flux enhancement in one membrane exceeds the reduction in the other membrane.

The largest flux enhancements are observed at low inlet base concentration in the dialysate channel. The reason can be related to the transport mechanism. The imposed electrical potential gradient competes with the concentration gradient and the induced electrical potential gradient. The latest is generated by the hydroxide flux from the dialysate to the feed channel. At low base concentration in the dialysate channel, hydroxide and lactate fluxes are low, therefore there is a stronger response to changes in current density.

The total fluxes of lactate and hydroxide are plotted in Fig. 3.13. The large flux enhancement observed at low base concentrations in the dialysate channel, under current load conditions, means that the flux at high current densities is almost independent of the base concentration. Under Donnan dialysis operation mode, the way to enhance the flux is by increasing the OH^- in the dialysate channel. However under current load conditions, there is not a big influence of the base concentration at high current densities. These results are very promising since high fluxes will be achieved at low base concentration, which reduces the base requirements during operation and the potential membrane damage due to the less aggressive pH environment.

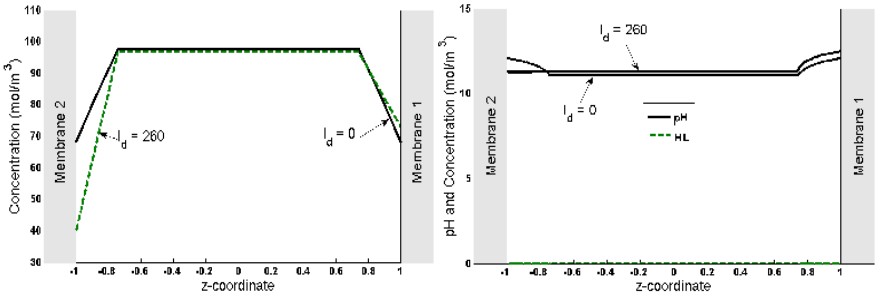

(a) Lactate in feed channel **(b)** pH in the feed channel

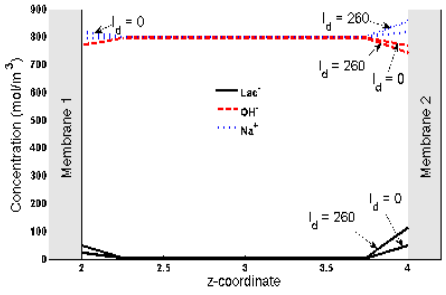

(c) Ions in the dialysate channel

Figure 3.11: Steady state ion concentration profiles in the channels and boundary layers under current load conditions, during membrane controlled transport ($C^{dbin}_{OH^-}$=800 mol/m^3). Concentration profiles during Donnan dialysis and current density of 260 A/m^2 are depicted. The channel widths have been scaled for illustration purposes

3.5.3 Current saturation conditions

In any electrically driven membrane separation process, it is expected to have a maximum allowed current density beyond which the current efficiency decreases. The presented model was derived to describe the ion transport under sub-limiting current conditions, therefore it is very important to know the operating window for the current density. In the literature the same situation is referred to as the limiting current density or current saturation (Mulder, 1997; Strathmann, 2004; Sonin and Grossman, 1972).

The term limiting current density is used in electrodialysis when, due to concentration polarization, the salt concentration at the membrane surface is reduced to zero and there are no more ions available to carry the imposed electrical current. The required ions are then provided by water dissociation resulting in a loss of current utilization (Strathmann, 2004). The current saturation term has been used for a more general situation when ion transport through layered ion exchange membranes was studied (Sonin and Grossman, 1972). Current saturation is achieved when the Donnan potential across an interface becomes infinity at a finite value of current density.

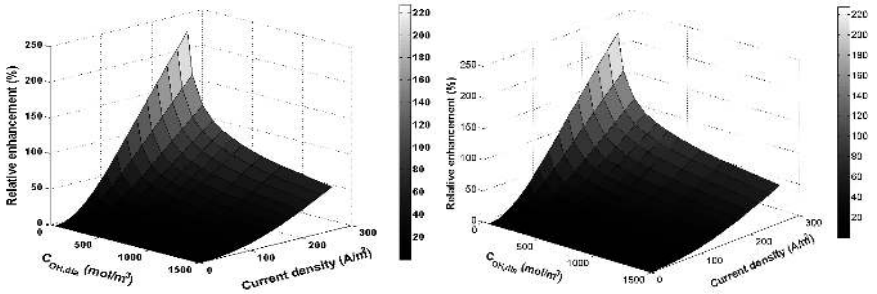

(a) Lactate flux enhancement toward dialysate channel **(b)** Hydroxide flux enhancement toward feed channel

Figure 3.12: Relative ion flux enhancement to Donnan dialysis as a function of the imposed current densities and inlet base concentration in dialysate channel

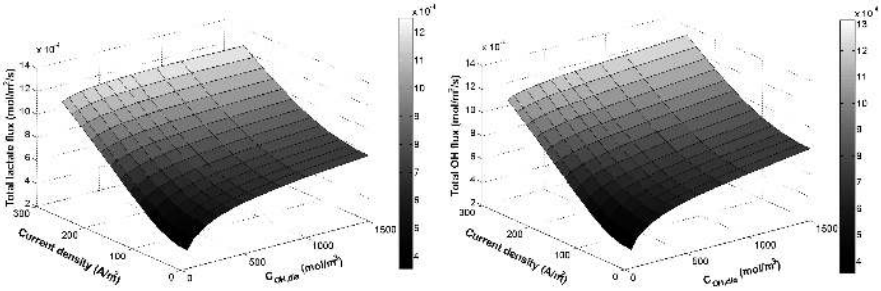

(a) Total Lactate flux toward dialysate channel **(b)** Total hydroxide flux toward feed channel

Figure 3.13: Total ion flux as a function of the imposed current densities and inlet base concentration in dialysate channel

Due to the complex mathematical description of the system, it is not feasible to find a analytical equation to determine the current saturation value for a given set of input variables. Instead, a convergence issue during the solution of the system of differential algebraic equations is exploited to obtain an idea about when current saturation occurs. For a given input hydroxide concentration in the dialysate channel, a simulation is performed by increasing stepwise the current density until the point where the solver does not converge. The last successful step is analyzed to find the interface where the current is saturating. In the evaluated scenarios, the saturation of the current was seen in the interface between the AEM2 and BL IV. The hydroxide concentration profiles in BL IV are shown in Fig. 3.14.

By increasing the current density further than the hydroxide flux inversion in AEM2 (as is depicted in Figs. 3.4(b) and 3.6(b) for high and low hydroxide concentration in the dialysate channel), the concentration profiles in the boundary layer between AEM2 and feed channel, BL IV, have an inversion point as it is shown in

Fig. 3.14.

In both simulated cases, the hydroxide concentration is higher in the solution adjacent to the membrane surface than in the feed channel at low current densities. After concentration gradient inversion, the feed channel hydroxide concentration is higher than close to the membrane, the gradient increases by intensifying the strength of the electric field. At high imposed electrical potential gradients, the hydroxide concentration in the solution adjacent to AEM2 decreases and approaches zero. In the derived model, Donnan equilibrium is one of the equations used to describe the concentration discontinuity at the membrane surface. This equilibrium defines the ion distribution inside the membrane based on the ion concentration in the solution adjacent to the membrane surface. The Donnan potential is represented in Eq. 3.20.

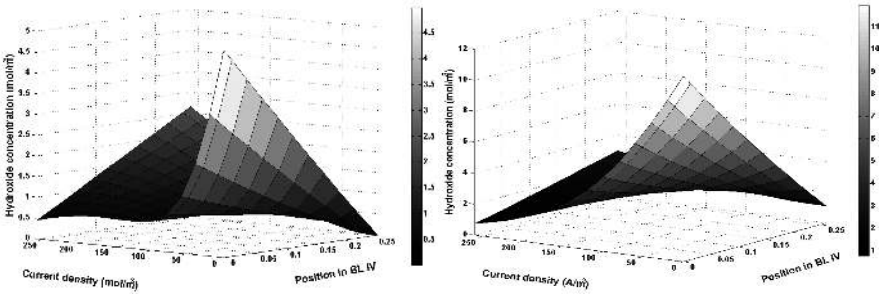

(a) Low base concentration ($C^{dbin}_{OH^-}$=50 mol/m^3) **(b)** High base concentration ($C^{dbin}_{OH^-}$=800 mol/m^3)

Figure 3.14: Hydroxide profile in the boundary layer between AEM2 and feed channel for low and high inlet base concentration in dialysate channel. Position in BL IV=0 corresponds to AEM2 surface and dimensionless position in BL IV=0.26 is the boundary between BL and feed channel

$$\Delta\psi_{Don} = \frac{RT}{z_{OH^-}F} ln\left(\frac{C^s_{OH^-}}{C^m_{OH^-}}\right) \tag{3.20}$$

The Donnan potential has a finite value. However, it can be seen that at some finite value of current density, the Donnan potential $\Delta\psi_{Don}$ can approach infinity. This is provoked by small values of the hydroxide concentration in the solution adjacent to the membrane surface ($C^s_{OH^-}$) combined with the somewhat higher concentration within the membrane ($C^m_{OH^-}$). The static hydroxide concentration ratio at the interface AEM2-BL IV is depicted in Fig. 3.15. It can be seen how this ratio grows almost exponentially while approaching the current saturation condition. At that point, it is difficult to solve the coupled system of algebraic and differential equations. Therefore, the saturating current density value can not be accurately predicted. However, it is expected that the Donnan potential increases fast for higher current densities since the $C^s_{OH^-}$ is decreasing. At moderate and high hydroxide concentrations in the dialysate channel, the current is saturated in the vicinity of

260 A/m^2. Nevertheless, this value dramatically decreases at low hydroxide concentrations ($C^{dbin}_{OH^-} \approx 5$ mol/m^3). To overcome this situation, the model should be extended to account for water splitting at the membrane surface.

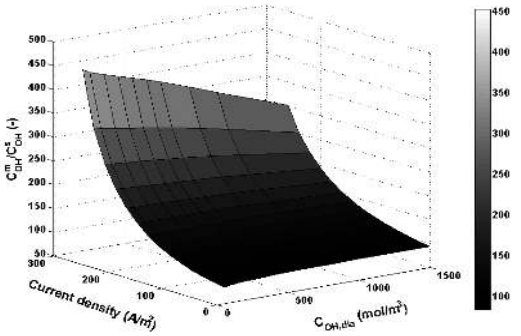

Figure 3.15: Static hydroxide concentration ratio ($C^s_{OH^-}/C^m_{OH^-}$) at the interface between AEM2 and BL IV as a function of the current density and $C^{dbin}_{OH^-}$

3.6 Conclusions

A model based study has been performed to investigate the electro-enhanced dialysis process, as a potential method to improve the lactate recovery over that for Donnan dialysis. A previously derived first principles dynamic model was employed to elucidate the simultaneous transport of multiple ions across ion exchange membranes under current load conditions. The parameters employed during the simulations have been taken from literature and estimated based on experimental data for lactate dialytic recovery. The flux behavior after applying an electrical potential gradient to the Donnan dialysis process was investigated. Different ion transport scenarios are predicted due to a flux inversion phenomenon. The current necessary to invert a certain ion flux strongly depends on the ion concentrations in the bulk solutions.

The concentration profiles in the modeled sections are studied at high and low inlet hydroxide concentration in the dialysate channel. Important changes in the ion concentration were seen compared to Donnan dialysis operation, especially within the membranes. The potential flux enhancement by imposing an electrical field was quantified. Lactate fluxes were increased up to 230% compared to Donnan dialysis operation at moderate and high base concentration in the dialysate channel. At low hydroxide concentration, the fluxes can be further increased but the current is saturated at a lower value. A numerical restriction is exploited to reveal that this system possesses an interface where the current is saturated. This point is the limit of the model validity since the water splitting reaction is not modeled.

Based on the simulation results, the operating window for current density and inlet hydroxide concentration to the dialysate channel was defined. The operating constraints for current density are Donnan dialysis and current saturation conditions.

Very low hydroxide concentration in the dialysate channel should be avoided since the current saturation value dramatically decreases under those conditions. The maximum base concentration in the dialysate channel is experimentally associated to the membrane stability. However, the ion fluxes have shown low sensitivity to the hydroxide concentration for high current densities. Therefore, it is beneficial to operate the system using moderate base concentration in the dialysate channel. Information about the system operating window is vital for further investigations on the operability of this membrane separation process.

The derived model has shown a great potential to contribute to the understanding of transport phenomena in electrochemical systems. It can be used for process design and optimization.

3.7 Acknowledgment

The authors acknowledge the support from the Sixth framework project of the European Union: NMP2-CT-2007-O2b515 IP "BIOPRODUCTION".

3.8 List of symbols

Abbreviations

AEM 1-2	Anion Exchange Membrane 1-2
BL I-IV	Boundary layer I-IV
EED	Electro-enhanced dialysis
MW	Molecular weight
PLA	Polylactic acid

Symbols

AEM	Anion Exchange Membrane
BL	Boundary layer
C	Concentration (mole m^{-3})
D	Diffusion coefficient (m^2 s^{-1})
E	Fractional membrane water content (-)
F	Faraday constant (C $mole^{-1}$)
I_d	Current density (A m^{-2})
J	Flux (mole m^{-2} s^{-1})
h_i	Channel i height (m)
k	Kinetic parameter (-)
L	Channel length (m)
q	Flow rate (m^3 s^{-1})
R_k	Total reaction rate of k (mol m^{-3} s^{-1})
R	Universal gas constant (J mol^{-1} K^{-1})

t	Time (s)
T	Absolute temperature (K)
x	Spatial direction (m)
y	Spatial direction (m)
W	Channel width (m)
z	Dimensionless distance $z = x/\delta_m$ (-)
z_k	Valence of k (-)

Greek letters

δ_m	Membrane thickness (m)
γ	Parameter in the diffusion model (-)
ψ	Electrical potential (V)
ψ_n	Nominal potential ($\psi_n = RT/F$) (V)
σ	Parameter in the WC model (-)
τ	Dimensionless time ($\tau = t/\tau_n$) (-)
τ_{dia}	Residence time in dialysate channel ($\tau_{dia} = h_{dia}WL/q_{dia}$) (s)
τ_{diff}	Diffusion time ($\tau_{diff} = \delta_m^2/D_{k,p}$) (s)
τ_{feed}	Residence time in feed channel ($\tau_{feed} = h_{feed}WL/q_{feed}$) (s)
τ_n	Nominal time ($\tau_n = 1$) (s)
φ	Dimensionless potential ($\varphi = \psi/\psi_n$) (-)

Subscripts

AEM	Anion Exchange membrane
BL	Boundary layer
dia	Dialysate channel
$feed$	Feed channel
fix	Fixed charges in the membrane
HL	Lactic acid
HP	Undissociated protein
in	inlet
i	Specie
j	Discretization point j=0,...,7
k	Specie
L^-	Lactate ion
Na^+	Sodium ion
OH^-	hydroxide ion
P^-	Dissociated protein
p	Zone (phase)
tot	Total
z	specific location (z-coordinate)

Superscripts

db	Dialysate bulk
$dbin$	Dialysate bulk inlet
fb	Feed bulk
$fbin$	Feed bulk inlet
m	Membrane
s	Solution

4

Reverse Electro-Enhanced Dialysis for Lactate Recovery from a Fermentation Broth

4.1 Abstract

A model based investigation is performed on the potential lactate recovery under current reversal conditions in a dialytic module. This technology has been referred to as the Reverse Electro-Enhanced Dialysis (REED). A description of the process, operation modes and antifouling mechanism is presented. A previously developed first principles dynamic model is employed to perform simulations. The model can describe simultaneous transport of ions through anion exchange membranes and Nernst diffusion layers in a section of the REED module. The approach leads to a system of multiregion partial differential equations that are solved numerically. The ion fluxes are studied predicting preferable ion transport at the interfaces, transient flux inversion and accumulation/depletion of ions within the membranes. These phenomena can explain the moderate loss of current efficiency during current reversal operation, which has been experimentally demonstrated. The average lactate productivity is estimated as a function of the reversal time. Experimental data are used to regress a simple electrical potential build up model and calculate the module energy consumption. This value is compared to a similar experimental setup. The trade off between the current efficiency loss and energy consumption is identified, which defines an optimal reversal time. Potentially, the model can be applied to optimize the design and the operation of the REED module for different production scenarios.

4.2 Introduction

The work presented in this contribution is part of our efforts investigating a novel process for *in situ* lactate recovery from dilute solutions. This investigation is driven by the wide range of applications of lactic acid in chemical, pharmaceutical, cosmetic and food industries. Recently, a research acceleration has been evidenced due to the increasing number of applications of biodegradable lactide polymers in biomedical, textile and plastic industries (Kharas *et al.*, 1996). Fermentation of carbohydrates using lactic acid bacteria (LAB) is mostly used at industrial scale, even though lactic acid can be produced by chemical synthesis. The main limitations during sustainable bioproduction of lactic acid are: that lactic acid bacteria are impaired by product

inhibition plus difficult downstream processing. It has been shown that lactic acid recovery and concentration can represent up to 70% of the total production cost (Stanbury *et al.*, 1995). Therefore, Polylactic acid polymers (PLA) only will be able to substitute petrochemical based products when the production costs of the main bulk raw material are considerably reduced. The application of new purification technologies and integrated process configurations appear to be efficient ways to render PLA production economically feasible.

A dynamic model has been derived previously, from first principles, to describe simultaneous ion transport across ion exchange membranes in a dialysis cell (Prado-Rubio *et al.*, 2010b). The model parameters were regressed to reproduce experimental steady state recovery of monoprotic carboxylic anions by Donnan Dialysis. The model structure satisfactorily reproduced anion fluxes as function of the base concentration in the dialysate channel. The estimated average diffusion coefficients within the membrane showed good agreement with experimentally determined values presented in literature. Additionally, simulated concentration profiles within the modeled sections matched the previously predicted profiles, both under boundary layer and membrane controlled transport.

The main limitation of lactate recovery using Donnan Dialysis is a rather low anion flux, since the driving force behind lactate transport is the hydroxide concentration gradient between dialysate and feed channels. Therefore, simulations were used to evaluate the potential flux enhancement under current load conditions, referred to as Electro Enhanced Dialysis (EED) (Prado-Rubio *et al.*, 2011b). The static analysis of EED showed the potential performance of the module and how recovery can be enhanced by applying an external potential gradient. The limiting current density was indirectly estimated as a function of the base concentration in the dialysate channel. For the range of concentrations employed in this contribution, the limiting current density is in the vicinity of 260 A/m^2. EED constitutes an ideal scenario and corresponds to the best achievable separation under current load conditions. The reason is that the model was solved for carboxylic anion recovery from ideal solutions. However, when the separation is performed from a fermentation broth, the picture is slightly different. There, membrane fouling and a pH buffer effect both become relevant (Hongo *et al.*, 1986; Lee *et al.*, 1998a; Garde, 2002; Rype, 2003).

Periodic operation has been researched and exploited in many chemical processes whereby intensification or higher efficiency may be obtained. One of the early examples was periodic forcing of chemical reactors, e.g. to improve conversion in equilibrium limited chemical reactions (Matros, 1989; Neophytides and Froment, 1992) and to ensure reduction of volatile organic compounds in industrial exhaust gases in tubular catalytic reactors (Eigenberger and Nieken, 1988; Matros and Bunimovich, 1996) through reverse flow operation. In separation processes periodic forcing has been employed to enhance the driving force between phases, e.g. in pressure swing adsorption which has been suggested (Jasra *et al.*, 1991; Ruthven *et al.*, 1994; Ruthven, 2000; Sircar, 2002) and applied for bulk gas separations, e.g. air purification (Ritter and Yang, 1991) propane propylene separation (Rege and Yang, 2002) and hydrogen purification (Sircar and Golden, 2000). Periodic forcing has also been demonstrated to improve the efficiency in vapor liquid tray separation processes (Toftegård and Jørgensen, 1988).

Periodic operation has also been investigated and applied in membrane processes to

compensate the adverse influence of membrane fouling during long term operation. Enhanced separation from fouling suspensions has been achieved using dynamic microfiltration with vibrating membrane filters (Beier *et al.*, 2006; Holm *et al.*, 1986; Postlethwaite *et al.*, 2004). Non stationary periodic operation during ultrafiltration and microfiltration units is obtained using hydraulic membrane cleaning through back-flushing (Mulder, 1997) or high frequency back-flush (Gekas and Hallström, 1987; Jonsson and Wenten, 1994; Guerra *et al.*, 1997). Probably the most similar periodically operated membrane separation process to REED, is Electrodialysis Reversal (EDR) (Katz, 1979). During EDR, the transport of ions is reversed during certain time intervals. Since the Electrodialysis stack is composed of anion and cation exchange membranes, concentrate and diluate compartments must be switched when the current is reversed. An advantage of the REED technology is that the channel switching is not required.

The purpose of this contribution is to investigate the periodic operation of the Reverse Electro-Enhanced Dialysis (REED) module and to elucidate the potential lactate recovery under periodic current reversal conditions. These insights are vital to reveal how the system should be operated according to a given production objective and thus evaluate the technical feasibility of REED.

The paper is structured as follows: REED process is introduced. Operation modes and the self-cleaning membrane mechanism in REED are described. Subsequently, the dynamic model is briefly described. Simulations are performed to investigate the dynamic ion fluxes, lactate bulk concentrations, lactate productivity and energy consumption. Finally, conclusions are drawn.

4.3 Process description

The Reverse Electro-Enhanced Dialysis design emerges as a potential method to enhance the lactate flux in conventional Donnan Dialysis operation, while reducing the adverse influence of membrane fouling (Garde, 2002; Rype, 2003). The REED module combines elements from Electrodialysis Reversal (EDR) and Donnan Dialysis (DD) separations.

The REED module setup is basically the same as for Donnan Dialysis, including electrode chambers at the left and right sides of the module stack. In addition, it includes a mechanism that allows a polarity reversal of the imposed electrical potential gradient. The qualitative understanding of the REED process prior to this investigation is depicted in Fig. 4.1 (Rype, 2003; Møllerhøj, 2006). A relatively low pH cultivation broth is introduced in every even numbered channel in the membrane stack (feed channels), while sodium hydroxide solution is fed into the remaining channels (dialysate channels) (see Fig. 4.1). When current load conditions are imposed, concentration and electrical potential gradients are the main driving forces for the separation. A competitive ion transport in the electrochemical system is generated. Lactate is preferably transported from the feed to the dialysate channels while hydroxide is transported in the opposite direction (Prado-Rubio *et al.*, 2011b). Due to this transport mechanism, the REED system recovers lactate while simultaneously facilitating pH control of the fermentation broth operating at defined current densities.

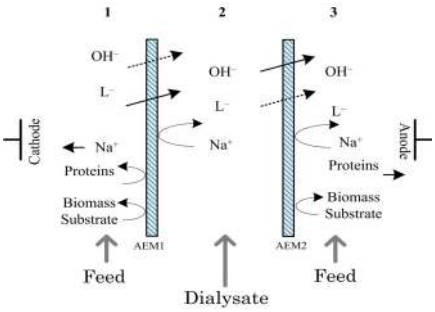

Figure 4.1: Sketch of the expected ion transport under negative current density condition and completely effective Donnan exclusion. Dominant fluxes are depicted with solid lines. For positive current density, the ion fluxes are the mirror image

Due to the symmetry of the modeled section, it is expected to have a mirror image of the ion fluxes when the polarity of the current is reversed. The presented sketch of flux directions is however valid only at sufficiently high current densities, but useful for the process introduction. How the fluxes are enhanced/reduced under continuous current load conditions has been previously investigated (Prado-Rubio *et al.*, 2011b).

4.3.1 REED operation modes

Analogous to Electrodialysis, REED module has two operation modes. The system can be operated at constant voltage or at constant current density. If the separation problem involves clear solutions of the carboxylic acids, practically there is no difference between the two operation modes. However, in the case of a fermentation broth, the selected operation mode defines the actual separation capabilities and operability of the device (Lee *et al.*, 1998a).

The difference between the mentioned operation modes can be seen from Ohm's law (Eq. 4.1). Where ψ represents the electrical potential difference across the module, I is the imposed current and R is the cell resistance.

$$\psi = IR \tag{4.1}$$

The total resistance of the membrane cell is composed by the summation of different resistances in series (Mulder, 1997; Timmer *et al.*, 1994):

- R_m: resistance of clean membranes in the cell, given by the summation of the resistances of the two anion exchange membranes.

- $R_{channel}$: resistance of channels, it is the summation of the resistance of the feed and dialysate channels.

- R_{td}: time dependent resistance

The first two resistances could be condensed into a single term denoted as initial or intrinsic cell resistance R_i, which is time independent. The time dependent resistance is generated by diverse sources such as concentration polarization, precipitation of salts, deposition of colloidal material and biomaterial attachment to the membrane surfaces. The colloidal matter and macromolecules can generate a layer adjacent to the membrane surface, either electrically neutral or carrying some fixed charges (Korngold *et al.*, 1970). An inert film increases the resistance to ion transport. Besides, if the formed layer is constituted of negatively charged components, i.e. organic macromolecules, the fouling layer is cation selective. This situation leads to a composite membrane that behaves as a bipolar membrane. The transport resistance largely increases, even if the thickness of the cation exchange layer is small (Korngold *et al.*, 1970; Grossman and Sonin, 1973).

Due to the increasing electrical resistance, operation at constant electrical potential implies a decreasing current density. From Faraday's law (Eq. 4.2), it is clear that a lower current density means lower ion fluxes.

$$I_d = F \sum_k z_k J_k \tag{4.2}$$

Only increasing the strength of the imposed electrical potential gradient across the cell allows operation at constant current density (constant ion fluxes). The REED module is operated at constant current density, analogously to a filtration unit operated at constant flux (Mulder, 1997).

From the modeling point of view, this operation is convenient since the predicted ion fluxes do not depend on the fouling layer formation.

4.3.2 Membrane cleaning effect in REED

In Electrodialysis, diverse procedures have been proposed to reduce the adverse influence of fouling. Mechanical cleaning has shown to be a temporal solution which works for short time. A chemical cleaning of the membrane with an alkali solution after a defined fouling level is regularly used achieving complete regeneration.

Some experiments were performed in the REED module to investigate the self-cleaning mechanism (Garde, 2002; Rype, 2003). The experiments used a fermented brown juice from food pellet industry. The feed was a 7% lactic acid solution with 5.5 pH. The electrical potential drop across a REED cell under current reversal conditions is depicted in Fig. 4.2. The current density was kept constant at 250 A/m^2 and the reversal time is 60 s.

From Fig. 4.2, the increasing electrical resistance generated by the fouling build-up is clear. The most interesting aspect is that after every current reversal, the initial cell resistance was regained. It means, that most of the fouling layer was reversibly removed by inversing the current direction with a suitable periodicity of the current reversal. By reducing the severe effect of fouling, the REED module can achieve long term operation for lactate extraction from a fermentation broth. In this paper, the first current imposed is negative with a selected magnitude. When the current is reversed, it becomes positive. The two half periods are equally long. The current reversal time is defined as half the period time.

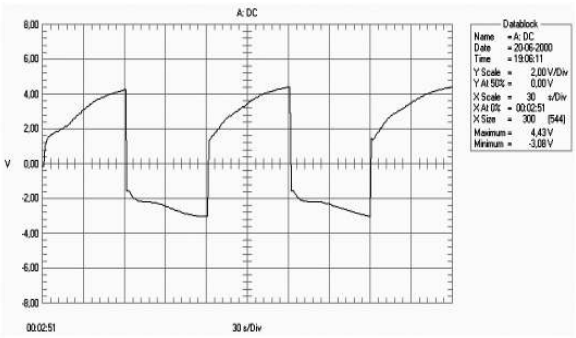

Figure 4.2: Sampling of the electrical potential drop in a cell of REED module during experiments with fermented brown juice with current reversal every 60 s (Garde, 2002; Rype, 2003)

4.4 Model description

A dynamic model has been derived from first principles to describe the simultaneous ion transport in a section of a Dialysis module (Prado-Rubio *et al.*, 2010b). The model accounts for convective transport of dissociated and undissociated species in the channels, and diffusion and migration across the boundary layers and membranes. The ion transport across the potential fouling layers is not currently included into the model. This is due to a lack of information about the nature of the fouling layer and of its rate of formation. However, the adverse influence on the energy consumption is quantified.

Donnan equilibrium is employed to describe the concentration and potential discontinuity on membrane-solution interfaces. The Nernst-Planck approach is used to describe the multicomponent diffusion and migration through boundary layers and membranes. A tank in series approach was employed to approximate the convective flow in channels in the y-direction. The most important field conditions are: electroneutrality and Faraday's law. At the boundaries, there is flux continuity of transported ions and equilibrium conditions. A more detailed model description has been previously published and employed (Prado-Rubio *et al.*, 2010b, 2011b). In the present contribution, the pH buffer model is highlighted since it has not been used in our previous work.

A sketch of the modeled section of the Dialysis module is depicted in Fig. 4.3. The section includes two anion exchange membranes and three bulk channels. This configuration was chosen in order to have symmetry under current reversal conditions. The main assumptions are:

1. General: electroneutrality at any location in the system, ideal solution and the current is carried only by ions. The species included in the model are: Lactate (L^-), hydroxide (OH^-), sodium (Na^+), dissociated protein (P^-), lactic acid (HL) and undissociated protein (HP).

2. Membrane: convective transport is not investigated, transport of water by

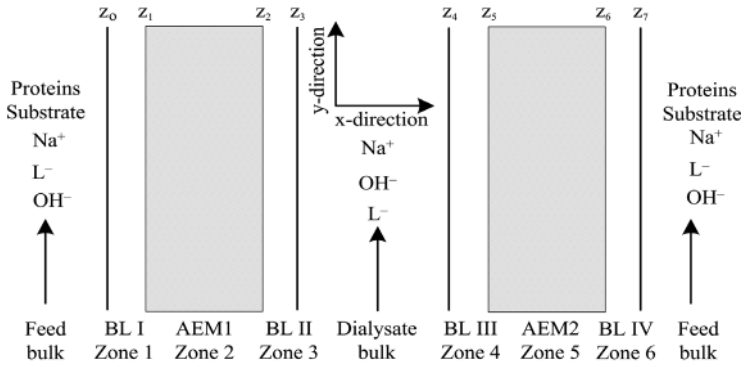

Figure 4.3: Sketch of the modeled section of the dialysis module for lactate recovery from a fermentation broth. The zones in the section and ions present in each zone are depicted. BL: boundary layer and AEM: anion exchange membrane. Dimensionless location $z_j \ \forall \ j$=0,...,7 are the interface locations (Prado-Rubio *et al.*, 2010b). In REED, the electrodes are located at the left and right sides on the section

osmosis and electro-osmosis is neglected, there is no transport of uncharged or large molecules through the membrane, equilibrium at the membrane surface and constant membrane dimensions.

3. Boundary layer: convective transport is neglected and the thickness of the boundary layers are constant for a given flow condition.

The most relevant model equations are depicted in Tables 4.1 and 4.2. The substances and phases are denoted by the subscripts k and p, respectively. For simplicity, the index for the tank in series description in the y-direction is not shown.

Algebraic expressions are employed to describe the electrical potential gradient and concentration discontinuities at membrane-boundary layer interfaces (z_1, z_2, z_5 and z_6 in Fig. 4.3) and electrical potential gradient at the bulk solution-boundary layer interfaces (z_0, z_3, z_4 and z_7). Those algebraic equations are derived from boundary and field conditions. It is assumed that ion concentrations at the membrane surface is in equilibrium with the adjacent solution. Electrochemical potential in the ionic solution and the membrane surface must be the same, which is referred to as the Donnan potential. Donnan equilibrium determines the ionic distribution of transported ions (Eq. 4.3). Faraday's law states that all the electrical current is carried by ions (Eq. 4.4). There is no accumulation of transported ions at the interfaces (Eq. 4.5), for the non-transported ions the flux equals zero. Finally, the electroneutrality condition affects the concentration distribution in both membrane and solution (Eqs. 4.6 and 4.7). The ion diffusion coefficients within the membrane are estimated through the Mackie and Meares' expression (Eq. 4.8, (Jonsson, 1980)). That relation accounts for the increasing ion diffusivity when free volume in the membrane increases. A power function is employed to describe the increasing membrane free volume as a function of the inlet hydroxide concentration in the dialysate channel (Eq. 4.9).

A mass balance for each species in each phase are represented by Eq. 4.10 (Taylor and Krishna, 1996). The ion flux $J_{k,p}$ through boundary layers and membranes is estimated using the Nernst-Planck equation for ideal solutions (Eq. 4.11), where the convective transport term was neglected (Strathmann, 2004). Dimensionless parameters are used to group constants and have dimensionless distance and time in the mass balances (see list of symbols). Substituting the flux term in Eq. 4.10 with the Nernst-Plank equation, the mass balance can be rewritten as Eq. 4.12. The electrical potential gradient is estimated explicitly by substituting the ion fluxes into Faraday's law (Eq. 4.13). Subsequently, the derivative of the electrical potential is obtained (Eq. 4.14). The convective transport in the bulk channels is modeled using a tank in series approach. Along a channel, there are migration and diffusion transport toward the adjacent boundary layers plus dissociation reactions. The mass balance for each tank in the feed and dialysate channels are depicted in Eqs. 4.15 and 4.16. In the dialysate channel mass balance the reaction term is neglected, since the high pH makes the ions completely dissociated.

Table 4.1: Interfacial boundary conditions to describe the ion concentrations and electrical potential gradients, and model parameter expressions (Prado-Rubio *et al.*, 2011b)

Equations at the interfaces

$$\left(\frac{C_k^s}{C_k^m}\right)^{\frac{1}{z_k}} = \left(\frac{C_i^s}{C_i^m}\right)^{\frac{1}{z_i}} = \ldots \quad k \neq i \tag{4.3}$$

$$I_d = F\sum_k z_k J_{k,p} \tag{4.4}$$

$$J_k|_{z=z_j^-} = J_k|_{z=z_j^+} \tag{4.5}$$

$$\sum_k z_k C_k^s = 0 \tag{4.6}$$

$$\sum_k z_k C_k^m + z_{fix} C_{fix}^m = 0 \tag{4.7}$$

Diffusion model

$$D_k^m = D_k^s \left(\frac{E}{2-E}\right)^2 \tag{4.8}$$

$$E = \gamma (C_{OH}^{dbin})^{\sigma} \tag{4.9}$$

The presence of proteins in the fermentation broth induces a pH buffer effect. In the mass balances a reaction term is included, to account for the species dissociation. It is expected that the present macromolecules are polyprotic species. However, if the biomolecules are modeled as a highly charged macromolecule, the stiffness of the system of model equations could increase considerably. To overcome this situation, proton acceptor groups in the protein are considered in terms of equivalents, i.e. the

Table 4.2: Summary of the differential equations employed in the first principles model for simultaneous ion transport through the Reverse Electro-Enhanced Dialytic module (Prado-Rubio *et al.*, 2011b). The index for the tank in series in the y-direction is not shown

Transport in boundary layers and membranes

$$\frac{\partial C_{k,p}}{\partial t} + \nabla J_{k,p} - R_k = 0 \tag{4.10}$$

$$J_{k,p} = -D_{k,p}\left(\frac{\partial C_{k,p}}{\partial x} + \frac{z_k F C_{k,p}}{RT}\frac{\partial \psi_p}{\partial x}\right) \tag{4.11}$$

$$\frac{\partial C_{k,p}}{\partial \tau} = \frac{\tau_n}{\tau_{diff}}\left(\frac{\partial^2 C_{k,p}}{\partial z^2} + z_k\Big(\frac{\partial C_{k,p}}{\partial z}\frac{\partial \varphi_p}{\partial z} + C_{k,p}\frac{\partial^2 \varphi_p}{\partial z^2}\Big)\right) + \tau_n R_k \tag{4.12}$$

$$\frac{\partial \varphi_p}{\partial z} = \frac{-I_d\delta_m/F - \sum_k z_k D_{k,p}\partial C_{k,p}/\partial z}{\sum_k z_k^2 D_{k,p} C_{k,p}} \tag{4.13}$$

$$\frac{\partial^2 \varphi_p}{\partial z^2} = \frac{-\sum_k z_k D_{k,p}\partial^2 C_{k,p}/\partial z^2}{\sum_k z_k^2 D_{k,p} C_{k,p}} \cdots + \frac{I_d\delta_m/F + \sum_k z_k D_{k,p}\partial C_{k,p}/\partial z}{\left(\sum_k z_k^2 D_{k,p} C_{k,p}\right)^2}\left(\sum_k z_k^2 D_{k,p}\frac{\partial C_{k,p}}{\partial z}\right) \tag{4.14}$$

Bulk channel model

$$\frac{dC_k^{fb}}{d\tau} = \frac{\tau_n}{\tau_{feed}}\left(C_k^{fbin} - C_k^{fb}\right) + \frac{\tau_n}{h_{feed}}\Big(J_k|_{z=z_7} - J_k|_{z=z_0}\Big) + \tau_n R_k \tag{4.15}$$

$$\frac{dC_k^{db}}{d\tau} = \frac{\tau_n}{\tau_{dia}}\left(C_k^{dbin} - C_k^{db}\right) + \frac{\tau_n}{h_{dia}}\Big(J_k|_{z=z_3} - J_k|_{z=z_4}\Big) \tag{4.16}$$

protein concentration is defined as moles of acid equivalents per volume. Therefore, the dissociation of a polyprotic species is simplified to an apparent monoprotic acid reaction (Prado-Rubio *et al.*, 2010b). The protein species represents a wide range of components in the fermentation broth from low molecular weight proteins to colloidal material. The system of reactions are given by the following equilibrium expressions:

$$HL + OH^- \underset{k_2}{\overset{k_1}{\rightleftharpoons}} L^- + H_2O$$

$$HP + OH^- \underset{k_4}{\overset{k_3}{\rightleftharpoons}} P^- + H_2O$$

where the dissociation constants (K_d) correspond to the acid dissociation constant (K_a) divided by the ionic product of water (K_w). Stoichiometric matrices are used to systematically handle the reaction term in each mass balance (Nielsen *et al.*, 2003).

4.4.1 Model solution

The dynamic model is a system of multiregion partial differential equations that are solved numerically. A sixth order asymmetric Taylor expansion is used to discretize the spatial dimension. The step length is reduced toward boundaries in order to have higher accuracy. Discretization leads to a system of algebraic differential equations (DAEs). A variable order multistep solver is employed based on the numerical differentiation formulas (NDFs) (Shampine *et al.*, 1999). An initialization procedure was used in order to guarantee convergence in all evaluated scenarios (Prado-Rubio *et al.*, 2010b).

4.5 Results and Discussion

4.5.1 Input parameters

For all simulations performed in this paper the extra pH buffer effect is activated by using a sufficient but relatively small concentration of total protein at the inlet of the feed channel. Preliminary simulations were performed under Donnan Dialysis to estimate that threshold. This model feature has not been used in previous work (Prado-Rubio *et al.*, 2010b, 2011b). Besides, sub-limiting current conditions are employed since the model has been derived for such a scenario. The required inputs are depicted in Table 4.3.

The physicochemical properties required to solve the model are listed in Table 4.4. Forced by the limited availability of ion diffusion coefficients in solution as a function of concentration, infinite dilute solution values are employed. The anion exchange membrane used is Neosepta-AMH which has been produced by ASTOM Corporation (Tokyo, Japan), earlier Tokuyama Soda Company, Inc. This is a strongly basic membrane with $-NC_7H_7^+$ as fixed charge groups (Ayyildiz and Kara, 2005). The characteristic properties are presented in Table 4.5.

4.5.2 Numerical issues related to current reversal conditions

Some preliminary simulations were performed to determine if there were convergence problems during the simulations under current reversal conditions. At the beginning of each period current is imposed to the system, then after a half period time the current density is reversed. As a result, a square wave function is obtained.

A current density function with an amplitude of 100 A/m^2 is applied. The first current applied is negative (-100 A/m^2). The initial conditions correspond to the steady state for Donnan dialysis operation, for the given inputs. For very short and long reversal times (shorter than 3 and longer than 20 min), simulations crashed. The numerical method was unable to achieve the integration tolerance without reducing the step size below the smallest allowed value ($h=5.820766x10^{-11}$) (Mathworks, 2006). It was noticed that after the current was reversed, the flux responses are characterized by two different dynamics. There is a fast response after the step disturbance followed by slow settling. The fast dynamic behavior increases considerable the stiffness of the system of equations. Thus if the step change amplitude in the current density is very high, there is a point where the numerical method can

Table 4.3: Operational parameters for REED operation at constant current intensity. The feed and dialysate channels have the same dimensions

Parameter	Value	Units
Channel length	0.373	m
Channel width	0.15	m
Channel height	$0.6\text{x}10^{-3}$	m
Current density	± 100	A/m^2
q_{feed}	120	L/h
q_{dia}	120	L/h
δ_{BL}	$70\text{x}10^{-6}$	m
δ_m	$270\text{x}10^{-6}$	m
E	0.1779	-
$C_{HL}^{fbin} + C_{L^-}^{fbin}$	100	mol/m^3
$C_{HP}^{fbin} + C_{P^-}^{fbin}$	10	mol/m^3
C_{NaOH}^{dbin}	50	mol/m^3
$C_{L^-}^{dbin}$	0	mol/m^3
pH_{in} feed	5.75	-

not achieve the required tolerance.

In order to ensure convergence for a wider range of current reversal times, the square wave function was modified. The step changes were softened by employing a ramp between initial and final value, with a t_{shift} duration. The selected shifting time is negligible compared to the reversal time ($t_{shift} = 1 \times 10^{-3}$s). In this way, convergence of the model is obtained within a reversal time window of $10 \leq t_{rev} \leq 8000$s (these values correspond to the minimum and maximum reversal times employed in the simulations).

4.5.3 Dynamic fluxes

Simulations are performed to investigate the dynamic ion fluxes through all interfaces at different current reversal times. Two different scenarios were studied. First, the complete dynamic response until steady state fluxes are achieved is investigated. In the second scenario, the short transient is studied before the change in the polarity.

4.5.3.1 Long current reversal time

The objective of this simulation is to study the complete dynamic response until static operation is achieved before the polarity of the current is reversed. The selected reversal time was sufficiently long to assure steady state fluxes, t_{rev} =8000 s. All the dynamic fluxes through each interface were investigated, but only the most relevant results for lactate are shown.

In Fig. 4.4, the lactate flux through both interfaces of the two anion exchange membranes is depicted. During Donnan Dialysis separation, static ion fluxes across

Table 4.4: Species properties in the model implementation

Parameter	Value	Units	Source
pK_a for HL	3.860	-	(Lide, 2008)
pK_a for HP	5.000	-	(Møllerhøj, 2006)
D_{L^-} in solution	$1.033x10^{-9}$	m^2/s	(Lide, 2008)
D_{OH^-} in solution	$5.273x10^{-9}$	m^2/s	(Lide, 2008)
D_{Na^+} in solution	$1.334x10^{-9}$	m^2/s	(Lide, 2008)
D_{P^-} in solution	$0.090x10^{-9}$	m^2/s	(Bowen *et al.*, 2000)
D_{HP} in solution	$0.090x10^{-9}$	m^2/s	(Bowen *et al.*, 2000)
D_{HL} in solution	$0.848x10^{-9}$	m^2/s	(Ribeiro *et al.*, 2005)
ρ_{HL} 0.1 M	1000.2	kg/m^3	(Lide, 2008)
ρ_{NaOH} 1 M	1042.8	kg/m^3	(Lide, 2008)
μ_{HL} 0.1 M	$1.027x10^{-3}$	kg/m/s	(Lide, 2008)
μ_{NaOH} 1 M	$1.248x10^{-3}$	kg/m/s	(Lide, 2008)
MW_{HP}	≈66500	g/mol	(Bowen *et al.*, 2000)
MW_{HL}	90.08	g/mol	-
γ	0.24	-	(Prado-Rubio *et al.*, 2010b)
σ	0.10	-	(Prado-Rubio *et al.*, 2010b)

both membranes are equal in magnitude due to the symmetry around the dialysate channel (represented schematically in Fig. 4.6a). When current is applied, asymmetric flux conditions at steady state are imposed, since the ion fluxes are enhanced in one membrane but diminished in the other one (Prado-Rubio *et al.*, 2011b). It can be seen in Fig. 4.4 that after the first step change, the static lactate flux through AEM1 is enhanced while a reduction is observed in AEM2 (notice that the flux sign indicates its direction). The opposite situation happens when the current is reversed.

After every step, the dynamic response of the fluxes through the interfaces (-/+) of each membrane differ, this generates a positive or negative accumulation of lactate in the membrane. When the steady state is achieved, fluxes are constant and equal across both interfaces for each membrane. This accumulation is clear when the dynamic concentration profiles are studied. In Fig. 4.5, the lactate concentration profile within AEM1 is depicted for a period and a half of stationary operation. In the first half period, lactate is accumulated in AEM1 while it is depleted from AEM2. After the second step change, the lactate is depleted from AEM1 while AEM2 is filled.

Under current reversal conditions, a dynamic flux symmetry situation is established with a half period time delay. It means that the lactate flux response through $AEM1^-$ is a half period delayed mirror image of the flux across $AEM2^+$, these interfaces are facing the boundary layers in the feed channel. Analogous behav-

Table 4.5: Properties of the Neosepta-AMH membrane (Ayyildiz and Kara, 2005; Palatý *et al.*, 2006). The water content and fixed charges concentration of the membrane were regressed (Prado-Rubio *et al.*, 2010b)

Parameter	Range	Value	Units
Thickness	0.25-0.28	0.27	mm
Water content	17-22	17.79	%
Ion exchange capacity	1.30-1.50	-	meq/g
C_{fix}	-	$7.5x10^3$	mol/m^3

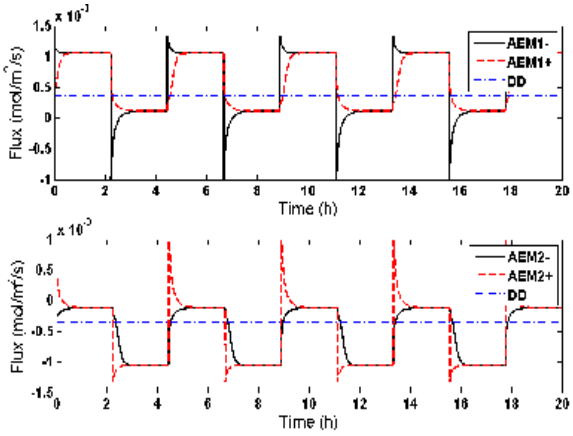

Figure 4.4: Dynamic lactate flux through both sides of each anion exchange membrane (AEM) for a reversal time of 8000 s (2.22 h). The signs -/+ stand for the left and right hand side of the membrane, respectively. The static Donnan Dialysis flux is depicted in each plot. AEMi: anion exchange membrane (i=1,2 see Fig. 4.3), DD: Donnan Dialysis

ior is observed for the membrane interfaces adjacent to the boundary layers in the dialysate channel. This half period delayed flux symmetry implies that the stationary total lactate flux is independent of polarity of the imposed electrical potential gradient.

Previous calculations have shown that there is a current density value that can invert the static ion flux when the reference is Donnan Dialysis separation (see Fig. 4.6a) (Prado-Rubio *et al.*, 2011b). In this first simulated scenario, there is a transient flux inversion at the membrane interfaces facing the feed channel. The flux inversion lasts for approximately 20 min. The transient flux directions and qualitative magnitudes are represented in Fig. 4.6, according to the polarity of the electrical potential gradient.

It is interesting that lactate flux response at the interface facing the feed channel has a pronounced overshoot which is not seen at the opposite interface. Additionally,

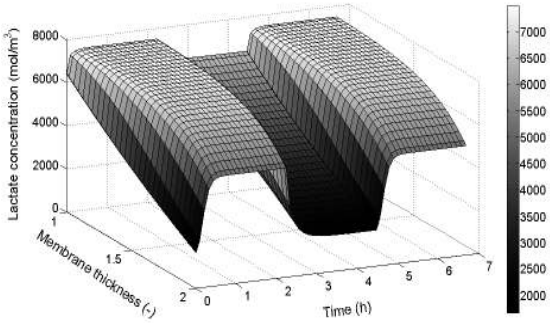

Figure 4.5: Dynamic lactate concentration in the membranes for a reversal time of t_{rev}=8000s (2.22 h). 1.5 operating period is depicted. Membrane thickness equal to 1 and 2 represent the interfaces facing the feed and dialysate channels, respectively (See Fig. 4.3 for the dimensionless references)

the overshoot is more pronounced for negative current in AEM2$^+$ and for positive current in AEM1$^-$, where the transient lactate flux inversion takes place. If only lactate flux is investigated, the reason for the overshoot is definitely not clear. The explanation for this behavior was found when all fluxes where investigated at the interfaces, since the hydroxide flux presents an analogous behavior.

A preferable ion transport was investigated statically for this system (Prado-Rubio *et al.*, 2011b). It was predicted that, under current load conditions, lactate is preferably transported from the feed to the dialysate channel through one membrane while hydroxide is transported in the other membrane. In other words, lactate is transported to the dialysate channel and most of it remains there. This phenomenon enables larger lactate recovery under current load conditions than in Donnan Dialysis separation.

Under current reversal conditions, a dynamic preferable ion transport is predicted at each interface. For instance, the lactate flux enhancement at the AEM1$^-$ interface is faster than the hydroxide flux reduction under negative current conditions. This is connected to Faraday's law condition that must be fulfilled dynamically. The ion fluxes react instantaneously at every sampling time. Therefore, lactate flux overshoot is the complement of the hydroxide flux to fulfill Faraday's law. The difference in the lactate flux overshoot magnitude is provoked by the fact that the hydroxide flux enhancement is slower that its reduction. It is believed that this happens since lactate is preferably transported at that interface. The high lactate concentration at the membrane interfaces facing the feed channel favor the lactate transport. To illustrate our interpretation, lactate and hydroxide fluxes across AEM1$^-$ are depicted in Fig. 4.7.

It is important to mention that in the feed channel and the adjacent boundary layers the lactate is present in both dissociated and undissociated form. To quantify total lactate both species must be accounted for.

Sodium flux was investigated in order to evaluate the effectiveness of Donnan exclusion. From previous work in this electrochemical system, it was concluded that

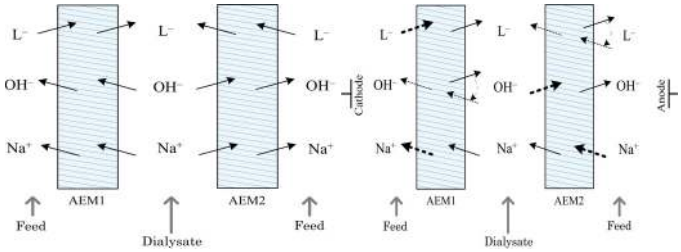

(a) Static Donnan Dialysis **(b)** Negative current density

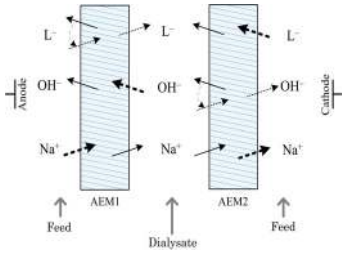

(c) Positive current density

Figure 4.6: Schematic representation of ion transport under current reversal conditions until steady state is achieved before the current is reversed. The strength of the imposed current density is $I_d = 100$ A/m^2 and it is reversed every 8000 s (2.22 h). Bold hatched lines represent large transient fluxes. Dashed and solid lines correspond to diminished and enhanced fluxes, respectively. Transient flux inversions are depicted by double arrows besides the respective ion

statically Donnan exclusion is very effective during Donnan Dialysis and Electro-Enhanced Dialysis (Prado-Rubio *et al.*, 2010b, 2011b). It was confirmed that Donnan exclusion effectiveness remains dynamically, since sodium flux is at least three orders of magnitude smaller than lactate and hydroxide fluxes.

In Fig. 4.8b, total dynamic lactate flux arriving to the dialysate channel is depicted. Additionally, the static Donnan Dialysis total lactate flux is shown (the total flux is quantified using according to Eq. 4.17). It is clearly seen that the current reversal generates periodic operation. Fig. 4.8a shows lactate total flux during one period of operation. The lactate flux through the boundary layers in the dialysate channel are depicted as well (J_{BLII^+} and J_{BLIII^-}, respectively). The static lactate flux is approximately 65% larger than during Donnan Dialysis. In a fair comparison, the static flux is expected to be much larger than under Donnan Dialysis conditions. The reason is that the fouling issue is not accounted for during Donnan Dialysis calculations. Due to the increasing resistance with time, the ion flux will decrease when there is no external electrical potential gradient. On the other hand, the ion fluxes obtained during REED operation potentially can be recovered after each time reversal, thereby ensuring longer operation time without a significant flux decrease.

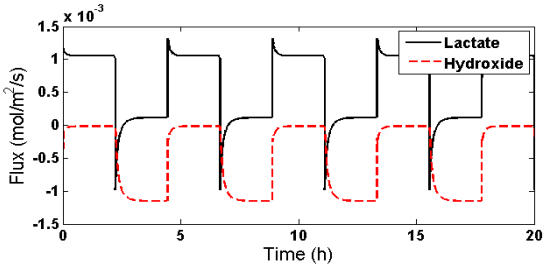

Figure 4.7: Dynamic lactate and hydroxide flux through AEM1$^-$ for a reversal time of 8000 s (2.22 h)

$$J_{L^-,tot} = \frac{1}{2}\left(J_{L^-,BL\ II^+} - J_{L^-,BL\ III^-}\right) \tag{4.17}$$

After the current polarity is reversed, there is a steep reduction of the total lactate flux. This model predicts that lactate flux arriving to the dialysate channel is reduced faster than the flux enhancement after every polarity change (see Fig. 4.8a). As a consequence, the total lactate flux decreases at first but recovers afterwards. The minimum lactate flux is achieved approximately 4.7 min after the half period time. There is a time interval ($\approx$ 8.3 min) where the total lactate flux is lower than during Donnan Dialysis.

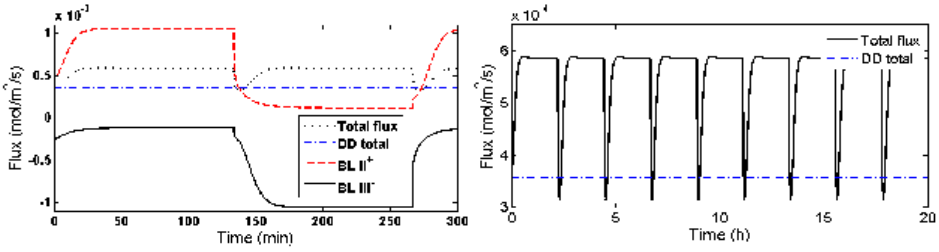

(a) One period **(b)** 4.5 periods

Figure 4.8: Dynamics of total lactate flux to the dialysate channel for a reversal time of 8000 s (2.22 h). The steady state Donnan Dialysis flux is depicted. One period operation is enlarged including J_{BLII^+} and J_{BLIII^-}

Preliminary experiments with REED operation using prepared solutions of lactic acid, showed a loss of current efficiency compared to Electro-Enhanced Dialysis (Rype, 2003). Using a simple mathematical description of the process, the experimental current efficiency loss was explained by shorter process operation at not fully developed concentration profiles.

From our simulation results, the loss of current efficiency has shown to be a consequence of the transient ion transport under current reversal conditions. After the

current is reversed, the anion exchange membranes are filled either with lactate or hydroxide ions. During the next current reversal the accumulated material is released toward both dialysate and feed channels. The ions returning to the source channel are quantified by the transient ion flux inversion after the current reversal. In a qualitative way, current is used building the lactate concentration profile within an anion exchange membrane. When the current is reversed and lactate returns to the feed channel, then part of this energy is lost. The symmetry of the modeled section permits to have the same phenomena independently of the polarity of the current.

4.5.3.2 Short current reversal time

This second scenario is investigated to understand the system when it does not achieve steady state before the current is reversed. The state values before the current polarity is reversed are the initial conditions for the following half period simulation. Consequently, the dynamic response shows additional features than analyzed above. The selection of the operating period time is a trade off between the carboxylic anion recovery and the energy consumption, subject to the operational constraints (Prado-Rubio *et al.*, 2009b). For illustration purposes, a period time of 600 s was selected. This value also has been used experimentally (Rype, 2003). The calculated dynamic lactate flux response in the two anion exchange membranes is depicted in Fig. 4.9.

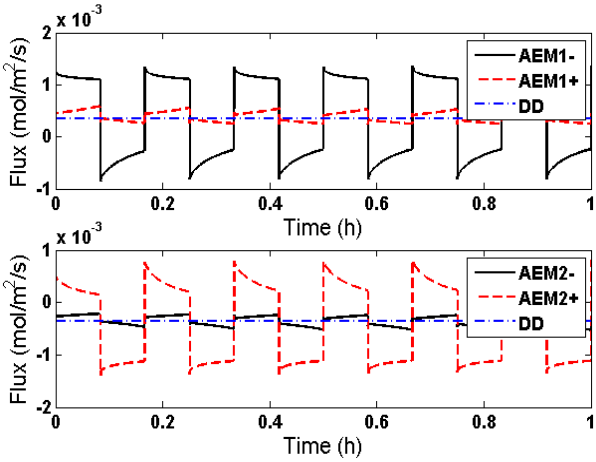

Figure 4.9: Dynamic lactate fluxes through the both sides of each anion exchange membrane (AEM) for a reversal time of 300 s (5 min). The signs -/+ stand for the left and right side of the membrane, respectively. The static Donnan Dialysis flux is depicted in each plot

The half period delayed symmetry situation predicted for a long period time, remains in this simulation. This is expected since the symmetry is due to the modeled section. The transient lactate flux inversion at the membrane interfaces

adjacent to the feed channel ($AEM1^-$ and $AEM2^+$) is clearer here, since the current is reversed before the lactate flux settles. During the first half period, the lactate flux entering the membrane across $AEM1^-$ is more than double the flux leaving through $AEM2^+$. Therefore, lactate ions fill the membrane during this half period. When the current is reversed, the accumulated ions are depleted from the membrane toward both channels. A larger amount is going back to the feed channel. This implies that shorter reversal times adversely affect the total lactate flux toward the dialysate channel. The lactate flux through the membrane interfaces facing the dialysate channel is very similar to the Donnan Dialysis lactate flux.

A schematic representation of the ion flux direction, magnitude and tendency is illustrated in Fig. 4.10. Lactate and hydroxide fluxes are very similar in magnitude but opposite in direction, in order to fulfill Faraday's law. This similarity is due to Donnan exclusion and the absence of protein within the membrane. Under negative current density, lactate accumulates in AEM1 due to the enhanced anion migration flux toward the anode. In this case, the fast lactate flux enhancement at $AEM1^-$ is represented by a dashed bold line.

For short periods, the total lactate flux is illustrated in Fig. 4.11. Clearly, the ion fluxes do not achieve steady state values before the current is inversed. This situation implies that several pulses are required to achieve stationary periodic operation. As anticipated, short period time implies that the total lactate flux is just slightly higher than during Donnan Dialysis.

From a current efficiency point of view, there is a radical effect when the current reversal time is reduced. The current is consumed filling the membrane with lactate/hydroxide ions but just a fraction passes through it before the current is reversed.

4.5.4 Lactate productivity

A dynamic productivity function was employed (Prod) to quantify the lactate removed from the feed stream. Productivity is defined as the molar lactate flow rate into the dialysate channel:

$$Prod_{L^-}(t) = q_{dia}\left(C_{L^-}^{db}(t) - C_{L^-}^{dbin}(t)\right) \tag{4.18}$$

For different reversal times, an average productivity is employed. The average productivity per half period is defined as follows:

$$\overline{Prod_{L^-}} = \frac{\int_0^{t_{rev}} Prod_{L^-}(t)dt}{t_{rev}} \tag{4.19}$$

The average lactate productivity is evaluated for each reversal time under stationary operation. Stationary periodic operation is achieved when the average lactate productivity is constant from period to period. The integral was evaluated employing the composite Simpson rule. The average productivity as a function of the reversal time is depicted in Fig. 4.12. Donnan Dialysis operation is used as reference point.

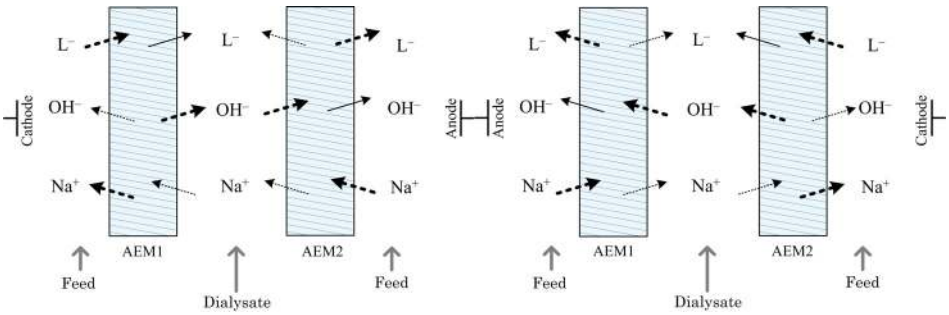

(a) Negative current density **(b)** Positive current density

Figure 4.10: Schematic representation of ion transport under current reversal conditions during short period operation. The strength of the imposed current density is $I_d = 100$ A/m^2 which is reversed every 300 s. Dashed and solid lines correspond to diminished and enhanced fluxes, respectively. Bold dashed lines represent larger transient fluxes

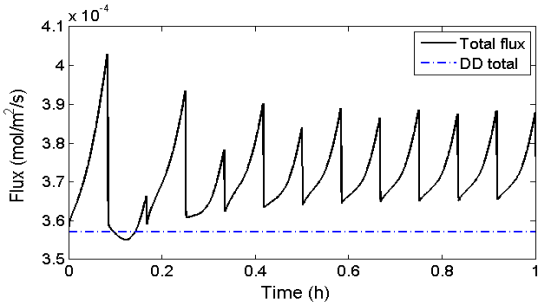

Figure 4.11: Dynamic total lactate flux arriving the dialysate channel for a reversal time of 300 s (5 min). The steady state Donnan Dialysis flux is also depicted

It can be seen that for short reversal times, the average lactate productivity increases almost linearly. This conditions remains up to a reversal time of approximately 20 min. For higher reversal times, the average lactate productivity does not improve considerably by increasing the operating time before the current is reversed. For long operating periods, the ion flux practically achieve steady state before the current is reversed. This condition implies that the average lactate productivity does not increase substantially.

From these results, the first intuitive conclusion is to operate REED using a relatively long reversal time, and then achieve higher lactate recoveries. Eventually, if the current is not reversed it corresponds to operate the module as Electro-Enhanced Dialysis. However, using high current reversal times has a price which has been qualitatively discussed in section 4.3.1, and further investigated in the next section.

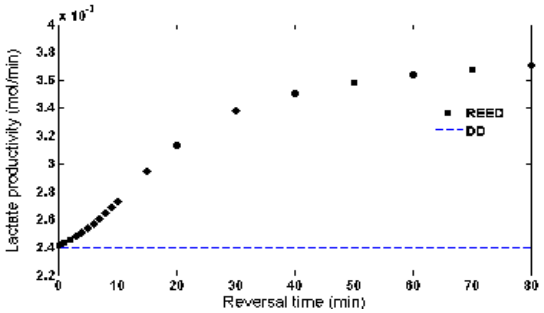

Figure 4.12: Average lactate productivity as a function of the reversal time for a current of $I_d = \pm 100$ a/m^2 and C^{dbin}_{NaOH}=50 mol/m^3. The maximum Donnan Dialysis productivity is depicted

4.5.5 Resistance build-up and energy consumption

The main drawback of using long reversal times is the energy requirement to maintain constant current density operation. For that reason, it is important to identify a potential REED reversal time operating window. The influence of other operational variables, such as the hydroxide concentration in the dialysate channel and imposed current density, is not currently investigated. The reason is that those inputs can be used to facilitate the pH control in the fermenter (Prado-Rubio *et al.*, 2010a).

At this point, it is desired to quantitatively illustrate the adverse influence of a fouling layer formation during periodic operating conditions. Even though the nature of the fouling layer is unknown in this specific application, i.e. charged or neutral fouling layer, some experimental data can be used. Previous experimental work has measured the electrical potential gradient across a REED cell during lactate recovery from brown juice from food pellet industry (Rype, 2003). The numerical values are depicted in Fig. 4.2. From these data, the potential gradient build up was approximated with a linear function.

$$\Delta V(t) = \Delta V_o + \lambda t \tag{4.20}$$

where ΔV is the time variant electrical potential gradient, ΔV_o is the electrical potential gradient corresponding to the initial cell resistance and λ is the electrical potential build up rate. It can be seen in Fig. 4.2 that the initial potential gradient of the cell (ΔV_o) is practically regained after the current is reversed regardless the polarity. The average value is used for the model. In contrast, the electrical potential gradient build up rate is characterized by two different values, according to the direction of the current. The positive electrical potential gradient build up rate (λ_+) is larger than for negative electrical potential build up (λ_-). Numerically, $\overline{\lambda_+}$ is more than twice $\overline{\lambda_-}$. The reason for this asymmetric condition might have been due to physical differences between the two channels. For illustration purposes, the larger slope is used in the linear potential gradient model. The values are $\Delta V_o = 1.4446$ V and $\lambda = \pm 3.0118$ V/min. In order to render this model compatible with the simulations performed previously, the potential gradient was scaled due

to the differences in the employed current densities. The scaling was done using Ohm's law, assuming that the resistance model is dependent of the imposed current density. This procedure leads to $\Delta V_o = 0.5778$ V and $\lambda = \pm 1.20472$ V/min.

The energy density consumed in a reversal time interval can be estimated from the following expression:

$$E = I_d \Delta V(t) t = I_d t_{rev} \Delta V_o + \lambda I_d t_{rev}^2 \tag{4.21}$$

where E is the energy density consumption, I_d is the imposed current density and t_{rev} is a half period of time. The maximum potential gradient that must be imposed and the energy density consumption as a function of reversal time are depicted in Fig. 4.13.

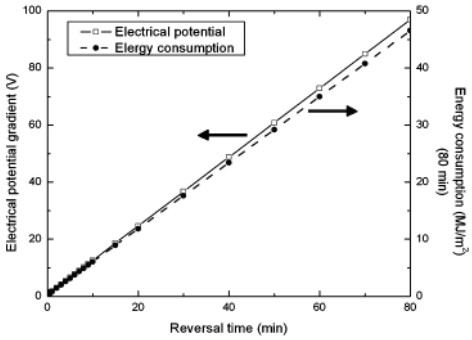

Figure 4.13: Maximum required potential gradient and energy density consumption of a REED cell, as a function of the reversal time for pulse changes in current density $I_d = \pm 100$ A/m^2 and C_{NaOH}^{dbin}=50 mol/m^3

Eq. 4.21 estimates the energy density consumed during half period of operation. In order to compare the energy consumed for all reversal times, the value estimated from the equation is scaled to be the energy consumed by the cell if it is operated during 80 min, which is the maximum reversal time employed in these simulations.

The energy consumption in an electrochemical system was investigated previously (Narbęska and Staniszewski, 1998b). Electrodialysis was applied to recover lactate from a solution of sodium lactate. Through that example, the substantial adverse influence of working with a fermentation broth can be seen. There are important differences between the Electrodialysis experimental setup and the REED module, especially: the feed solution, the membrane configuration and the operational mode. However, it is believed that the relevant difference regarding energy consumption is the fouling issue. The energy consumed by Electrodialysis was 0.297 MJ/mol/h, while an energy consumption up to 13.16 MJ/mol/h was predicted for REED (max t_{rev}=80 min, See Fig. 4.14). The large differences can be explained by the increasing electrical resistance which is not evidenced when clear solutions are used. Comparable energy consumptions are achieved with REED by operating at relatively short reversal times (around 40 s.).

Prolonged operation at constant current requires a higher potential gradient and therefore the energy consumption increases as well. However, there is a maximum potential gradient allowed due to the power source constraint, which defines the operating window for the REED unit. Once the current source reaches its limit, operation at constant current conditions is no longer feasible. This means that the operational mode switches to constant voltage conditions, implicating a reduction in the ion flux and lactate productivity. It must be stressed that the presented model was not developed to predict operation under constant voltage conditions.

This qualitative illustration can not be numerically relevant due to the lack of information about the fouling layer characteristics. However, the objective of this section was to identify the factors which define the constraints for an optimization problem. The trade off between the current efficiency loss and energy requirements as a function of the reversal time is clear in Fig. 4.14. The current efficiency (η) is used in Electrodialysis to measure the fraction of the energy added which is utilized for the target separation. The average current efficiency is estimated using the Eq. 4.22.

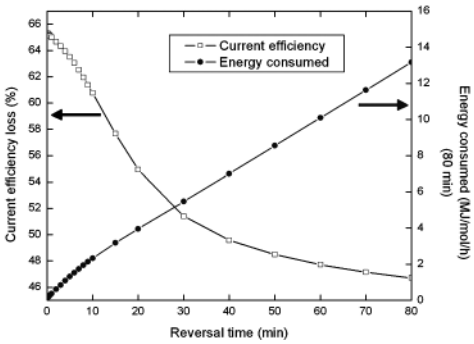

Figure 4.14: Stationary average current efficiency loss and energy density consumption as a function of the reversal time

$$\overline{\eta} = -\frac{z_{L^-} F q_{dia} (\overline{C_{L^-}^{db}} - C_{L^-}^{dbin})}{n I_d A_m} \tag{4.22}$$

where z_{L^-} is the lactate valence, F is the Faraday constant, $q_{dia}(\overline{C_{L^-}^{db}} - C_{L^-}^{dbin})$ is the average lactate productivity, n is the number of cell pairs in the stack and $I_d \cdot A_m$ corresponds to the total current through the module. The numerator of the current efficiency equation can be understood as the average amount of electrical current that the recovered lactate ions carried. The denominator normalizes that magnitude by the total current added to the system. Implicitly, the current efficiency equation assumes that the target ion was recovered only by means of the imposed current. The contribution of migration by the induced electrical potential gradient and diffusion are not accounted for. The ion transport due to the mentioned phenomena can influence the total target productivity either positively or negatively. Therefore,

the average current efficiency is biased. To calculate the current efficiency loss, we assumed that the maximum efficiency is 100% ($\overline{\eta_l} = 1 - \overline{\eta}$).

Under current reversal conditions, the maximum current efficiency is obtained just before the polarity is reversed, analogously to the lactate productivity function presented in Fig. 4.16. Thus, long reversal time implies a better current utilization, especially when the concentration profiles are fully developed. At short reversal time, there is a high current efficiency loss since the current is utilized to fill the membrane with ions, and just a fraction is transported through as shown in Fig. 4.9. On the other hand, longer operation without reversing the current requires more energy due to the electrical resistance build up.

Experimentally, the current efficiency was estimated during REED operation using a clear lactic acid solution (Rype, 2003). The experimental conditions were: type of anion exchange membrane (Neosepta ASC), feed lactate concentration (7%), current density (250 A/m^2), flow conditions (16.2 l/h), no pH buffer effect (lactic acid solution) and reversal time (60 s). Over a large pH range, the experimental current efficiency was approximately 55%.

For the simulations, Neosepta ASC properties were taken from literature (Sarmidi *et al.*, 2001) and the flow conditions are kept as shown in Table 4.3. The total lactate concentration at the inlet is reproduced but to ensure numerical stability, the employed current density is 200 A/m^2. The predicted current efficiency for t_{rev}=60 s is 51%. Despite the model parameters were estimated for a different membrane and flow conditions, the results are fairly similar.

The large adverse influence of reversal conditions on the current efficiency is mainly due to the large capacity of the membrane relative to the amount of ions transported. The high membrane fixed charge is crucial for the permselectivity, but the thinner Neosepta ACS showed a substantially better current utilization than Neosepta AMH.

From the current efficiency trend, it can be concluded that the optimal reversal time represents a trade off between the carboxylic anion productivity and the energy consumption, subject to the power and safety constraints introduced by the selected design. The location of optimum reversal time depends on the weights of both contributions on the objective function.

4.6 Conclusions

A Reverse Electro-Enhanced Dialysis process has been investigated as a novel technology to recover lactate from a fermentation broth. This model based study is supported by prior experimental and modeling work. The main goal of this investigation is to provide insights, vital for the REED process design and operation.

Simulations were performed to investigate the dynamic ion fluxes through each interface in the system. The transport mechanism has shown to be more complex than predicted in previous research. The system has shown to have lactate accumulation or depletion in the membranes, transient flux inversion, flux symmetry and preferable ion transport at the interfaces. The interpretation of those phenomena is an important contribution of the presented investigation, since they trigger the development of a transient lactate recovery when the current is reversed. Therefore, the experimentally observed loss of current efficiency can be explained.

From this modeling work, the total lactate flux independence of the current polarity was predicted. This result is relevant from control point of view, since the current density could be used as manipulated variable without account for the polarity. Additionally, the influence of the base concentration in the separation makes it interesting to investigate for control purposes. However, the REED operation might be challenging due to the non linear system behavior within the period and from period to period.

The relatively large ion exchange capacity of the Neosepta AMH has shown to be crucial for the separation. However, it has a negative influence on the current utilization under current reversal conditions. Therefore, a thinner membrane like Neosepta ASC would be more appropriate from a current utilization point of view. Additionally, it was predicted that the reversal time must be selected as a trade off between current efficiency loss and energy consumption. Therefore, REED technology only should be used when fouling has a considerably negative impact on the separation. Validation of the dynamics can be improved by dedicated dynamic experiments designed for parameter estimation.

Finally, this model was implemented as a tool which can be used to study the competitive ion transport through ion selective membranes. Therefore it is useful for development of an optimal design and operation of REED in dependence of different production objective functions.

4.7 Acknowledgment

The authors acknowledge the support from the Sixth framework project of the European Union: NMP2-CT-2007-O2b515 IP "BIOPRODUCTION".

4.8 Appendix

Here, complementary information about the system behavior is presented.

4.8.1 Dynamic Bulk concentrations

The dynamic lactate concentration in bulk channels displays a direct reflection of the fluxes calculated above. To illustrate the concentration evolution in the channels, the simulation for short current reversal time is employed. The lactate concentration in the feed and dialysate channels when t_{rev}=300 s is depicted in Fig. 4.15.

Analyzing the fluxes, it was predicted that accumulated lactate ions within a membrane during half operating period are depleted by reversing the current polarity. A larger amount of lactate ion is returning to the feed channel, as seen in Fig. 4.15a. After the reversal in polarity, lactate concentration in the feed channel rises fast but starts decreasing slowly since lactate is extracted as well. The lactate concentration in the dialysate channel follows exactly the same evolution as the total lactate flux calculated previously.

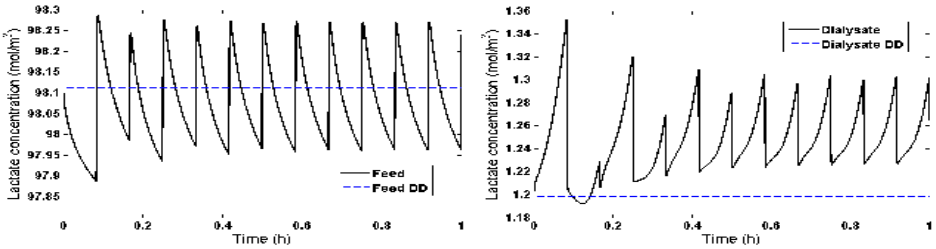

(a) Feed channel **(b)** Dialysate channel

Figure 4.15: Lactate bulk concentration in the feed and dialysate channel. Current reversal time t_{rev}=300 s (5min). Static Donnan Dialysis concentration of lactate are shown

4.8.2 Dynamic lactate productivity

As an example, lactate productivity for a current reversal time of 600 s is depicted in Fig. 4.16. The dynamic behavior completely follows the lactate concentration profile in the dialysate channel, since the dialysate flow rate q_{dia} is a constant value.

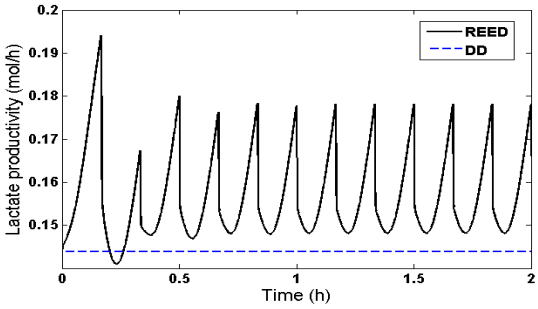

Figure 4.16: Lactate productivity evolution for a current of $I_d = \pm 100$ a/m^2 when it is reversed every 600 s (10 min) and C^{dbin}_{NaOH}=50 mol/m^3. Dashed line represents the maximum productivity achievable during Donnan Dialysis

4.9 List of symbols

AEM	Anion Exchange Membrane
BL	Boundary layer
C	Concentration (mol m^{-3})
D	Diffusion coefficient (m^2 s^{-1})
DD	Donnan Dialysis
E	Fractional membrane water content (-)

E	Energy density consumption (J m^{-2})
EDD	Electro-Enhanced Dialysis
F	Faraday constant (C mol^{-1})
I	Current (A)
I_d	Current density (A m^{-2})
J	Flux (mole m^{-2} s^{-1})
h_i	Channel i height (m)
k	Kinetic parameter (-)
K_a	Acid dissociation constant (mol m^{-3})
K_d	Dissociation constant (mol m^{-3})
K_w	Ionic product for water (mol^2 m^{-6})
L	Channel length (m)
$Prod$	Productivity (mol/h)
$\overline{Prod}$	Average productivity (mol/h)
q	Flow rate (m^3 s^{-1})
R	Electrical resistance (Ohm)
R	Universal gas constant (J mol^{-1} K^{-1})
$REED$	Reverse Electro-Enhanced Dialysis
R_k	Total reaction rate of k (mol m^{-3} s^{-1})
t	Time (s)
T	Absolute temperature (K)
t_{rev}	Reversal time (s)
V	Electrical potential (V)
x	Spatial direction (m)
y	Spatial direction (m)
W	Channel width (m)
z	Dimensionless distance $z = x/\delta_m$ (-)
z_k	Valence of k (-)

Greek letters

δ_m	Membrane thickness (m)
η	Current efficiency (-)
η_l	Current efficiency loss (-)
γ	Parameter in the diffusion model (-)
λ	Potential build up rate (V/min)
ψ	Electrical potential (V)
ψ_n	Nominal potential ($\psi_n = RT/F$) (V)
σ	Parameter in the diffusion model (-)
τ	Dimensionless time ($\tau = t/\tau_n$) (-)
τ_{dia}	Residence time in dialysate channel ($\tau_{dia} = h_{dia}WL/q_{dia}$) (s)
τ_{diff}	Diffusion time ($\tau_{diff} = \delta_m^2/D_{k,p}$) (s)
τ_{feed}	Residence time in feed channel ($\tau_{feed} = h_{feed}WL/q_{feed}$) (s)
τ_n	Nominal time ($\tau_n = 1$) (s)

φ	Dimensionless potential ($\varphi = \psi/\psi_n$) (-)

Subscripts

AEM	Anion Exchange membrane
BL	Boundary layer
dia	Dialysate channel
$feed$	Feed channel
fix	Fixed charges in the membrane
HL	Lactic acid
HP	Undissociated protein
in	Inlet
i	Species
j	Discretization point $j = 0, ..., 7$
k	Species
L^-	Lactate ion
Na^+	Sodium ion
OH^-	Hydroxide ion
P^-	Dissociated protein
p	Zone (phase)
tot	Total
z	specific location (z-coordinate)

Superscripts

db	Dialysate bulk
$dbin$	Dialysate bulk inlet
fb	Feed bulk
$fbin$	Feed bulk inlet
m	Membrane
s	Solution
$-/+$	Left/Right side of a section

Part II

Integrated system analysis

5

Unstructured fermentation model development

5.1 Abstract

This work is focused on modeling lactic acid fermentation suitable for integration with the previously derived model for Reverse Electro-Enhanced Dialysis (REED) (Prado-Rubio *et al.*, 2011a). In order to further understand the interaction between the Reverse Electro-Enhanced Dialysis module and the bioreactor, it is desirable to develop a dynamic model for the fermentation. This model should describe the lactate production rate as a function of key operating variables such as substrate, biomass and product concentrations. The structure of a published fermentation model is modified. The kinetic parameters are estimated using experimental data from literature and mathematical and statistical tools. As a result, a reasonable model which is feasible for integration with the REED module is obtained. The developed kinetic model is employed to estimate the dilution rate and input substrate concentration to achieve the best total lactate productivity, in a continuous fermentation.

5.2 Introduction

In bio-systems modeling the present trend is to exploit the growing fond of knowledge of intracellular metabolism, to increasingly substitute heuristic-based models by mechanistic representations of the cell behavior. As a consequence, the predictive power of the models is augmented. The complexity of the metabolism of a cell lies in the hundreds of reactions subject to internal regulatory mechanisms. However, the cellular control systems are not yet well understood, therefore it is necessary to employ different assumptions and modeling approaches according to the specific model purpose. Traditionally, fermentation processes have been modeled employing unstructured biomass models. The model parameters are estimated from measurement of extracellular metabolite and biomass concentrations. Even though these models do not provide insight into cellular physiology and thus their predictive power is limited, they have been widely used in engineering since they provide a simple representation of cell growth especially for prokaryotic organisms (Nielsen *et al.*, 2003).

The main challenges during parameter estimation of a large number of kinetic parameters have been investigated and summarized by Kristensen (2003). The non linear nature of the model makes the estimation problem most likely non convex,

thus it has local minima. The global minimum is the target solution since it hopefully provides the most biologically reasonable set of parameters. In order to ensure that the solution is close to a reasonable minimum, a good quality of initial parameters guesses is vital. The selection of the initial estimates must be supported by physiological understanding. The robustness of the solution must be verified using different sets of initial conditions. It has been noticed that in biological systems there is a strong correlation between the rate and affinity constants in Monod based kinetic expressions (Holmberg, 1981). Therefore, they are difficult to estimate from standard batch experiments. The insensitive set of model parameters can be reduced by using experimental data from different operation modes.

In order to reduce the influence of model structure error, the model development procedure should be supported by statistical tools. In this contribution, sensitivity based metrics are employed to increase the reliability of the proposed model. Sensitivity analysis can be described as a variance analysis where the output variance is decomposed with respect to each model parameter (Salteri *et al.*, 2006). In that way, the influence of an individual input parameter on the predicted output is quantified. Thus, a sensitivity analysis can assist both parameter estimation and model unfalsification stages. Additionally, the results of the sensitivity analysis can be exploited to design future experiments that potentially can reduce the uncertainty. It should be stressed that sensitivity analysis is a powerful framework, but absolute conclusions can not be obtained from it. The main limitations are firstly that it is based on local sensitivity calculations that become a limitation in non convex optimization problems. Secondly, the results can be affected by the selection of scale factors and therefore these factors must be carefully selected. Finally, prior knowledge of the model parameters is crucial. For those reasons, the statistical analysis must be coupled to expert knowledge of the process and model. Uncertainty and sensitivity analysis methodologies have been successfully employed in other applications (McKlay *et al.*, 1999; Brun *et al.*, 2002; Sin *et al.*, 2009, 2010).

The purpose of this chapter is to develop a model for the fermentation which may be usable for investigating the integrated operation of the REED separation with the bioreactor. Therefore, this model should (ideally) be able to describe the disturbance dynamics which are imposed by the REED operation in order to obtain a valid representation of the integrated system. The operational requirements of the integrated system are to handle start up, i.e. batch or fedbatch operation, as well as continuous operation. In addition, the integrated system should also enable control of pH. In the case of the continuous operation additional variables should be controlled, i.e. lactate, substrate, biomass, etc.(determined by the analysis of the operational degrees of freedom).

Since control during batch/fedbatch as well as continuous operation is desired, a fairly reasonable accuracy of the fermentation model is required at low to medium frequencies. However, the pH dynamics from period to period in the REED module will also influence the fermenter behavior, thus ideally also high frequency pH disturbances should be well described by the bioreactor model. These requirements are rather high for a fermenter model.

Due to experimental work was not available within this project, it is decided to search in the literature for a model which can describe both batch and continuous operation. A model developed by Boonmee *et al.* (2003) is able to describe both

batch and continuous fermentations of *Lactococcus lactis*. Therefore this model will be analyzed to reveal to which extend this type of model structure and experimental data behind may be used as basis for modeling the bioreactor in this work.

This contribution is structured as follows: lactic acid fermentation is introduced and the fermentation model presented. The reported kinetic model is described and the proposed structural modification introduced. Subsequently, the methodology for parameter estimation is depicted and the required tools presented. Afterwards, the structure of the kinetic model is investigated and the relation with the published model is elucidated. The full model parameter set is regressed. Due to the correlation between parameters, an identifiable parameter subset is estimated. Finally, the kinetic model is used to find the best operating conditions for total lactate productivity during continuous fermentation.

5.3 Model development

The most important reactions taking place in the reactor during lactic acid fermentation are modeled. In this multicomponent system, a carbon source is transformed by the microorganisms into lactate and biomass. A dynamic model is derived to represent the substrate consumption, biomass growth and lactate production. Additionally, the model accounts for the dissociation of the main monoprotic acids. The fermentation is performed in a stirred bioreactor operated in either batch/fed batch or continuous mode with a recycle stream coming from the REED module. A sketch of the fermenter and involved streams are depicted in Fig. 5.1.

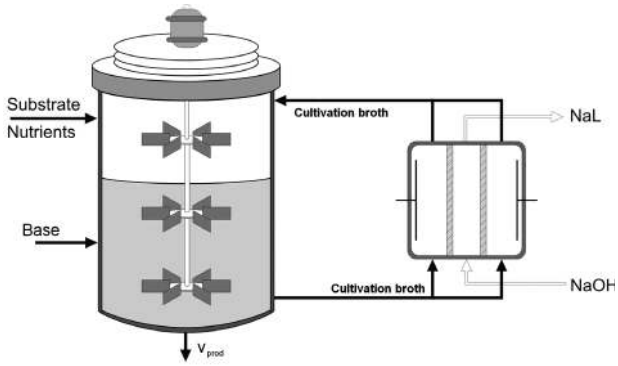

Figure 5.1: Sketch of the integrated bioreactor with the REED module for a batch/fed-batch/continuous fermentation

The bioreactor has two input streams, one for the required substrate and nutrients and another that allows pH control by adding a base solution. The cultivation broth is continuously sent to the REED module where lactate is exchanged by hydroxide while substrate and biomass are recirculated. The lactate is recovered as sodium lactate in the dialysate channels in the REED module. During continuous operation, a purge stream in the fermenter is necessary to avoid accumulation.

5.3.1 Model assumptions

The main assumptions for the fermenter model development are (FA):

FA1. The biomass growth is influenced by carbon source limitation and inhibition at low and high concentrations, respectively. Additionally, growth is also inhibited by the primary fermentation product concentration. Substrate limitation is modeled using a Monod expression and substrate inhibition follows a non-competitive inhibition function. The biomass growth is not affected by pH.

FA2. There is only one carbon source.

FA3. The feed stream contains the main carbon source at a known pH. Phosphate, nitrogen source, salt and vitamin uptakes are not investigated, presently.

FA4. The fermentation is considered homofermentative with lactic acid as product. However, the product inhibition is caused by the total lactate concentration in the media (L^- and HL).

FA5. The assumption MA2, where the transport of water by osmosis and electro-osmosis is neglected in REED, implies that there are no changes in the volumetric flow rate of the recycle stream.

FA6. Mass balances are formulated for: biomass, carbon source, lactate, dissociated protein, sodium, lactic acid, undissociated protein and hydroxide.

FA7. The pH of the fermenter is perfectly controlled. When the pH regulation is investigated, pH is adjusted by adding a solution of sodium hydroxide.

FA8. The protein production rate has been chosen such that the total protein concentration in the fermenter remains constant. In that way the buffer effect induced by the protein dissociation is kept constant. The hypothetical protein species (HP and P^-) represent a wide range of molecules that could induce a pH buffer effect in the fermentation broth. Due to the lack of understanding of the pH buffer source, it is assumed a protein production rate which keeps the total concentration constant.

FA9. Substrate uptake and product formation are similarly to growth rate limited at low and high substrate concentrations, respectively ($K_{ss} = K_{sp}$ and $K_{is} = K_{ip}$).

FA10. Lactic acid inhibition term affects substrate uptake and product formation equally ($C_{L,1/2s} = C_{L,1/2p}$)

FA11. The separation effect of the REED module is not accounted for in the fermenter model development. This is done by eliminating the recirculation flow rate ($q_{feed} = 0$).

FA12. For lactate concentrations higher than the maximum value for cell growth (P_{mx} in the reported model), the biomass concentration remains constant. It means, there is no viability loss or cell lysis.

5.3.2 Mass balances

The generalized mass balance for component k and the volume change in a bioreactor with recycle can be written as follows:

$$\frac{dC_k}{dt} = \frac{q_{feed}}{V}\left(C_k^{rec} - C_k\right) + \frac{\upsilon_{base}}{V}\left(C_k^{base} - C_k\right) + \frac{\upsilon_{feed}}{V}\left(C_k^{in} - C_k\right) + R_k \qquad (5.1)$$

$$\frac{dV}{dt} = \upsilon_{feed} + \upsilon_{base} - \upsilon_{prod} \qquad (5.2)$$

where C_k is the concentration of the species k in the bioreactor. A recycle stream is included with a flow rate of q_{feed}. In this mass balance, the bioreactor has a purge stream that allows to remove material with a flow rate υ_{prod}. An extra input flow rate is added to the mass balances so called υ_{base}. This stream is used to allow for pH regulation by base addition. The reaction term R_k is composed by the bioreactions plus the dissociation reactions. The dissociation reactions are shown in Chapter 2.

5.3.3 Kinetic model development

5.3.3.1 Unstructured kinetic model

The kinetics is the core of the fermenter model. An appropriate description of the microorganism growth is vital for the bioprocess design. The selection of a model structure is a crucial step during system identification. This choice must be based both on an understanding of the system identification procedure and on system insights (Ljung, 1999). A variety of unstructured models have been applied to lactic acid fermentation, those models account for the growth dependency on substrate concentration and product inhibition. The substrate concentration influence on the growth rate is usually modeled using Monod kinetics, i.e. where the growth is inhibited at certain concentration of the rate limiting substrate. The point where substrate inhibition occurs is very important, especially in batch cultivations. For the product inhibition, different types of linear and non linear functions have been investigated. A linear inhibition term has shown to be useful in several applications (Nielsen *et al.*, 2003; Boonmee *et al.*, 2003). However, for other cases the functionality of the product inhibition term is highly non linear, mainly exponential (Cachon and Divès, 1993; Amrane and Prigent, 1994; Åkerberg *et al.*, 1998; Burgos-Rubio *et al.*, 2000).

The growth kinetics proposed here for the prokaryote is based on the Luedeking-Piret model with inhibition (Boonmee *et al.*, 2003). This model is attractive since is capable of describing experimental data for batch and continuous fermentations with the same model parameters. This flexibility is convenient for our ultimate goal which is the investigation of the operability of the integrated bioreactor with the REED module. The published growth model includes a linear product inhibition term and substrate limitation. The substrate influence on the growth rate is modeled using an extended Monod expression, similar to Haldane equation. Besides, lactate inhibition is considered to work within a concentration band. It means, there is a threshold

lactate concentration (P_i) which is required to initiate the inhibition. On the other hand, there is a maximum lactate concentration (P_m) where complete inhibition is reached. Different values of P_i and P_m for growth and lactate production/lactose consumption were found by Boonmee *et al.* (2003). The published kinetic model, as presented by Boonmee *et al.* (2003), is shown in Eqs. 5.3 - 5.5.

$$q_x = \mu_{max}\left(\frac{s}{K_{sx}+s}\right)\left(\frac{K_{ix}}{K_{ix}+s}\right)\left(1-\frac{p-P_{ix}}{P_{mx}-P_{ix}}\right) \tag{5.3}$$

$$q_p = \alpha\frac{dx}{dt} + q_{p,max}\left(\frac{s}{K_{sp}+s}\right)\left(\frac{K_{ip}}{K_{ip}+s}\right)\left(1-\frac{p-P_{ip}}{P_{mp}-P_{ip}}\right) \tag{5.4}$$

$$q_s = q_{s,max}\left(\frac{s}{K_{ss}+s}\right)\left(\frac{K_{is}}{K_{is}+s}\right)\left(1-\frac{p-P_{is}}{P_{ms}-P_{is}}\right) \tag{5.5}$$

The number of parameters to be estimated are 16 (μ_{max}, K_{sx}, K_{ix}, P_{ix}, P_{mx}, α, $q_{p,max}$, K_{sp}, K_{ip}, P_{ip}, P_{mp}, $q_{s,max}$, K_{ss}, K_{is}, P_{is}, P_{ms}). Based on the assumptions proposed by Boonmee *et al.* (2003), the number of parameters in this model is slightly reduced (to 12). It is assumed that $K_{ss} = K_{sp}$ and $K_{is} = K_{ip}$ (FA9); $P_{is} = P_{ip}$ and $P_{ms} = P_{mp}$ (implicit in FA10). This means that substrate uptake and lactate production are affected in the same way by substrate and product concentrations.

5.3.3.2 Kinetic model structure modification

The motivation to modify the kinetic model structure lies in how the no biomass viability loss assumption is handled in the reported model (F12). The assumption states that when the maximum growth inhibiting lactate concentration (P_{mx}) is reached, the biomass concentration remains constant with no viability loss or cell lysis.

It can be seen in the Eq. 5.3, that when the product concentration is higher than P_{mx} the product inhibition term becomes negative. From a mathematical point of view, it means that the growth rate is negative. In other words, the model predicts biomass death. This contradicts the initial assumption of no viability loss. Another inconsistency can be seen when the product concentration is lower than P_{ix}, since the product inhibition term is larger than 1. Under that condition, the model predicts that the biomass growth is enhanced by the presence of the product. That scenario should be supported by experimental evidence. In order to avoid the above listed situations, the growth rate must be saturated. It can be achieved using constraints in the product inhibition term which must be between zero and one. However, using a simple saturation function for the inhibition term is a potential problem for gradient based calculations, such as the parameter estimation procedure.

Our contribution lies in modifying the lactate inhibition functionality. The basic concept is preserved for the inhibition term, but the function describing it is substituted by a normalized Boltzmann two parameter sigmoid function. Boltzmann sigmoid functions are interesting since they are continuous and monotonically increasing/decreasing between 2 defined boundaries, therefore they have smooth derivatives. These characteristics make them useful in neural networks training and gradient based calculations (Baughman and Liu, 1995; Rutledge and Steward, 2008).

The proposed growth model is:

$$q_x = \mu_{max}\left(\frac{C_s}{K_{sx}+C_s}\right)\left(\frac{K_{ix}}{K_{ix}+C_s}\right)\left(1-\frac{1}{1+exp\left(\frac{C_{L,1/2x}-C_L}{k_x}\right)}\right) \tag{5.6}$$

Analogously, the substrate uptake is:

$$q_s = -q_{s,max}\left(\frac{C_s}{K_{ss}+C_s}\right)\left(\frac{K_{is}}{K_{is}+C_s}\right)\left(1-\frac{1}{1+exp\left(\frac{C_{L,1/2s}-C_L}{k_s}\right)}\right) \tag{5.7}$$

The lactate production rate is given by the Luedeking-Piret model. When the product inhibition is low, the dominant lactic acid production rate has shown to be growth associated. However, at high lactate concentrations the lactic acid production rate follows a non growth associated pattern (Luedeking and Piret, 1959).

$$q_p = \alpha q_x + q_{p,max}\left(\frac{C_s}{K_{ps}+C_s}\right)\left(\frac{K_{ip}}{K_{ip}+C_s}\right)\left(1-\frac{1}{1+exp\left(\frac{C_{L,1/2p}-C_L}{k_p}\right)}\right) \tag{5.8}$$

Based on the assumptions proposed by Boonmee *et al.* (2003), the number of parameters in this model may be slightly reduced. It is assumed that $K_{ss} = K_{ps}$ and $K_{is} = K_{ip}$ (FA9), $C_{L,1/2s} = C_{L,1/2p}$ and $k_s = k_p$ (FA10). The number of parameters to be regressed is reduced from 16 to 12, analogously to the reported model.

A limitation for the kinetic model is how to define the total protein production rate. The hypothetical protein species (HP and P^-) represent a wide range of components contained in the cultivation broth from moderate molecular weight proteins to colloidal material, that could induce a pH buffer effect which is not associated to lactic acid dissociation. Due to the lack of knowledge of the source and nature of such components, it is assumed that the total protein production rate compensates for the protein which is removed/diluted in the reactor. As consequence, the total protein concentration in the fermenter is constant (FA8). Notice, that the ratio between dissociated and undissociated form of the protein still is a function of the fermenter pH.

5.4 Methodology for kinetic parameter estimation

Once the model structure is defined, a methodology is employed to estimate the kinetic parameters in the unstructured model. The parameters to be estimated are allocated in the parameter vector θ. At this stage the system identification problem is to estimate θ, evaluate the quality of estimates and confront the model to extra experimental information. For those purposes, the available experimental

data must be divided into 2 sets, one for parameter identification and the second for model validation. The purpose of the model validation is to ensure that the process noise is not modeled, e.g. through model over parametrization. That is investigated through a residual analysis test (Ljung, 1999). Another issue is to ensure the identifiability of the model parameters, which is investigated using correlation and sensitivity analysis.

The first step is to obtain initial guesses for the parameters. Secondly, the model parameters are regressed using a parameter estimation procedure. Thirdly, the model is falsified or unfalsified employing a statistical analysis. If the model is falsified, a sensitivity analysis is performed to propose a way to unfalsify the model given the existing experimental data.

5.4.1 Initial parameter guesses

In order to regress the model parameters through an optimization procedure, initial guesses are required. Those values can be obtained from (based on the ideas presented by Lei (2001)):

- Literature review to find approximate values for the kinetic parameters.
- Preliminary calculations using experimental data.
- Rough guesses based in the model structure and some experimental evidence.

If the model complexity is high, probably a manual tuning of the parameters is required to ensure convergence to a physiologically reasonable minimum. This tuning is based on a prior knowledge of the system.

5.4.2 Parameter regression

During a parameter estimation procedure, the model's ability to describe experimental data is exploited. A suitable model is able to reproduce the observed data with a small prediction error. In other words, the parameter estimation process must compute a set of parameters such as the prediction errors become as small as possible. This guiding principle can be stated as an optimization problem. Usually, the least-squared criterion is employed as shown in Eq. 5.9.

$$min_{\theta} F = \sum_{l=1}^{L} W_l \sum_{i=1}^{I_l} w_{li}^2 \sum_{n=1}^{N_{li}} \left(y_{lin} - \bar{y}_{lin}\right)^2 \tag{5.9}$$

where L is the number of different experiments, I_l the number of different measurements in the *l'th* experiment and N_{li} is the number of data points for the *i'th* measurement in the *l'th* experiment. F is the sum of the squared residuals, y are the experimental data while $\bar{y}$ are the model prediction. W_l and w_{li} are weights. When the vector θ contains many parameters, due to the stochastic nature of data it will not be possible to estimate the parameters accurately. In addition, there may be parameters about which data does not have any information, therefore, there

are advantages to force those parameters towards a fixed value. This is achieved by adding a regularization term in the objective function as follows (Ljung, 1999; Lei, 2001).

$$min_\theta F = \sum_{l=1}^{L} W_l \sum_{i=1}^{I_l} w_{il}^2 \sum_{n=1}^{N_{li}} \left(y_{lin} - \bar{y}_{lin}\right)^2 + W_{reg} \sum_{j=1}^{n_p} \lambda_j \left(\frac{\theta^{in} - \theta}{\theta^{in}}\right)^2 \tag{5.10}$$

where n_p is the number of parameters and θ^{in} is the initial value of the parameter vector. W_{reg} and λ_j are weights. During the solution of the regularized optimization, the model parameters that have a small influence on the objective function, given the available data, will be affected the most by the regularization term. Another advantage of the regularization term is when the Hessian of the least-squared part is ill-conditioned. In that case, the minimization problem will be ill-conditioned. By adding regularization, the penalty λI is added to the Hessian matrix and makes it better conditioned (Ljung, 1999).

5.4.3 Model falsification or unfalsification

After the best parameter vector is obtained, it is important to evaluate the quality of the model prediction. A number of tools are available to estimate the parameter significance and correlation between them based on a residuals analysis. Correlation between parameters indicates that the data contains insufficient information to estimate the model parameters uniquely. This analysis can be performed on the estimation or validation data set. The same conclusion can be obtained from a test for whiteness of cross-validation residuals, but it must be necessarily performed on the validation data set (Ljung, 1999). In that case, the model is said to be falsified with respect to the available information. Thus, the model structure should be reconsidered, further experiments performed or the parameter set should be reduced to a subset that can be estimated from the available data. In case the model is not falsified through the correlation analysis, the modeling cycle is terminated. Notice that the methods employed in this work employ estimation data sets and not cross-validation data, therefore the model can only be falsified. In order to unfalsify the model, new data are required to perform the residual analysis test.

5.4.3.1 Parameters confidence interval

The covariance matrix of the parameters estimators can be approximated by Eq. 5.11 (Seber and Wild, 2003).

$$COV(\theta) = \frac{1}{W_l} \left(\frac{F(\hat{\theta})}{m - n_p}\right) H^{-1} \tag{5.11}$$

where $F(\hat{\theta})$ is the objective function evaluated at the optimum solution $\hat{\theta}$, m is the number of observations, n_p corresponds to the number of parameters and H is the parameter Hessian. The Hessian is usually approximated using the Jacobian, which is the sensitivity of the model outputs $\bar{y}$ to the parameters θ ($H = J^T J$) (Nocedal

and Wright, 1999). Based on the covariance matrix, the confidence intervals of the parameters can be estimated using Eq. 5.12.

$$\Delta\theta = \theta_s \pm \sqrt{diag(COV(\theta))} \times \Big(t(m - n_p, \alpha_s/2)\Big) \tag{5.12}$$

where $diag(COV(\theta))$ represents the diagonal elements of the covariance matrix and $t(m-n_p, \alpha_s/2)$ is the t-distribution value corresponding to $\alpha_s/2$ percentile for $m-n_p$ degrees of freedom.

5.4.4 Sensitivity analysis

In order to obtain an identifiable parameters set, two conditions must be fulfilled. The available experimental data must be sensitive to individual changes in each parameter and the parameters must be uncorrelated. The first condition may be addressed by an average sensitivity measure δ_j^{msqr} calculated for every parameter θ_j. This sensitivity measure assesses the average individual parameter significance. The significance of individual parameters is important to investigate the structure of the model. In principle, insignificant parameters must be eliminated since their presence indicates that the model is overly complex (Kristensen, 2003). The absolute sensitivity matrix S is built on the model output sensitivity y_i to each parameter θ_j around the optimal solution:

$$s_{ij} = \left.\frac{dy_i}{d\theta_j}\right|_{\hat{\theta}} \tag{5.13}$$

In a dimensionless form:

$$s_{ij}^{nd} = \frac{\Delta\theta_j}{sc_i}\frac{dy_i}{d\theta_j} \tag{5.14}$$

where $\Delta\theta_j$ is an *a priori* measure of the range of θ_j and sc_i is a scale factor with the same dimension as the corresponding y_i observation. The dimensionless form of the sensitivity accounts for the different scales of the model outputs and parameters. For this analysis, it is very important to have an appropriate selection of the scale factors since the results are highly influenced thereby. The average sensitivity measure is quantified using the quadratic mean of the dimensionless sensitivity factors through Eq. 5.15.

$$\delta_j^{msqr} = \sqrt{\frac{1}{m}\sum_{i=1}^{m}(s_{ij}^{nd})^2} \tag{5.15}$$

The second condition is quantified employing the so called collinearity index, γ_K, which is calculated for a parameter subset K. K is an index given to a specific combination of parameters. According to the number of parameters in the subset,

the combinatorial is calculated as the k-combination $C_k^{n_p}$, $k \in \{2, 3, ..., n_p\}$. The collinearity index measures the degree of linear dependence between the columns of a submatrix $\tilde{S}_K$ of the normalized sensitivity matrix ($\tilde{S}$), the latest developed using Eq. 5.16 (Brun *et al.*, 2001). $\tilde{S_K}$ is an $m \times k$ submatrix containing the columns that correspond to parameters in the index K. The collinearity index equals one if the columns are orthogonal, meaning they are linearly independent. An increasing linear dependency is reflected in an increasing collinearity index.

$$\tilde{s}_{ij} = \frac{s_{ij}^{nd}}{\left\| s_j^{nd} \right\|} \tag{5.16}$$

where $\left\| s_j^{nd} \right\|$ is the Euclidean norm of the j^{th} column of the dimensionless sensitivity matrix. The collinearity index is defined as:

$$\gamma_K = \frac{1}{\sqrt{\lambda_K}} \tag{5.17}$$

where λ_K is the smallest eigenvalue of the product $\tilde{S_K}^T \tilde{S_K}$. If the columns in the submatrix $\tilde{S_K}$ are dependent, a change in the model output due to a small change in θ_j can be compensated by a change in other parameters in parameter subset K. It has been observed empirically that collinearity indexes larger than 15, the subset is poorly identifiable. An interesting characteristic of this measure is that it is independent of $\Delta\theta_j$ due to the normalization, making more general the interpretation of the results (Brun *et al.*, 2001).

5.5 Results and discussion

Our main objective is to show how the proposed kinetic structure can satisfactorily reproduce experimental data from the literature. The experimental data obtained by Boonmee *et al.* (2003) are used to re-estimate the model parameters of the proposed kinetic structure. Therefore, a reasonable model is obtained which is suitable for the integrated system analysis.

5.5.1 Experimental data

Boonmee *et al.* (2003) performed a series of batch and continuous fermentations using *Lactococcus lactis* NZ133. The cultivations were carried out in a one liter Quickfit fermenter with 400 ml working volume. The experiments took place at 30°C. The pH was controlled at 6.5 by adding 5M NaOH. The series of batch and continuous fermentations used a modified M17 medium with 20, 40, 60, 80 and 100 g/l of initial lactose. In Boonmee *et al.* (2003), the batch experiments were used for the model parameters estimation, while the continuous culture data was employed to evaluate the model quality. This strategy may be questioned since very different dynamics take place in batch versus continuous operation. When the model quality is assessed using the continuous fermentation data, only the low frequency part of the model is evaluated.

From the published simulation results, a reasonable qualitative agreement was found. Additionally, the estimated parameters values show significant similarities with values estimated for other microorganisms. However, no statistical analysis was performed.

5.5.2 Product inhibition term

When a non conventional black box model is proposed to substitute an existing unstructured function, it is relevant to reveal the meaning of the model parameters and the connection with the previous model. It can be shown analytically that the term $C_{L,1/2}$ (in Eqs. 5.6, 5.7 and 5.8) corresponds to the product concentration at the inflexion point of the Boltzmann function. Besides, the constant k is related to the inhibition function (IT) slope evaluated at the inflexion point ($C_{L,1/2}$):

$$k = -\left(4\frac{dIT}{dC_L}\Big|_{C_{L,1/2}}\right)^{-1} \tag{5.18}$$

Using the saturated kinetic model employed by Boonmee *et al.* (2003) (Eqs. 5.3 - 5.5), the product inhibition term for biomass and substrate were plotted as a function of the product concentration. This calculation is performed in order to evaluate if the proposed model structure can follow the saturated inhibition term proposed in the literature.

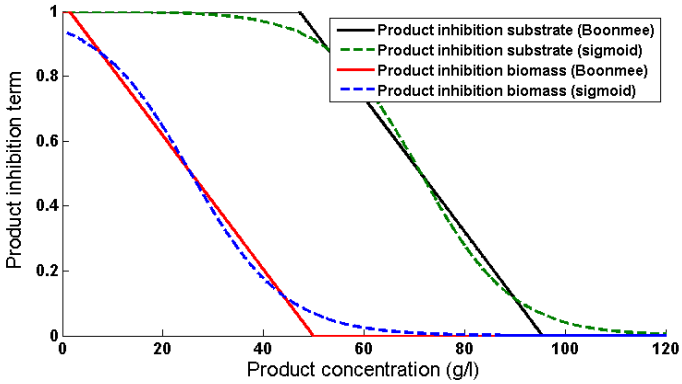

Figure 5.2: Saturated product inhibition term (solid lines) according to Boonmee *et al.* (2003) and the regressed Boltzmann sigmoid functions (dashed lines), for biomass and lactose/lactate product inhibition

From these data, the parameters required by the Boltzmann inhibition function were regressed. The methodology used for parameter estimation is a numerical method for large scale optimization, this algorithm is a subspace trust region method based on the interior reflective Newton method for non linear minimization subject to bounds (Coleman and Li, 1994), available in Matlab 2007a using the function

"lqscurvefit"(Mathworks, 2006). The objective function is the sum of the squared residuals according to Eq. 5.9, using W_l=1/2 and w_{li}=1.

The estimated parameters are depicted in Table 5.1 and the function fitting is depicted in Fig. 5.2. It can be seen in the figure how the s-shaped threshold function smoothly adjusts to the saturated product inhibition term. In general the results satisfactorily describe the location of the inhibition band, the largest differences are evidenced in the biomass model at low product concentrations.

Table 5.1: Estimated parameters for the Boltzmann inhibition term and the equivalent in the reported model (Boonmee *et al.*, 2003). The $C_{L,1/2}$ value in the literature column is estimated as the average value of P_i and P_m

Parameter	Estimated	Literature
$C_{L,1/2x}$	25.54	25.64
$C_{L,1/2s}$	71.30	71.30
k_x	9.37	-
k_s	9.13	-

From the results can be seen that the inflexion point of the Boltzmann function ($C_{L,1/2}$) can be considered as the average value of P_i and P_m for both biomass and product kinetics (see Table 5.1). The results also indicate that there are small differences between the k values in the rate expressions for biomass and substrate. For that reason, k can be considered constant in the three reaction rates, i.e. $k_x \approx k_s = k_p = k$ (Eqs. 5.6 - 5.8). Thus, the number of parameters in the proposed model structure is reduced further lower than in the published model, being at the end eleven. The product inhibition affects the biomass growth and substrate uptake at the same rate but at different product concentration. Differences in the inflexion point of the Boltzmann functions can be explained by the low biosynthetic ability of the lactic acid bacteria. Therefore the substrate uptake is usually considered decoupled of the biomass growth (Stephanopoulos *et al.*, 1998).

5.5.3 Initial parameter guesses

A reasonable set of initial conditions for the parameter estimation are the regressed values presented in Boonmee *et al.* (2003). The model structure and parameter interpretation are discussed in the paper.

5.5.4 Model parameter estimation

The initial purpose was to use the experimental data obtained by Boonmee *et al.* (2003) and then re-estimate the model parameters for the proposed model structure. Therefore, it is reasonable to use only information from the batch experiments for parameter estimation, as was done in the referred paper.

The batch data sets were divided into two groups. The first group is used for parameter estimation and the second to evaluate the model quality. The data sets used initially for model parameters regression are batch experiments with initial

substrate concentration of 20, 60 and 100 g/l of initial lactose. The kinetic model is substituted in the mass balance equation (Eq. 5.1) and it is solved according to the type of experimental data used for the parameter estimation, i.e. batch or continuous fermentation. There is a total of eleven parameters: μ_{max}, K_{sx}, K_{ix}, $C_{L,1/2x}$, k, α, $q_{p,max}$, K_{sp}, K_{ip}, $C_{L,1/2p}$, $q_{s,max}$.

The model parameters are estimated by minimizing the sum of the squared residuals employing again the interior reflective Newton method (Coleman and Li, 1994). A modification is introduced into the residual objective function compared to the method employed by Boonmee *et al.* (2003). The experimental data are normalized using the maximum value for each concentration in each experiment, as consequence all concentrations remain within zero and one. This is done through the weight vector w_{li} in the objective function. The purpose of this modification is to compensate for differences in orders of magnitude between the biomass, substrate and product concentrations. Therefore, all substances have the same weight in the objective function. The weight $W_l = 1/2$ as it is commonly used in the least squares method (Nocedal and Wright, 1999).

Due to the large number of parameters plus the non linear behavior of the system, it was expected to have a non convex optimization problem. In this investigation, different distribution of the data set for regression and quality evaluation were tested, combined with a grid of initial guesses close to the values reported by Boonmee *et al.* (2003). The solution with minimum value of the objective function was selected. The model regression on the experimental data is depicted in Fig. 5.3. The estimated parameters are listed in Table 5.2. The model prediction using the validation data set is shown in Fig. 5.4. From the figures, a qualitatively reasonably description of the experimental data is seen.

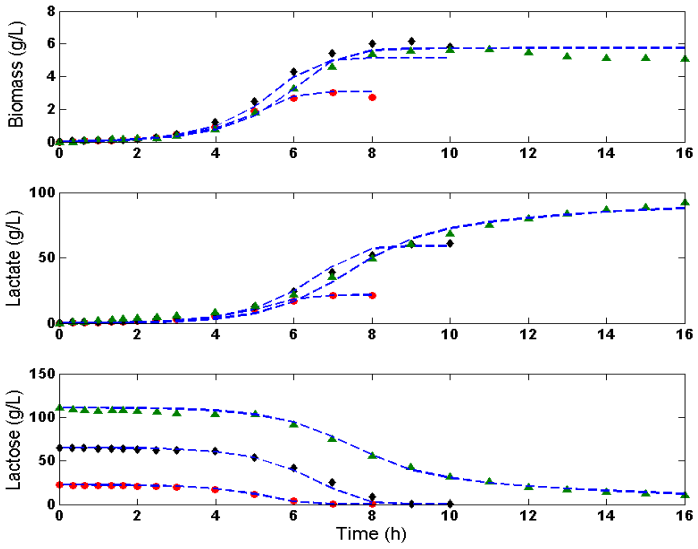

Figure 5.3: Model regression (dashed lines) on experimental data for batch fermentations (points). (•) 20 g/l lactose, (◇) 60 g/l lactose and (△) 100 g/l lactose

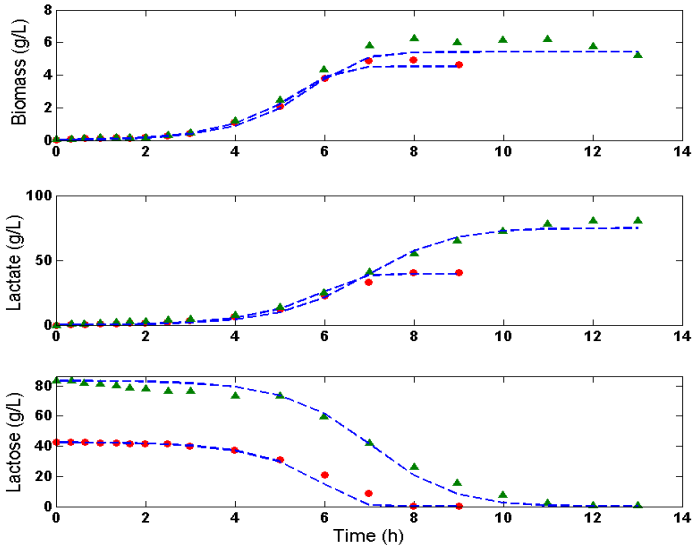

Figure 5.4: Model confrontation (dashed lines) with experimental data for batch fermentations (points). (•) 40 g/l lactose, (△) 80 g/l lactose

Table 5.2: Estimated kinetic parameters for the proposed fermentation model

	Parameter	Estimated	95% CI	Deviation	Units
1	μ_{max}	1.2471	0.1366	11 %	1/h
2	K_{sx}	6.315	0.0047	0.1%	g/l
3	K_{ix}	302.7832	151.1118	50%	g/l
4	$C_{L,1/2x}$	22.8693	5.1297	22%	g/l
5	k	8.6147	1.9371	23%	g/l
6	$q_{s,max}$	6.7458	0.5049	7.5%	g/g/h
7	K_{ss}	4.6069	2.3052	50%	g/l
8	K_{is}	145.1781	74.5589	51%	g/l
9	$C_{L,1/2s}$	63.3429	3.0572	5%	g/l
10	$q_{p,max}$	5.7108	0.2775	5%	g/g/h
11	α	0.7493	0.9291	124%	g/g

Despite the simulation results agreement, the considerable large number of parameters to estimate from the experimental data provides a motivation for estimating the parameter set using the least squares method combined with the regularization (see Eq. 5.10). However, no substantial improvements are obtained using regularization and thus only the parameters calculated through the least squared optimization are employed. The results using regularization are shown in Appendix D.

5.5.5 Model falsification or unfalsification

The confidence intervals of the estimated parameters are shown in Table 5.2. Large confidence intervals are provoked by significant correlation between the parameters. From the correlation matrix (not shown) it was found that the pairs K_{sx}-K_{ix}, $C_{L,1/2x}$-k, K_{ss}-K_{is} and $C_{L,1/2s}$-$q_{p,max}$ are highly correlated. Besides, there is significant correlation between other parameter pairs. This situation is undesired, since a parameter can take any value within the confidence interval and this unbalance is compensated by appropriate change of the correlated parameters.

It must be stressed that this analysis is local, since the Jacobian is evaluated around the optimal solution found by the parameter estimation procedure. It has been noticed that the obtained optimal parameters depend on the initial parameter guesses. This is an indication that the optimization problem is not convex and local minima are obtained. A change in the initial guesses can potentially generate a different solution and thus correlation matrix. From the above correlation analysis, it is clear that all the parameters can not be estimated uniquely from the available experimental data, even though the model reproduces the validation data sets satisfactorily. Therefore, the model with the full parameter set is falsified.

5.5.6 Sensitivity analysis

In order to have a fully identifiable parameter set, a reduction of the number of parameters to be estimated is investigated using a sensitivity analysis. This is not a straight forward task since it must be supported by an expert knowledge filter which excludes parameters from the search space that can not be reasonable estimated from the available data (Brun *et al.*, 2002). However, this exclusion can be assisted by the identifiability analysis.

As mentioned above, an important factor for these calculations is the selection of the scale factors to transform the sensitivity matrix into a non dimensional form. Previous studies have used different scale factors such as the standard deviation of the inputs and outputs (Sin *et al.*, 2009) or the mean value of the output (Brun *et al.*, 2002). In this investigation the scale factor of the output sc_i has been chosen as the mean value of the output, depending of the *i'th* measurement and the within the *l'th* experiment (according to the nomenclature used in Eq. 5.9). On the other hand, the scale factor of the parameters $\Delta\theta_j$ is the estimated value of the parameter $\hat{\theta}$. Other scale factors than the presented here were investigated, the δ_j^{msqr} has shown to be very sensitive to these. The estimated average sensitivity measure is depicted in Fig. 5.5. It can be seen that the model output is practically insensitive to parameters such as μ_{max}, K_{ix}, $q_{s,max}$ and α. Besides, K_{ss} and K_{is} have a small contribution. While the model output is significantly sensitive to K_{sx}, $C_{L,1/2x}$, k, $C_{L,1/2s}$ and $q_{p,max}$. The average sensitivity measure just confirms the results obtained in the correlation analysis and regularized optimization, since only parameters with significant influence on the output can be expected to be identified from the experimental data. However, the parameters with low sensitivity measure can not be directly excluded from the parameter set due to the results highly dependent on the selection of the scale factor.

The second part of the identifiability analysis is the estimation of the collinearity

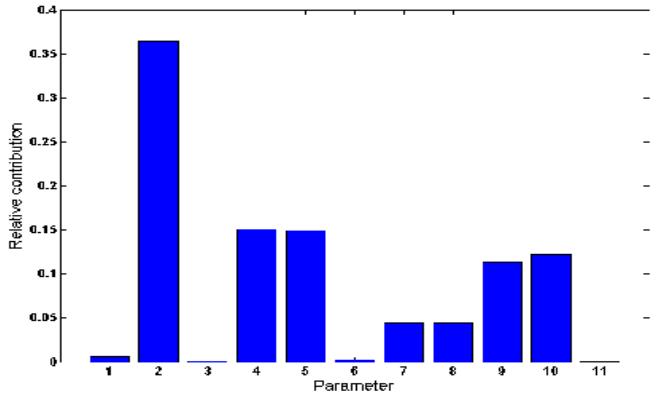

Figure 5.5: Relative average sensitivity measure of the output to each parameter numbered as in Table 5.2

index. The number of parameter combinations starts from 2 up to the number of parameters n_p. The results are shown in Fig. 5.6. From the figure is not straightforward to distinguish the subsets that are qualified as potentially identifiable subsets (the collinearity index is lower than the threshold γ_K <15). The number of the identifiable parameter subsets according to the parameters is summarized in Table 5.3. For this calculation, there are 948(46.6%) parameter subsets of 2036 possible combinations that can be identified. It is concluded that a maximally 8 parameters can be estimated from the experimental data (see the last column of Table 5.3).

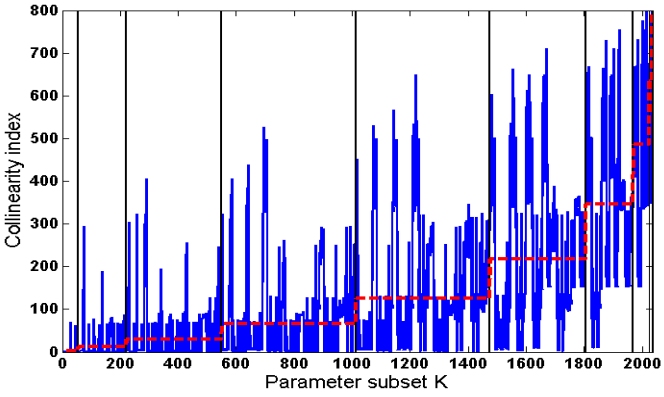

Figure 5.6: Collinearity index of each parameter combination in the set. The vertical black lines separate the parameter subset by number of parameters within the subset. Dashed line corresponds to the mean collinearity index in the subset with the same number of parameters

Table 5.3: Total number and identifiable combinations according to the number of parameters considered. The percentage of the identifiable combinations according to the number of parameters is depicted

Parameters	Total Combinations	Identifiable Combinations	Percentage (%)
2	55	53	96.36
3	165	145	87.88
4	330	245	74.24
5	462	261	56.49
6	462	171	37.01
7	330	63	19.09
8	165	10	6.06
9	55	0	0
10	11	0	0
11	1	0	0
Total	2036	948	46.56

5.5.6.1 Parameter re-identification

It is intended to determine the number of parameters which may be reliably estimated from the available experimental data. In order to define an identifiable subset, some of the parameters must be fixed using information from literature. An alternative is to change the model structure. Both solutions were investigated.

Parameters for comparable unstructured growth models of lactic acid bacteria were collected from different sources (Nielsen *et al.*, 2003; Burgos-Rubio *et al.*, 2000; Cachon and Divès, 1993; Amrane and Prigent, 1994; Boonmee *et al.*, 2003). Unfortunately, the estimated parameters are very different since they depend on factors such as the employed microorganism, fermentation conditions, substrate, the model structure and parameter identification methodology. Initially, a modification of the model structure was studied including a maintenance term into the substrate uptake rate. No improvement of the results was obtained. Subsequently, different combinations of fixed parameters were studied, especially highly correlated parameters. The identifiability analysis is performed for each parameter subset. It was noticed that reducing the size of the parameter set also affects the maximum number of identifiable parameters and their correlation. This makes it non trivial to find an identifiable parameter subset.

During this analysis the following insights were obtained: the correlation between α and μ_{max} was very high. This correlation could be decreased if the data from the continuous cultivation are employed for the parameter estimation. The reason might be that during batch experiments, growth rate changes along the experiment as well as the product formation, which make more difficult to estimate μ and α from the same batch data sets.

Additionally, if too many batch experiments are used for parameter estimation, objective function will contain more data from the batch experiments that may

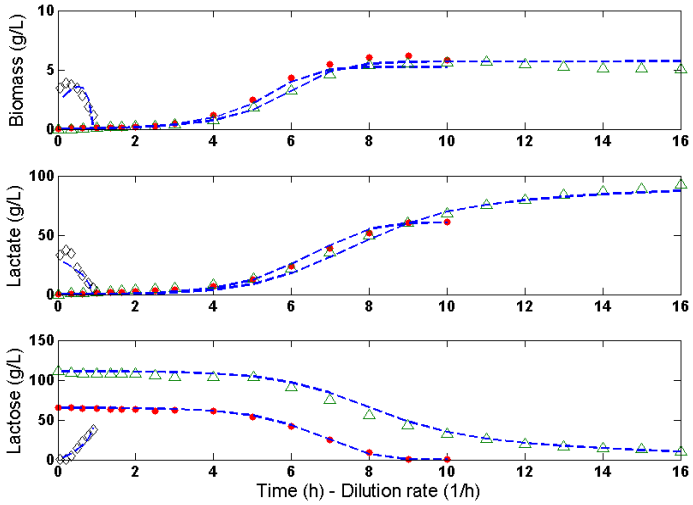

Figure 5.7: Model regression (dashed lines) on experimental data for batch and steady state continuous fermentations (points). (●) 60 g/l lactose, (△) 100 g/l lactose and (◇) steady state continuous fermentation

dominate the information contained in the continuous culture. This issue should be dealt with using the weighting factors in the objective function. The weight factors selection is tightly related to the modeling purpose. From the evaluated experiments combination, the best fitting was obtained employing for parameter estimation the continuous fermentation plus the batch experiments with 60 and 100 g/l of initial substrate. A seven parameter set that is identifiable from the available data: μ_{max}, K_{ix}, $C_{L,1/2x}$, $q_{s,max}$, $C_{L,1/2s}$, $q_{p,max}$ and α.

The model fitting to the experimental data and model quality evaluation are depicted in Figs. 5.7 and 5.8. The estimated parameters and the fixed values are depicted in Table 5.4. The qualitative agreement between the model prediction and the experimental data remains comparing with the initial parameter estimation in Figs. 5.3 and 5.4. The largest deviations during model regression are obtained for lactate concentration at low dilution rates. For the model quality evaluation, there are considerable differences in biomass and lactate concentrations for the batch using 80 g/l of initial lactose.

The statistical analysis of the best parameter set showed a substantial reduction of the parameter correlation. This can be seen from the confidence intervals depicted in Table 5.4. The maximum confidence interval for the complete parameter set was calculated for α and it was with 124% larger than the parameter value. That confidence interval was reduced to 35% after the model parameter reduction.

From the identifiability analysis of the set of seven estimated parameters, the sensitivity measure is depicted in Fig. 5.9. It can be seen how for this parameter set, the relative parameter significance is better distributed between the parameters

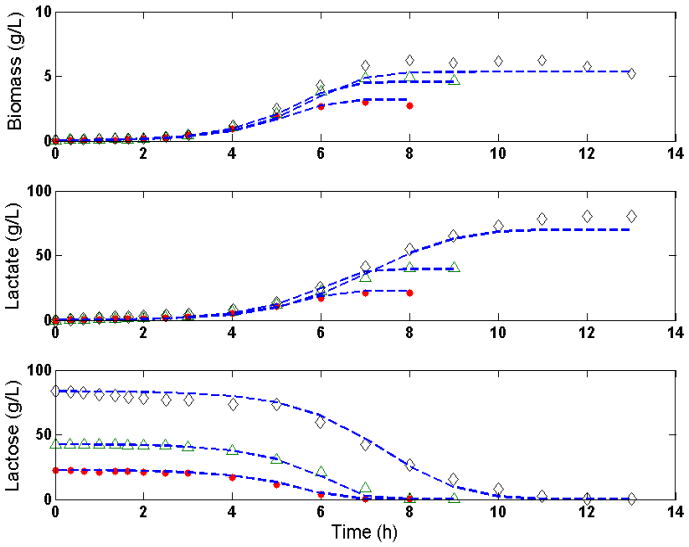

Figure 5.8: Model confrontation (dashed lines) with experimental data for batch fermentations (points). (•) 20 g/l lactose, (△) 40 g/l lactose and (◇) 80 g/l lactose

than the initial estimated set (compare to Fig. 5.5). This means that the output is actually sensitive to each of those parameters and thus they are might be identifiable from the given experimental data.

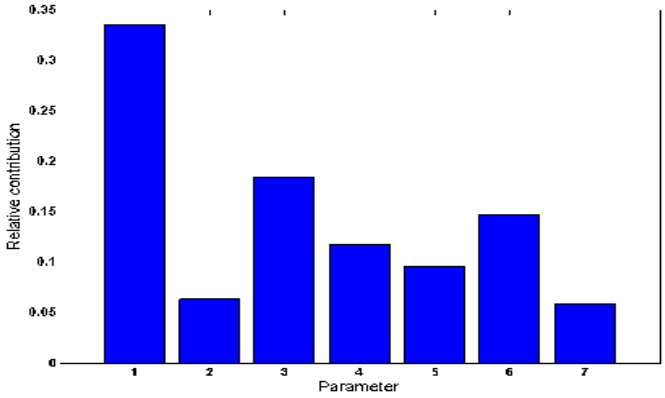

Figure 5.9: Relative average sensitivity measure of the output to each parameter numbered as in Table 5.4

The collinearity index for the seven parameter subset is shown in Fig. 5.10. From the collinearity index figure, it can be seen that the collinearity index is lower than the linear dependency threshold ($\gamma_K < 15$) for all the possible parameter combinations in the set. This indicates that all parameters in the set are identifiable.

Table 5.4: Reduced set of estimated kinetic parameters for the proposed fermentation model. Parameters without number were fixed during the parameter estimation procedure

Parameter		Estimated	95% CI	Deviation	Units
1	μ_{max}	1.2212	0.1183	9.7 %	1/h
-	K_{sx}	6.315	-	-%	g/l
2	K_{ix}	299.9919	96.2399	32%	g/l
3	$C_{L,1/2x}$	23.9953	3.617	15%	g/l
-	k	7.8875	-	-%	g/l
4	$q_{s,max}$	5.6659	1.2573	22%	g/g/h
-	K_{ss}	4.6069	-	-%	g/l
-	K_{is}	145.1781	-	-%	g/l
5	$C_{L,1/2s}$	68.0736	2.7019	4%	g/l
6	$q_{p,max}$	4.0971	0.9177	22%	g/g/h
7	α	2.5412	0.9056	35%	g/g

The number of parameter combinations starting from 2 up to 7 parameters and the number of identifiable subset are summarized in Table 5.5. There is a total of 120 parameter subsets (K) and all of them are identifiable.

Table 5.5: Total number and identifiable combinations according to the number of parameters considered. The percentage of the identifiable combinations according to the number of parameters is depicted

Parameters	Total Combinations	Identifiable Combinations	Percentage (%)
2	21	21	100
3	35	35	100
4	35	35	100
5	21	21	100
6	7	7	100
7	1	1	100
Total	120	120	100

The selection of any model structure implies a degree of approximation to the actual phenomena involved in the modeled process and hence so the uncertainty of the predictions. Despite the diverse sources of uncertainty, the concern was to avoid an increase of structural uncertainty when the model proposed by Boonmee *et al.* (2003) was modified.

It can be concluded from the presented analysis that despite the apparently good quality of the model structure evaluated through the agreement between the full model (eleven parameter set) and experimental data, the large number of parameters is not identifiable from the available experimental data. Therefore, the model

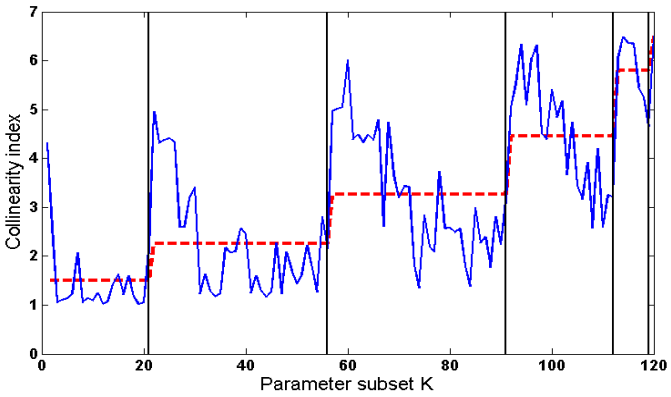

Figure 5.10: Collinearity index of each parameter combination in the set. The vertical black lines separate the parameter subset by number of parameters within the subset. Dashed line corresponds to the mean collinearity index in the subset with the same number of parameters

structure may be appropriate to reproduce the experimental data but the model can not be validated. The methods and tools employed in this contribution only allows to falsify a model, thus to obtain a reasonable model. However, there is not enough information to validate the model. In order to render the model parameters better identifiable, new experiments must be performed. The information obtained from the sensitivity analysis can be used to design new experiments.

Despite these concerns, the obtained model will be used for the further to investigate the integrated system behavior.

5.5.7 Optimal continuous fermentation

The developed kinetic model is employed to estimate the optimal static lactate productivity as a function of dilution rate and inlet substrate concentration during a continuous fermentation. This calculation is performed since the lactate productivity without *in situ* product removal is the reference to evaluate the impact of the fermenter and REED integration. The total lactate productivity is estimated through the total lactate productivity function (Eq. 5.19).

$$PF = D\,(C_{HL} + C_{L^-}) \tag{5.19}$$

In the lactate productivity function, both dissociated and undissociated lactates are accounted for. Since there are only 2 variables to optimize, the productivity surface is estimated at steady state for a given set of input variables. In this way we can have more information about the system that will be useful during the processes integration. A grid of dilution rates and inlet substrate concentrations is formed based on the experimental data for this fermentation (Boonmee *et al.*, 2003). For each combination of variables in the grid, the steady state productivity function

is evaluated. The total lactate productivity and concentration are depicted in Figs. 5.11 and 5.12.

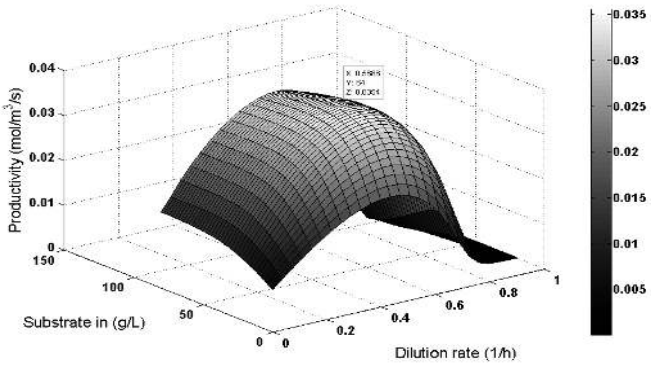

Figure 5.11: Total lactate productivity function for a continuous fermentation as function of inlet substrate concentration and dilution rate. The optimal productivity is depicted

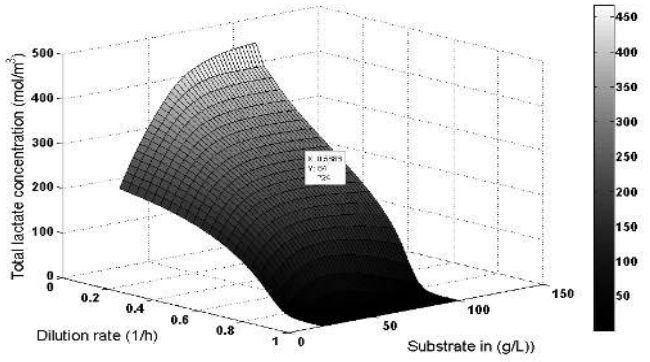

Figure 5.12: Total lactate concentration for a continuous fermentation

As expected, it is a convex surface where the best productivity is clearly visible. The maximum total lactate productivity ($PF = 0.0354\ mol/l^{-1}h^{-1}$) is found for a dilution rate of $D = 0.5688$ h^{-1} and $C_s^{in} = 64$ g/l. This point corresponds to a total lactate concentration of 224.03 mol/m^3, which is an intermediate concentration in the surface. Notice that the highest productivity is the best solution to the problem but not the optimal. The reason is that this methodology evaluates only the productivity function for each combination of input variables defined. However, it is expected that the optimal solution is close the above value.

5.6 Conclusions

An unstructured kinetic model is proposed for lactic acid fermentation, based on a model in the literature (Boonmee *et al.*, 2003). A modification is introduced in the product inhibition term, where a constrained linear function has been substituted by a normalized Boltzmann two parameter sigmoid representation. The model describes the substrate uptake, biomass growth and product generation rates. The model includes the ion dissociation reactions and assumes perfect pH control of the pH in the fermenter.

The full model parameters are regressed to describe *Lactococcus lactis* batch growth on lactose as main carbon source with eleven parameters to be determined from experimental data. The model is able to satisfactorily reproduce the experimental data. However, identifiability problems of the full set of parameters were encountered. Regularized optimization method was shortly investigated to overcome the poor parameter identifiability, but not satisfactory results were obtained. Therefore, reduction of the parameter set was used in order to decrease the correlation between parameters. Sensitivity based metrics and an identifiability analysis were employed to assist the selection of an appropriate parameter subset, where all parameters could be identified from the available experimental data. As a result, a subset of 7 parameters was identifiable. Using the validation data set, it was evidenced that the quality of the model fitting basically remains.

However, the reliability of the developed model is rather limited, since several parameters could not be reliably estimated from available data. It is noteworthy that four parameters had to be given constant values during parameter estimation. To further validate or improve the accuracy of this model, additional experimental work is required. Preferably with experiments in regions where the measured variables are more sensitive to the values of the unknown model parameters.

Due to an unstructured model is used, it is expected to have better model accuracy in the low frequency range (steady state cultivation). Since it is assumed that the internal composition of the cell is in balance with the cultivation composition, situation which is referred to as balanced growth. In other words, when the anabolic processes immediately utilize the energy generated by the catabolism. Dramatic and very fast changes in the cultivation conditions can change the energetic state of the cell or modify its genetic activity, thus the assumption of balanced growth does not hold. Under those conditions, the unstructured model may have less predictive power. Additional experiments are thus necessary to improve the model accuracy at higher frequencies. However, models with much higher biochemical details might be required at some point.

Despite these (rather significant) shortcomings, the developed model is used in the further work to investigate the operational aspects of integrating the bioreactor and the REED module.

5.7 Nomenclature

C Concentration (g l^{-1})

CI	Confidence interval
$C_{L,i}$	Threshold product concentration (g l^{-1})
$C_{L,m}$	Total inhibiting product concentration (g l^{-1})
$C_{L,1/2}$	Average inhibiting product concentration (g l^{-1})
$C_k^{n_p}$	k-combinatorial with n_p parameters
COV	Covariance matrix
D	Dilution rate (h^{-1})
F	Residuals objective function (-)
I	Number of measurements in experiment *l'th*
IT	Inhibition term
H	Hessian
J	Jacobian
k	Product inhibition kinetic parameter (g l^{-1})
k	Number of parameters in a subset
K	Subset
K_S	Limiting substrate concentration (g l^{-1})
K_i	Inhibitory substrate concentration (g l^{-1})
L	Number of experiments
m	Number of observations
N_{li}	Number of data points in measurement *i'th* in experiment *l'th*
n_p	Number of parameters
p	Product concentration (g l^{-1})
PF	Productivity function (mol l^{-1} h^{-1})
P_i	Threshold product concentration (g l^{-1})
P_m	Total inhibiting product concentration (g l^{-1})
q	Recirculation flow rate (l h^{-1})
q_k	Reaction rate (biological) (g l^{-1} h^{-1})
$REED$	Reverse Electro-Enhanced Dialysis
R_k	Total reaction rate of k (g l^{-1} h^{-1})
s	Element in the sensitivity matrix
s	Substrate concentration (g l^{-1})
$\tilde{s}$	Element in the normalized sensitivity matrix
S	Sensitivity matrix
$\tilde{S}$	Normalized sensitivity matrix
$\tilde{S}_K$	Normalized sensitivity submatrix
sc	Scale factor
t	Time (s)
t	t-distribution
V	Volume (l)
W_l	Weight
w_{li}	Weight
W_{reg}	Weight
x	Biomass concentration (g l^{-1})
y	Experimental data
$\bar{y}$	Predicted values

Greek letters

α_s	Percentile for t-distribution
δ_j^{msqr}	Average sensitivity measure
μ	Specific growth rate (g l^{-1} h^{-1})
υ	Flow rates in the fermenter (l h^{-1})
θ	Parameter vector
$\hat{\theta}$	Optimal parameter vector
α	Growth associated constant (g g^{-1})
$\Delta\theta$	Scale factor
γ_K	Collinearity index
λ_K	Minimum eigenvalue of $\tilde{S}_K^T \tilde{S}_K$
λ_j	Weight

Subscripts

$base$	Concentrated NaOH solution
$feed$	Feed channel
HL	Lactic acid
HP	Undissociated protein
i	Inhibiting
i	Data point
j	Parameter
k	Specie
L^-	Lactate ion
max	Maximum
Na^+	Sodium ion
OH^-	Hydroxide ion
p	Product
P^-	Dissociated protein
$prod$	Product stream
s	Substrate
tot	Total
x	Biomass

Superscripts

in	Inlet
in	Initial
nd	Non dimensional
rec	Recirculation
T	Transpose

6

Analysis and design of a pH control system of Reverse Electro-Enhanced Dialysis

6.1 Abstract

A bioreactor integrated with an electrically driven membrane separation process (Reverse Electro-Enhanced Dialysis - REED) is under investigation as potential technology for intensifying lactic acid bioproduction. In this contribution the pH regulation issue in the periodically operated REED module is investigated. A methodology for goal driven control system development is adjust to easily handle the dynamic system. A sensitivity analysis is used as criterion for the conceptual design of the control structure. The analysis leads to a periodic input-resetting control structure. The system controls pH using the imposed current density and resets the latest employing the hydroxide inlet concentration to the dialysate channel. The proposed structure is implemented and evaluated using a set point tracking test. The performance of the control structure is satisfactory achieving a desired pH at the outlet of the feed channel in REED from period to period and resetting the current density.

6.2 Introduction

An integrated bioreactor coupled with electrically driven membrane separation processes (Reverse Electro-Enhanced Dialysis - REED and Electrodialysis with Bipolar membranes - EDBM) has been recently proposed as a method for *in situ* lactate removal from the fermentation broth (Garde, 2002; Rype, 2003). The fermentation and first extraction stage are depicted in Fig. 6.1 (Rype, 2003). The novelty of the process is the innovative electro-membrane separation process which selectively extracts the lactate and simultaneously in principle facilitates the pH control in the fermenter. This is possible since the lactate ions are exchanged by hydroxide ions through the anion exchange membranes (Strathmann, 2004). In addition, the adverse influence of the membrane fouling is diminished by periodically reversing the polarity of the electrical field, ensuring longer operation compared to other continuously operated membrane based separations (Rype, 2003).

A model based approach has been employed to investigate the operating window of the REED process under Donnan Dialysis (Prado-Rubio *et al.*, 2010b), Electro-Enhanced Dialysis (Prado-Rubio *et al.*, 2011b) and Reverse Electro-Enhanced Dialysis (Prado-Rubio *et al.*, 2011a). Details of the system operation and model are

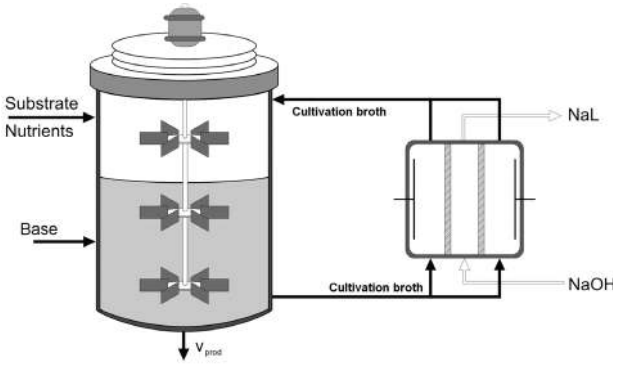

Figure 6.1: Sketch of the integrated bioreactor with the REED module for a batch/fed-batch/continuous fermentation (adjusted from (Rype, 2003))

described in those contributions. In order to facilitate integration of the bioreactor and membrane separation process models, a systematic procedure for control system design at the regulatory layer is employed to the periodically operated REED module. The objective of this contribution is then the design and implementation of a pH control structure based on a systematic but non trivial sensitivity analysis for the periodically operated separation process.

Early discussions about control structure design and its impact on industrial processes has been given by Foss (1973); Morari *et al.* (1980); Morari (1982); Stephanopoulos (1983, 1989). In a simple manner, control structure design refers to which variables should be measured, which inputs should be manipulated and which links should be made between the two sets (Foss, 1973). Therefore, this analysis involves all the structural decisions that lead to the selection of controlled variables, measurements, manipulated variables, control configuration and controller type according to an operational goal. In addition, the decomposition of the overall problem into smaller subproblems (Larsson and Skogestad, 2000; Skogestad, 2004). The control structure design involves a number of tasks that ideally are performed sequentially through the so called "top-down" analysis. The controllers implementation and their performance are evaluated using the "bottom-up" design.

This chapter is structured as follows. First, a methodology is described for control system development for the REED module as a subsystem of the integrated process. The pH control subgoal of the REED module is addressed and the limitations within the framework discussed. Afterwards, a brief overview of the REED model is provided and the pH model is highlighted. A sensitivity based criterion is introduced to assist the top-down analysis during the control structure design. The pH behavior is investigated as a function of the potential manipulated variables and the sensitivity analysis is performed. A control structure is proposed to exploit the pH sensitivity towards the potential manipulated variables and fulfill the input constraints. The control structure is implemented and its performance evaluated. Finally, the conclusions are drawn.

6.3 Methodology for designing a monitoring system

The control system in a process is structured in different hierarchically organized layers, these layers are interconnected and the upper layers compute information required as inputs to lower layers. The control structure can be divided into two sections, the upper section corresponds to optimization layer and lower level is the control layer. The control layer can be divided into two subsections, the supervisory and regulatory layers. The structure is illustrated in Fig. 6.2 (Skogestad, 2000, 2004; Jørgensen, 2006).

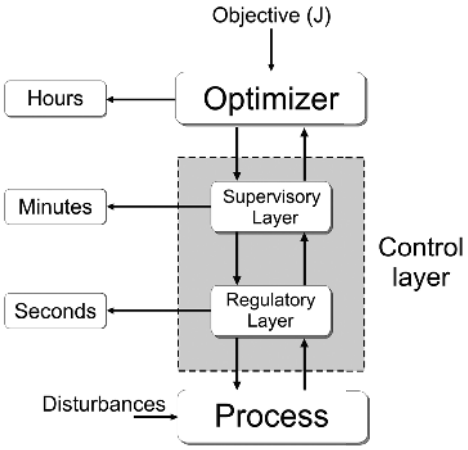

Figure 6.2: Hierarchical structure for control design (adapted from (Skogestad, 2000))

The principal parts of the hierarchical structure for control design are (from the bottom to the top) (Skogestad, 2000, 2004):

- Regulatory layer: the main purposes of this control layer are stabilization and local disturbance rejection. In this stage, some variables are stabilized using low complexity controllers, like single input - single output PI control, to avoid long control loops.

- Supervisory layer: the main aim is to keep the primary controlled outputs at their set points. Multivariable controllers may be required at this stage.

- Optimization: the objective is to calculate the optimal set points for given product specifications based on market conditions. The optimization procedure can be executed off line or in real time (RTO). The real time optimization is costly and requires (at least) a steady state model that should be continuously updated. The solution of the optimization problem consists in the maximization of a productivity function. This function is used to quantify the plant performance.

In the literature, a methodology based on the analysis of the operational degrees of freedom is proposed to develop monitoring systems (Skogestad, 2000, 2004; Jørgensen, 2006). However, existing guidelines for the conceptual control structure design of a goal driven control system needs extension. For instance, in the actual case here where the selection of manipulated variables is not evident or existing tools are inappropriate for a periodically operated process.

The herein employed methodology is divided into 3 main parts: Goal definition, Top-down analysis and Bottom-up design.

6.3.1 Goal definition

The starting point of the control structure design procedure is to define the primary plant operating goal.

Interesting industrially relevant primary objective functions for the process are: lactate productivity as potential feedstock for the production of the biodegradable Poly-Lactic Acid (PLA), probiotic culture productivity (higher biomass activity) or extracellular protein productivity based on genetically modified lactic acid bacteria. To maximize these productivities, an important subgoal is to to reveal how the REED process can facilitate pH control in the fermenter. This is selected as a main subgoal and further investigated in this contribution. To control pH at the outlet of the REED module is important because it is a measure of the amount of lactate which is separated, since the lactate flux towards the dialysate channel is almost identical to the hydroxide flux towards the feed channel. This equality is due to the exchange-diffusion mechanism and Donnan exclusion in the anion exchange membranes (Prado-Rubio *et al.*, 2011a).

The next step in the methodology analyses how the available degrees of freedom may be used to provide the desired functionality to satisfy the primary operating goal, or in this case the pH control.

6.3.2 Top-down analysis

The operational degrees of freedom (DOF) for the system are determined (details shown in Appendix C). The DOF that can ensure that the goals and subgoals can be achieved become actuator variables and define the axes of the operating window for the process. The remaining degrees of freedom are considered as disturbances. The measurements provide information concerning goal/subgoal achievements through key performance indexes. Revealing the coupling between monitored variables and key performance indexes requires a prior knowledge of the system. Key performance indexes can be classified as productivity achievement, regulatory performance, yield achievement and quality achievement.

In linear systems, the selection of the manipulated variables according to a specific goal can be handled in a relatively simple way based on the system understanding and guidelines, e.g. large and fast effects on the controlled variables are desired, corresponding to a large steady state gain and relatively small time constants. Methodologies as Bristol's Relative Gain Array (RGA) and Singular Value Analysis (SVA) have been proposed in literature to screen subsets of possible pairing of manipulated variables and controlled variables (Skogestad and Postlethwaite, 2004; Seborg

et al., 2004). However for this non squared periodically operated system, the manipulated/controlled variables pairing is investigated in more detail using a dynamic analysis. A sensitivity based index is defined to quantify the mentioned guidelines.

Performing dynamic simulations within the operating window provide useful information concerning: the shape of the operating surface for the system, the operational constraints, possible input or output multiplicities and operating conditions. Additionally, the simulation results help refining the selection of the manipulated variables in order to achieve the operational goal. As mentioned above, the pH regulation structure design in the REED module is chosen to illustrate this control structure design procedure.

The selected criterion to assist the selection of the manipulated variables according to the operative goal, is the dynamic sensitivity of the controlled variable to changes in the potential manipulated variables. Dynamic simulations of the periodically operated system within the operating window are performed and the sensitivity is evaluated. From the analysis of those results, a control configuration can be proposed.

6.3.3 Bottom-up design

Once the control structure is designed, the controllers can be implemented. Usually a multilevel hierarchical structure is employed. It is of particular interest to reveal the potential benefit of multivariable control over a fully decentralized control structure. The performance of the implemented control structure is investigated through dynamic simulations. Performance indexes such as overshoot and settling time provide relevant indicators for the integrated plant monitoring.

6.4 pH control structure development

6.4.1 pH model in the REED module

Previously, a dynamic model was developed to describe simultaneous ion transport across anion exchange membranes in a dialysis cell (Prado-Rubio *et al.*, 2010b). Investigations were performed for operation without imposing current density and subsequently for operation applying an external potential gradient and operation under current reversal conditions (Prado-Rubio *et al.*, 2010b, 2011b,a). In those contributions, the operating window of the device was explored. Here, we investigate pH changes in the outlet of the REED module as a function of the potential manipulated variables, therefore the pH model is highlighted. The mass balances within the boundary layers and membranes in the REED model can be summarized as follows. A mass balance for component k in phase p is:

$$\frac{\partial C_{k,p}}{\partial t} + \nabla J_{k,p} - R_k = 0 \tag{6.1}$$

The reaction term (R_k) is used to introduce acid dissociation into the model. The flux $J_{k,p}$ is estimated using the Nernst-Planck equation for ideal solutions, neglecting convective transport (Strathmann, 2004).

$$J_{k,p} = -D_{k,p}\left(\frac{\partial C_{k,p}}{\partial x} + \frac{z_k F C_{k,p}}{RT}\frac{\partial \psi_p}{\partial x}\right) \tag{6.2}$$

where $D_{k,p}$ is the diffusion coefficient, z_k the valence, F is the Faraday number, R is the ideal gas constant, T is temperature and ψ is the electrical potential. The potential gradient can be calculated using the assumption that all current I_d is carried by ions, through Faraday's law (Eq. 6.3).

$$I_d = F\sum_k z_k J_{k,p} \tag{6.3}$$

Donnan equilibrium is used to describe the concentration and potential discontinuities at the membrane surfaces. The bulk channel models are approximated using tanks in series model, where in each tank there is mass transport towards the membrane and the dissociation reactions are present. Experimentally, it has been verified that a pH buffer effect is induced by the presence of biomolecules in a fermentation broth. When those components are modeled as highly charged macromolecules, multiple dissociation reactions must be introduced. That increases the complexity of the model unnecessarily. To deal with this situation, the proton acceptor groups in the proteins are considered in terms of equivalents, i.e. the protein concentration is represented as mol of acid equivalents per volume. Therefore, the dissociation of a polyprotic species is simplified to a monoprotic acid reaction (Prado-Rubio *et al.*, 2010b). The protein species represent a wide range of components in the fermentation broth from low molecular weight proteins to colloidal material. The system of reactions is therefore given by the following reversible reactions:

$$\mathrm{HL} + \mathrm{OH^-} \underset{k_2}{\overset{k_1}{\rightleftharpoons}} \mathrm{L^-} + \mathrm{H_2O}$$
$$\mathrm{HP} + \mathrm{OH^-} \underset{k_4}{\overset{k_3}{\rightleftharpoons}} \mathrm{P^-} + \mathrm{H_2O}$$

where the dissociation constants for those reactions (K_d) correspond to the acid dissociation constant (K_a) divided by the ionic product of water (K_w). Using a stoichiometric matrix, the dissociation reaction rates are systematically introduced into the model. The reaction rate term R_k can be written as a vector using the the reaction rates r_1 and r_2, plus the stoichiometric vectors α and β. The values for α and β for each species are depicted in Table 6.1.

$$\mathbf{r}_1 = k_2\left[\mathrm{L^-}\right] - k_1\left[\mathrm{HL}\right]\left[\mathrm{OH^-}\right] \tag{6.4}$$

$$\mathbf{r}_2 = k_4\left[\mathrm{P^-}\right] - k_3\left[\mathrm{HP}\right]\left[\mathrm{OH^-}\right] \tag{6.5}$$

$$R_k = \alpha_k \mathbf{r}_1 + \beta_k \mathbf{r}_2 \tag{6.6}$$

The model consists of a system of multiregion partial differential equations. The method of lines is employed to discretize the spatial x-dimension, resulting in a

Table 6.1: Stoichiometric vectors for reactions $\mathbf{r}_1$ and $\mathbf{r}_2$

Specie	**Symbol**	α_k	β_k
Lactate	L^-	-1	0
Hydroxide	OH^-	1	1
Sodium	Na^+	0	0
Protein ion	P^-	0	-1
Lactic acid	HL	1	0
Undissociated Protein	HP	0	1

system of differential and algebraic equations (DAEs). A feasible set of initial conditions must be specified in order to ensure convergence. An initialization procedure is developed in order to guarantee, at least in all evaluated scenarios, convergence (Prado-Rubio *et al.*, 2010b).

6.4.2 Operational Degrees of freedom

The potential manipulated variables to control hydroxide flux towards the REED feed channel, and implicitly the lactate flux towards the dialysate channel, are: the feed and dialysate input flow rates (q_{feed} and q_{dia}), the polarity reversal time (t_{rev}), the imposed current density (I_d) and the inlet hydroxide concentration in the dialysate channel ($C^{in}_{OH,dia}$). A first screening is performed based on the knowledge earned from previous investigations (Prado-Rubio *et al.*, 2010b, 2011b,a). The first variables discarded are the flow rates, the reason is the lack of information about how the thickness of boundary layers changes as a function of the flow conditions. Therefore, the model predictive power during flow rate changes is very limited. The reversal time, or operation time before the polarity of the potential gradient is inversed, is not investigated since it is a design variable that is chosen by trading off lactate recovery and the energy consumption subject to the power source constrains (Prado-Rubio *et al.*, 2011a). These choices leave the current density and the inlet base concentration to the dialysate channel as potential manipulated variables, restricting the operating window to two dimensions.

6.4.3 Selection of the manipulated variables

The question to answer at this stage is: what is the most appropriate manipulated variable which can control pH at the outlet of the feed channel in REED? A model based study is performed to answer that question.

In order to evaluate the pH changes during REED module operation, a simulation scenario is proposed. Feed channel input concentrations to REED are assumed constant, corresponding to hypothetical fermentation broth at constant pH. Simulations are performed to estimate the pH at the end of the feed channel based on changes of the potential manipulated variables around certain nominal values (ΔI_d and $\Delta C^{in}_{OH,dia}$). The dynamic dimensionless sensitivity (NS) of pH to the potential manipulated variables is calculated through Eqs. 6.7 and 6.8.

$$NS_{I_d} = \frac{|I_d|\Big|_{t_0}}{pH\Big|_{t_0}} \frac{dpH(t)}{dI_d} \tag{6.7}$$

$$NS_{C_b} = \frac{C^{in}_{OH,dia}\Big|_{t_0}}{pH\Big|_{t_0}} \frac{dpH(t)}{dC^{in}_{OH,dia}} \tag{6.8}$$

where the derivatives are approximated using forward finite differences:

$$\frac{dpH(t)}{dI_d} \approx \frac{pH(I_d + \Delta I_d, t) - pH(I_d, t)}{\Delta I_d} \tag{6.9}$$

$$\frac{dpH(t)}{dC^{in}_{OH,dia}} \approx \frac{pH(C^{in}_{OH,dia} + \Delta C^{in}_{OH,dia}, t) - pH(C^{in}_{OH,dia}, t)}{\Delta C^{in}_{OH,dia}} \tag{6.10}$$

Dimensionless sensitivity is selected in order to make a fair comparison between both actuator variables. The scale values chosen are the initial conditions before the disturbance is applied, i.e. at $t_0 = 0$. The truncation error of the numerical approximation of the derivatives is of the order of magnitude of the applied disturbance ($\mathcal{O}(\Delta I_d)$ or $\mathcal{O}\left(\Delta C^{in}_{OH,dia}\right)$).

The simulation procedure to estimate the sensitivity around each operating point involves three steps.

a. The dynamic model is initialized from a known operating point to stable periodic operation. This point is function of I_d and $C^{in}_{OH,dia}$. The other input variables required to solve the model are fixed. The purpose of this step is to determine the stationary operation at nominal values of the potential manipulated variables. The last simulation point during the period is selected as the initial condition for the following simulations.

b. The model is solved from the new initial conditions and the previous input variables. The simulation results correspond to stationary operation, and become the reference to estimate the sensitivity. The target variable is either $pH(I_d, t)$ or $pH(C^{in}_{OH,dia}, t)$.

c. The model is solved again introducing the disturbance in the potential manipulated variable at $t = 0$ using the initial conditions obtained in step (a). The target variable is either $pH(I_d + \Delta I_d, t)$ or $pH(C^{in}_{OH,dia} + \Delta C^{in}_{OH,dia}, t)$.

6.5 Results and discussion

Initially, the system is simulated in open loop in order to understand the dynamic pH behavior as function of the potential manipulated variables. Afterwards, the sensitivity analysis is performed resulting in the control structure design. Finally, PI controllers are implemented and their performance evaluated.

6.5.1 Operating conditions

The ion physicochemical properties, module dimensions, flow conditions and membrane properties required to solve the model are taken from previous work (Prado-Rubio *et al.*, 2010b, 2011a). For the all simulations performed in this contribution the extra pH buffer, due to the presence of the ideal monoprotic protein (HP and P^-), is activated by using a relatively small concentration of total protein at the inlet of the feed channel. The required inputs are depicted in Table 6.2. The membrane water content, which defines the ion diffusion coefficients within the membrane, is estimated according to the diffusion model presented by Prado-Rubio *et al.* (2010b).

Table 6.2: Operational parameters for REED operation

Parameter	Value	Units
q_{feed}	120	L/h
q_{dia}	120	L/h
$C_{HL}^{fbin} + C_{L^-}^{fbin}$	100	mol/m^3
$C_{HP}^{fbin} + C_{P^-}^{fbin}$	10	mol/m^3
$C_{L^-}^{dbin}$	0	mol/m^3
pH_{in} feed	5.75	-
t_{rev}	5	min

6.5.2 pH behavior during REED operation

The understanding of system dynamics is vital to assist the control system development. During REED operation at constant values of the potential manipulated variables (I_d and $C_{OH,dia}^{in}$), the system is driven by the periodicity and strength of the current density plus the hydroxide concentration gradient between channels. At the beginning of each period current is imposed to the system, then after a half period time the polarity of the imposed electrical potential is reversed. As a result, a square wave function is obtained as depicted in Fig. 6.3, with a period time for the current of 1200 s. The initial condition is static Donnan Dialysis recovery (I_d=0) and the amplitude on the step changes are defined by the desired current density.

The system dynamics has been investigated previously (Prado-Rubio *et al.*, 2011a). For illustration, the pH behavior at the outlet of the feed channel in REED is computed during step changes of the potential manipulated variables.

Stationary REED operation at I_d=100 A/m^2 and $C_{OH,dia}^{in}$=50 mol/m^3 is used as initial condition. Step changes in current density to 200 A/m^2 and hydroxide concentration to $C_{OH,dia}^{in}$=150 mol/m^3 are applied separately. The results are shown in Figs. 6.4 and 6.5.

The period to period dynamics is visible before periodic stationary operation is achieved after a few cycles. In both scenarios, the cycles required to achieve stationary operation after the disturbances are basically the same. However, under other operating conditions they may be different. After the polarity is reversed, there is a steep pH reduction due to a temporal hydroxide flux inversion at the interface

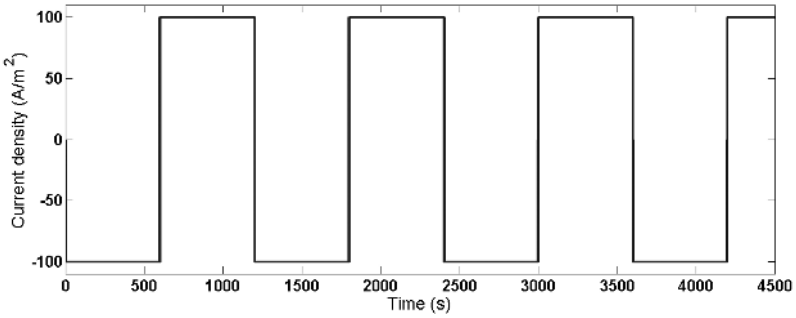

Figure 6.3: Representation of the squared wave function employed for the current density with an strength of I_d=100 A/m^2. In this example the reversal time is 600 s

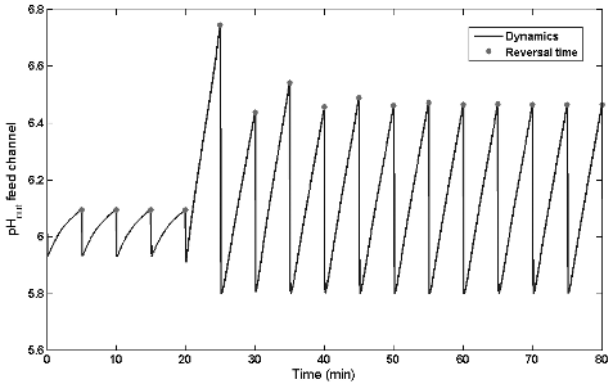

Figure 6.4: Feed channel pH behavior for t_{rev}=5 min and $C^{in}_{OH,dia}$=50 mol/m^3. When I_d is changed from 100 A/m^2 to 200 A/m^2 at t=20 h. The highlighted points are every half period time

between bulk channel and boundary layer. Transient fluxes inversion in this system have been predicted previously (Prado-Rubio *et al.*, 2011a). Due to the symmetry of the unit, the pH behavior is not a function of the polarity of the electrical field under stationary operation, but of the absolute current density. The last result is very important from a control point of view, since the manipulated variable can be the magnitude of the current density instead of the current magnitude plus the polarity.

The half period pH response to the applied disturbances is characterized by a different behavior, which is highlighted with red points in Figs. 6.4 and 6.5. The half period system response to the step change in current density corresponds to the mapping of an underdamped second order transfer function. On the other hand, the pH response to the change in the hydroxide concentration in the dialysate channel maps a first order transfer function.

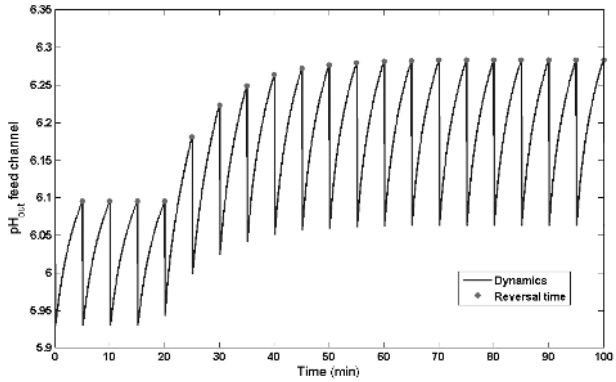

Figure 6.5: Feed channel pH behavior for t_{rev}=5 min and I_d= 100 A/m^2. When the $C^{in}_{OH,dia}$ is changed from 50 mol/m^3 to 150 mol/m^3 at t=20 h. The highlighted points are every half period time

Previous work with this system revealed other relevant issues related to pH in the REED module:

- Large pH changes in the REED feed channel have an adverse influence on the biomass growth and activity.
- At low lactate concentrations, current saturation condition can be achieved along the feed channel. This issue is relevant especially during a fedbacth fermentation or the start up of a continuous cultivation (Prado-Rubio *et al.*, 2011b).
- Computationally speaking, large concentration gradients along the REED channels are undesired, since several tanks in series must be used to model the concentration profile along them (Prado-Rubio *et al.*, 2010b). It implies a substantial increase in the computational time.

6.5.3 Conceptual control structure design

The pH sensitivity functions are evaluated dynamically, however a comparison is only performed when the derivative has been approximated at the same point in time within subsequent periods. The chosen points are at the time just before the polarity is reversed - highlighted in Figs. 6.4 and 6.5. Following the simulation procedure described above, the sensitivity is investigated within a selected operating window of the potential manipulated variables. The window size selection is based on our present understanding of the REED process.

The operative window for current density is defined by Donnan Dialysis (I_d=0) and the current saturation condition. It is desired to operate the process at within that window since the current utilization decreases after current saturation threshold (Sonin and Grossman, 1972; Strathmann, 2004). The current saturation point is a function of the ion bulk concentrations in both channels. In this investigation the

total lactate concentration in at the feed channel does not significantly change as a function of the potential manipulated variables. On the other hand, hydroxide concentration is changing within a wider concentration range. For a feed solution with 100 mol/m^3 of total lactate, it has been predicted that the maximum operative current density is not very sensitive to large changes in the hydroxide concentration when the nominal value is higher than 50 mol/m^3 (Prado-Rubio *et al.*, 2011b). Nevertheless, it drops dramatically for concentrations lower than the mentioned threshold. The operative window for current density defines clearly the operational constraints.

The maximum hydroxide concentration in the dialysate channel is defined by the membrane resistance to the pH environment. Neosepta-AMH (produced by ASTOM Corporation (Tokyo, Japan), earlier Tokuyama Soda Company, Inc.) has been used in caustic environment using solutions up to 2M of sodium hydroxide. However, we have estimated that static lactate and therefore hydroxide fluxes are not very sensitive to the hydroxide concentration in the dialysate channel at high current densities (Prado-Rubio *et al.*, 2011b). Therefore, it is interesting to explore the pH sensitivity at relatively low base concentrations.

The dimensionless pH sensitivity to disturbances in current density and hydroxide inlet concentration to the dialysate channel are depicted in Figs. 6.6 and 6.7, respectively. The disturbance is approximately 0.1% of the nominal value. Analogously to the pH behaviour evidenced after the step disturbances, the dimensionless sensitivity response is underdamped and overdamped after introducing disturbances in I_d and $C^{in}_{OH,dia}$, respectively. The settling time for both responses is comparable. During the calculations a numerical issue raised in the simulations involving disturbances in $C^{in}_{OH,dia}$. The sensitivity did not achieve a constant value at pH stationary operation under current reversal conditions. This problem was significantly reduced by lowering the tolerance during the solution of the set of differential algebraic equations (from 1x10^{-8} up to 1x10^{-11}).

In order to compare the simulation results, the ratio between the two dimensionless sensitivities was investigated at one point during the transient response -the first middle point- and at stationary operation after the transient has settled. Disturbances in the potential manipulated variables where evaluated around nominal values of current density from 75 to 200 A/m^2 and $C^{in}_{OH,dia}$ of 50 and 150 mol/m^3. The results are shown in Fig. 6.8.

Fig. 6.8a shows that the stationary dimensionless sensitivity ratio increases almost linearly as a function of the nominal current density where the disturbances are applied. Differences between the pH sensitivity towards I_d and $C^{in}_{OH,dia}$ increase at higher operative hydroxide concentrations. At low current densities, there are no practical differences between the dimensionless sensitivities. At high nominal current densities, the pH is 5 to 10 times more sensitive to I_d than to $C^{in}_{OH,dia}$. The results indicate that the stationary pH of the outlet of the REED channel could be potentially controlled using either I_d or $C^{in}_{OH,dia}$, especially at low nominal current densities.

On the other hand, the dimensionless sensitivity ratio evaluated in the first middle point carries more information which is relevant for the control structure design. The sensitivity ratio is not increasing linearly with current density. This behavior is introduced by the differences in the sensitivities responses as can be seen in Figs.

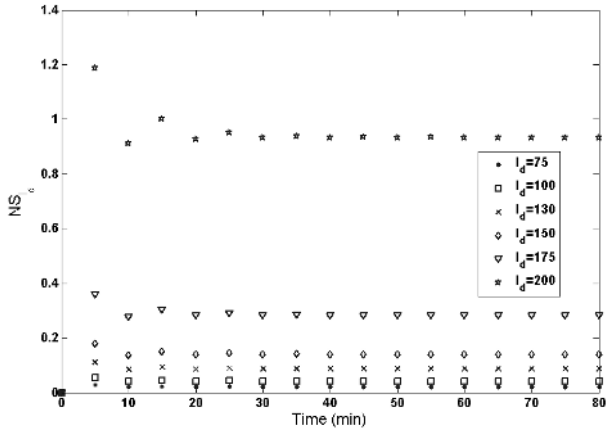

Figure 6.6: Dynamic dimensionless feed channel pH sensitivity to current density at every half period time for t_{rev}=5 min and $C^{in}_{OH,dia}$=150 mol/m^3. The disturbances are applied around the shown current densities

6.6 and 6.7. More importantly, larger differences are clear since the normalized pH sensitivity is approx. 20 to 50 times higher for current density than for base concentration changes (Fig. 6.8b).

A fast view to these results indicates that I_d is the appropriate manipulated variable to control the pH, since the sensitivity ratio is higher in both scenarios evaluated. However, the current density constraints are an issue from both numerical and an operative point of view. The numerical constraints come from the mathematical

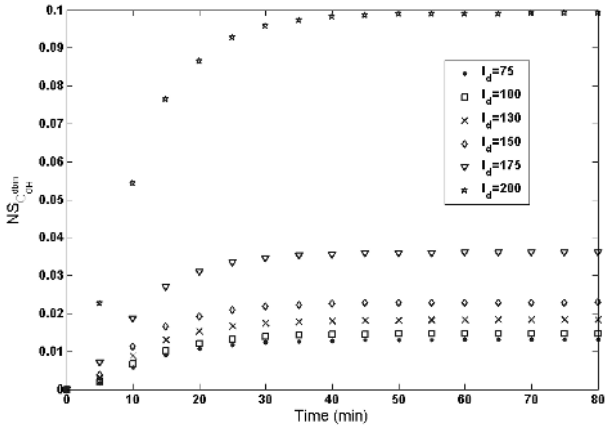

Figure 6.7: Dynamic dimensionless feed channel pH sensitivity to $C^{in}_{OH,dia}$ at every half period time for t_{rev}=5 min and $C^{in}_{OH,dia}$=150 mol/m^3. The disturbances are applied around the shown current densities

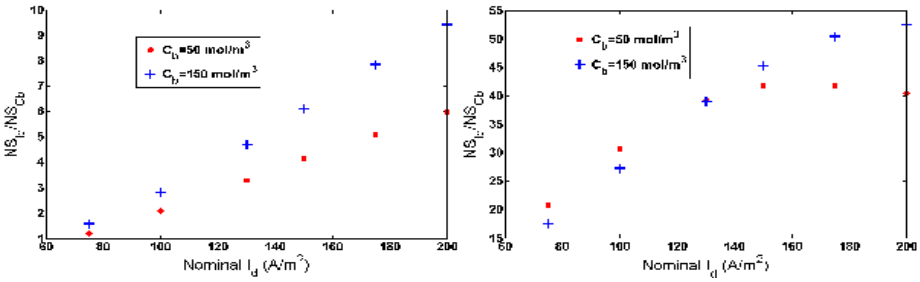

(a) Stationary **(b)** First middle point

Figure 6.8: Dimensionless feed channel pH sensitivity ratio of current density over base concentration at the first middle point and stationary operation for t_{rev}=5 min

description of the equilibrium conditions at the membrane surface. By employing Donnan equilibrium equation, convergence problems appear when the current density approaches saturation conditions (Prado-Rubio *et al.*, 2011b). On the other hand, at current saturation the current density would be insufficient to reject disturbances. Therefore, in this specific application is interesting to exploit the fact that $C^{in}_{OH,dia}$ can facilitate the pH control and has larger operative window. This can be done through an input-resetting control structure, which has some resemblance to cascade control.

Cascade control structures have been employed in order to enhance the response of a control loop by using an intermediate measurement and two feedback controllers (Seborg *et al.*, 2004). Due to the hierarchical arrangement of the controllers in the cascade control structure, the feedback signals are interconnected but the implementation has the advantage of a decoupled design of the controllers (Skogestad and Postlethwaite, 2004). In a cascade control structure, one manipulated variable takes care of the fast control action and the second of the long term control. When the extra measurement employed is an output, the design leads to a conventional cascade control configuration. However if the extra measurement is an input, then the so called input-resetting control implementation emerges (Faanes and Skogestad, 1999). The input-resetting control configuration is a non-conventional control structure where a fast controller regulates the controlled variable, while the slow controller uses the extra input to drive the fast controller manipulated variable to a desired value. This avoids saturation of the measured input, thus input constraints can be handled. A special characteristic of this control structure is that if both inputs have a positive effect in the output the gain of the slow controller must be negative (Skogestad and Postlethwaite, 2004).

For pH regulation of the outlet of the REED module, the input reseting control architecture enables a fast dynamic response using the current density as manipulated variable. Additionally, manipulation of the inlet hydroxide concentration to the dialysate channel resets the imposed current density to a desired value, thereby avoiding current saturation conditions. The desired pH value is given by the regulation performance index, and the current density set point may be provided by

a higher layer in the control system. The conceptual design of the cascade control structure is depicted in Fig. 6.9.

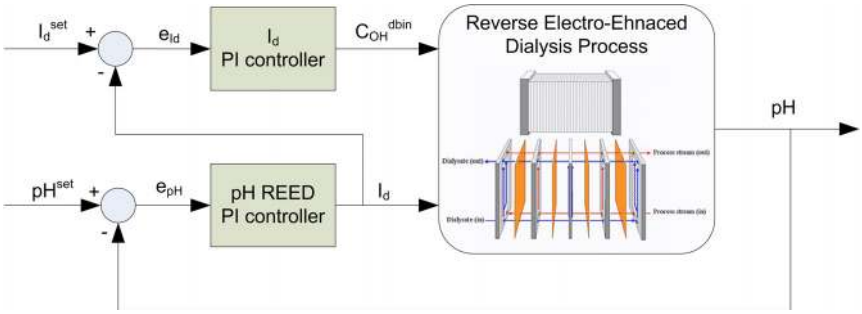

Figure 6.9: Input-resetting control structure for pH control of the outlet of the REED module

6.5.4 Control structure implementation

Once the control structure has been designed, the controllers implementation and performance evaluation are performed. Discrete time Proportional-Integral controllers are employed to build the periodic input-resetting control structure. The controllers are discrete time since our sensitivity analysis was based on the periodicity of the REED system. This choice implies that we can aim to control the pH at the end of each period and not within the period. Taking advantage of the vertical decomposition of the structure, the decoupled design of the two feedback controllers facilitates the implementation. The Proportional-Integral controllers use the following control law:

$$p_k = \bar{p} + K_c \left(e_k + \frac{\Delta t}{\tau_i} \sum_{k}^{j=1} e_j \right) \tag{6.11}$$

where k is the actual sampling time, p is the controller output, $\bar{p}$ is the nominal value of the controller output, K_c is the controller gain, e is the error (see Fig. 6.9), Δt is the sampling time and τ_i is the integral time. The controllers are tuned using IMC method based on an approximated continuous time transfer function. The transfer function is obtained mapping system response at half period time after applying a step disturbance in the manipulated variable (Seborg *et al.*, 2004). If the sampling time is relatively small compared to the process response, then the controller settings obtained for a continuous controller can be employed by the discrete time controller. This condition holds as long as $\Delta t/\tau_i \leq 0.1$ (Isermann, 1989). When the condition is not fulfilled, the discrete time control system must be modified since the zero-order hold plus the sampler introduce an effective time delay in the system response. It has been proposed to approximate the introduced time delay to one half of the sampling period $(\Delta t/2)$(Franklin *et al.*, 1997). Thus, the approximated time delay is added

to the process time delay before tuning the controller. Since the controller settings are based on an approximated system response, it is expected that the controller tuning may be refined manually.

The pH response to a step change in the current density is approximated using a second order transfer function. The controller is tuned using IMC expressions, and the condition $\Delta t/\tau_i \leq 0.1$ is not fulfilled. The half period time delay is introduced and the controller settings updated. The fast control loop is closed and the slow controller is tuned using the same approach. The current density response to a step change in $C^{in}_{OH,dia}$ follows a first order transfer function. In this case the condition $\Delta t/\tau_i \leq 0.1$ is fulfilled and no correction is required. The final controller settings are obtained by manual tuning. Those are depicted in Table. 6.3.

Table 6.3: Discrete input reseting controller settings

Controller	Gain	Integral time (s)
Fast controller	130	200
Slow controller	-0.5	1000

The discrete time input-resetting controller performance is evaluated using a set point tracking test. The controllers output are saturated in order to avoid numerical problems. The minimum $C^{in}_{OH,dia}$ is 50 mol/m^3, since the limiting current density dramatically falls at lower hydroxide concentration in the dialysate channel (Prado-Rubio *et al.*, 2011b). The minimum current density is zero, due to its sign is defined by the reversal time. The maximum current density is the current saturation value which is in the vicinity of 260 A/m^2 (Prado-Rubio *et al.*, 2011b). The initial conditions are defined by stationary Donnan dialysis operation with $C^{in}_{OH,dia}$=150 mol/m^3. Under those conditions the pH at the outlet of the feed channel in REED equals pH=6.074. At time t=0, the control loops are closed with $pH_{set} = 6.25$ and $I_{d,set}$=80 A/m^2. The periodic input-resetting controller performance is depicted in Fig. 6.10.

Due to the positive step change in the desired pH set point, the fast controller response increases the strength of the imposed current density. The initial conditions are given by Donnan dialysis (I_d=0 A/m^2), thus it is expected that a higher current density is required. The end period pH value at the outlet of the feed channel in REED achieves the set point after 5 cycles.

By using one period as sampling time, the fast controller objective is to achieve the pH target at the end of each period. However, the stationary pH behavior is a function of the strength of the imposed electrical field and not of the current polarity. As a consequence, when the end of the period pH set point is achieved implies that the half period pH also reaches that desired point. This can be seen in the top plot in Fig. 6.10, where the circles highlight the pH at the period time which clearly is seen to achieve the stationary goal of the control system design, i.e zero set point error. At the same time, the pH at half period time achieves the set point (shown with triangles).

The slow controller aims to reset the value of the current density. It implies that at the beginning the controller reduces the inlet hydroxide concentration in the

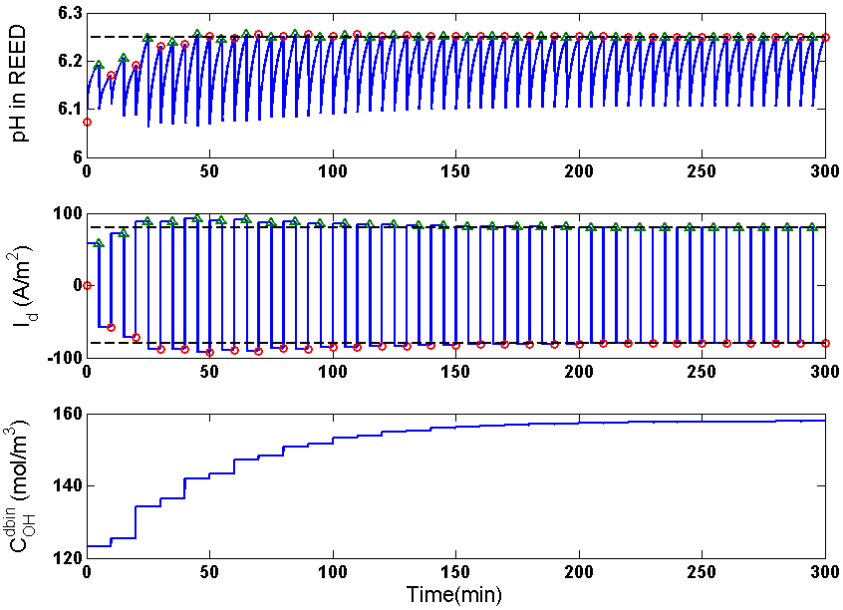

Figure 6.10: Performance of the input-resetting control structure for a set point tracking test when the initial conditions are Donnan dialysis operation. Solid lines represent the dynamic response, (○) corresponds to the value at period time and (△) corresponds to the half period time. Dashed lines are the set points

dialysate channel in order to have a faster rise of the current density magnitude. Afterwards, $C_{OH,dia}^{in}$ slowly increase to compensate the I_d overshoot obtained when the desired pH is achieved. The current density strength settles after 12 cycles, which is more than double the cycles required by the fast controller. In the second plot of Fig. 6.10, the circles and triangles are employed every half period time to show the convergence to the desired current density magnitude.

6.6 Conclusions

This contribution illustrates how to perform a quantitative systematic analysis, which leads to select an appropriate combination of manipulated variables to satisfy a specific control goal for a highly non linear and dynamic system, when the selection is neither intuitive nor trivial. As case study, the pH control at the end of the feed channel of the REED module is selected as subgoal. A quantitative defined operating window was explored using a dynamic model derived from first principles. The model describes the simultaneous transport of multiple ions across anion exchange membranes in a REED cell during lactate recovery from a fermentation broth. The solution of the system of multiregion partial differential equations was approximated numerically (Prado-Rubio *et al.*, 2010b, 2011b,a).

Here, the pH model in the cultivation is highlighted including a pH buffer effect

which was been experimentally evidenced (Møllerhøj, 2006). The dimensionless pH sensitivity, towards I_d and $C^{in}_{OH,dia}$, was used as the quantitative criterion. The sensitivity was evaluated at specific points within the periodic shifting of the imposed gradient polarity. The results show that pH can be controlled, during stationary operation, by either of the manipulated variables; especially around low current densities. However, pH has shown a considerably higher sensitivity towards current density in the first middle period point after a step change in the actuator. That behavior leads to propose that the dynamic pH response can be controlled by manipulating the current density. Additionally, the base concentration in the inlet of the dialysate channel can control the stationary response since the I_d operating window is much narrower than for $C^{in}_{OH,dia}$.

The control structure was implemented, tuned and its performance evaluated using a set point tacking test. The controller performance is satisfactory. It should be stressed that the found controller settings strongly depend of the operating point. The last is defined by the pH and I_d set points that must be provided by a higher layer in the hierarchical control structure. Therefore, a lost in the controller performance must be compensated by a re-tuning. In practice, the actual controllers tuning must clearly depend upon the specific location within the operating window. This dependence follows directly from the large variation on the sensitivities within the operating window as shown in Fig. 6.8.

6.7 Nomenclature

C	Concentration (mol m^{-3})
D	Diffusion coefficient (m^2 s^{-1})
DD	Donnan Dialysis
e	Output error
EDD	Electro-Enhanced Dialysis
F	Faraday constant (C mol^{-1})
I_d	Current density (A m^{-2})
J	Flux (mole m^{-2} s^{-1})
k	Kinetic parameter (-)
K_a	Acid dissociation constant (mol m^{-3})
K_c	Controller gain
K_d	Dissociation constant (mol m^{-3})
K_w	Ionic product for water (mol^2 m^{-6})
NS	Dimensionless sensitivity
p	Controller output
$\overline{p}$	Nominal controller output
q	Flow rate (m^3 s^{-1})
R	Universal gas constant (J mol^{-1} K^{-1})
$REED$	Reverse Electro-Enhanced Dialysis
R_k	Total reaction rate of k (mol m^{-3} s^{-1})
r_i	Reaction rate i (mol m^{-3} s^{-1})
t	Time (s)

t_s	Settling time
T	Absolute temperature (K)
t_{rev}	Reversal time (s)
x	Spatial direction (m)
z_k	Valence of k (-)

Greek letters

α	Sign vector for r_1 (-)
β	Sign vector for r_2 (-)
ψ	Electrical potential (V)
	($\tau_{dia} = h_{dia}WL/q_{dia}$) (s)
τ_i	Integral time

Subscripts

C_b	Base concentration
dia	Dialysate channel
$feed$	Feed channel
HL	Lactic acid
HP	Undissociated protein
I_d	Current density
in	Inlet
i	Specie
k	Specie
L^-	Lactate ion
Na^+	Sodium ion
OH^-	Hydroxide ion
P^-	Dissociated protein
set	Set point
t_0	At time zero

Superscripts

$dbin$	Dialysate bulk inlet
$fbin$	Feed bulk inlet
in	Inlet

7

Integrated bioreactor and Reverse Electro-Enhanced Dialysis system

7.1 Abstract

From a goal driven analysis for process design and control design, the role of the individual units in the integrated system is defined as well as a sequential strategy to design the integrated system based on the design constraints. The integration of lactic acid fermentation and Reverse Electro-Enhanced Dialysis is investigated based upon previously developed mathematical models. The degrees of freedom analysis reveals the process integration requirements which implies additional model assumptions and mass balances. The conceptual analysis of the processes integration based upon an existing design of the separation unit shows the potential need of an additional pH controller in the fermenter. A Proportional-Integral (PI) controller is implemented and tested for pH regulation. The complete control structure for the integrated system consists of this PI controller in the fermenter plus an input resetting control structure in the REED module. The integrated system design and operation is studied in two case studies: batch production of starter culture and the continuous production of lactic acid. Substantial productivity improvements are predicted in both cases using the integrated process, despite a not entirely satisfactory control performance. The simulation results lead to propose challenges in the design and control of the integrated membrane bioreactor system.

7.2 Introduction

Process design and process control design are still considered separated disciplines which supplement the process synthesis. Process design and control system development are traditionally performed sequentially despite they are tightly coupled. First, the process is designed to achieve the design objectives, assuming that a control system can be designed to keep the process in the desired operating point. Once the process is designed, the achievable system operability is investigated resulting in the control structure design. The sequential approach may be inconvenient since process control challenges may arise due to an inadequate or inflexible process design, which can lead, e.g. to dynamic constraint violations where feedback control may not guarantee robust performance (Malcolm *et al.*, 2007). As a consequence, the control system would be unable to meet its design specifications. When process design is evaluated sequentially to process control design it may lead to the elimination of easily controlled designs which are not economically optimal.

Due the interactions between process and control design decisions, there is a trend towards the combining process design and operability considerations. As evidenced by the increasing number of publications that address this issue. These methodologies may be classified into two types: methods which enable screening designs for controllability and methods which integrate the design of the process and the control system development (Lewin, 1999). In the first group, different process designs can be compared and classified based on open and closed loop controlability metrices such as relative gain array, condition number and disturbance condition number (Bristol, 1966; Morari, 1983; Palazoglu and Arkun, 1986; Skogestad and Morari, 1987). The second group is based on the simultaneous optimization of the process and control design, often called integrated process design and control design (IPDC methods) (Bahri *et al.*, 1997; Bansal *et al.*, 2000; Kookos and Perkins, 2001; Malcolm *et al.*, 2007; Patel *et al.*, 2008; Ricardez-Sandoval *et al.*, 2010; Hamid *et al.*, 2010). The objective has been to obtain a profitable and operable process as well as the control structure through a systematic procedure. Therefore, controllability and process design issues are resolved simultaneously. The main drawback in an IPDC problem is that the application of these methods is constrained by the computational resources available. Thus, the nature of the process might limit their applicability.

The study of integrated systems involves even more challenges for the process design and control. Despite process integration is becoming common in industry, their design, behavior and operability are still fertile research areas. In simple cascade processing, the knowledge on the independent units can be applied since the units are linked sequentially (Luyben, 1993). The operability may not be a problem when the manipulated variables in each unit are internal, and disturbances will not propagate to other units in the plant. When single variable control loops are present in the system, interaction between control loops can be a limitation. However, if some controllers are faster than others, the interaction may not be a problem. The challenging problems arise when the disturbances propagates through the plant, thus conventional single variable local loops may be insufficient to control inventories (Faanes and Skogestad, 1999).

Additional challenges are prevailing in recycle systems due to the positive material and/or energy feedback. The dynamics and operational aspects of these integrated processes have not been thoroughly investigated. Their dynamics are more complex and may not be sufficiently well understood. Recycle systems can exhibit interesting behaviors such as: high sensitivity, unexpected changes in the plant time constants due to the integration, propagation and recirculation of disturbances, infeasibility and state multiplicity (Recke and Jørgensen, 1999; Jacobsen, 1999; Pushpavanam and Kienle, 2001; Seborg *et al.*, 2004).

Research in integration of process and control design for integrated reactor-separation systems, has focused on coupled reactor and distillation columns using mainly linear models (Luyben, 1993). The reactor is chosen as key unit since it is expected that the separation section is efficient and robust. This can be achieved by assuming good quality local control loops and overdesign of the separation unit (Kiss *et al.*, 2007). However in the particular case investigated in this contribution, an integrated bioreactor and membrane separation process, both process dynamics are relevant. The complexity of the interaction between these process units makes the integrated

system very interesting to investigate.

The purpose of this chapter is to investigate the goal driven integrated process design and operability to identify potential limitations. The chapter is structured as follows: a strategy for goal driven process and operability design of the integrated system is presented and analyzed. From that analysis, the required extra considerations to integrate previously developed unit models are identified. These requirements also include a PI controller to regulate the pH in the fermenter which is implemented and its performance evaluated. The final control structure for the integrated bioreactor and REED module is completed. The design and operability of the integrated system is investigated using two case studies: the batch production of a starter culture and the continuous production of lactic acid. Limitations in the design and control of both processes are analyzed. Based on the results, some research challenges are described. Finally, the conclusions are drawn.

7.3 Goal driven integrated process and control design

The design of the integrated processes under investigation is challenging since it is tightly coupled to the partially developed monitoring system design. A conceptual representation of the interactions between the process and operability design is depicted in Fig. 7.1.

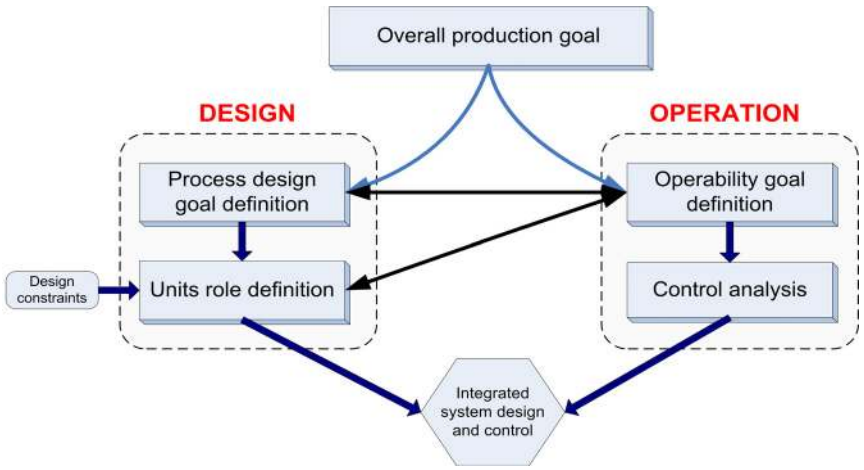

Figure 7.1: Conceptual sketch of the interaction between process design and control system development within a goal driven framework

The overall production goal is broken down into a process design goal and an operability goal. The design and operability goals are defined by the desired target product and its production mode. For instance, if a production process requires fedbatch operation, then the operational requirements are quite different from a case where continuous operation is the most desired operation form. The process

design and operability goals must of course be feasible and are interdependent. The achievement of the goals result in the process design, a operating point or trajectory and the means (i.e. control structure) to operate at that point or to follow the trajectory.

From these goal definitions follow selection of the unit roles to fulfill the required production goal and the identification of potential design constraints. At this point, another interaction between process design and control goal definition arises. The reason is the control subobjectives become the means to achieve the role of the individual units in the integrated process. Additional control subobjectives may be required, for local regulation and/or supervision purposes.

Subsequently follows the design of the unit(-s). For the operational design follows first an analysis of available degrees of operational freedom, which is used to select the actuators for controlling the operation to satisfy the operational goal. In accordance the process design must ensure sufficient power in the actuators to enable coverage of the desired operating window for the process. It is interesting to evaluate how the degrees of freedom of the individuals units are moved by the integration of the two processes.

The IPDC problem can be formulated as an optimization problem where a performance objective function in terms of design, control and cost is optimized subject to constraints such as: process (dynamic and steady state) and conditional (process-control specifications) (Hamid *et al.*, 2010). In the present highly integrated process, the complexity of the models, model validity constraints and potential infeasible simulation scenarios of the integrated system are the main limitations to apply a simultaneous process design and control design approach. Therefore, the solution of the problem is attempted in a sequential manner but accounting for the conceptual interaction between design and control of the integrated process. The formulation of the two problems separately can provide relevant information for the appropriate design of the integrated system.

Relevant processing objectives can be: continuous lactic acid production, biomass production with higher activity (starter cultures for probiotics cultivations) or the production of extracellular proteins using genetically modified bacteria. Those objectives define the overall production goal and indirectly the fermenter operation mode, i.e. batch, fedbatch or continuous. If the target is lactic acid production as commodity chemical, continuous processing is the clear option. On the other hand, a batch or fedbatch fermentation is most appropriate for the production of starter cultures or extracellular proteins (Boonmee *et al.*, 2007).

In the next step, the design constrains have a large influence in the design strategy of the integrated system. In this application, the main design constraints are possessed by the available model of the REED unit. The idea is to use the developed model without compromising its validity. Additionally, the integrated process model might not be solved without revealing how REED should be operated. Therefore, the design strategy is to fix the membrane unit dimensions and then design the fermenter in accordance with the goal of the integrated process.

According to this design strategy, the role of the REED module in the integrated system is defining the fermenter operating volume. During REED operation, lactate ions are dynamically exchanged by hydroxide ions. Therefore, REED can play two different roles in the integrated system that leads to different designs: it can be

designed to control the lactate concentration in the fermenter or to facilitate the pH control in the fermenter. In an ideal scenario, when the REED is capable to remove the lactate that is produced in the fermenter, the hydroxide introduced to the cultivation broth is the required to keep the pH. Therefore, the REED module completely substitutes the pH control in the fermenter and control the total lactate concentration at the desired operating point.

In the modeled system, several situations can cause that REED can not totally regulate the pH in the fermenter: the Donnan exclusion is not 100% efficient, the potential incapability of REED to remove the lactate produced and the influence of purge stream (during continuous operation). The mentioned sources of non ideality, define implicitly another subobjective for the control structure design layer. The REED may not be able to completely substitute the pH regulation in the fermenter. Thus, the previously developed input resetting control structure for the REED separation must be complemented by a pH controller in the fermenter.

Experimentally yet another issue has been identified: the current efficiency loss due to the transport of other anions (mainly nutrients) present in the fermentation broth, which means lower lactate fluxes. In addition, nutrient loss (anions) can generate lag periods in the biomass growth (Ishizaki *et al.*, 1990; Boonmee *et al.*, 2007; Jurag-Separation, 2009). The latest problems have not been investigated here since that requires a more detailed fermenter and REED models than developed during this work.

7.4 Model extensions for process integration

This investigation is a knowledge based approach, represented in the forms of models for the units to be integrated. The previously derived models for the individual units were developed for defined purposes. In order to make the models suitable for process integration, some adjustments are revealed by a degree of freedom analysis for the integrated system. These model adjustments imply extra assumptions and equations. The extra considerations are listed below. The operational degrees of freedom analysis for the integrated system is shown in the Appendix C.

7.4.1 Mass balances extension in the REED module

The mass balances presented in Prado-Rubio *et al.* (2010b) consider the presence of the following substances in the fermentation broth which is fed to the REED unit: lactate (L^-), hydroxide (OH^-), sodium (Na^+), dissociated protein (P^-), lactic acid (HL) and undissociated protein (HP). However, according to the bioreactor model previously developed, the substrate and biomass are outputs of the reactor and thus their mass balances must be added to the REED model. Recalling the assumption **MA3** presented in the model development, there is assumed to be no transport of uncharged species or large molecules through the anion exchange membranes. Meaning that the substrate and biomass are 100% retained in the feed channels of the REED module (Prado-Rubio *et al.*, 2010b). On the top, the following extra assumptions are added (EA):

EA1. The biomass is uncharged and thus it is transported through the boundary layers just by diffusion.

EA2. The biomass diffusion coefficient in solution is assumed equal to the value assigned for the hypothetical protein species ($D_x^s = 9.0 \times 10^{-11}$ m^2/s) (Bowen *et al.*, 2000). The diffusion coefficient for the lactose is taken from literature ($D_s^s = 0.38 \times 10^{-9}$ m^2/s) (Lide, 2008).

EA3. The substrate and biomass do not intervene in the pH balance already defined for the system.

EA4. There are neither biomass production nor substrate consumption in the feed channel of the REED module. This assumption is reasonable since the residence time in REED considerably shorter than in the fermenter. This condition largely depends on the integrated system design and operational conditions. Therefore, it must be confirmed in every simulated scenario.

EA5. The biomass and substrate do not strongly modify the rheology of the system and therefore the flow conditions. This assumption implies that for the previously investigated flow rates, the thickness of the boundary layers remains.

EA6. The substrate and biomass are not accumulating in the REED module. Therefore, the potential material attachment to the membrane surface is not investigated. This assumption is reasonable considering the REED antifouling mechanism (Prado-Rubio *et al.*, 2011a)

The mass balances and boundary conditions defining the substrate and biomass transport along the y-direction and x-direction (see Fig. 2.2), are completely analogous to the undissociated protein or lactic acid (depicted in Chapter 2). The reason is that they are uncharged molecules that are only present in the feed channel. Therefore, the terms involving migration in the mass balance do not apply for those components (Eq. 2.8, shown below), and the zero flux condition at the boundary layer-membrane interface remains.

$$\frac{\partial C_{k,p}}{\partial \tau} = \frac{\tau_n}{\tau_{diff}} \left(\frac{\partial^2 C_{k,p}}{\partial z^2} + z_k \left(\frac{\partial C_{k,p}}{\partial z} \frac{\partial \varphi_p}{\partial z} + C_{k,p} \frac{\partial^2 \varphi_p}{\partial z^2} \right) \right) + \tau_n R_k$$

7.4.2 Protein production rate in the fermenter

As stated in the bioreactor modeling using assumption **FA8** (Chapter 5), the two forms of protein production rate (P^- and HP) have been chosen such that the total protein concentration in the fermenter remains constant at the reactor pH. This assumption can be understood in different ways according to the operational mode of the fermenter. The following scenarios were investigated:

- Batch reactor with perfect pH control: in this ideal scenario, the pH is kept constant by the addition of sodium hydroxide molecules that compensate for the lactic acid formation. Therefore, there is no change in the reactor operating volume. If the initial total protein concentration is the desired value, the protein production rates equal zero.

- Fed-batch reactor: this operation mode also includes the case of a batch reactor with pH regulation employing a solution of a strong base, since there is expected a change of the reactor operating volume. In this case, the protein production rate must compensate for the concentration change due to the dilution which is generated by the input flow rate and/or the base solution addition (see Fig. 7.4).

- Continuous reactor with pH control: the protein production rate is assumed to compensate for the protein that leaves the reactor in the exit stream (see Fig. 7.4).

7.4.3 Models units

The bioreactor model presented in Chapter 5, was developed in weight basis in order to easily compare the results with relevant experimental data. On the other hand, the mass balances proposed for the REED module are on molar basis.

The molar basis is selected for the integrated system. This choice means that the units of the model parameters and variables in the fermenter mass balances must be changed to make the model compatible with the REED model. In some of the results depicted in this chapter, the concentrations are switched back to weight basis for comparison with data reported in literature.

7.5 Results and discussion

From the goal driven integrated process design, it was identified that under a non ideal scenario a pH controller in the fermenter might be necessary to enable maintaining pH. Introduction of a fermenter pH control loop corresponds to a regulatory layer control problem which is handled initially. Subsequently, the goal driven design and operation of the integrated process is investigated considering two different production goals: the batchwise production of a starter culture and the continuous production of lactic acid. The integration issues of these two cases are analyzed separately.

7.5.1 pH control in the fermenter

A conventional problem in bioreactor control is regulation of abiotic variables, such as pH and temperature, to guarantee optimal conditions for the biological reaction or microbial growth.

A continuous PI controller in the fermenter is implemented to keep the pH using the base input stream so called υ_{base} as manipulated variable (see Fig. 7.4). As pH control agent, a solution of sodium hydroxide is employed, its concentration depends on the application. Satisfactory controller settings are obtained by manual tuning ($K_p = 0.0001$ and $\tau_I = 100$). The controller performance was evaluated simulating a 5 liters continuous fermenter start up employing the best inputs variables previously estimated (see Chapter 5). The objective is to regulate the pH at 5.75 using a 2M solution of sodium hydroxide. The fermenter behavior and actuator are shown in Fig. 7.2.

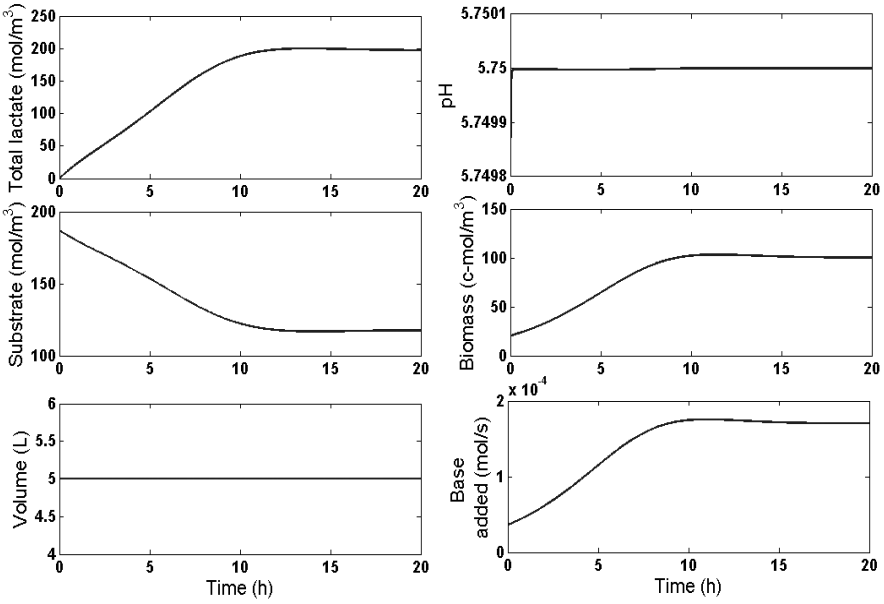

Figure 7.2: Simulated continuous fermentation start up to best operating point using a continuous PI pH controller, where the setpoint is pH=5.75

At this stage, the pH controller performance is tested rejecting periodic disturbances in hydroxide ion concentration. The idea is to evaluate how the pH controller in the fermenter will behave when the REED module is integrated during a batch fermentation (properly speaking is a fedbatch fermentation, due to the volume change). Employing the minimum and maximum hydroxide fluxes estimated previously for REED operation under $I_d = 100$ A/m^2 and $C^{in}_{OH,dia}$=50 mol/m^3 (depicted in Table 7.1), a periodic function is constructed. Then the disturbance is applied to the pH controlled batch fermentation previously investigated using 80 g/l of initial substrate (see Chapter 5), between 5h$\leq$ t $\leq$8.667h (300 min$\leq$ t $\leq$520 min). The disturbance duration time was estimated based on the fermenter hydroxide requirements. A enlarged picture of the disturbance and the actuator response are depicted in Fig. 7.3.

The simulation results indicate that the pH in the fermenter remains constant (not shown since it is constant at the desired value), while the controller output oscillates to reject a periodic disturbance with the same period time as the disturbance. The comparison between the actuator behavior with and without the disturbance is shown in Fig. 7.3(b). This high frequency response may be a problem for the actuator. For that reason, a discrete time pH controller is also implemented and its performance evaluated in during the processes integration (the two case studies).

The pH controlled fermentation is integrated with the REED module which uses the input resetting control pH structure. The complete control system architecture is depicted in Fig. 7.4. The pH in the fermenter is regulated by the developed

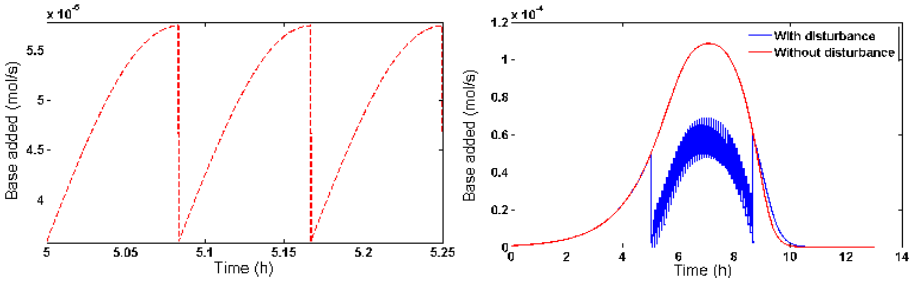

(a) Disturbance **(b)** Actuator response

Figure 7.3: Enlarged periodic hydroxide concentration disturbance function during a batch fermentation and PI actuator response to reject the disturbance (the actuator behavior without disturbance is also shown) . The periodic disturbance (period time is 5 min) is applied between 5h$\leq$ t $\leq$8.667h

controller herein, while the input resetting control structure controls the pH change along the feed channel. Conceptually, the REED module operation facilitates pH control in the fermenter and the extra hydroxide, if necessary, is provided by the pH regulator in the fermenter. This control structure has the potential problem that the controllers may fight if they do not know how the other controller behaves. This issue should be handled at different levels of complexity: by an appropriate controllers tuning, a feedforward action or perhaps a multivariable control design.

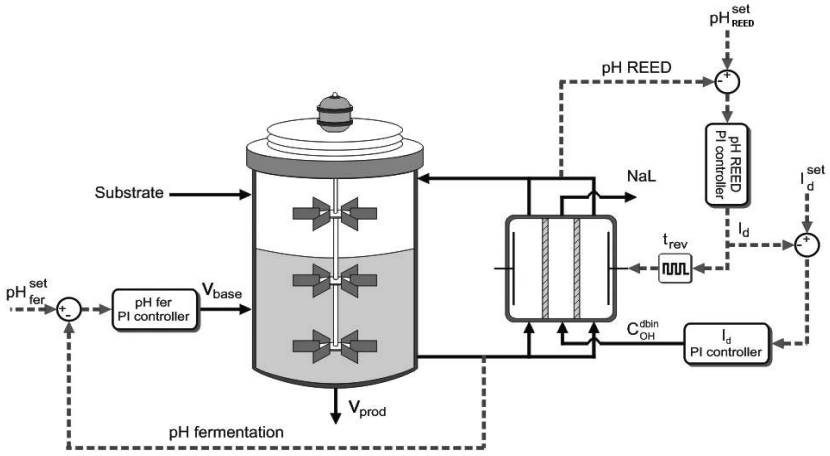

Figure 7.4: Sketch of the complete pH control architecture of the integrated system. Solid lines are flow streams while dashed lines are signals. The input resetting control structure controls the separation in REED while there is a PI pH controller in the fermenter

7.5.2 Facilitated pH control in the fermenter during batch fermentation

Batch or fedbatch cultivations have been used to produce starter cultures of lactic acid bacteria for dairy industry. During this type of fermentation, lactate is accumulated in the cultivation broth and therefore progressively inhibits biomass growth. Therefore it is relevant to investigate the usage of REED to increase the potential bacterial productivity during batch operation. The selected case study is a pH controlled batch fermentation coupled to the REED module. The fermenter is a fedbatch reactor since there is an operating volume evolution when the addition of a solution of sodium hydroxide is necessary for pH control.

Experimentally, a batch fermentation coupled with electrodialysis has been investigated for production of *Lactococcus lactis* starter culture (Boonmee *et al.*, 2007). Their study is the continuation of a previous experimental and modeling work on lactic acid fermentation (Boonmee *et al.*, 2003). The experimental data presented in that contribution were used for the bioreactor model development in Chapter 5. The batch experiment of the integrated system started using 80 g/l substrate. After 5 hours, the recirculation through the electrodialysis unit was initiated. These experimental results will be compared to the performance of the integrated bioreactor and REED module.

7.5.2.1 Batch integrated system design

The integrated system design is handled using the above presented strategy, where the design and operability problems are solved sequentially.

The batch cultivation starts with a low biomass concentration in a cultivation broth rich in substrate and required nutrients. At the beginning, the membrane separation process is not coupled to the fermenter. The reason is that when lactate concentration is rather low, current saturation conditions may be achieved in REED module generating numerical problems (Prado-Rubio *et al.*, 2011b). Therefore, a certain lactate concentration is required in the fermentation broth before the REED can be started. The role of the REED module in the integrated system is to provide the hydroxide necessary to neutralize the lactic acid produced during the fermentation, thus to maintain a constant pH in the bioreactor.

This design problem is particularly interesting due to the dynamic nature of both the bioreactor and REED. There are 2 design issues:

a. The minimum average hydroxide flux provided by REED can not be excessively higher than the bioreactor base requirements at the process integration time. Otherwise, there is the risk that the pH in the fermenter increases and adversely may influence the biomass growth. Even though the loss of biomass viability as a function of the increased pH is not accounted for in the model, this situation is undesired.

b. In order to completely substitute the pH control in the fermenter by operating the REED with pH control, the membrane separation process must be capable of providing sufficient hydroxide to neutralize the produced lactic acid during the entire fermentation.

The solution strategy is based on simulations of the pH controlled fermenter and REED module. First, the range of hydroxide flux that can be provided by the fixed design of REED module is calculated. Then the volumetric hydroxide requirements in the fermentation are estimated. The fermenter volume is estimated by matching the lowest amount of hydroxide provided by the REED module and the base requirements at the integration time. From the calculations, it is interesting to reveal if the integrated system design can match both design constraints. If that is not the case, then the objective is to determine to which extent the REED module facilitates the pH control in the fermenter.

The first step is to estimate amount of hydroxide that can introduced to the cultivation by the REED module. This is important since different hydroxide fluxes are required along the operation which it mostly is batch, although the volume increase makes it a fedbatch (approximately 15%). The batch cultivation broth concentrations after 5 hours of operation are used as constant inputs for the membrane separation process. A summary of the stationary REED simulation results are depicted in Table 7.1.

Table 7.1: Summary of average hydroxide flux in REED using a cultivation broth at 5 hours of batch fermentation. The average hydroxide flux ($\overline{F_{OH}}$) is estimated using the composite Simpson rule. The reversal time used in the simulation is 5 min

Case	I_d (A/m^2)	$C^{in}_{OH,dia}$ mol/m^3	F^{max}_{OH} mol/s	F^{min}_{OH} mol/s	$\overline{F_{OH}}$ mol/s
Donnan	0	50	4.929x10^{-5}	4.929x10^{-5}	4.929x10^{-5}
REED	100	50	3.589x10^{-5}	5.745x10^{-5}	4.949x10^{-5}
REED	250	250	1.112x10^{-4}	-7.689x10^{-6}	6.785x10^{-5}
REED	250	500	1.444x10^{-4}	-6.781x10^{-6}	7.095x10^{-5}

The first design constraint is that Donnan dialysis can take over the pH control when the system is integrated. Donnan dialysis separation is chosen since the minimum ion fluxes are obtained (Prado-Rubio *et al.*, 2011a). The hydroxide requirements during the batch fermentation are calculated using the previously presented continuous pH controller in the fermenter. This controller provides the evolution of the hydroxide requirements which directly depends on the lactic acid production during the fermentation. Therefore, the fermenter volume is estimated by matching the REED module and fermentation results at the processes integration time. It means matching $\overline{F_{OH\,Donnan}}$ to the hydroxide requirements per reactor volume of the fermentation. The later value equals the lactic acid productivity in the fermenter during a pH controlled fermentation. The solution leads to a bioreactor volume of approximately 2 l.

The bioreactor is simulated for a 13 hours batch fermentation using 80 g/l of initial substrate and the estimated volume. The pH is controlled employing a 5M solution of sodium hydroxide. The fermentation simulation results together with available experimental data without lactate separation are shown in Fig. 7.5 (Boonmee *et al.*, 2003) (notice that the experimental data set was used previously in the Chapter 5).

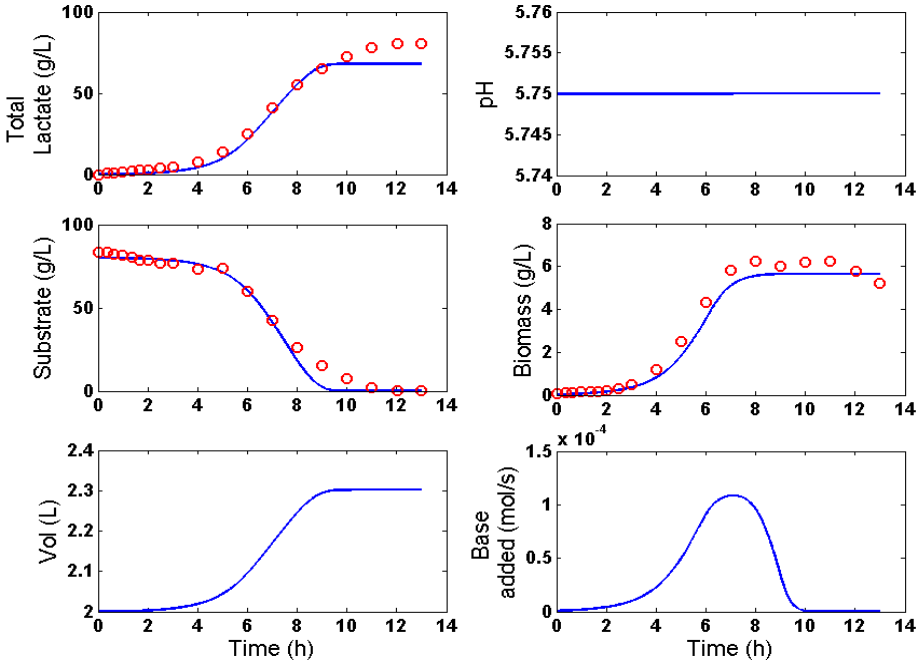

Figure 7.5: Simulation of a pH controlled batch fermentation using 80 g/l of initial substrate without lactate separation. Red open dots represent the experimental data (Boonmee *et al.*, 2003). Solid lines are the model prediction

The most important fermentation result is the behavior of pH control actuator. At t=5h, the sodium hydroxide molar flow rate is 4.98x10^{-5} mol/s. The maximum molar flow rate is 1.09x10^{-4} mol/s at 7.1 hours of operation. Comparing the fermenter requirements and the REED separation capabilities, it can be concluded that the two design issues can not be fulfilled simultaneously, given the fixed design of the REED module. When the system is integrated, Donnan dialysis adds to the fermentation broth approximately the hydroxide which is required. However, at the maximum lactic acid production point, REED could at most supply 65% of the hydroxide required. Therefore, the REED module can only facilitate the pH control in the fermenter.

Another issue during the system design is not so evident at first look. The continuous pH control in the fermenter employs a solution of sodium hydroxide that modifies the bioreactor volume (see Fig. 7.5). However, the hydroxide addition by REED does not affect the reactor volume since water transport through the membrane has not been modeled. Therefore, there is an imbalance within the calculations that generates a biased design.

7.5.2.2 Batch integrated system behavior

In order to reveal the potential benefit of process integration it is relevant to compare the performance of conventional batch fermentation (simulated), batch fermentation coupled with electrodialysis (experimental, (Boonmee *et al.*, 2007)) and the integrated fermentation and REED system (simulated), the same experiment is reproduced as reported in the literature. The batch fermentation simulation results are depicted in Fig. 7.5.

The initial conditions for the integrated system simulation are the fermentation concentrations at t=5 hours. The simulation is stopped when the lactic acid production is rather low and the REED module forces the fermenter to high pH values. The entire control structure with a discrete time pH controller in the fermenter is tested for this case study. Due to the problems evidenced during the continuous system, especially the potential pH drops in the fermentation broth, a different strategy is investigated during batch operation (see section 7.5.3.2). In the continuous fermentation case, the pH at the outlet of the feed channel in the REED module is the setpoint. It defines which separation is desired in REED when the pH is constant at the entrance of the module. However when the pH decreases in the fermentation broth, actuators in REED are forced to saturate to achieve the desired pH setpoint at outlet of the feed channel. Thus the control objective cannot be satisfied. An alternative is to define a desired pH change along the channel, instead of defining a fixed pH at the outlet of REED. In that way, the constant pH setpoint is transformed into a trajectory. The desired pH change along the feed channel in the REED module is ΔpH=0.25 (this value was estimated as achievable through closed loop simulations).

The response of the actuators in the input resetting control structure is shown in Fig. 7.6. It can be seen how at the beginning REED operation under current load conditions is not necessary, as was expected from the first condition in the design. Once the process evolves, current starts to be applied from around 5.4 hours, and subsequently the amplitude increases. The trajectory of the desired pH setpoint in REED is depicted. The fast controller input resetting structure has a small off set especially between one and two hours after the integration. The I_d controller, which is the slower controller in the input resetting structure, is not sufficiently fast to reset the current density. The point where the REED module should be detached is clear since the pH at the outlet of the membrane module increases rapidly.

Fig. 7.7 shows the evolution of the fermenter concentrations. The unsatisfactory pH control in the fermenter is clear. However, the biomass growth is not influenced by this bias (according to FA1). The lactate concentration is reduced initially, but round 1 hour after the integration, the lactic acid production overcomes the lactate removal and therefore it accumulates in the bioreactor. There is no substantial difference between the biomass growth between the batch fermentation alone and the integrated system before 7 hours of operation (Figs. 7.5 and 7.7). The difference arises after 7 hours of the fermentation where inhibition completely stops biomass growth in the batch fermentation. While in the integrated system, the growth is prolonged achieving higher biomass density. Additionally, the final reactor volume is lower than the case without REED due to it facilitates the pH in the fermenter, then the base requirements are lower as well.

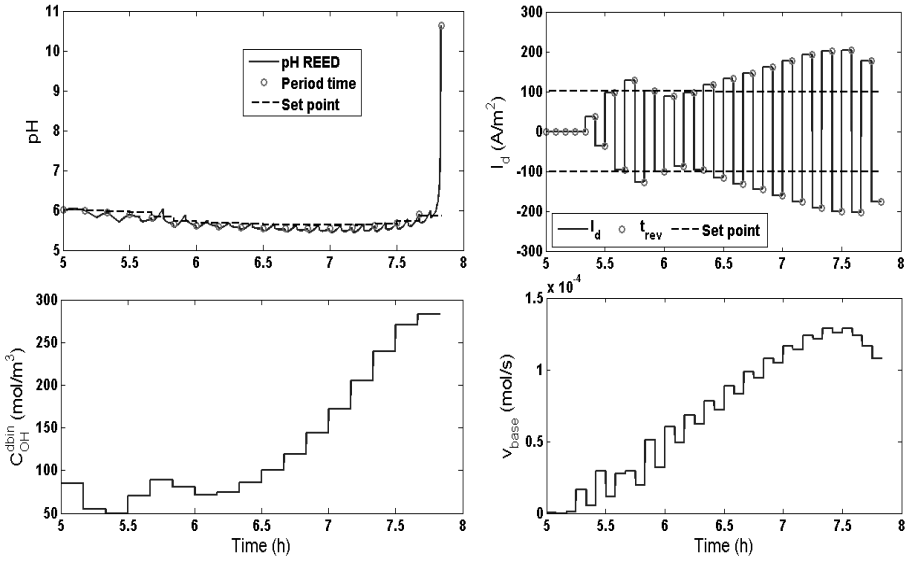

Figure 7.6: pH values at the outlet of the REED module and actuator values during batch operation of the integrated system. Current density (I_d) and input hydroxide concentration to the dialysate channel (C_{OH}^{dbin}) are defined by the input resetting control structure in REED. The base addition to the fermenter (v_{base}) is the output of the discrete time pH controller. The desired pH change along the feed channel is ΔpH=0.25

Some key performance indexes are summarized in Table 7.2, where the batch fermentation is compared to the experimental batch+electrodialysis and predicted batch+REED. The batch fermentation and integrated fermentation and electrodialysis data are taken from the literature (Boonmee *et al.*, 2003, 2007).

Despite the pH is not satisfactorily controlled in the fermenter in the integrated bioreactor with the REED unit, this technology is promising for the production of starter cultures. Comparing the key performance indexes, both integrated systems increase the biomass concentration, biomass yield and biomass productivity compared to the batch fermentation. The significant differences between using the electrodialysis and REED can be explained by the following facts. Lower biomass concentration in the experimental setup can be due to loss of cells that are attached to the electrodialysis membranes (Boonmee *et al.*, 2007; Ishizaki *et al.*, 1990). Another potential problem is the nutrient transport through the membranes. This problem is significantly larger during batch than for continuous fermentation since higher nutrient concentration is used. There are two effects due to the transport of other species: loss of current efficiency and potential nutrient deficiency. Experimentally, if there is a nutrient lack in the fermenter biomass will not grow as much as expected.

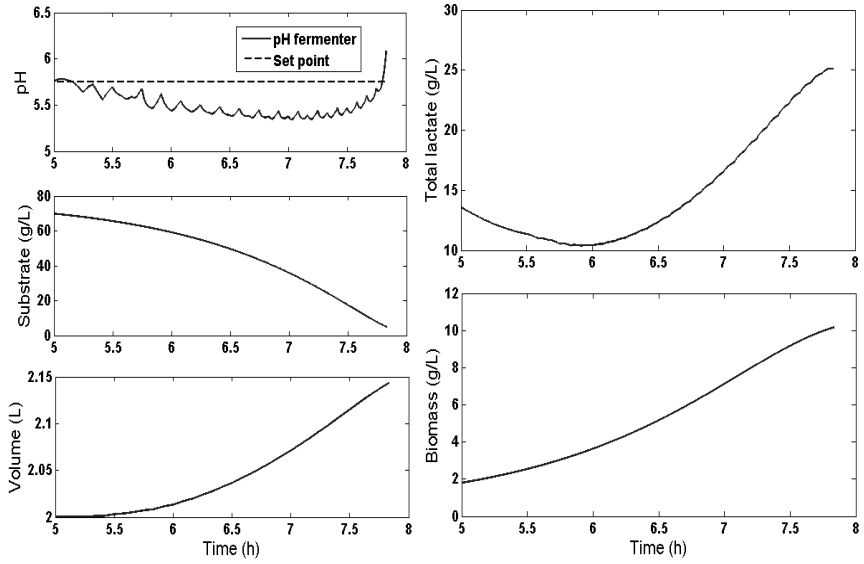

Figure 7.7: Batch fermentation behavior when REED is integrated with the bioreactor

7.5.3 Process Integration for Continuous Operation

In order to make the production of the commodity lactic acid economically feasible by employing REED technology, and most likely any other technology, the fermentation must be operated continuously. Such an integrated process is designed below using the described goal driven methodology for process and control design. Afterwards, the integrated system behavior is studied.

7.5.3.1 Continuous integrated system design

The fermenter design follows the described goal driven integrated system design strategy, where the production goal is to produce lactic acid. In this case, the REED module role in the integrated system is to remove the lactate produced in the fermenter. By separating the lactate that is produced in the bioreactor, its concentration can be maintained at a desired value in the fermenter. The best product concentration must be estimated through an optimization procedure for the integrated system, which is at the highest level of a process design methodology (Skogestad, 2000; Jørgensen, 2006).

When the REED module dimensions are fixed as is the case here, the bioreactor volume is estimated by matching the lactate productivity in the fermenter and the lactate which can be removed in the REED module. Those values are estimated from simulations of the individual units as follows. The initial step is to select the lactate productivity point in the fermenter. Subsequently, the REED model is simulated under Donnan dialysis conditions to determine the potential lactate separation. This simulation scenario is selected as a reference since average lactate extraction under

Table 7.2: Key performance indexes for batch bioreactor (simulated), integrated bioreactor and electrodialysis (experimental) and Integrated bioreactor and REED (simulated). The batch bioreactor with REED improvement is relative to batch bioreactor with ED

Performance Index	Batch Bioreactor (B)	Batch B+ED	Batch B+REED	REED improvement	Units
Batch time	10	11	7.8	-29%	h
Final lactate	68.09	13.32	25.09	88%	g/l
Final biomass	5.65	6.55	10.17	55%	g/l
Final substrate	≈0	≈0	4.77	-	g/l
Biomass yield	0.0706	0.0819	0.1352	65%	g/g
Biomass Productivity	0.565	0.596	1.304	118%	g/l/h

Donnan dialysis is the minimum achievable separation (Prado-Rubio *et al.*, 2011b,a). The minimum separation is selected since the lactate productivity increases by the *in situ* lactate removal. Using lactate productivity and the hydroxide fluxes in the REED module, the fermenter volume can be estimated.

Two operating points have been selected to investigate the design of the integrated process, an optimal and a suboptimal point. The suboptimal conditions are a scaled version of the optimal operation point, where the same amount of substrate is provided using a five times more concentrated substrate input stream. As a consequence, the fermenter input flow rate is reduced in the same proportion. The fermenter model outputs in both scenarios are summarized in Table 7.3.

Table 7.3: Selected bioreactor operating points for continuous production of lactic acid. The lactate productivity is depicted as well as the calculated bioreactor volume

Output	Optimal point	Suboptimal point	Units
C_{L^-}	221.18	381.89	mol/m^3
C_{OH^-}	5.62x10^{-6}	5.62x10^{-6}	mol/m^3
C_{Na^+}	229.67	381.89	mol/m^3
C_{P^-}	8.49	8.49	mol/m^3
C_{HL}	2.85	4.91	mol/m^3
C_{HP}	1.51	1.51	mol/m^3
C_s	127.34	634.11	mol/m^3
C_x	106.86	97.73	mol/m^3
Productivity	0.0354	0.015	mol/m^3/s
Lactate removal	6.25x10^{-5}	8.95x10^{-5}	mol/s
Fermenter volume	1.76	5.97	l

Using the outlet concentrations of the fermenter as inputs to the REED module,

the model is solved in Donnan dialysis mode using a q_{feed}=q_{dia}= 120 l/h and a base concentration at the inlet of the dialysate channel of C_{OH}^{dbin}=150 mol/m^3 (These values correspond to a scenario previously investigated (Prado-Rubio *et al.*, 2010b)). Using the total lactate flux and the REED dimensions (depicted in Table 4.3) the lactate that can be removed by the Donnan dialysis is estimated. The bioreactor volume can be calculated as the ratio between the the Donnan dialysis potential separation and the fermenter lactate productivity. The results are shown also in Table 7.3.

It can be seen from simulation results, that total lactate productivity of the optimal operating point is more than twice the suboptimal point. Besides, the lactate removal under no current conditions is lower for the optimal operating point. The reason is the lower lactate concentration present in the fermentation broth. The combination of both situations reveals that the membrane separation process can handle an optimal bioreactor which is basically three times smaller than the suboptimal operating point. This is because the ratio between lactate removal and lactate productivity of the suboptimal point is approximately 1/3 of the ratio evaluated in the optimal point.

A problem of this simple design approach is that the bioreactor size is based on the lactate productivity when the inhibition is present. By the *in situ* lactate removal from the cultivation broth, productivity is increased. Then the question is to which extent the REED module is capable of handling the additional load. During the simulation of the integrated system this issue is studied.

7.5.3.2 Continuous integrated system behavior

The integrated system behavior is investigated using the suboptimal operating point. This point is selected since it is well know that tight control is required to operate a system at the optimal value of the fermentation alone. The estimated operative fermenter volume has slightly increased to V=6.1 L for the following simulation.

The system is integrated in a 3 step procedure:

a. The continuous bioreactor is simulated using the optimal inputs in order to estimate the static concentrations.

b. REED module is simulated under Donnan dialysis conditions, using the inputs from the simulated fermenter. Additional simulations under current reversal conditions are performed to define achievable setpoints for the input resetting control structure.

c. The static concentrations estimated in the previous two steps become the initial conditions for the integrated system simulation. The control structure is closed and the system is simulated.

Notice that the first two simulations were performed during the design stage. The fermentation response when the controlled REED is integrated is depicted in Fig. 7.8. The desired setpoints correspond to the values from preliminary simulations (pH_{set}^{fer} = 5.75, pH_{set}^{REED} = 6.1 and $I_{d_{set}}^{fer}$=100 A/m^2). Firstly, it is relevant to corroborate that the total protein concentration is constant in the fermenter, this

has not been shown in previous simulations but has been confirmed in each scenario by checking the total protein concentration in the fermenter.

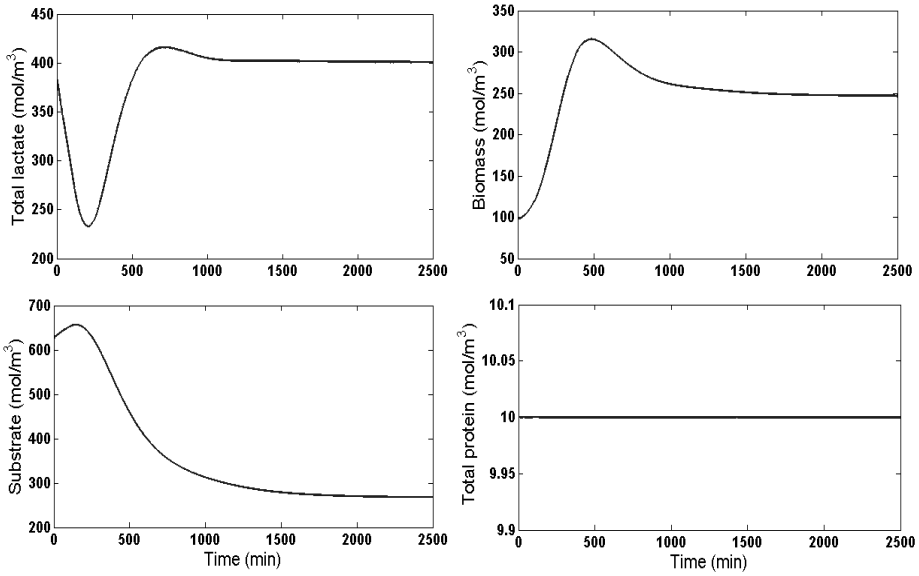

Figure 7.8: Continuous fermentation behavior after REED is integrated with the bioreactor which is in the static suboptimal operating point

From the concentrations in the fermenter, the influence of dynamic and stationary REED operation can be evaluated. By starting the membrane separation process, the fermentation is disturbed since lactate starts being removed from the cultivation broth. Lower lactate concentration in the fermenter promotes biomass growth and thus substrate utilization. A summary of the results at stationary conditions is shown in Table 7.4. The integrated system has shown a lactate productivity 2.4 times higher than the continuous fermentation with a comparable biomass concentration increment. Additionally, the biomass consumes more than 50% of the substrate still available.

Table 7.4: Stationary comparison of the performance between continuous fermentation and the integrated system

Subject	Fermentation	Integrated system	Relative difference	Units
Total lactate	386.80	400.90	3.7%	mol/m^3
Biomass	97.73	246.90	152.6%	mol/m^3
Substrate	634.11	267.70	-56.4%	mol/m^3
Lactate productivity	0.015	0.036	140%	$mol/m^3/s$

The pH value evolutions at the outlet of the REED module and the fermenter are shown in Fig. 7.9. The actuator actions are depicted in Fig. 7.10. After the system is integrated, the pH in the fermenter increases since the amount of hydroxide added to the cultivation is slightly larger than required to maintain pH. As consequence, the pH controller in the fermenter switches off. Due to the reduced lactate concentration in the fermenter, the lactic acid production is enhanced and the pH starts decreasing. When the pH in the fermenter is below the desired value, the pH controller starts providing the extra hydroxide ions necessary to neutralize the produced lactic acid. The elapsed time of inactivity of the pH controller is approximately 120 min.

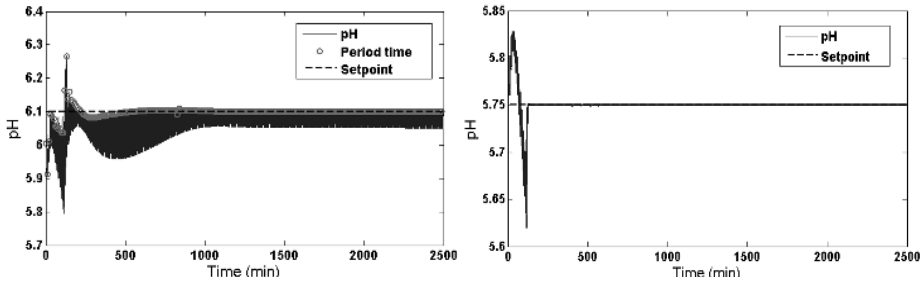

(a) pH value at the outlet of REED **(b)** Fermenter pH

Figure 7.9: pH behavior at the outlet of REED and in the fermenter for the controlled integrated system. In (a), the end period pH at the outlet of the REED module is highlighted

When the pH controller in the fermenter starts the base supply, it acts as a disturbance to the input resetting control structure of the REED module. The effect can be seen in the pH at the outlet of the REED module as an overshoot at time 130 min (see Fig. 7.9(a)). The desired value of the pH at the outlet of the REED module is achieved earlier than the current density setpoint, which is expected from a previous simulation shown in Chapter 6. The effect of the increased fermenter productivity can be seen in the actuator efforts to keep the setpoints (see Fig. 7.10).

Regarding the control performance, there is still an issue in the continuous pH controller output in the fermenter that was evidenced in the simulation performed and briefly discussed in section 7.5.1 (see Fig. 7.3). The issue is the oscillations of the base input flow rate to the fermenter to reject continuously the periodic disturbance introduced by REED. A discrete time pH controller in the fermenter is therefore evaluated.

- **A discrete time pH controller in the fermenter**: several problems appeared using this approach, related to the controller tuning and initial conditions. Manual tuning was attempted to overcome the poor controller performance. A grid of controller gains and integral times were tested. Low gain pH control in the fermenter leads to a transient pH decay in the cultivation broth. Actuators in the REED module achieve saturation conditions trying to

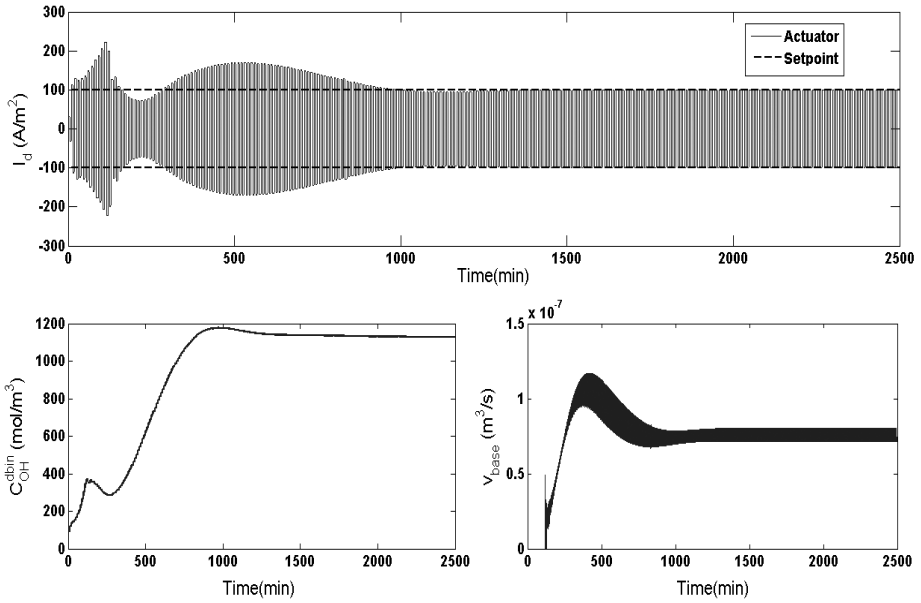

Figure 7.10: Actuator values during continuous operation of the integrated system. Current density (I_d) and input hydroxide concentration to the dialysate channel (C_{OH}^{dbin}) are defined by the input resetting control structure in REED. The base addition to the fermenter (v_{base}) is the output of the continuous pH controller. The pH behavior of the fermenter and outlet of the REED module are shown in Fig. 7.9

control the pH at the outlet of the feed channel. It must be stressed that the input resetting control structure in REED was designed for a constant inlet pH to the REED. If the pH decreases in the cultivation broth, REED is forced to work harder to keep the pH setpoint. If the setpoint cannot be achieved, the situation is known as unreachable setpoint. Using higher gain pH control for the fermenter, the controllers start fighting causing system instability.

Some alternative strategies were implemented to decrease the adverse effect of the decentralized control structure. The setpoints used in the previous implementation of the input resetting control structure were relaxed, for instance $pH_{set}^{REED} = 5.95$ and $I_{d_{set}}^{fer}$=125 A/m^2 (the pH in the fermenter is still $pH_{set}^{fer} = 5.75$). This modification attempts to reduce the REED effort during transient pH drops in the fermenter. Additionally, new initialization is performed were both control systems are not closed simultaneously. The continuous fermentation is simulated just with the discrete pH controller and when static conditions are achieved, the REED is integrated.

Despite the efforts trying to improve the performance of the block decentralized control structure, no satisfactory behavior was obtained. For the continuous integrated system, the system becomes unstable in a long term simulation. For illustration, results obtained using a moderate gain and a rather low inte-

gral action in the tested grid are shown (K_{pH}^{fer}=5x10^{-8} and $\tau_{I,pH}^{fer}$=3000). The actuator performances are depicted in Fig. 7.11.

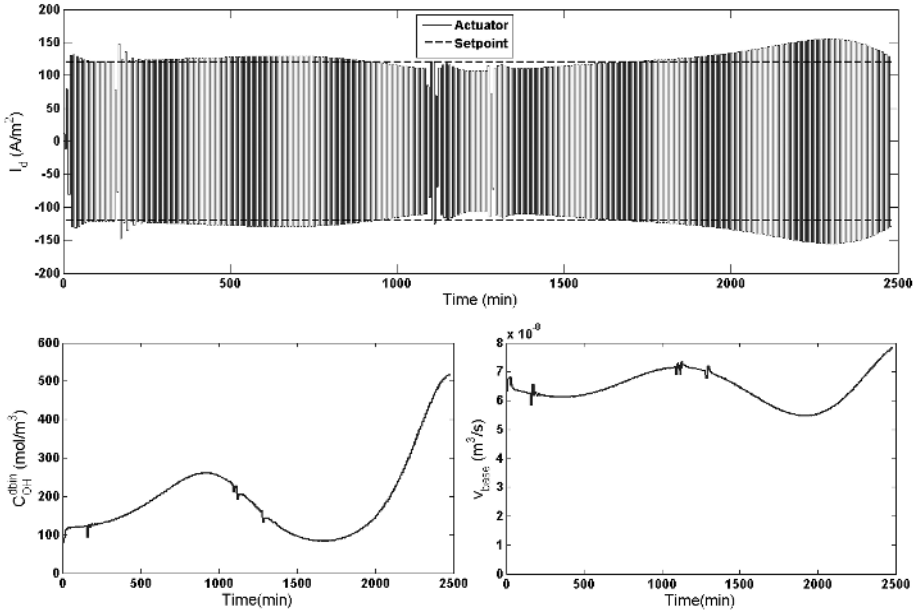

Figure 7.11: Actuator values during continuous operation of the integrated system. Current density (I_d) and input hydroxide concentration to the dialysate channel (C_{OH}^{dbin}) are defined by the input resetting control structure in REED. The base addition to the fermenter (v_{base}) is the output of the discrete pH controller

The main purpose of implementing a discrete time pH controller is to attempt to remove the oscillations of the pH controller in the fermenter. If the v_{base} discrete time actuator is compared to the continuous in Fig. 7.10, the high frequency oscillatory behavior was removed. The reason is that the controller is aiming to control the pH at the end of the REED period and not within the period. However, the oscillations are transferred to the pH in the fermenter as can be seen in Fig. 7.12(b).

The main two problems obtained with the discrete simulations can be seen from the actuators and pH behavior in the fermenter. The integrated system becomes unstable as can be seen in Figs. 7.11 and 7.12. The second issue is the simulation crashing at some points. It is believed that this is a consequence of the dynamic behavior of the fermenter pH, since it could considerably increase the stiffness of the integrated system. Therefore, the solver can not achieve the required integration tolerance using the the smallest allowed step value (h=5.820766x10^{-11}) (Mathworks, 2006). Due to the model implementation algorithm, the simulation can continue taking the last successful step as initial conditions for the following current value. The crashing points are clear in Figs. 7.11 and 7.12. The simulation crashing as such is not really interesting

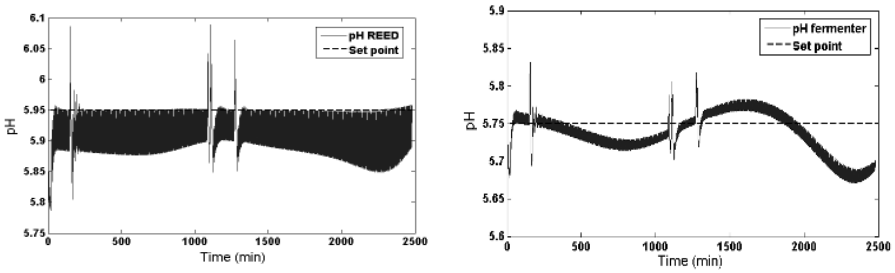

(a) pH value at the outlet of REED **(b)** Fermenter pH

Figure 7.12: pH behavior at the outlet of REED and in the fermenter for the controlled integrated system. Interruptions in the plots correspond to cycles where the simulation crashed

except as an issue.

7.5.4 Challenges in the integrated system design and operability

The process and control design of the continuous integrated system is challenging due to nature of the models and design constraints. The main limitation of the employed approach is that lactate productivity changes in dependence of the REED operation. If biomass growth is not limited by the carbon source, the productivity enhancement by the *in situ* lactate removal can be significant (as evidenced in the calculations). By using the lactate productivity in an inhibitory environment for the bioreactor design, the employed design strategy results in an overdesigned fermenter. Therefore, the need of an alternative problem formulation becomes clear. However, the nature of the models and design constraints make infeasible at this point to consider an IPDC approach. For that reason, alternative ideas are proposed.

An iterative design procedure could be initiated. However, some issues might arise. Firstly, a smaller reactor requires tighter control, otherwise there is a risk that the system becomes unstable before achieving stationary operation. Additionally, the dilution rate of the system changes when the pH control take over by REED. The fermenter pH control is regulated by the addition of a sodium hydroxide solution, which influences the system dilution rate. On the other hand, REED facilitates pH control by adding hydroxide ions without modifying the flow rate. This behavior implies that the dilution rate changes once REED is integrated with the bioreactor, thus the productivity moves to another point different than the initially calculated. Due to the mentioned reasons, it is difficult to predict if the iterative design of the integrated system actually converges.

An unexplored alternative is to control the productivity of the fermenter, e.g. by controlling the biomass concentration using the purge flow rate a (slow) actuator. However, this strategy implies the design of an effective system to separate biomass, which could be difficult to implement in practice.

The design problem during the batch fermentation is not only associated with the increased productivity. The main problem is that the defined REED module is not capable of supplying the range of hydroxide flow rate to neutralize the lactic acid. In that case, a more flexible design of the integrated system must be proposed. An alternative that does not compromise the REED model validity constraints is to use multiple parallel REED modules. This strategy adds the additional feature of using different phases in the periodic pH control, thereby enabling a much reduced impact of the pH oscillations in the fermenter. Thereby significantly improved productivity may be obtained.

At the control level, the main limitation is the decentralized control structure and the interaction between controllers. When the propagation of disturbances in cascade systems is sequential, a feedforward control action has shown improvements in the product quality control (Luyben, 1993). However, the addition of feedforward information is sensitive to model errors that can lead to a worse performance (Faanes and Skogestad, 1999). Feedforward control action has been investigated in benchmark case studies using mainly linear models. In this application, obtaining feedforward information should be investigated. Initially, an approximate feedforward coupling could be used since any misalignment will be handled by feedback action.

The monitoring system design can be extended including alternative potential manipulated variables to control pH in the fermenter. In practice, to use the flow rate through the REED as manipulated variable could be relevant. However, the presented model has not been validated at different flow conditions and therefore this aspect has not been investigated in the present work.

7.6 Conclusions

The process and operability design of an integrated bioreactor and membrane separation process has been investigated in the present contribution. The investigation has been based on dynamic models previously developed to investigate lactic acid fermentation and Reverse Electro-Enhanced Dialysis. The original process models are adapted for the purpose of the processes integration. Due to the model complexity and the design constraints, an ideal simultaneous process design and process control could not be applied. A sequential goal driven process design and control strategy is adopted. From a goal methodology, the requirements to integrate the processes model were identified. Biomass and substrate mass balances are included in the REED model and the total protein production rate in the fermenter defined.

In order to fulfill model validity constraints, the design strategy is limited to fix the dimensions of the REED module and then fermenter is designed according to the particular role of the REED unit in the integrated process. From the goal driven design methodology, the need of a pH control in the fermenter was identified. A continuous PI pH controller is implemented for the bioreactor and its performance evaluated during a simulated reactor start up. The pH controller is able to regulate the fermenter pH at the desired point until static operation is achieved. Incorporating this controller with the input resetting control structure, the final integrated system control pH architecture is obtained. Where the pH in the fermenter is regu-

lated by the continuous PI controller and the pH change along the feed channel in the REED is controlled by the input resetting control structure of this unit.

The integrated process is investigated for two different production targets: the fetbatch production of lactic acid bacteria starter culture and the continuous production of lactic acid. In both cases, controllability problems are encountered either in the actuator behavior or pH regulation with the proposed decentralized control structures.

During the batch integrated process, the fixed REED module design is not capable to supply the required hydroxide along the process. Thus, the rigid design of REED can only partially facilitate the pH control in the fermenter. The final biomass concentration, biomass yield and productivity are increased in the REED process compared to the batch fermentation and the integrated fermentation and electrodialysis.

In the second case study, a suboptimal productivity operation point is investigated. Once again, it was evidenced that the rigid design strategy leads to over designed fermenter and therefore REED only can facilitate pH control and not substitute it. Under stationary operation, the total lactate productivity is 2.5 times larger than during the continuous fermentation. Besides, there is a higher biomass growth and better substrate utilization.

The issues evidenced during the design and control of the integrated system are challenging and are the motivation to continue investigating this type of dynamic system. A promising approach which may be useful for both scenarios is to use multiple REED modules sequentially as biomass concentration in the fermenter increases. The different REED modules may then also using different phasing in their periodic controls such that the load on the fermenter control would be significantly reduced. The limitation for such a design would then be the operation of the REED at high biomass concentrations.

7.7 Nomenclature

C	Concentration (mol m^{-3})
D	Diffusion coefficient (m^2 s^{-1})
HL	Lactic acid
HP	Undissociated protein
I_d	Current density (A m^{-2})
K_p	Controller gain
L^-	Lactate ion
Na^+	Sodium ion
OH^-	Hydroxide ion
P^-	Dissociated protein
q	Flow rate (m^3 s^{-1})
$REED$	Reverse Electro-Enhanced Dialysis
R_k	Total reaction rate of k (mol m^{-3} s^{-1})
r_i	Reaction rate i (mol m^{-3} s^{-1})
s	Substrate concentration (mol m^{-3})

t	Time (s)
t_{rev}	Reversal time (s)
x	Spatial direction (m)
x	Biomass concentration (mol m^{-3})
z	Dimensionless distance $z = x/\delta_m$ (-)
z_k	Valence of k (-)

Greek letters

δ_m	Membrane thickness (m)
ψ	Electrical potential (V)
ψ_n	Nominal potential ($\psi_n = RT/F$) (V)
τ_{diff}	Diffusion time ($\tau_{diff} = \delta_m^2/D_{k,p}$) (s)
τ_i	Integral time
τ_n	Nominal time ($\tau_n = 1$ (s))
υ_{base}	Base inlet flow rates to the fermenter (m^3 s^{-1})
φ	Dimensionless potential ($\varphi = \psi/\psi_n$) (-)

Subscripts

dia	Dialysate channel
$feed$	Feed channel
k	Specie
OH^-	Hydroxide ion
p	Zone (phase)
s	Substrate
set	Setpoint

Superscripts

$dbin$	Dialysate bulk inlet
$fbin$	Feed bulk inlet
fer	Fermenter
in	Inlet
$REED$	Reverse Electro-Enhanced Dialysis

8

Conclusions

In this thesis a model based approach for design, operation, control and optimization of an integrated process for lactic acid fermentation has been investigated. Especial focus has been paid to the Reverse Electro-Enhanced Dialysis process due its novelty and lack of understanding. This thesis' contributions can be classified into two main areas: transport phenomena in membranes and process system engineering.

In membrane separation processes area, the developed modeling work constitutes the pillar for the Reverse Electro-Enhanced Dialysis analysis. The static and dynamic simulation results have been combined to the available experimental evidence in order to provide insights of the membrane separation process, vital for the integrated system design and operation as a function of different production objectives.

A short review of membrane based separations employed to remove lactate from a diluted solution has been presented in a chronological manner. The most important achievements and limitations of each application are highlighted. The Reverse Electro-Enhanced Dialysis understanding prior to this thesis is described. The novel membrane separation system analysis has been divided into three contributions.

The starting point is the dynamic model development from first principles to describe the simultaneous ion transport in a Dialytic module. The model is based on diffusion, convection and migration of the modeled species. Additionally, the dissociation reactions are accounted for in order to model their influence in the pH of the cultivation broth. The model structure has been evaluated statically using experimental data for Donnan Dialysis recovery of monoprotic carboxylic anions, where the unknown model parameters are regressed. The model has satisfactorily reproduced the anion fluxes and qualitatively described previously predicted concentration profiles in the module.

A step further in this investigation is aimed to contribute in the understanding of the competitive ion transport in the dialytic module under current load conditions, so called Electro-Enhanced Dialysis operation. By imposing an external electrical field, the target ion static fluxes has been enhanced more than two times compared to Donnan Dialysis recovery. The static analysis predicted ion fluxes inversion and asymmetric concentration profiles within the module, which are responsible for the total flux enhancements. From the simulation results, the system operative window has been identified for the current density and inlet base concentration to the dialysate channel. The most important inlet constraint is found for the imposed current density, referred to as current saturation conditions.

The periodic operation of the REED module is studied employing a wave function for the imposed electrical field. A more diverse set of phenomena have been predicted that can explain the transient lactate recovery after the current is reversed. These transient phenomena are the lactate accumulation within the membranes,

flux inversion and preferable ion transport at the interfaces. A comparison of lactate separation has been presented between the Donnan Dialysis and Reverse Electro-Enhanced Dialysis operation. Despite the current efficiency loss by reversing the current density, the average lactate recovery under current reversal conditions is higher than during Donnan Dialysis. The tradeoff between input variables in the REED module is predicted. As consequence, the reversal time must be selected as a function of the energy consumption and the current efficiency loss.

From the modeling work some model advantages can be highlighted:

- The general description of the accounted transport phenomena and species allows to apply this model in diverse electrically driven membrane separation setups. Especially under no current, current load and variable current density conditions.
- The dynamic nature of the model make it suitable to perform both static and dynamic predictions
- The introduction of the dissociation reactions in the mass balances allows to model the pH either for pure solutions and fermentation broths.
- The tank in series description of the concentration profiles along the channels (y-direction) make the model flexible enough to apply for larger equipment setups
- The initialization procedure guarantees, at least in all evaluated scenarios, to have a suitable set of initial conditions to perform the simulations.
- The model implementation is made as a tool which is very flexible to use for different purposes such as simulation of the individual unit, control systems development and integration with the bioreactor.

On the other hand, the presented model of the REED process has the following limitations:

- The model validity under current load conditions maybe questionable. The issue is that the model parameters were estimated under Donnan Dialysis conditions. Due to the absence of experimental data under current load and current reversal conditions, it remains to corroborate the validity of the ion diffusion coefficient model under current load conditions.
- The model parameters were estimated for well defined flow conditions. Different flow regime will require the re-estimation of the model parameters.
- Despite the model was derived for any multicomponent system, the model implementation was developed for monoprotic anions. In the case of a polyprotic system, modifications should be introduced in the model solution.
- The presence of other ions, such as nutrients and fermentation subproducts, are not included in the model. Therefore, the current efficiency loss due to their transport is not currently predicted.

- Water transport due to electro-osmosis is not investigated in this application. In a long term batch or fedbatch fermentation it may be relevant since it will affect the fermentation volume.

The investigation of the Electrodialysis with bipolar membranes is an example of the developed model flexibility. Only few modifications are required to include the effect of ideal bipolar membranes into the mathematical description of the system. The module static analysis has confirmed the potential ion flux enhancement under current load conditions. However for this system arrangement, the lactate and hydroxide ions must be present in a certain concentration ratio to favor lactate transport. When hydroxide is transported through the anion exchange membrane, water is formed in the acid channel instead of lactic acid, resulting in a current efficiency loss. The tradeoff between simulation time and numerical accuracy of the concentration profiles along the channels has been investigated, concluding that for the used module, the tank is series approach is not required.

In the process system engineering area, there are three main contributions which have been investigated in separated chapters. These contributions can be classified as: dealing with parameter estimation issues in bioprocesses modeling, extension of the available methodology for control structure design for dynamic systems and the goal driven process design and control issues of the integrated system.

Using correlation and sensitivity analyses, a parameter identifiability problem has been found in the proposed unstructured model for the fermentation. Therefore, despite the reasonable good agreement of the predictions and experimental data, the full model is falsified. Extra experimental work was not possible to perform within this project, thus a parameter set reduction has been the adopted strategy to obtain an identifiable set of parameters. The selection of the appropriate seven parameter subset is assisted by an identifiability analysis and sensitivity based metrics. A reasonable model has been obtained but there is no sufficient experimental data to validate the model.

The analyzed bioreactor model is advantageous since it is simple and can reproduce experimental data of either batch or continuous cultivations. However, it barely provides insight of the microorganism growth and it predictive power is limited to the neighborhood of conditions where the experiments were performed. The sensitivity analysis results could be used in order to design future experiments and eventually validate the model.

Investigation of the REED module operability led to other contribution to the process engineering area. The conventional methodology for goal driven control system design is adapted to handle this periodically operated system. The drawback during the top down analysis lies on the coupling between manipulated and controlled variables for non linear dynamic systems. Therefore, the available guidelines for selection of the appropriate manipulated variable according to a specific goal have been expressed as a quantitative index. This index is based on the controlled variable dimensionless sensitivity towards each potential manipulated variable. From the proposed analysis, a non conventional input resetting control structure for pH control at the outlet of the REED module is obtained. Its performance is satisfactory during a set point tracking test, where the desired pH can be achieved while the input is reset. This control structure is more powerful than single control loops,

it can handle the present input constraints and the controllers can be tuned separately. However, the controllers must be re-tuned if the setpoints change due to the large variation on the pH sensitivities towards the manipulated variables within the operating window.

The study of the integrated system through the continuous and batch case studies has revealed the potential of this technology to increase the target product productivity and substrate utilization while reducing the operation time (for batch case). Despite the promising results, several design and operability problems have been encountered during this investigation that are encouraging to further investigate such integrated system. The main limitation is the sequential process design and control strategy, which is adopted due to the model complexity and design constraints. From the investigated case studies it is concluded that in the proposed REED module design is only able to facilitate the pH control in the fermenter and not completely substitute it.

The sources operability problems in the integrated system set up are: the decoupled control structure plus the process design issues, since the system controllability is tightly related to the process design. Therefore the issues in both layers are expected to be coupled. The main concern lies in an inherent characteristic of the recycle system, since disturbances propagate through the system. The attempts to mitigate this issue converged to two different control approaches: discrete and continuous pH controllers in the fermenter. The actuator of continuous pH controller in the cultivation has shown oscillations in order to keep constant the pH within the REED periods. On the other hand, the discrete time pH controller translated those oscillations to the pH behavior in the cultivation, generating convergence problems and system instability. Different solutions were proposed to improve the system design and controllability.

8.1 Future work

Several open problems and potential future work have become apparent during the writing of this thesis, those have not been pursued due time limitations.

- Reverse Electro-Enhanced Dialysis modeling: it would be relevant to have more static and dynamic experimental data that allows at least estimating the model parameters under current load conditions and different flow scenarios. This would improve the quality of the estimates for the ion diffusion coefficient and thickness of the boundary layers estimates.

  Additionally, potential model extensions might be relevant to further understand the membrane separation process. Including in the model phenomena, such as the water and other ions transport through the anion exchange membranes, can have a relevant influence on the process behavior. Thus, affect the role of the REED module in the integrated process. The lack of experimental evidence is the main obstacle to achieve a proper representation of those phenomena. Therefore, further modeling development must be supported by experimental work for both parameter estimation and model validation.

- Bioreactor Parameters identifiability: the parameters identifiability issue has

been the main limitation during the bioreactor modeling. In order to estimate the full set of parameters, new experiments should be performed to obtain the required information. The experimental design could be partially supported by the employed sensitivity analysis. Therefore, the methods and tools described in this thesis can be employed to fine-tune the model parameters.

- Integrated system: the investigation of the integrated system is probably the most fertile area for future work. A discussion of the potential challenges and future work was presented in Chapter 7. In summary, the major challenge is to overcome the issues of the design strategy that could limit the controllability of the integrated system. A more appropriate integrated system design might reduce the operability issues. In that way, problems as the controllers fighting and poor performance could be avoided. This work might extend or adapt the available methodologies for solving IPDC problems. In addition, it would be interesting to evaluate the integrated system operability using more advanced controller design. Starting with simple feedforward control actions up to model based control.

Appendices

A

Mathematical tools employed during the REED model solution

A.1 REED model solution

The dynamic model is based on first engineering principles for diffusion, migration and convection. Combining the equations for all sections in the REED cell leads of a system of multiregion partial differential equations. Method of lines is commonly used to solve partial differential equations where the spatial dimension is discretized using Taylor expansion, resulting in a system of ordinary differential equations (ODEs) or differential algebraic equations (DAEs) where the independent variable is time. The obtained set of equations can be integrated simultaneously along the line of constant spatial dimension, by employing the any of the developed methods for the numerical integration of ODEs and DAEs (Schiesser, 1994). In this case, variable order multistep solver for is employed based on the numerical differentiation formulas (NDFs) (Shampine *et al.*, 1999). This method is recommended for solving stiff system of ordinary differential equations or a index-1 differential algebraic problem represented by equation A.1.

$$M(t)y' = f(t, y) \tag{A.1}$$

Initially, in order to obtain a low truncation error during the discretization, a considerable high number of cheap steps were used in the an asymmetric centered differences second order Taylor expansion. Nevertheless, the reduction of the truncation error leaded to intractable long computation time, due to the high number of discretization steps. For that reason high order Taylor expansion was employed instead, substituting the cheap by expensive steps and then diminishing the number of nodes to achieve the desired accuracy. Sixth order Taylor expansion series to the function $f(x)$ around the point x_0 is represented by the following expression.

$$\begin{aligned} f(x) = f(x_0) + (x - x_0)f'(x_0) + \frac{(x - x_0)^2}{2!}f''(x_0) + \frac{(x - x_0)^3}{3!}f^{(3)}(x_0) + \\ \frac{(x - x_0)^4}{4!}f^{(4)}(x_0) + \frac{(x - x_0)^5}{5!}f^{(5)}(x_0) + \frac{(x - x_0)^6}{6!}f^{(6)}(x_0) + \\ \mathcal{O}\left(\frac{(x - x_0)^7}{7!}\right) \end{aligned} \tag{A.2}$$

The truncation error in this case is reduced up to $\mathcal{O}\left((x-x_0)^7/7!\right)$. The function value for x is calculated using another six points. This method is referred to as seven point difference equations. It means, each phase in the REED module must have at least seven discretization points. As mentioned above, asymmetric centered differences are used, it means the step length can change from point to point, smaller steps are used close to the interfaces as it can be seen in Fig. A.1. In each discretization point, a system of six algebraic equations must be solved (obtained from Taylor expansion). The steps are summarized in table A.1.

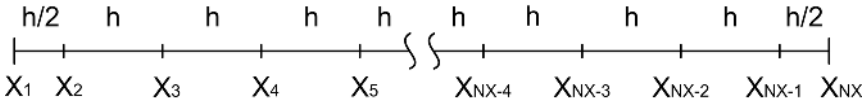

Figure A.1: Step distribution for the 7 point asymmetric centered differences

Table A.1: Steps used for the seven points asymmetric centered differences

(x_0)	1	2	3	4	5 to NX-4	NX-3	NX-2	NX-1	NX
x-x_0	h/2	-h/2	-3h/2	-5h/2	-3h	-3h	-4h	-5h	-11h/2
	3h/2	h	-h	-2h	-2h	-2h	-3h	-4h	-9h/2
	5h/2	2h	h	-h	-h	-h	-2h	-3h	-7h/2
	7h/2	3h	2h	h	h	h	-h	-2h	-5h/2
	9h/2	4h	3h	2h	2h	2h	h	-h	-3h/2
	11h/2	5h	4h	3h	3h	5h/2	3h/2	h/2	-h/2

The derivation and implementation of the difference equations was validated by comparison of the analytical solution of the first and second derivative of the function $f(x) = sin(x)$ with those computed numerically (Møllerhøj, 2006). For the numerical implementation, 12 discretization points were employed between x=[0 1]. The results are depicted in Fig. A.2. As it can be seen, the largest absolute errors are obtained at the interval endpoints with a value of approximately $10^{-7.5}$ and $10^{-5.7}$ for the first and second derivatives, respectively. The smallest errors are obtained for the inner points x5 to x8, since symmetric centered differences have been applied for these.

A.2 Initialization of the REED model

After the discretization of the system of PDEs, a system of equations such as equation A.1 is obtained where $M(t)$ is a singular matrix, meaning that it is a set of DAEs. The algebraic states correspond to the concentrations of the species at both sides of the interface located at z_j ($C_k|_{z=z_j^-} = C_k|_{z=z_j^+}$) and the electrical potential gradients int he interfaces. The number of total equations depends basically on the

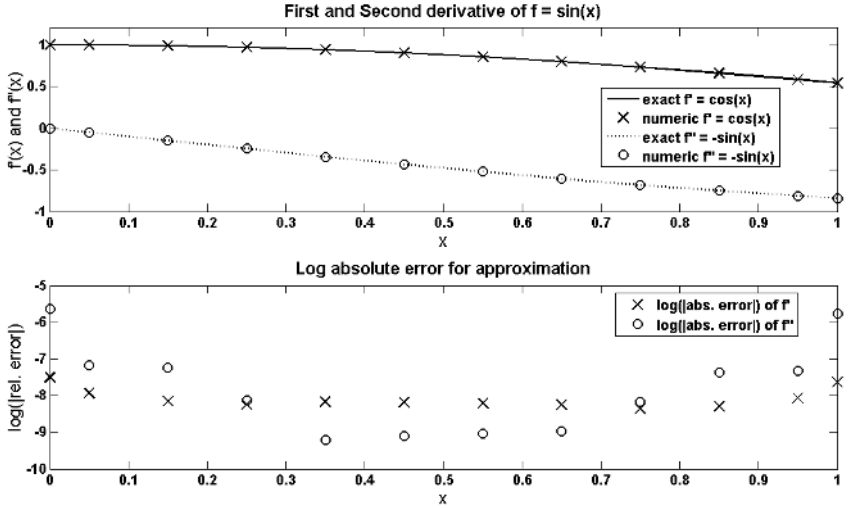

Figure A.2: Validation of the derivation and implementation of the 7 point difference equation

summation of discretization points in each phase times the number of species in each phase, that product is amplified by the number of tanks in series in the y-direction.

Solving a DAE system of equations is complex since it only has a solution if the set of initial conditions are consistent, it means that a feasible set of initial conditions must be known in order to have convergence. The most important limiting conditions are the algebraic equations at the interfaces, then an inconsistent set of initial conditions leads to numerical problems (index of the DAE's is larger than one). Møllerhøj (2006) proposed an initialization procedure in order to guaranty, to some extend, convergence. Experimental data are used as initial condition for the procedure using a high pH value of the feed solution (pH=10). When the steady state is achieved, the pH value is reduced to 5.75, corresponding to an experimental data for a fermentation broth. After the step change, there is a fast change in pH. This period is the most time consuming part of the initialization procedure. Reasonable changes in parameters such as input concentrations, liquid flow rates, boundary layer thickness and membrane water content do not require a new initialization. However, changes in the dissociation constants or fixed charge concentration of the membrane demand the estimation of a new initial profile.

A.3 Optimization methodology

The methodology used for parameter estimation is a numerical method for large scale optimization, this algorithm is a subspace trust region method based on the interior reflective Newton method for non linear minimization subject to bounds (Coleman and Li, 1994; Mathworks, 2006). The nonlinear data-fitting problem was

solved by defining a function to compute the vector-valued expression $F(x, xdata)$. Where x is a vector containing the parameter to be estimated, $xdata$ is the vector with the independent variable and $F(x, xdata)$ is the model prediction. The size of the vector returned by the defined function is the same as the size available experimental data set. The optimization method, referred as interior points method provides an alternative means of solving bound-constrained problems. The idea is to trace approximate minimizers of $\phi(x, \mu)$ as μ approaches zero, where μ is a positive parameter called *barrier*:

$$\phi(x, \mu) = f(x) - \mu \sum_{i=1}^{n} \log(x)_i \tag{A.3}$$

Then, ϕ is a logarithmic barrier function. Under reasonable assumptions, and for a sufficiently small positive values of μ, local minimizers of $\phi(x, \mu)$ describe continuous trajectories converging to the local solutions of the required problem (Gould *et al.*, 2004). The interior reflective Newton approach generates strictly feasible iterates by using a scaling transformation and following the reflections paths (Coleman and Li, 1994).

B

Donnan dialysis modeling using back box models

The experimental data for lactate, acetate and propionate fluxes are depicted in the Fig. B.1. From the figure, it can be seen that experimental fluxes for lactate and propionate don not achieve a maximum value for the flux (J_{max}) as it is predicted by the reaction-diffusion model, which follows a Langmuir behavior as function of the inlet base concentration in the dialysate channel. This could be the evidence of a dual mechanism. Using the experimental data, the parameters for the proposed models are estimated by minimizing the squared prediction error. The estimated parameters for each model are summarized in Table B.1 and the prediction shown in Fig. B.1.

Table B.1: Estimated parameters for Reaction-Diffusion (RD) model and Reaction-Diffusion+Solution-Diffusion (RD+SD) model

Ion	Model	Parameter			Squared norm
		J_{max}	K	P	of Residuals
Lactate	RD	$7.9996\text{x}10^{-4}$	$1.2882\text{x}10^{-2}$	-	$6.765\text{x}10^{-9}$
	RD+SD	$6.7139\text{x}10^{-4}$	$1.8819\text{x}10^{-2}$	$1.03467\text{x}10^{-7}$	$2.938\text{x}10^{-9}$
Acetate	RD	$8.9673\text{x}10^{-4}$	$9.2518\text{x}10^{-3}$	-	$2.638\text{x}10^{-9}$
	RD+SD	$8.9807\text{x}10^{-4}$	$9.1907\text{x}10^{-3}$	$2.2000\text{x}10^{-14}$	$2.643\text{x}10^{-9}$
Propionate	RD	$4.8304\text{x}10^{-4}$	$2.8462\text{x}10^{-2}$	-	$7.111\text{x}10^{-9}$
	RD+SD	$4.2139\text{x}10^{-4}$	$4.8694\text{x}10^{-2}$	$8.76443\text{x}10^{-8}$	$4.489\text{x}10^{-9}$

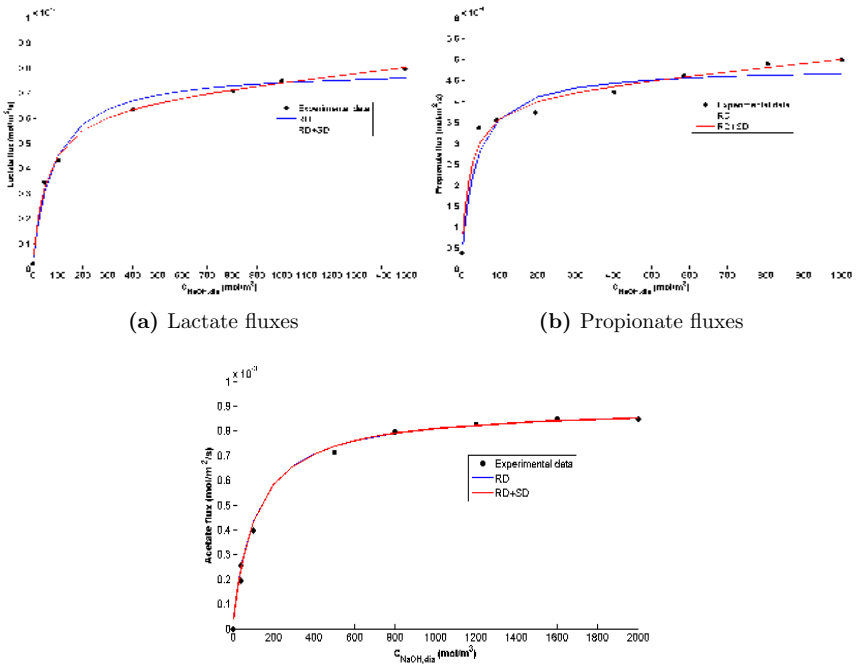

(a) Lactate fluxes

(b) Propionate fluxes

(c) Acetate fluxes

Figure B.1: Lactate, propionate and acetate fluxes through an anion exchange membrane as a function of the base concentration in the dialysate channel. Besides, fitted model for different mechanisms. RD: reaction-diffusion mechanism, SD: solution-diffusion mechanism

C

Operational degrees of freedom analysis

The degree of freedom analysis is a methodology used to identify the number of variables to be specified such that the system can be solved. For an operating plant these degrees of freedom includes both the disturbances and the variables which will be used to reject the disturbances, i.e. manipulated variables, such that the operational goal of the plant may be fulfilled. The division of degrees of freedom between manipulated inputs and disturbances is performed through the top-down analysis during the control structure design (Skogestad, 2000, 2004; Jørgensen, 2006). Once the disturbance variables have been selected, the plant operating window can be mapped and the required span of the manipulated variables can be determined. The degrees of freedom (DOF) of a system are calculated from the following expression:

$$DOF = N_x + N_u - N_e \tag{C.1}$$

Where N_x is the number of dependent variables, N_u is the number of inputs or disturbances and N_e is the number of equations available. The DOF analysis is performed for the REED module, the fermenter separately and for the integrated system (tables C.1, C.2 and C.3). In this analysis it is considered that the initial conditions, kinetic model parameters and equipment design are defined. In order to simplify, the analysis is performed for one tank in the y-direction for the REED module. If more tanks are used, the number of variables and equations are increased by the changed number of tanks, without affecting the degrees of freedom. In addition, the algebraic variables that can be substituted in the PDEs or ODEs are not counted since they are explicitly given, this means that there is and extra variable but also an extra equation. Therefore, the degrees of freedom do not change.

The REED module has 15 degrees of freedom, the fermenter has 14 and the integrated system has 12, as it is shown in the last row of the presented Tables. For the three cases, some of these degrees of freedom can be used as possible manipulated variables in order to achieve a desired goal. The remaining degrees of freedom are considered as disturbances. The introduction of a control law modifies the degrees of freedom since the controller relates the target state and the manipulated actuator variable by an additional equation. The degrees of freedom are reduced if the set points are known. Furthermore, the variation required to reject the disturbance or fulfill the required set point change is shifted to the manipulated variable which is supposed to have the necessary range to accommodate this variation.

Table C.1: Degrees of freedom analysis for the REED module. PDE, ODE and AE stand for Partial differential equation, Ordinary differential equation and Algebraic equation, respectively

Variable		**Inputs**		**Equations**	
Variable	**#**	**Variable**	**#**	**#**	**Type of equation**
$C_{L^-}^{rec}$	6			6	PDE equations
$C_{OH^-}^{rec}$	6			6	PDE equations
$C_{Na^+}^{rec}$	6			6	PDE equations
$C_{P^-}^{rec}$	2			2	PDE equations
C_{HP}^{rec}	2			2	PDE equations
C_{HL}^{rec}	2			2	PDE equations
C_{s}^{rec}	2			2	PDE equations
C_{x}^{rec}	2			2	PDE equations
Boundary conditions	56			16	ODE mass balances in feed channel
				6	ODE mass balances in dialysate channel
				8	Donnan equilibrium (AEs)
				4	Faraday's law (AEs)
				12	No accumulation (AEs)
				10	Zero flux (AEs)
Potential gradient	12			8	Electroneutrality condition
				4	Faraday's law
		q_{feed}	1		
		q_{dia}	1		
		I_d	1		
		t_{rev}	1		
		$C_k^{feed,in}$	8		
		$C_k^{dia,in}$	3		
Total	96		15	96	

Table C.2: Degrees of freedom analysis for the fermenter. ODE stand for Ordinary differential equation

Variable		**Inputs**		**Equations**	
Variable	**#**	**Variable**	**#**	**#**	**Type of equation**
C_{L^-}	1			1	ODE mass balance equation
C_{OH^-}	1			1	ODE mass balance equation
C_{Na^+}	1			1	ODE mass balance equation
C_{P^-}	1			1	ODE mass balance equation
C_{HP}	1			1	ODE mass balance equation
C_{HL}	1			1	ODE mass balance equation
C_{s}	1			1	ODE mass balance equation
C_{x}	1			1	ODE mass balance equation
V	1			1	ODE mass balance equation
		q_{feed}	1		

Continued on next page

Table C.2 – continued from previous page

Variable		Inputs		Equations	
Variable	**#**	**Variable**	**#**	**#**	**Type of equation**
		υ_{feed}	1		
		υ_{base}	1		
		C_k^{in}	3		
		C_k^{rec}	8		
Total	9		14	9	

Table C.3: Degrees of freedom analysis for the integrated system. PDE, ODE and AE stand for Partial differential equation, Ordinary differential equation and Algebraic equation, respectively

Variable		Inputs		Equations	
Variable	**#**	**Variable**	**#**	**#**	**Type of equation**
REED	96			96	PDE's + ODE's + AE's
Fermenter	9			9	ODE mass balance equations
		q_{feed}	1		
		q_{dia}	1		
		I_d	1		
		t_{rev}	1		
		$C_k^{dia,in}$	3		
		υ_{feed}	1		
		υ_{base}	1		
		C_k^{in}	3		
Total	105		12	105	

D

Parameter estimation of the bioreactor model through regularized optimization

The parameter estimation problem shown section 5.5.4, was solved using the least squared method combined with a regularization according to the following expression:

$$min_{\theta}F = \sum_{l=1}^{L} W_l \sum_{i=1}^{I_l} w_{il}^2 \sum_{n=1}^{N_{li}} (y_{lin} - \bar{y}_{lin})^2 + W_{reg} \sum_{j=1}^{n_p} \lambda_j \left(\frac{\theta^{in} - \theta}{\theta^{in}} \right)^2 \tag{D.1}$$

The optimization problem is implemented in Matlab 2007a and solved using the function "fmincon"(Mathworks, 2006). The regularization weights, λ_j, are set to 1 since the contribution of each parameters is already normalized in the objective function (division by θ^{in}). The regularization term weight W_{reg} must be carefully selected in order to make negligible the model bias that is introduced by the regularization, this is done using the L-criterion (Hansen, 1996). The objective function is evaluated for a wide range of W_{reg} using the experimental data, the $\hat{\theta}$ obtained from the pure least squared optimization and θ^{in} shown in Table D.1. For very low regularization weight, the objective function is not sensitive. However, there is a W_{reg} where the objective function starts growing very fast. The regularization weight is selected in that neighborhood, the used regularization term is $W_{reg} = 300$.

When the optimization problem was solved using different sets of initial guesses, the solution was very close to the initial values. Therefore, a set of initial guesses relatively close to the solution found with the pure least squares method is used, since it was the best solution found. The initial guesses and optimal parameters are listed in Table D.1. The results obtained using regularization confirm the identifiability problem. It can be seen how most of the parameters are basically the same initial values, since the function of the regularization term in the objective function is to keep close to the initial value the parameters with a small significance.

It could be argued that the weight factor is responsible for this result. However, the optimization is repeated with different W_{reg} withing a range of three orders of magnitude and there is not a significant difference in the results.

If regularization is used, the quality of the set of initial parameter guesses is even more important than in the conventional least squares optimization problem.

Table D.1: Estimated kinetic parameters for the proposed fermentation model using the regularized objective function

Parameter		Initial guess	Estimates	Units
1	μ_{max}	1.2500	1.2505	1/h
2	K_{sx}	6.0000	6.0034	g/l
3	K_{ix}	302.0000	301.9929	g/l
4	$C_{L,1/2x}$	22.0000	22.0041	g/l
5	k	9.0000	9.0001	g/l
6	$q_{s,max}$	7.0000	7.0035	g/g/h
7	K_{ss}	5.0000	5.0022	g/l
8	K_{is}	145.0000	144.9969	g/l
9	$C_{L,1/2s}$	63.0000	62.9891	g/l
10	$q_{p,max}$	6.0000	5.9957	g/g/h
11	α	1.0000	1.0004	g/g

E

Dynamic modeling of Electrodialysis with bipolar membranes for lactic acid recovery

MSc. Thesis by Sijing Liu
Supervisor: Gunnar Jonsson
Co-supervisor: Oscar Andrés Prado-Rubio

E.1 Abstract

An integrated bioreactor and electrically driven membrane separation processes is under investigation to recover lactic acid from the fermentation broth. A previously developed dynamic model for ion transport in a dialytic module is extended to account for the presence of bipolar membranes. This model describes convective transport of the dissociated and undissociated species in the channels with diffusion and migration across the boundary layers and membranes. The model consists of a system of multiregion partial differential equation which is solved numerically. The operative window is explored by investigating the influence of the imposed current density and the lactate/hydroxide concentration ratio on the ion fluxes and concentration profiles. Finally, a numerical study of the concentration changes along the bulk channel is performed.

E.2 Introduction

A novel process was proposed to integrate lactic acid fermentation and *in situ* main product removal. This integrated system consists of one fermenter and two electrically driven membrane modules (Rype, 2003). The cultivation broth coming out of the fermenter contains lactate, which is separated by means of anion exchange membranes and sodium hydroxide using Reverse Electro-Enhanced Dialysis (REED). The sodium lactate obtained from REED is further converted to lactic acid, and sodium hydroxide is generated in an Electrodialysis process with Bipolar Membranes (EDBM).

Electrodialysis with bipolar membranes is used in the production of an acid or base from the corresponding salt in a cell arrangement consisting of cation and/or anion exchange membranes and bipolar membranes in alternating series (Strathmann, 2004).

Previously, some models have been developed for the ion transport through bipo-

lar membranes. Lee *et al.* (1998b) proposed a simple dynamic model for a batch operation mode. Two-compartment configuration with a cation exchange membrane was used. Sodium ion was assumed to be the only transported ion across the membrane. During the water-splitting electrodialysis, volume changes due to electroosmosis were significant for feed and the permeate solutions. Water transport index (litre of water per mol of ion) was determined with sodium lactate and with sodium ion. The calculated results for these two cases are 0.286 and 0.043 (litre water per mol of NaL/Na^+). The drawbacks of this model are that it excludes the transport phenomenon caused by diffusion, and that it does not account for the Donnan equilibrium at the interfaces.

Wilhelm (2001) in his thesis proposed a more concrete model which employs Nernst-Planck approach including both concentration and electrical potential gradients. Additionally, coupling phenomena such as Donnan equilibrium and electroneutrality conditions are also included. The model uses identical salt solutions in both sides of the bipolar membrane, and is developed for quasi-symmetric membranes (the layer thicknesses, the fixed charged group concentrations and the diffusion coefficients of both permeable layers are the same). However, in this static model, the average concentration at the solution-membrane interface is taken as the concentration inside the membrane. Furthermore, the boundary layer effects in the salt solutions are neglected, which results in a constant ion concentration at the membrane surface adjacent to the solution. A limitation of this model is the assumption that acids, bases and salts are completely dissociated under all conditions. But in practice, the dissociations of these solutions are strongly dependent on the pH value of where they locate.

Sonin and Grossman (1972) studied the ion transport of laminar membrane consisting of alternating layers of cation and anion exchange materials. Up to four layers are considered. The motion of the ions is governed by the transport law (Nernst-Planck model is used) of the dilute solution. Donnan equilibrium is employed to describe interfacial conditions. Only the dissociated salt is considered, the undissociated forms of the solution (weak acid) are not investigated. Transport number is defined for the positive and negative ions. The sum of these transport numbers should equal unity. Usually these numbers are positive and less than unity, but when the current density approaches zero, one of them might become larger than unity thus causing the other number becomes negative. The negative transport number signifies that, due to diffusion in a concentration gradient, the net ion flux is in an opposite to the expected direction of migration. Therefore, even if there is no current, salt ions can still be transported from one side to the other side of the membrane as long as the concentrations of the solutions in both sides do not equal. Similar to Wilhelms study, this paper also only deals with ion transport at steady state.

Jaime-Ferrer *et al.* (2009) proposed a dynamic model for formic acid production by a cell design consisting of cation exchange membranes and bipolar membranes. Both diffusion and migration phenomena are considered, and the mass balances for acid, salt, and hydroxide ions are specified. This study found out that it is possible that the formed formic acid can diffuse through bipolar membrane and enter the channel of sodium hydroxide solution. Besides, formate ion leaks through the bipolar membrane and contaminate the sodium hydroxide solution. Furthermore,

the hydroxide ion leaks through the cation-exchange membrane. The impacts of the diffusion of formic acid and the leakage of formate ion through the bipolar membrane on the current efficiency are small. The current efficiency is defined by the leakage of hydroxide ion through CEM. The current efficiency decreases as time increases. This is because the sodium hydroxide concentration increases, which leads to an increase of hydroxide ion leakage. The leakage of formate ion is proportional to the current density and sodium hydroxide concentration. The sodium hydroxide concentration needs to be low (but not too low, at an optimal value) in order to maintain a high current efficiency.

This contribution is structured as follows. The Electrodialysis with bipolar membranes process is described and the current process understanding is presented. The previously derived model is briefly summarized and the model extensions presented. Based on a degrees of freedom the model inputs and parameters identified. Afterwards, simulations are performed to investigate the influence of the current density and inlet ion concentrations to the base channel. A numerical study of the convective transport along the bulk channels is performed. Finally, the conclusions are drawn.

E.3 Process description

In this investigation, a two compartment electrodialysis cell design with anion exchange membranes is studied. This configuration is selected since it separation purpose is to recover and concentrate lactic acid from the corresponding salt solution (sodium lactate). A sketch of the modeled cell is depicted in Fig. E.1.

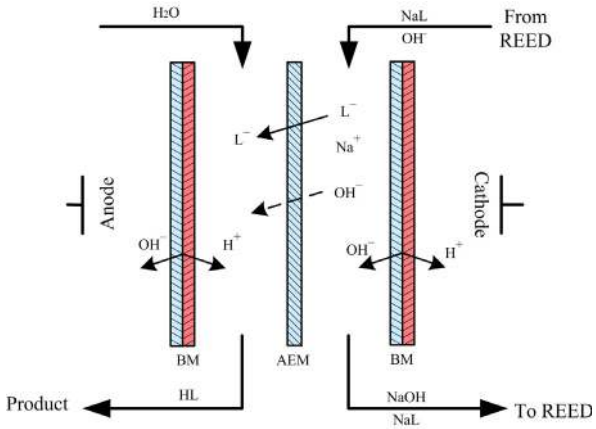

Figure E.1: Schematic drawing illustrating the expected ion transport in a two compartment electrodialytic cell with anion exchange membrane (AEM) and bipolar membranes (BM)

In this configuration, both the salt and acid solution flow in parallel separated by the membranes arrangement. Lactate and hydroxide ions present in the salt stream can be transported through the anion exchange membrane driven by concentration

and electrical potential gradients. The hydrogen and hydroxide ions required to recover the lactic acid and sodium hydroxide are produced by the bipolar membranes adjacent to the channels. Those ions are generated by the water splitting in the contact region between the cation permeable layer and anion permeable layer. This phenomenon originates from a reaction between the water molecule and the catalysts, which are immobilized on the surface of the membrane. Water is diffused into the contact region by a concentration gradient. The catalysts reduce the electric potential of a bipolar membrane and the activation energy requirement for water dissociation (Wilhelm, 2001). The reactive parts of the catalysts are the cation exchange group such as the carboxylic acid and the phosphoric acid groups, and the weak anion exchange groups such as tertiary and secondary amines. Not all fixed groups in the membranes show catalytic properties. Sulfonic acid group is known not enhancing the water splitting reaction (Mafé *et al.*, 1998), while all membranes with weakly basic amino and weakly acidic carboxylic acid groups involve in water splitting process (Simons, 1985).

One model that explains this reaction in the contact region is proposed by Simons (1985). With a weak acid (AH) as the catalyst:

$$A^- + H_2O \underset{k_{-1}}{\overset{k_1}{\rightleftharpoons}} AH + OH^-$$

$$AH + H_2O \underset{k_{-2}}{\overset{k_2}{\rightleftharpoons}} A^- + H_3O^+$$

With the corresponding acid BH^+ of a weak base B as a catalyst:

$$B + H_2O \underset{k_{-1}}{\overset{k_1}{\rightleftharpoons}} BH^+ + OH^-$$

$$BH^+ + H_2O \underset{k_{-2}}{\overset{k_2}{\rightleftharpoons}} B + H_3O^+$$

The rate constants for all the forward reactions are generally larger than the one found in free solution situation. This might be caused by the favorable orientation of water molecules under high electric field in the contact region (Mafé *et al.*, 1998). According to Simons (1985), the reactions which involve amino and phenol groups have rate constants that are up to 50 times higher than in free solution in general. Looking into different kind of membranes, during water splitting, for strongly basic membrane, k_2 value is two orders of magnitude greater than the free solution value. For sulfonic membrane, as explained previously the functioning group on sulfonic membrane does not enhance water splitting, thus electrolyte solutions are added. When doing so, the rate constants in the forward reactions between the surrounding electrolyte solutions and the water molecule would be six to thirty times greater than the free solution value. On the other hand, for weakly basic or acidic membrane, the rate constants are in the same order of magnitude (Simons, 1985). A model employing an exponential function was even developed to rationalize the relation between these rate constants under two different conditions (Mafé *et al.*, 1998).

The major limitation of EDBM process is the coion transport. Due to the interface equilibrium, the salt coions can also pass the membrane. This means, that in Fig.

E.1, the cations of the salt in the base chamber diffuse across the anion permeable layer and reach the acid chamber. This undesired transport is driven by the concentration gradients, and could finally result in contamination of the desired products. Additionally, EDBM also faces other limitations such as accumulated electrical resistance and instability under alkaline solutions. However, those problems are beyond the scope of this study.

E.4 Model development

The modeled section of two compartment bipolar membrane employing an anion exchange membrane is sketched in Fig. E.2. The effluent of REED module containing sodium (Na^+), lactate (L^-) and hydroxide (OH^-) ions, enters the base channel. The bipolar membrane (BM2) to the right side of anion exchange membrane (AEM) produces hydroxide. Under an electrical field, lactate and hydroxide might be transported towards the anode side. Due to the concentration gradient, a small amount of the sodium ions might pass through the AEM and reach the acid chamber. In the acid channel, diluted sodium lactate is added as the electrolyte solution. The bipolar membrane (BM1) to the left side of AEM produces hydrogen ion, which, together with lactate forms lactic acid (HL) due to the low pH. Assuming that hydrogen and lactic acid do not pass AEM, there are thus five components acid channel and adjacent boundary layer (BL1). However, there are only three components in base channel and corresponding boundary layer (BL2). The interfaces are denoted from z_0 to z_3. Relating to the current direction, positive fluxes are towards the cathode, while negative fluxes are towards the anode.

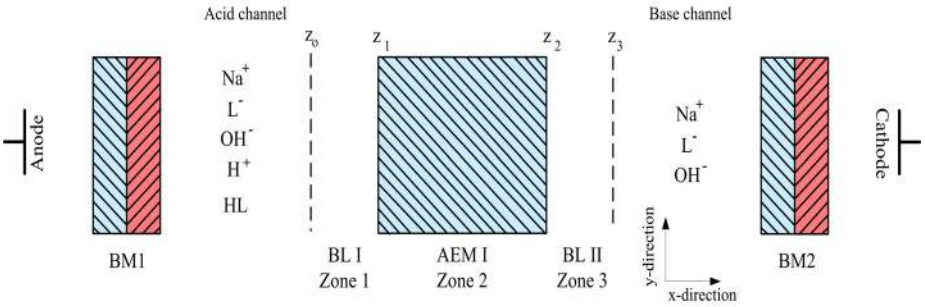

Figure E.2: Schematic drawing of a two compartment cell configuration using anion exchange membrane (AEM) and bipolar membranes (BM). z_0 to z_3 indicate the interfaces between the solution and boundary layers, boundary layers and anion exchange membranes. Components in the acid and base channels are depicted

The previously developed model for simultaneous ion transport through ion exchange membranes and adjacent boundary layers is employed as starting point for the development of the model for the EDBM cell. The details of the model are described in Prado-Rubio *et al.* (2010b). Basically, all the assumptions presented previously holds. Those are summarized as follows:

General assumptions (GA)

GA1. Electroneutrality condition is valid at any location.

GA2. The electrical current is only carried by ions.

GA3. Constant temperature.

GA4. The diffusion coefficients of the components in the solution are constant.

GA5. The solutions are ideal (activity coefficient equals 1).

GA6. There is no osmotic pressure difference between the solution and the membrane phase.

GA7. The bipolar membrane is 100% efficient. It means that the current is carried just by hydrogen and hydroxide ion in the cation and anion exchange layers, respectively.

GA8. Ion transport through the boundary layers adjacent to the bipolar membranes is not investigated.

GA9. Species included in the model are: lactate (L^-), hydroxide (OH^-), sodium (Na^+), hydrogen (H^+) and lactic acid (HL). H^+ and HL exist only in the acid bulk channel and boundary layer 1, while the other ions exist everywhere.

The extra assumptions that are required in this model are GA7 and GA8, that account for the bipolar membranes contribution. The bipolar membranes on both sides of the anion exchange membrane produce proton and hydroxide ions, respectively. The complexity of the bipolar membrane requires a separate modeling work. In this model it is assumed that the bipolar membranes are 100% efficient on producing proton and hydroxide. In other words, the fluxes of these two ions are completely controlled by Faraday's law, since only OH^- and H^+ are transported. As a consenquence of GA7, the ion transport across the boundary layers adjacent to the bipolar membranes is not investigated. As can be noticed in GA9, in this model the hypothetical protein which generates an extra pH buffer is eliminated. The reason is that that specie is not transported through the anion exchange membranes in the REED module.

Membrane assumptions (MA)

MA1. The transport through the membrane in the x-direction is defined by multicomponent diffusion and migration transport.

MA2. Convective transport is neglected.

MA3. The membrane surface is in equilibrium with the solution.

MA4. The influence of the water content on the size of the membrane is neglected.

MA5. Water flux caused by electroosmosis is not investigated.

Boundary layer assumptions (BLA)

BLA1. There are only diffusive and migrational transports in the x-direction.

BLA2. Convective transport is neglected.

BLA3. The diffusion coefficients for each ion in BL1 and BL2 are equal.

BLA4. The thickness of BL1 and BL2 are equal.

E.4.1 Model extension

As mentioned before, the mass balances describing the concentration profiles across boundary layers and the anion exchange membrane that were developed for the REED module remain in this model. The mass balances in the bulk channels are modified in order to account for the presence of the bipolar membranes. There are two changes that are introduced, the hydrogen and hydroxide fluxes from the bipolar membranes and how the acid channel inlet concentrations are estimated.

E.4.2 Bulk channels model

The concentration profile along the channels are estimated using tanks in series approach. Analogously to the REED model, a system of differential algebraic equations describes the convective transport along the bulk channels (y-direction). In each tank there is mass exchange with the adjacent boundary layers and the dissociation reactions are present. The dimensionless mass balances for the acid channel is expressed in the following way (Prado-Rubio *et al.*, 2010b):

$$\frac{dC_k^{acid}}{d\tau} = \frac{\tau_n}{\tau_{acid}}\left(C_k^{acid,in} - C_k^{acid}\right) + \frac{\tau_n}{h_{acid}}\left(J_{k,BM1} - J_k|_{z=z_0}\right) + \tau_n R_k \tag{E.1}$$

It can be noticed that the term $J_{k,BM1}$ was introduced. This term represent the ion flux which come from the bipolar membrane (BM1), and can be estimated from Faraday's law.

$$I_d = F\sum_k z_k J_{k,BM1} \tag{E.2}$$

Since only hydrogen ion (H^+) is transported from bipolar membrane to the acid chamber, then:

$$J_{H^+,BM1} = \frac{I_d}{z_{H^+}F} \tag{E.3}$$

The mass balance in the base channel is expressed as following:

$$\frac{dC_k^{base}}{d\tau} = \frac{\tau_n}{\tau_{base}}\left(C_k^{base,in} - C_k^{base}\right) + \frac{\tau_n}{h_{base}}\left(J_{k,BM2} - J_k|_{z=z_3}\right) \tag{E.4}$$

where the reaction term is not included due to the high pH in this channel, thus the species are completely dissociated. The terms involved in this expression are analogous to the acid channel. Since only hydroxide ion (OH^-) is transported from bipolar membrane to the base chamber, then:

$$J_{OH^-,BM1} = \frac{I_d}{z_{H^+}F} \tag{E.5}$$

E.4.3 Acid channel inlet concentration model

The inlet concentrations to the acid channel need to be specified for the model. This would include five species: lactate, hydroxide, sodium, hydrogen and lactic acid. Therefore a small model is made for acid channel initial concentrations.

The water dissociation is expressed as following:

$$H_2O \overset{K_w}{\rightleftharpoons} H^+ + OH^-$$

$$K_w = C^{acid}_{H^+} C^{acid}_{OH^-} \tag{E.6}$$

where K_w is the water dissociation constant. The dissociation of lactic acid can be expressed in the base form:

$$HL + OH^- \overset{K_b}{\rightleftharpoons} L^- + H_2O$$

$$K_b = \frac{C^{acid}_{HL} C^{acid}_{OH^-}}{C^{acid}_{L^-}} \tag{E.7}$$

The total lactate concentration consists of both the concentration of lactate ion and of lactic acid.

$$C^{tot}_{L^-} = C^{acid}_{L^-} + C^{acid}_{HL} \tag{E.8}$$

Due to the electroneutrality condition in the acid chamber,

$$C^{acid}_{L^-} + C^{acid}_{OH^-} = C^{acid}_{H^+} + C^{acid}_{Na^+} \tag{E.9}$$

Therefore if the pKa value the total lactate concentration and the sodium concentration at the inlet of the acid channel are given, the four unknowns ($C^{acid}_{L^-}$, $C^{acid}_{OH^-}$, $C^{acid}_{H^+}$ and C^{acid}_{HL}) can be calculated from four equations (E.6, E.7, E.8 and E.9).

E.4.4 Model solution

The extended dynamic model from REED which is used to model the EDBM module consists of a system of multiregion partial differential equations (PDEs). Once again, the method of lines is used to discretize the spatial dimension using sixth order Taylor expansion with asymmetric centered differences (Prado-Rubio *et al.*, 2010b).

E.5 Results and discussion

Simulations are performed in order to explore the operative window as a function of the imposed current density and lactate/hydroxide concentration ratio in the base channel. Finally, tank in series description of the convective transport along the channels is investigated.

E.5.1 Model parameters and inputs

Parameters and inputs are identified through a degree of freedom (DOF) analysis. Studies on parameters have been done by Prado-Rubio *et al.* (2010b). The relevant parameters to this model are summarized in Table E.1.

Table E.1: Parameters used in the EDBM model, taken from Prado-Rubio *et al.* (2010b)

Parameter	Value	Units
Gas constant (R)	8.3145	J/mol/K
Faraday number (F)	96487	C/mol or As/mol
pK_a for HL	3.860	-
D_{L^-} in solution	$1.033x10^{-9}$	m^2/s
D_{OH^-} in solution	$5.273x10^{-9}$	m^2/s
D_{Na^+} in solution	$1.334x10^{-9}$	m^2/s
D_{HL} in solution	$0.848x10^{-9}$	m^2/s
D_{H^+} in solution	$9.311x10^{-9}$	m^2/s
Membrane thickness	$0.27x10^{-3}$	m
Boundary layer thickness	$70x10^{-6}$	m
Fixed charge conc.	7500	mol/ m^3
Channels length	0.373	m
Channels width	0.15	m
Channels height	$0.6x10^{-3}$	m

The ion diffusion coefficients in the membrane are estimated using an empirical correlation that was previously regressed (Prado-Rubio *et al.*, 2010b). This expression proposed by Mackie and Meares expresses the tortuosity factor as a function of porosity of the membrane (Eq. E.10, cited by (Jonsson, 1980)). The smaller diffusion coefficient inside the membrane than in solution is explained by the fact that the membrane has an structural resistance to the transport. Additionally, that relation accounts for the increasing diffusivity of the ion when free volume in the

membrane increases. However, it neglects the coupling effect due to interactions between molecules, which means, that diffusion coefficients of all ions passing through the membrane are affected by the same factor.

$$D_k^m = D_k^s \left(\frac{E}{\tau_f} \right) = D_k^s \left(\frac{E}{2 - E} \right)^2 \tag{E.10}$$

Assuming that the membrane is completely wet, the free volume of the membrane is the water content. A black box model was proposed in Prado-Rubio *et al.* (2010b) in order to correlate the membrane water content with changes in the pH. In this model the water content of the membrane is believed to increase nonlinearly as the hydroxide concentration (thus also defining the average pH) in the base channel increases (Eq. E.11):

$$WC = \gamma \left(C_{OH^-}^{base,in} \right) \sigma \tag{E.11}$$

Where $C_{OH^-}^{base,in}$ is the inlet hydroxide concentration in the base channel (the units must be mol/L). γ and σ are empirical values which were estimated from experimental data. For lactate transport through Neosepta-AMH, $\gamma = 0.24$ and $\sigma = 0.1$ (Prado-Rubio *et al.*, 2010b). The fixed charge of the membrane and the thickness of the boundary layers adjacent to the AEM were estimated through a sensitivity analysis.

The model inputs need to be specified in order to run the simulation. Any of these variables can be changed so as to study its impact on the system. The first studied independent variable is the current density (I_d). The other inputs are studied and summarized in Table E.2.

Table E.2: Model inputs

Parameter	Value	Units
Current density range	100-550	A/m^2
q_{acid}	120	l/h
q_{base}	120	l/h
$C_L^{base,in}$	80	mol/m^3
$C_{OH}^{base,in}$	20	mol/m^3
$C_{Na}^{base,in}$	100	mol/m^3
$C_{HL}^{acid,in} + C_{L^-}^{acid,in}$	20	mol/m^3
$C_{Na^+}^{acid,in}$	10	mol/m^3

Where q_{acid} and q_{base} are the flow rates of acid and base channel. The value is taken from the operational parameters for Donnan dialysis operation mode in Prado-Rubio *et al.* (2010b). $C_L^{base,in}$, $C_{OH}^{base,in}$ and $C_{Na}^{base,in}$ are the inlet concentration of lactate, hydroxide, and sodium ions in the base channel, respectively. These ions exist as the composing ions of sodium lactate and sodium hydroxide which come from the REED module. Due to the high pH, all components are completely dissociated.

In REED module, hydroxide is transported through the anion exchange membrane to the feed channel, while lactate is recovered from the cultivation broth. In this investigation, the input to the base channel which comes from the dialysate channel in the REED module, is assumed to be alkaline and contains more lactate than hydroxide. Therefore, the lactate concentration at the inlet of the base channel is set 80 mol/m^3, while the hydroxide 20 mol/m^3. The sodium ion exists in the salt form with both lactate and hydroxide ions, thus the concentration of sodium at the inlet of base channel is the sum of the concentration of lactate and hydroxide (100 mol/m^3), fulfilling the electroneutrality condition.

In the acid channel, the concentrations of total lactate and sodium at the inlet need to be specified according to the initial condition model discussed in above. Both concentrations should be lower than the concentrations in the base channel as the starting solution in the acid channel is mainly used as the electrolyte solution. As H^+ ion is produced from the bipolar membrane adjacent to the acid channel, lactic acid is formed as the pH becomes low. Thus the lactate in this channel exists in either undissociated or dissociated form. Using the proposed model, a relation between sodium concentration and the pH value can be found. This is depicted in Fig. E.3. When the sodium concentration is smaller than 20 mol/m^3, the solution in the acid channel is acidic (pH below 6). But once the sodium concentration exceeds 20 mol/m^3 the pH value increases dramatically. So for the simulation 10 mol/m^3 is chosen as the inlet sodium concentration in the acid channel, and for total lactate is 20 mol/m^3.

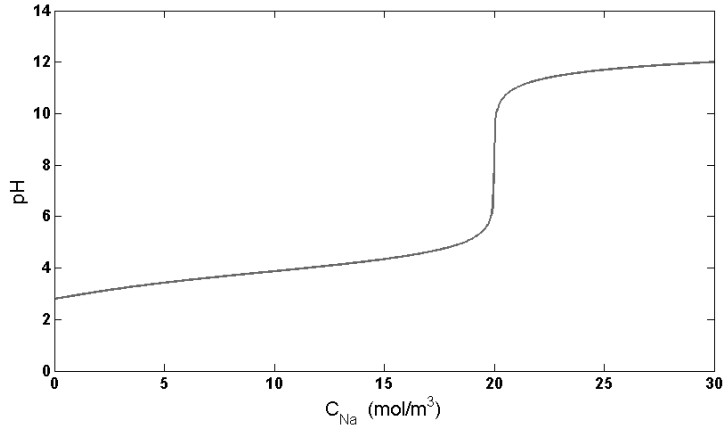

Figure E.3: pH changes at the inlet of the acid channel as a function of the Na^+ concentration

E.5.2 Static model analysis under current load conditions

The static system behavior is investigated as a function of the strength of the imposed electrical potential gradient. The current density is increased from 100 A/m^2 onwards until the solution of the system of equations becomes unfeasible (Prado-

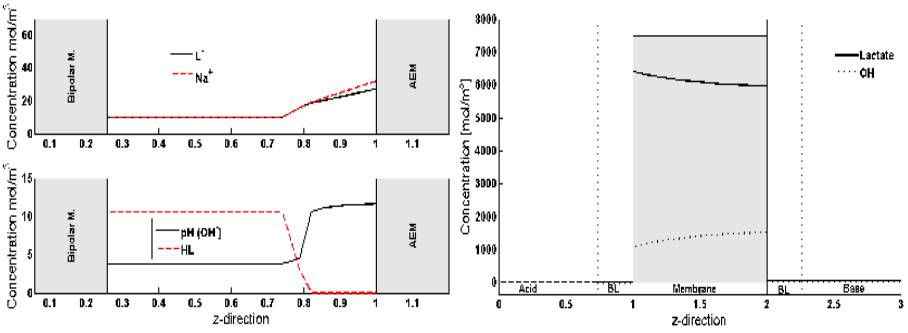

(a) Acid channel profile

(b) Membrane profile

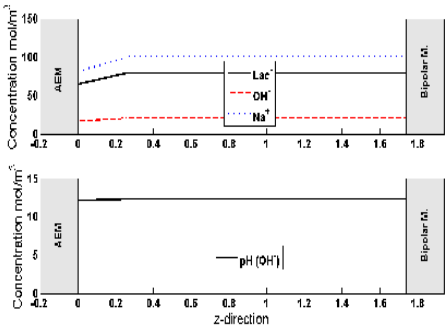

(c) Base channel profile

Figure E.4: Static concentration profiles of the system under low current density (I_d=100 A/m^2). (a) Acid channel; (b) Membrane and (c) Base channel

Rubio *et al.*, 2011b). In this simulation the current density can go up till 550 A/m^2. Two simulations under two different current densities are shown in Figs. E.4 and E.5, which shows the concentration profiles of the system under 100 A/m^2 and 550 A/m^2 current densities, respectively.

The Figs. E.4(a) and E.5(a) show that the concentrations of lactate and sodium at the interface between BL1 and AEM become three times higher by increasing the current density from 100 to 550 A/m^{-2}. The difference between C_{L^-} and C_{Na^+} at this location becomes five times larger. Under the higher current density, the concentration of lactic acid is slightly increased in the acid channel. Additionally, the pH has a sharper increase at the interface between the bulk solution and the boundary layer, which leads to less lactic acid concentration in the boundary layer.

The Figs. E.4(b) and E.5(b) depict that when the current density becomes high, the lactate concentration in the membrane drops, while the hydroxide concentration rises. Lactate concentration at the interface between AEM and BL2 decreases from 6000 to 5700 mol/m^3. Besides, hydroxide concentration at same interface increases from 1450 to 1750 mol/m^3. The lactate and hydroxide concentration inside the membrane become almost constant at the highest current density. Due to the

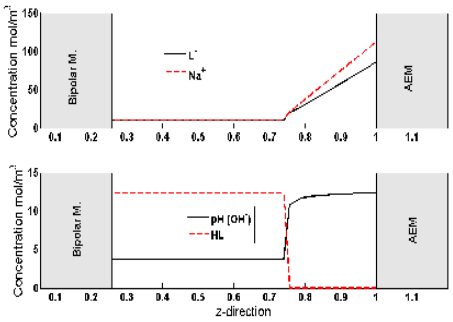

(a) Acid channel profile

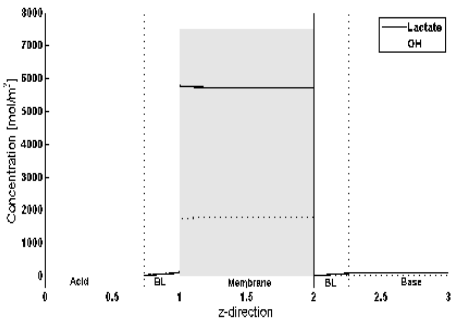

(b) Membrane profile

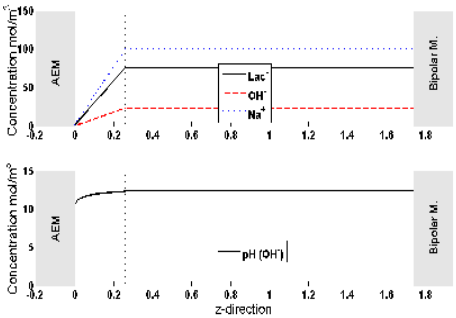

(c) Base channel profile

Figure E.5: Static concentration profiles of the system under high current density (I_d=550 A/m^2). (a) Acid channel; (b) Membrane and (e) Base channel

electroneutrality condition and effectiveness of Donnan exclusion, the sum of both concentrations basically equals the fixed concentration of the anion exchange membrane.

The last two plots in Figs. E.4 and E.5 show that the concentrations of lactate, hydroxide and sodium at the interface between AEM and BL2 are smaller and approach zero when the high current density is applied. By increasing the current density from 100 to 550 A/m^2, the lactate and sodium concentrations at the interface between AEM and BL2 become forty times smaller while hydroxide concentration is thirty times smaller. As the BL2 becomes deficient of hydroxide, the pH value also drops at this point compared to the case when 100 a/m^2 is applied.

Fig. E.6 shows the concentration of the lactic acid produced in the acid channel as a function of the current density. As the current density increases, more lactic acid is formed in the acid channel. There is however a plateau where either the increase of lactic acid production is somewhat hindered, or after certain period of saturation the lactic acid formation activated again. An explanation is proposed below.

The plateau in lactic acid concentration might be caused by a certain concentration ratio of lactate, hydroxide and sodium. The diffusion coefficient (which relates to

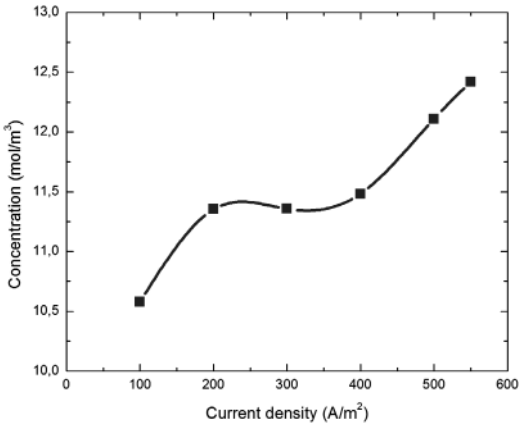

Figure E.6: Static lactic acid concentration in the acid channel as a function of current density

the ion mobility) of hydroxide is about five times larger than for lactate (as shown in Table E.1). This means that the lactate concentration gradient across the membrane has to be in a certain level higher than for hydroxide in order favor the production of lactic acid by increasing the current density. As shown in Fig. E.7, the concentration ratio between lactate and hydroxide at the interface in the base channel is high in at low current density, and tends to keep at the same level as both lactate and hydroxide concentrations start decreasing. This means that the production of lactic acid should stay at a constant level. However when the current density is increased to higher than 400 A/m^2, the lactic acid concentration increases again. This situation leads to interest in the bulk concentration behavior in the acid channel.

Fig. E.8 shows that between 200 and 400 A/m^2 the pH and sodium concentration increase. This situation can explain the plateau in lactic acid production. Meaning that the increase in lactic acid production by an increment in current density is compensated by the rise in pH. The pH wave behavior shown in Fig. E.8(a) is not investigated further in this study, but can be important for future work. Especially the dissociation phenomenon inside the boundary layer adjacent to the acid channel might play an import role in this case.

Fig. E.9 depicts the lactate and hydroxide fluxes as a function of current densities. Under current densities from 100 to 550 A/m^2, the both ion fluxes are negative since the ions are transported in the opposite direction to the spatial direction reference. As the current density increases both fluxes become bigger. Besides, the hydroxide flux is all the time higher than lactate flux and becomes even much higher when the current density becomes larger.

The first round model simulations gives a clear result about the impact of current density to the behavior of the system. When all other inputs and parameters are fixed, increasing the current density enhances the fluxes of both hydroxide and lactate, the latter of which leads to a higher production of lactic acid. At intermediate values of the imposed current density (200 to 400 A/m^2), sodium concentration

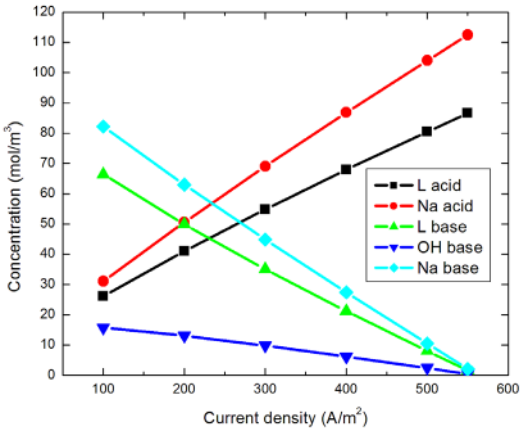

Figure E.7: Static ionic concentrations at the interface between membrane and the boundary layers as a function of the current density. Acid and base refer to the acid and base channels, respectively

and pH increase at the acid channel while lactic acid concentration is kept almost constant. The lactic acid production rises when the pH decreases.

The concentration profiles in the membrane as well as in the boundary layers also change significantly when the current density increases. The concentrations of all ions at the interface between the membrane and the boundary layer in the base channel tend to approach zero, which results in a deficiency of ions when the current is increased. This point is referred to generates as limiting current density (Strathmann, 2004; Sonin and Grossman, 1972). The numerical problems generated at limiting current densities have been previously investigated for ion transport through AEM using the same approach Prado-Rubio *et al.* (2011b).

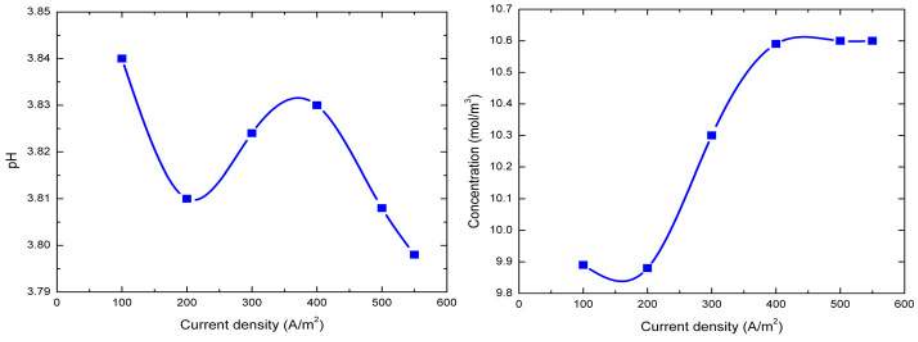

(a) pH in the acid channel **(b)** Sodium in the acid channel

Figure E.8: Static pH and sodium concentration in the acid channel as a function of the current density

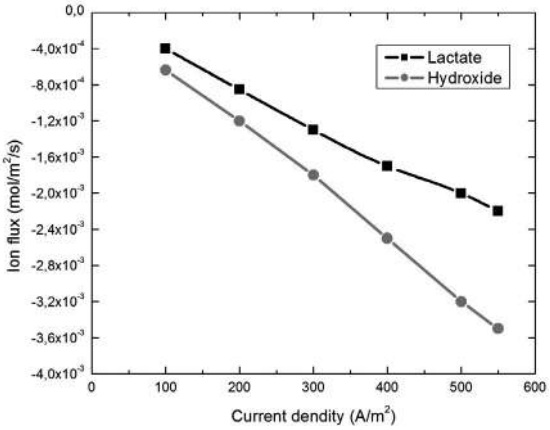

Figure E.9: Static lactate and hydroxide fluxes as a function of current density

E.5.3 Influence of lactate and hydroxide concentration ratio

After investigating the impact of current density, the concentration ratio of lactate and hydroxide in the base channel is changed (lactate: 90 mol/m^3; hydroxide: 10 mol/m^3) to study its impact on the system performance. The sodium is still the sum of the concentrations of lactate and hydroxide in order to keep the electroneutrality condition. The current density is set at 100 A/m^2, and all the other inputs are unchanged as shown in Table E.2. The concentration profile of the simulation under the condition of the new inputs is shown in Fig. E.10. This result can be compared with the (a), (b) and (c) graphs from Fig. E.4.

From Fig. E.10(a), it is possible to see that the concentration profile for lactic acid is slightly different, the change is significant in the boundary layer. More lactic acid penetrates the boundary layer compared with the result in Fig. E.4(a). This higher presence of lactic acid is accompanied by a lower pH value in the boundary layer. Fig. E.10(b) shows that the average lactate and hydroxide concentration ratio inside the membrane rises more than 2 folds compared to Fig. E.4(b). The lactate concentration gradient across the membrane decreases from 220 to 160 mol/m^3. Comparing the concentration profiles in the base channel, Fig. E.10(c) and E.4(c), it can be seen that the sodium concentration at the interface between AEM and BL2 decreases. This is mainly due to the decrement of hydroxide concentration at that point.

The simulation results show also that the fluxes of lactate and hydroxide vary considerably by modifying the concentration ratio of lactate and hydroxide at the inlet of the base channel. A comparison is depicted in Fig. E.11, which shows that when the lactate concentration in the base channel changes from 80 to 90 mol/m^3, the lactate flux increases from approximately -3x10^{-4} to -6x10^{-4} mol/m^2/s. Oppositely, the hydroxide flux decreases when the lactate concentration in the base channel increases.

One interesting phenomenon is that when fixing all the other variables and parameters, changing the concentration ratio in the base channel results in a different

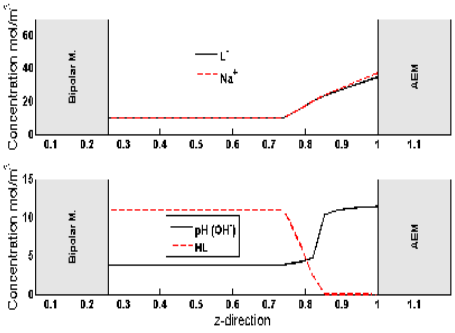

(a) Acid channel profile

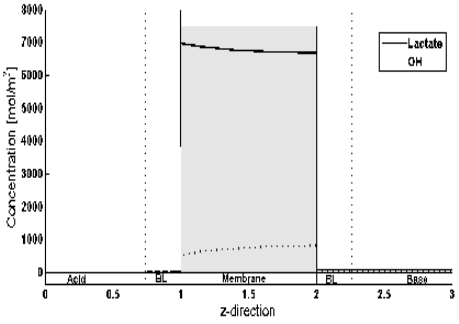

(b) Membrane profile

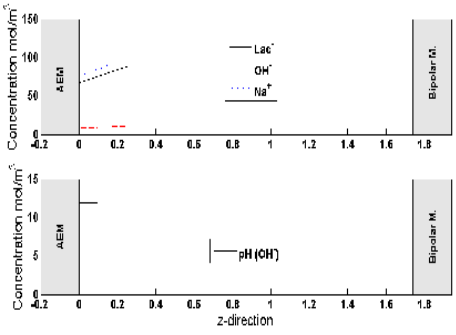

(c) Base channel profile

Figure E.10: Static concentration profiles of the system under 100 A/m^2 and inlet lactate and hydroxide concentration to the base channel of 90 and 10 mol/m^3, respectively. (a) concentration profile in the acid channel, (b) concentration profile in the membrane and (c) concentration profile in the base channel

preference on the ionic fluxes. As clearly shown in Fig. E.11, the hydroxide flux is larger than lactate flux when the concentration ratio of lactate and hydroxide is 4:1. However, when the lactate concentration is increased while the hydroxide concentration is decreased, the lactate flux becomes dominant. Since one of the purposes of the bipolar membrane electrodialysis is to produce purer lactic acid in the acid channel and sodium hydroxide in the base chamber, which depend largely on their fluxes, it is advantageous to reach a scenario when lactate flux surpasses the hydroxide flux. As previously discussed, the current density influences the flux. Therefore, plots are made for fluxes as a function of current density for both concentration ratios, and for a larger range.

In Fig. E.12 the lactate and hydroxide fluxes are plotted against the current density for two different inlet base channel concentration ratios. (b) shows that the fluxes of lactate and hydroxide are equal when the current density is around 50 A/m^2. Before this point, hydroxide flux is favored while after this point lactate flux becomes higher. This behavior is not observed in (a), where hydroxide flux is always

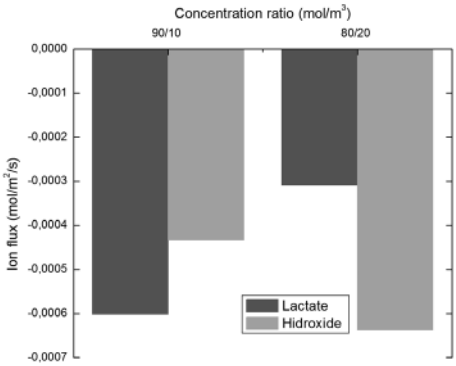

Figure E.11: Static lactate and hydroxide flux under different base channel concentration ratios. 90/10 and 80/20 indicate the lactate to hydroxide concentration ratio at the inlet of the base channel

higher than lactate flux, and this difference becomes even bigger when the current density increases. It can be seen when lactate concentration in the base chamber increases from 80 to 90 mol/m^3, the change of its flux as a function of current density tends to become steeper. Similarly, when the hydroxide concentration decreases from 20 to 10 mol/m^3, the change of its flux as a function of current density becomes steadier. Therefore, lactate flux has is able to overcome hydroxide flux. Based on above discussion, it can be hypothesized that there is a lactate/hydroxide threshold in order to favor the lactate transport.

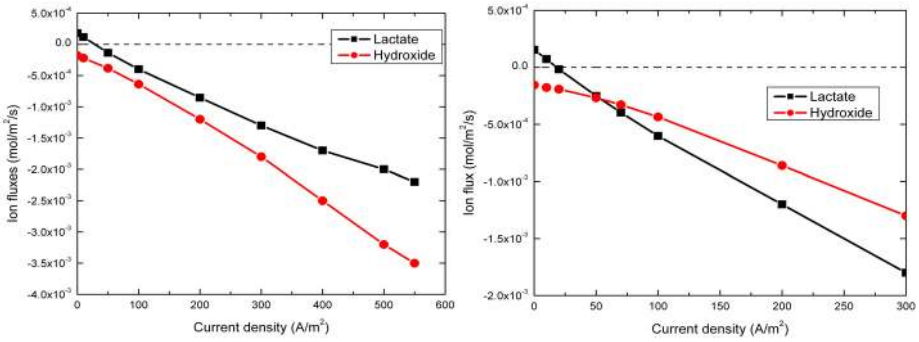

(a) Ion fluxes for 80/20 **(b)** Ion fluxes for 90/10

Figure E.12: Comparison of lactate and hydroxide static fluxes, under different base channel concentration ratios. (a) when lactate and hydroxide concentrations in the base channel are 80 and 20 mol/m^3, and (b) when lactate and hydroxide concentrations at the inlet of the base channel are 90 and 10 mol/m^3

Another interesting phenomenon can be observed in Fig. E.12 is that under very low current density the lactate flux becomes positive. This ion exchange transport is generated by the pH difference between the acid and base channels. Under no/low current conditions, the hydroxide tends to transport through the anion exchange membrane due to the concentration difference between the two channels. The hydroxide transport induces a potential gradient which drives the lactate flux out of the acid chamber, thus giving a positive value (Strathmann, 2004; Prado-Rubio *et al.*, 2010b). The induced potential gradient overcomes the lactate concentration gradient and the strength of the imposed electrical potential gradient.

As previously mentioned, the concentration of lactate, hydroxide and sodium at the interface between membrane and the bulk channel boundary layer all tend to be zero when the limiting current density is applied. This is checked for system with other concentration ratios in the base channel, and the result is shown in Fig. E.13. Interestingly, it shows that when the lactate concentration goes down and hydroxide concentration goes up in the base channel, the concentrations at the interface cannot really reach zero under the highest current densities that are applied. This might be caused by another numerical constraint during in the simulation under high current densities, which results in a current limitation that is actually lower than the expected limiting current density.

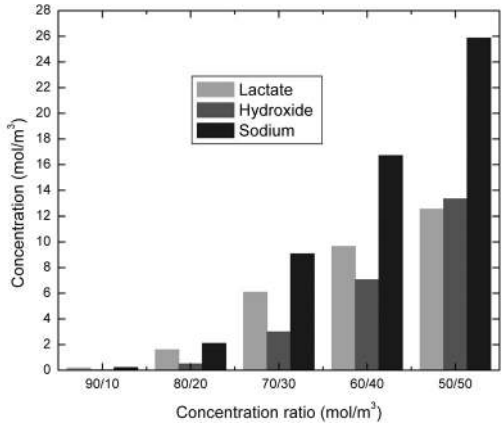

Figure E.13: Static interfacial ion concentrations between the anion exchane membrane and the boundary layer in the base channel at the maximum current density allowed, before the solution of the system of equations becomes unfeasible

Fig. E.14 shows the highest current densities that can be applied in the simulation for each simulation for different lactate/hydroxide concentration ration in the base channel. Based the previously concluded, when the lactate concentration is 90 mol/m^3, the highest current density correspond to the limiting current density. However, when the lactate concentration goes down, the limiting current densities should be higher than the highest current densities shown in Fig. E.14.

Summing up all the results given above, an operative window can be defined for further simulations. One key element of this operative window is that the concen-

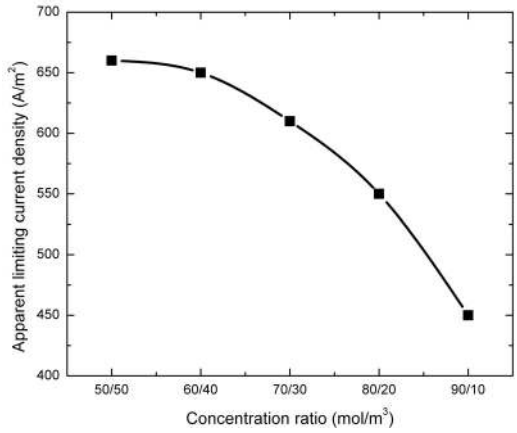

Figure E.14: Static highest current density that can be imposed as a function of the lactate/hydroxide concentration ratio in the base channel

tration ratio of lactate to hydroxide in the base channel should be preferably high, such as 9:1. This concentration ratio gives a reliable limiting current density in the simulation and generates a preferable lactate flux at high current density.

E.5.4 Numerical investigation of the tank in series approach

The purpose of this investigation is to reveal whether and when it is necessary to use tank-in-series model to describe the concentration changes in the bulk channel along the y-direction. Two and Five tank modules are investigated separately in order to gain the result of the gradual increase of the tank number. Additionally, the channel length is also amplified five times to see the impact of adding more tanks when the channel is longer.

Figs. E.15 and E.16 show the lactate and hydroxide concentrations at the outlet of each tank when there are one and five tanks and for short and long channels. When the channel length is small, five-tank module does not give a significant difference in the outlet concentrations of each tank (compare first result of 5 tanks and 5xAm with last point in 5 tanks and 1xAm, in Fig. E.15). However, when the channel length is increased five folds, the outlet concentration of the lactate at the fifth tank is significantly lower than the starting concentration. Similarly the hydroxide concentration at the outlet of the fifth tank is significantly higher than its starting concentration at the inlet of the first tank. As shown in both figures, the one tank module for the long channel (1 tank and 5xAm, in Fig. E.15) has a similar outlet concentration as the last outlet concentration of the five-tank module for the long channel (last point in 5 tanks and 5xAm, in Fig. E.15). The relative error of using only one tank is calculated using Eq. E.12. The error of using only one tank in the y-direction when the channel length is five times larger than the reference is 0.38% and 2.24% for lactate and hydroxide, respectively.

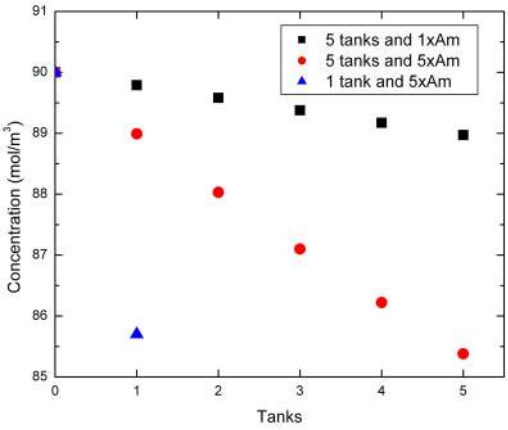

Figure E.15: Static lactate concentration at the outlet of each tank. Am stands for membrane area. The ion concentration at tank zero corresponds to the inlet concentration. 1xAm reference channel length (according to Table E.1). 5xAm refers to 5 times the reference channel length)

$$Error(\%) = \frac{\left|C_{(5\text{ tank }5\text{x}Am)} - C_{(1\text{ tank }5\text{x}Am)}\right|}{C_{(5\text{ tank }5\text{x}Am)}} \tag{E.12}$$

The influence of the tank in series approach can be evaluated using the mean fluxes of lactate and hydroxide for one, two and five -tank modules respectively, and for short and long channels. The mean flux of each tank is calculated from Eq. E.13.

$$\bar{J}_i = \frac{\left(C_i^{out_k} - C_i^{in_k}\right) q_{base}}{Am_k} \tag{E.13}$$

where $\bar{J}_i$ is the mean flux of ion i, Am is the membrane area of the k-th tank, and C_i^{out} and C_i^{in} are the outlet and inlet concentrations to each tank, respectively. The total average flux in the module is calculated averaging the mean fluxes of all individual tanks.

The results are shown in Fig. E.17. They show that by adding more tanks in the channel, the averaged lactate flux will increase while the averaged hydroxide flux decreases. These changes become clearer when the channel length increases. This means that when the channel is long it might be necessary to consider using tank-in-series module as higher deviations are obtained. Quantifying the error in the mean flux by using an expression analogous to Eq. E.12, it gives a results that the 1-tank approach for lactate is deviated 1.2% and 2% from the 2-tank and 5-tank description, respectively. For the longer channel, the differences are 4.5% and 7.5% respectively. Similar results are obtained for hydroxide mean flux.

When the channel is long, it might be necessary to include more tanks in the tank in series description, as the deviation from the 1-tank approach increases. On the

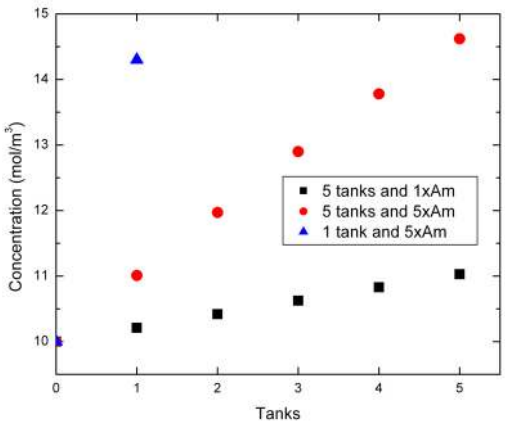

Figure E.16: Static hydroxide concentration at the outlet of each tank. The ion concentration at tank zero corresponds to the inlet concentration. Am stands for membrane area. 1xAm reference channel length (according to Table E.1). 5xAm refers to 5 times the reference channel length

other hand, when the channel length is small, adding more tanks does not make a big difference in the fluxes, thus one tank CSTR module can be considered as the appropriate setup.

Using tanks-in-series module might be beneficial for long channels regarding to the averaged fluxes, but might asks for a price when talking about the simulation time. Fig. E.18 shows the change of the simulation time as the tank number increases. It can be seen that the simulation time increases exponentially as the tank number increases. When the channel is longer, the simulation time is higher compared to the one for a short channel. This result confirms previous investigations where

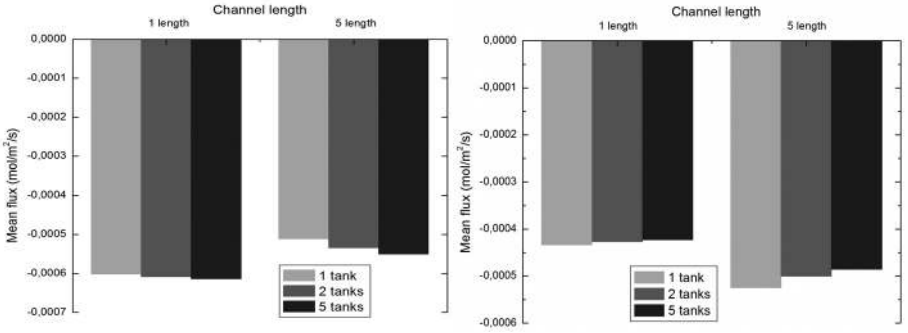

(a) Lactate **(b)** Hydroxide

Figure E.17: Comparison of static mean lactate and hydroxide fluxes between short and long channel systems

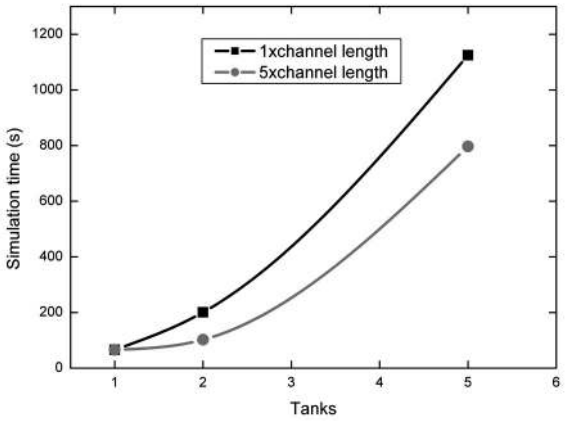

Figure E.18: Simulation time as a function of the number of tank in series employed

it was stated that the simulation time increases exponentially as the number of discretization points in the Taylor expansion series increases (Møllerhøj, 2006). As the channel length increases, the total number of equations increases analogously to have more discretization points. Thus, the simulation time exhibits a similar response.

Therefore, it is concluded that although adding more tanks in the channel leads to a higher accuracy, the dramatic increase in simulation should also be taken into account. The pros and cons should be well balanced when designing the simulation work.

E.6 Conclusions

A dynamic model was developed for the transport of ions in the two compartment electrodialysis with bipolar membranes for lactic acid recovery, employing an anion exchange membrane. The model is based on first principles for dissociation, diffusion and migration of the species. The transport phenomena through the boundary layer and the anion exchange membrane, in the bulk solutions and at the interfaces are modeled separately. The link between zones in the model are boundary and field conditions given by algebraic and differential algebraic equations. The combined model leads to a system of partial differential equations which is solved numerically. The major modifications to the original model are the dissociation model in the acid channel and the introduction of bipolar membranes. The model is able to predict concentration profiles as well as fluxes in the modeled zones in presence or absence of a current load. Thus it provides useful understanding for the interactions between the membrane separation processes involved in the entire lactic acid production process.

The operating window of the process was investigated as a function of the current density and the ion concentration ratio in the base channel. Increasing the current density, the ion fluxes were enhanced and thus the lactic acid production. However,

the observed pH wave behavior in the feed channel could be unfavorable. Therefore, future investigations are required to reveal the source that behavior. The concentration ratio between lactate and hydroxide in the base channel should be as high as 9:1. Such concentration ratio provides the necessary conditions for having preferable lactate transport through the anion exchange membrane and for obtaining reliable estimation of the limiting current density.

From the numerical investigation of the tank in series approach it was observed that for short channel lengths, only one CSTR is an appropriate assumption to model the ion concentration in the bulk channels. As the channel length increases, convective transport along the channel plays a significant role, thus requiring more tanks in the model. This modification leads to an exponential increase in the simulation time. Therefore, the selection of the number of tank in series represents a trade off between accuracy and simulation time.

E.7 Nomenclature

A^-	Acid ion
AEM	Anion exchange membrane
Am	Membrane area
B	Weak base
BL	Boundary layer
C	Concentration (mole m^{-3})
D	Diffusion coefficient (m^2 s^{-1})
E	Fractional membrane water content (-)
$EDBM$	Electrodialysis with bipolar membranes
F	Faraday constant (C $mole^{-1}$)
H^+	Hydrogen ion
HA	Weak acid
HL	Lactic acid
I_d	Current density (A m^{-2})
J	Flux (mole m^{-2} s^{-1})
h_i	Channel i height (m)
k	Kinetic parameter (-)
K_b	Dissociation constant (mol m^{-3})
K_w	Ionic product for water (mol^2 m^{-6})
L	Channel length (m)
L^-	Lactate ion
Na	Sodium ion
OH^-	Hydroxide ion
q	Flow rate (m^3 s^{-1})
R_k	Total reaction rate of k (mol m^{-3} s^{-1})
R	Universal gas constant (J mol^{-1} K^{-1})
$REED$	Reverse electro-enhanced dialysis
t	Time (s)
y	Spatial direction (m)

W	Channel width (m)
z	Dimensionless distance $z = x/\delta_m$ (-)
z_k	Valence of k (-)

Greek letters

δ_{BL}	Boundary layer thickness (m)
δ_m	Membrane thickness (m)
γ	Parameter in the WC model (-)
σ	Parameter in the WC model (-)
τ	Dimensionless time ($\tau = t/\tau_n$) (-)
τ_{acid}	Residence time in dialysate channel ($\tau_{acid} = h_{acid}WL/q_{acid}$) (s)
τ_{base}	Residence time in feed channel ($\tau_{base} = h_{base}WL/q_{base}$) (s)
τ_f	Tortuosity factor (-)
τ_n	Nominal time ($\tau_n = 1$ (s))

Subscripts

A^-	Anion
$acid$	Acid
$base$	base
BL	Boundary layer
fix	Fixed charges in the membrane
HL	Lactic acid
i	Specie
j	Discretization point
k	Specie
L^-	Lactate ion
Na^+	Sodium ion
OH^-	hydroxide ion
p	Zone (phase)
z	specific location

Superscripts

$acid$	Acid
$base$	Base
in	Inlet
m	Membrane
s	Solution
$-/+$	Left/Right side of a section

References

Abdekhodaie, M. and Wu, X. (2005). Modeling of Cationic Glucose-Sensitive Membrane with Consideration of Oxygen Limitation. *Journal of Membrane Science*, **254**, 119–127.

Åkerberg, C. and Zacchi, G. (2000). An economic evaluation of the fermentative production of lactic acid from wheat flour. *Bioresource Technology*, **75**(2), 119 – 126.

Åkerberg, C.; Hofvendahl, K.; Zacchi, G. and Hahn-Hägerdal, B. (1998). Modelling the Influence of pH, Temperature, Glucose and Lactic Acid Concentrations on the Kinetics of Lactic Acid Production by *Lactococcus lactis* ssp. Lactis ATCC 19435 in Whole Wheat Flour. *Appl. Microbiol. Biothenol*, **49**, 682–690.

Amrane, A. and Prigent, Y. (1994). Mathematical Model for Lactic Acid Production from Lactose in Batch Culture: Model Development and Simulation. *J. Chem. Tech. Biotechnol.*, **60**, 241–246.

Ayyildiz, H. and Kara, H. (2005). Boron Removal by Ion Exchange Membranes. *Desalination*, **180**, 99–108.

Bahri, P. A.; Bandoni, J. A. and Romagnoli, J. A. (1997). Integrated Flexibility and Controllability Analysis in Design of Chemical Processes. *AIChE Journal*, **43**, 997–1015.

Bansal, V.; Perkins, J. D.; Pistokopoulos, E. N.; Ross, R. and van Schijndel, J. M. G. (2000). Simultaneous Design and Control Optimization under Un. *Computers & Chemical Engineering*, **24**, 261–266.

Baughman, D. and Liu, Y. (1995). *Neural Networks in Bioprocessing and Chemical Engineering*. Academic Press.

Beier, S.; Guerra, M.; Garde, A. and Jonsson, G. (2006). Dynamic Microfiltration with Vibrating Hollow Fiber Membrane Module: Filtration of Yeast Suspensions. *Journal of Membrane Science*, **281**, 281–287.

Boonmee, M.; Leksawasdi, N.; Bridge, W. and Rogers, P. (2003). Batch and Continuous Culture of *Lactococcus lactis* NZ133:Experimental Data and Model Development. *Biochemical Engineering Journal*, **14**, 127–135.

Boonmee, M.; Leksawasdi, N.; Bridge, W. and Rogers, P. (2007). Electrodialysis for Lactate Removal in the Production of the Diary Starter Culture *Lactococcus lactis* NZ133. *International Journal of Food Science and Technology*, **42**, 567–572.

Bowen, W. R.; Liang, Y. and Williams, P. M. (2000). Gradient Diffusion Coefficients - Theory and Experiment. *Chemical Engineering Science*, **55**(13), 2359–2377.

Boyaval, P.; Corre, C. and Terre, S. (1987). Continuous Lactic Acid Fermentation with Concentrated Product Recovery by Ultrafiltration and Electrodialysis. *Biotechnology Letters*, **9**(3), 207–212.

Bristol, E. (1966). On a New Measure of Interaction for Multivariable Process Control. *IEEE Transactions on Automatic Control*, **11**(1), 133 – 134.

Brun, R.; Reichert, P. and Künsch, H. (2001). Practical Identifiability Analysis of Large Enviromental Simulation Models. *Water Resources Research*, **34**(4), 1015–1030.

Brun, R.; Kühni, M.; Siegrist, H.; Gujer, W. and Reichert, P. (2002). Practical Identifiability of ASM2d Parametes - systematic selection and tuning of parameters subsets. *Water research*, **36**, 4113–4127.

Burgos-Rubio, C.; Okos, M. and Wankat, P. C. (2000). Kinetic Study of the Conversion of Different Substrates to Lactic Acid Using *Lactobacillus bulgaricus*. *Biotechnology progress*, **16**, 305–314.

Cachon, R. and Divès, C. (1993). Modeling of Growth and Lactate Fermentation by *Lactococcus lactis* subsp. lactis biovar. Diacetylactis in Batch culture. *Applyed Microbiology and Biotechnology*, **40**, 28–33.

Coleman, T. and Li, Y. (1994). On the Convergence of Interior-Reflective Newton Methods for Nonlinear Minimization Subject to Bounds. *Mathematical Programming*, **67**, 189–224.

Cussler, E. (1984). *Diffusion-Mass Transfer in Fluid Systems*. Cambridge University Press.

Cwirko, E. H. and Carbonell, R. G. (1989). Transport of Electrolytes in Charged Pores: Analysis using the Method of Spatial Averaging. *Journal of Colloid and Interface Science*, **129**, 513–531.

Cwirko, E. H. and Carbonell, R. G. (1990). A Theoretical Analysis of Donnan Dialysis across Charged Porous Membranes. *Journal of Membrane Science*, **48**, 155–179.

Eigenberger, G. and Nieken, U. (1988). Catalytic combustion with periodic flow reversal. *Chemical Engineering Science*, **43**(8), 2109–2115.

Faanes, A. and Skogestad, S. (1999). Control Structure Selection for Serial Processes with Application to pH-Neutralization. In *Proceedings of the European Control Conferance, ECC 99*.

Fila, V. and Bouzek, K. (2003). A Mathematical Model of Multiple Ion Transport Across an Ion-Selective Membrane under Current Load Conditions. *Journal of Applied Electrochemistry*, **33**, 675–684.

Foss, A. (1973). Critique of Chemical Process Control Theory. *AIChE Journal*, **18**(6), 642–652.

Franklin, G.; Powell, J. and Workman, M. (1997). *Digital Control of Dynamic Systems*. Addison-Wesley, third edition.

Friedman, M. and Gaden, E. J. (1970). Growth and Acid Production by *Lactobacillus delbrueckii* in a Dialysis Culture System. *Biotechnol Bioeng*, **12**, 961–974.

Garde, A. (2002). *Production of Lactic Acid from Renewable Resources using Electrodialysis for Product Recovery*. Ph.D. thesis, Technical University of Denmark.

Gekas, V. and Hallström, B. (1987). Mass Transfer in the Membrane Concentration Polarization Layer under Turbulent Cross Flow - I. Critical Literature Review and Adaptation of Existing Sherwood Correlations to Membrane Operations. *Journal of Membrane Science*, **30**(2), 153–170.

Gerhardt, P. and Gallup, D. (1963). Dialysis Flask for Concentrated Culture of Microorganisms. *Applied Bacteriology*, **86**, 919–929.

Glassner, D. and Datta, R. (1990). Process for Production and Purification of Lactic Acid. Patent number, EP0393818A1.

Gould, N.; Orban, D. and Toint, P. (2004). Numerical Methods for Large-Scale Nonlinear Optimization. Technical report, Council for the Central Laboratory on the Research Concils.

Grossman, G. and Sonin, A. (1973). Membrane Fouling in Electrodialysis: A model and Experiments. *Desalination*, **12**, 107–125.

Guarner, F. and Schaafsma, G. J. (1998). Probiotics. *International Journal of Food Microbiology*, **39**(3), 237 – 238.

Guerra, A.; Jonsson, G.; Rasmussen, A.; Waagner Nielsen, E. and Edelsten, D. (1997). Low cross-flow velocity microfiltration of skim milk for removal of bacterial spores. *International Dairy Journal*, **7**(12), 849 – 861.

Hábová, V.; Melzoch, K. and Rychtera, M. (2004). Modern Method of Lactic Acid Recovery from Fermentation Broth. *Czech Journal of Food Sciences*, **22**, 87–94.

Hamid, M. K.; Sin, G. and Gani, R. (2010). Integration of Process Design and Controller Design for Chemical Processes using a Model-based Methodology. *Computers & Chemical Engineering. In press.*

Hansen, P. (1996). *Rank-deficient and Discrete ill-posed Problems*. Doctoral thesis, Polyteknisk Forlag.

Heriban, V.; Skára, J.; Sturdík, E. and Ilavský, J. (1993). Isolation of Free Lactic Acid using Electrodialysis. *Biotechnology Techniques*, **7**(1), 63–68.

Herold, J.; Schultz, J. and Gerhardt, P. (1967). Differential Dialysis Culture for Separation and Concentration of a Macromolecular Product. *Applied Microbiology*, **15**(5), 1192–1197.

Holm, S.; Malmberg, R. and Svensson, K. (1986). Method and Plant Producing Milk with Low Bacterial Content.

Holmberg, A. (1981). A Systems Engineering Approach to Biotechnical Processes - Experiences of Modelling, Estimation and Control Methods. *Acta Polytech. Scand.*, **33**, 1–45.

Hongo, M.; Nomura, Y. and Iwahara, M. (1986). Novel Method of Lactic Acid Production by Electrodialysis Fermentation. *Applied and Environmental Microbiology*, **52**(2), 314–319.

Hulse, J. (2004). Biotechnologies: Past History, Present State and Future Prospects. *Trends Food Sci. Technol.*, **15**, 3–18.

INCHEM, I. (2009). Chemical Safety Information from Intergovernmental Organizations. On line. Available http://www.inchem.org/.

Isermann, R. (1989). *Digital Control Systems*. Springer-Verlag, second edition.

Ishizaki, A.; Nomura, Y. and Iwahara, M. (1990). Built-in Electrodialysis Batch Culture, a New Approach to Release of End Product Inhibition. *Journal of Fermentation and Bioengineering*, **70**(2), 108 – 113.

Iversen, S.; Bhatia, V.; Dam-Johansen, K. and Jonsson, G. (1997). Characterization of Microporous Membranes for use in Membrane Contactors. *Journal of Membrane Science*, **130**, 205–217.

Izák, P.; Hovorka, S.; Bartovská, L. and Crespo, J. (2007). Swelling of Polymeric Membranes in Room Temperature Ionic Liquids. *Journal of Membranes Science*, **296**, 131–138.

Jacobsen, E. W. (1999). On the Dynamics of Integrated Plants-non-minimum Phase Behavior. *Journal of Process Control*, **9**(5), 439–451.

Jaime-Ferrer, J.; Couallier, E.; Viers, P. and Rakib, M. (2009). Two-compartment bipolar membrane electrodialysis for splitting of sodium formate into formic acid and sodium hydroxide: Modelling. *Journal of Membrane Science*, **328**(1-2), 75 – 80.

James, P.; McMaster, T.; Newton, J. and Miles, M. (2000). In situ Rehydration of Perfluorosulphonate Ion-Exchange Membrane studied by AFM. *Polymer*, **41**, 4223–4231.

Jasra, R.; Choudary, N. and Bhat, S. (1991). Separation of Gases by Pressure Swing Adsorption. *Separation Science and Technology*, **26**(7), 885–930.

Jørgensen, S. (2006). Plantwide Optimizing Control. Course 28451, A note on Optimizing control of process plants.

Jonsson, G. (1980). The Influence of the Porous Sublayer on the Salt Rejection and Reflection Coefficient of Asymmetric CA Membranes. *Desalination*, **34**, 141–157.

Jonsson, G. and Wenten, I. (1994). Control of Concentration Polarization, Fouling and Protein Transmision of Microfiltration Processes within the Agrobased Industry. In *Proceedings of the ASEAN-EC workshop on Membrane Technology in Agrobased Industry*, pages 157–166.

Jurag-Separation (2009). Reverse Electro-Enhanced Dialysis Technology. On line. Available http://www.jurag.dk/.

Kapoor, N. and McAvoy, T. (1987). An Analytical Approach to Approximate Dynamic Modeling of Distillation Towers. *Industrial & Engineering Chemistry Research*, **26**(12), 2473–2482.

Katz, W. (1979). The electrodialysis reversal (EDR) process. *Desalination*, **28**(1), 31 – 40.

Kharas, G.; Sanchez-Riera, F. and Severson, D. (1996). Polymers of Lactic Acid. In D. Mobley, editor, *Plastics from Microbes, Microbial Synthesys. Polymers and Polymers Precursors*. Hanser Publishers.

Kiss, A.; Bildea, C. and Dimian, A. (2007). Design and Control of Recycle Systems by Non-linear Analysis. *Computers & Chemical Engineering*, **31**(5-6), 601 – 611.

Kookos, I. K. and Perkins, J. D. (2001). An Algorithm for Simultaneous Process Design and Control. *Industrial & Engineering Chemistry Research*, **40**, 4079–4088.

Korngold, E.; Körösy, F.; Rahav, R. and Taboch, M. (1970). Fouling of Anionselective Membranes in Electrodialysis. *Desalination*, **8**, 195–220.

Kristensen, N. (2003). *Fed-batch Process Modelling for State Estimation and Optimal Control*. Ph.D. thesis, Technical University of Denmark.

Lake, M. and Melsheimer, S. S. (1978). Mass Transfer Characterization of Donnan Dialysis. *AIChE Journal*, **24**, 130–137.

Lakshminarayanaiah, N. (1969). *Transport Phenomena in Membranes*. Academic Press.

Larsson, T. and Skogestad, S. (2000). Plantwide Control - A Review and a New Design Procedure. *Modelling, Identification and Control*, **21**, 209–240.

Leaist, D. and Lyons, P. (1984). Diffusion in Dilute Aqueous Acetic Acid Solutions at 25°C. *Journal of Solution Chemistry*, **13**(2), 77–85.

Lee, E.; Moon, S.; Chang, Y.; Yoo, I. and Chang, H. (1998a). Lactic Acid Recovery Using Two-Stage Electrodialysis and its Modelling. *Journal of Membrane Science*, **145**, 53–66.

Lee, E.; Moon, S.; Chang, Y.; Yoo, I. and Chang, H. (1998b). Lactic acid recovery using two-stage electrodialysis and its modelling. *Journal of Membrane Science*, **145**(1), 53 – 66.

Lei, F. (2001). *Dynamics and Nonlinear Phenomena in Continuous Cultivations of Saccharomyces cerevisae*. Ph.D. thesis, Technical University of Denmark.

Lewin, D. (1999). Integration of Design and Control. In *Proceedings of 7th Mediterranean Conference on Control and Automation (MED99)*.

Lide, D., editor (2008). *CRC Handbook of Chemistry and Physics*. Taylor and Francis Group, LLC, 88th edition.

Ljung, L. (1999). *System Identification. Theory for the User*. Pretience Hall PTR.

Ljungh, A. and Wadström, T. (2006). Lactic Acid Bacteria as Probiotics. *Current Issues in Intestinal Microbiology*, **7**, 7390.

Luedeking, R. and Piret, E. (1959). A Kinetic Study of the Lactic Acid Fermentation. Batch Process at Controlled pH. *Journal of Biochemical and Microbiological Technology adn Engineering*, **1**(4), 431–459.

Luyben, W. (1993). Dynamics and Control of Recycle Systems. 1. Simple Open-Loop and Closed-loop Systems. *Industrial and Engineering Chemistry Research*, **32**, 466–475.

Madigan, M.; Martinko, H. and Parker, J. (2003). *Biology of Microorganisms*. Prentice Hall.

Mafé, S.; rez, R. and Alcaraz, A. (1998). Electric Field-assisted Proton Transfer and Water Dissociation at the Junction of a Fixed-charge Bipolar Membrane. *Chemical Physics Letters*, **294**(4-5), 406 – 412.

Malcolm, A.; Polan, J.; Zhang, L.; Ogunnaike, B. A. and Linninger, A. A. (2007). Integrating Systems Design and Control Using Dynamic Flexibility Analysis. *AIChE Journal*, **53**(8), 2048–2061.

Mathworks (2006). *Matlab Full Product Family Help*, version 7 (r14) edition.

Matros, Y. S. (1989). *Catalytic processes under unsteady-state conditions*. Elsevier: Amsterdam.

Matros, Y. S. and Bunimovich, G. A. (1996). Reverse-Flow Operation in Fixed Bed Catalytic Reactors. *Catalysis Reviews*, **38**(1), 1–68.

Mauritz, K. and Moore, R. (2004). State of Understanding of Nafion. *Chem. Rev.*, **104**, 4535–4585.

McKlay, M.; Morrison, J. and Upton, S. (1999). Evaluating Prediction Uncertainty in Simulation Models. *Computer Physics Communications*, **117**(1-2), 44–51.

Miyoshi, H. (1997). Diffusion Coefficients of Ions through Ion-Exchange Membranes for Donnan Dialysis using Ions of the same Valence. *Chemical Engineering Science*, **52**, 1087–1096.

Møllerhøj, M. (2006). *Modeling the REED Process*. Master's thesis, Technical University of Denmark.

Moon, P.; Sandi, G.; Stevens, D. and Kizilel, R. (2004). Computational Modeling of Ionic Transport in Continuous and Batch Electrodialysis. *Separation Science and Technology*, **39**(11), 2531–2555.

Morari, M. (1982). Integrated Plant Control: A Solution at Hand or a Research Topic for the Next Decade? In T. Edgar and D. Seborg, editors, *Chemical Process Control 2*, pages 467–495.

Morari, M. (1983). Flexibility and Resilience of Process Systems. *Computers & Chemical Engineering*, **7**(4), 423–437.

Morari, M.; Arkun, Y. and Stephanopoulos, G. (1980). Studies in the Synthesis of Control Structures for Chemical Processes: Part 1: Formulation of the Problem. Process Decomposition and the Classification of the Control Tasks. Analysis of the Optimizing Control Structures. *AIChE Journal*, **26**(2), 220–232.

Mulder, M. (1997). *Basic Principles of Membrane Technology*. Kluwer Academic Publishers.

Narbęska, A. and Staniszewski, M. (1997). Separation of Fermentation Products by Membrane Techniques. I. Separation of Lactic Acid/Lactates by Diffusion Dialysis. *Separation Science and Technology*, **32**(10), 1669–1682.

Narbęska, A. and Staniszewski, M. (1998a). Separation of Fermentation Products by Membrane Techniques. Part III. Continuous isolation of Lactic Acid by Facilitated Membrane Extraction. *Separation Science and Technology*, **33**(10), 1455–1465.

Narbęska, A. and Staniszewski, M. (1998b). Separation of Fermentation Products by Membrane Techniques. II. Conversion of Lactate to Lactic Acid by Electrodialysis. *Separation Science and Technology*, **33**(7), 959–973.

Neophytides, A. and Froment, G. F. (1992). A Bench Scale Study of Reversed Flow Methanol Synthesis. *Industrial & Engineering Chemistry Research*, **31**(7), 15831589.

Nielsen, J.; Villadsen, J. and Lidé n, G. (2003). *Bioreaction Engineering Principles*. Kluwer Academic/Plenum Publishers, second edition.

Nocedal, J. and Wright, S. J. (1999). *Numerical Optimization*. Springer.

Ohleyer, E.; Wilke, C. and Blanch, E. (1985). Continuous Production of Lactic Acid from Glucose and Lactose in a Cell-Recycle Reactor. *Applied Biochemestry and Biotechnology*, **11**, 457–463.

Palatý, Z.; Záková, A. and Prchal, P. (2006). Continuous Dialysis of Carboxylic Acids. Permeability of Neosepta-AMH Membrane. *Desalination*, **216**, 345–355.

Palatý, Z.; Stoček, P.; Zaková, A. and Bendová, H. (2007). Trasnport Characteristics of Some Carboxylic Acids in the Polymeric Anion-Exchange Membrane Neosepta-AMH: Batch Experiments. *Journal of Applied Polymer Science*, **106**, 909–916.

Palatý, Z.; Stoček, P.; Bendová, H.; Prchal, P. and Zaková, A. (2009). Continuous Dialysis of Carboxylic Acids: Solubility and Diffusivity in Neosepta-AMH Membranes. *Desalination*, **243**, 65–73.

Palazoglu, A. and Arkun, Y. (1986). A Multiobjective Approach to Design Chemical Plants with Robust Dynamic Operability Characteristics. *Computers & Chemical Engineering*, **10**, 567–575.

Patel, J.; Uygun, K. and Y., H. (2008). A Path Constrained Method for Integration of Process Design and control. *Computers & Chemical Engineering*, **32**, 13731384.

Postlethwaite, J.; Lamping, S.; Leach, G.; Hurwitz, M. and Lye, G. (2004). Flux and Transmission Characteristics of a Vibration Microfiltration System Operated at High Biomass Loading. *Journal of Membrane Science*, **228**(1), 89–101.

Prado-Rubio, O.; Jørgensen, S. and Jonsson, G. (2009a). Lactic Acid Recovery in Electro-Enhanced Dialysis: Modelling and Validation. In J. Jeżowski and J. Thullie, editors, *19th European Symposium on Computer Aided Process Engineering*, volume 26, pages 773–779. Elsevier.

Prado-Rubio, O.; Jørgensen, S. and Jonsson, G. (2009b). Tool for Optimizing the Design and Operation of Reverse Electro-Enhanced Dialysis of Monoprotic Carboxylic Acids. In R. Brito Alves; C. Nascimento and E. J. Biscaia, editors, *Computer-Aided Chemical Engineering*, volume 27A, pages 663–668. Elsevier. ISBN: 978-0-44-45345-4.

Prado-Rubio, O.; Jørgensen, S. and Jonsson, G. (2010a). Control System Development for Integrated Bioreactor and Membrane Separation Process. In S. Pierucci and G. Buzzi Ferraris, editors, *Computer-Aided Chemical Engineering*, volume 28, pages 289–294. Elsevier. ISBN: 978-0-444-53569-6.

Prado-Rubio, O.; Møllerhøj, M.; Jørgensen, S. and Jonsson, G. (2010b). Modeling Donnan Dialysis Separation for Carboxylic Anion Recovery. *Computers & Chemical Engineering*, **34**, 1567–1579.

Prado-Rubio, O.; Jørgensen, S. and Jonsson, G. (2011a). Reverse Electro-Enhanced Dialysis for Lactate Recovery from a Fermentation Broth. *Journal of Membrane Science*, **374**, 20–32.

Prado-Rubio, O.; Jørgensen, S. and Jonsson, G. (2011b). Model Based Investigation of the Potential Lactate Recovery using Electro-Enhanced Dialysis - Static Analysis. *Separation and Purification Technology*, **78**, 113–124.

Pushpavanam, S. and Kienle, A. (2001). Nonlinear Behavior of an Ideal Reactor Separator Network with Mass Recycle. *Chemical Engineering Science*, **56**(8), 2837 – 2849.

Raucourt, A.; Girard, D.; Prigent, Y. and Boyaval, P. (1989). Lactose Continuous Fermentation with Cells Recycled by Ultrafiltration and Lactate Separartion by Electrodialysis: Modelling and Simulation. *Applied Microbiology and Biotechnology*, **30**, 521–527.

Recke, B. and Jørgensen, S. (1999). Complex nonlinear behaviour of a fixed bed reactor with reactant recycle. *Computers & Chemical Engineering*, **23**(Supplement 1), S179 – S182. European Symposium on Computer Aided Process Engineering, Proceedings of the European Symposium.

Rege, S. and Yang, R. (2002). Propane/propylene Aeparation by Pressure Swing Adsorption: Sorbent Comparison and Multiplicity of Cyclic Steady States. *Chemical Engineering Science*, **57**(7), 1139–1149.

Ribeiro, A.; Lobo, V.; Leaist, D.; Natividade, J.; Veríssimo, L.; Barros, M. and Cabral, A. (2005). Binary Diffusion Coefficients for Aqueous Solutions of Lactic Acid. *Journal of Solution Chemistry*, **34**(9), 1009–1016.

Ricardez-Sandoval, L. A.; Budman, H. M. and Douglas, P. L. (2010). Simultaneous Design and Control: A New Approach and Comparisons with Existing Methodologies. *Industrial & Engineering Chemistry Research*, **49**, 28222833.

Ritter, J. and Yang, R. (1991). Pressure Swing Adsorption: Experimental and Theoretical Study on Air Purification and Vapor Recovery. *Industrial & Engineering Chemistry Research*, **30**(5), 10231032.

Ruthven, D. (2000). Past Progress and Future Challenges in Adsorption Research. *Industrial & Engineering Chemistry Research*, **39**(7), 2127–2131.

Ruthven, D.; Farooq, S. and Knaebel, K. (1994). *Pressure Swing Adsorption*. VCH Publishers.

Rutledge, R. and Steward, D. (2008). A Kinetic-Based Sigmoidal Model for the Polymerase Chain Reaction and Its Application to High-Capacity Absolute Quantitative Real-Time PCR. *BMC Biotechnology*, **8**, paper number 47.

Rype, J. (2003). *Modelling of Electrically Driven Processes*. Ph.D. thesis, Technical University of Denmark.

Salteri, A.; Ratto, M.; Tarantole, S. and Campolongo, F. (2006). Sensitivity Analysis Practices: Strategies for Model-based Inference. *Reliability Engineering and System Safety*, **91**(10-11), 1109–1125.

Sanders, M. (1993). Summary of Conclusions from a Consensus Panel of Experts on Health Attributes of Lactic Cultures: Significance to Fluid Milk Products Containing Cultures. *Jounal of Dairy Science*, **76**, 1819–1828.

Sarmidi, M.; Yunos, K. and Pee, L. (2001). Permselectivity Coefficient of Anion Exchange Membranes for Electrodialysis of Citric Acid. In *15^{th} Symposium of Malaysian Chemical Engineers (SOMChE)*, pages 109–114.

Schiesser, W. (1994). *Computational Mathematics in Engineering and Applied Science*. CRC Press.

Seber, G. A. F. and Wild, C. J. (2003). *Nonlinear Regression*. John Wiley and Sons, New Jersey.

Seborg, D.; Edgar, T. and Mellichamp, D. (2004). *Process Dynamics and Control*. John Wiley and Sons.

Shampine, L. F.; Reichelt, M. W. and Kierzenka, J. A. (1999). Solving Index-1 DAEs in MATLAB and Simulink. *SIAM Review*, **41**(3), 538 – 552.

Simons, R. (1985). Water Splitting in Ion Exchange Membranes. *Electrochimica Acta*, **30**(3), 275 – 282.

Sin, G.; Gernaey, K. V. and Lantz, A. (2009). Good Modeling Practice for PAT Applications: Propagation of Input Uncertainty and Sensitivity Analysis. *AIChE*, **25**(4), 1043–1053.

Sin, G.; Meyer, A. and Gernaey, K. (2010). Assessing Reliability of Cellulose Hydrolysis Models to Support Biofuel Process DesignIdentifiability and Uncertainty Analysis. *Computers & Chemical Engineering*. In press (doi:10.1016/j.compchemeng.2010.02.012).

Sircar, S. (2002). Pressure Swing Adsorption. *Industrial & Engineering Chemistry Research*, **41**(6), 1389–1392.

Sircar, S. and Golden, T. (2000). Purification of Hydrogen by Pressure Swing Adsorption. *Separation Science and Technology*, **35**(5), 667–687.

Skogestad, S. (2000). Plantwide control: The Search for the Self-optimizing Control Structure. *Journal of Process Control*, **10**, 487–507.

Skogestad, S. (2004). Control Structure Design for Complete Chemical Plants. *Computers & Chemical Engineering*, **28**, 219–234.

Skogestad, S. and Morari, M. (1987). Effect of Disturbance Directions on Closed-Loop Performance. *Industrial & Engineering Chemistry Research*, **26**, 2029–2035.

Skogestad, S. and Postlethwaite, I. (2004). *Multivariable Feedback Control: Analysis and Design*. John Wiley and Sons.

Sonin, A. and Grossman, G. (1972). Ion Transport through Layered Ion Exchange Membranes. *Journal of Physical Chemistry*, **76**(26), 3996–4006.

SRI-Consulting (2010). Lactic Acid, Its Salts and Esters. On line. Available http://www.sriconsulting.com.

Stanbury, P.; Whitaker, A. and S.J., H. (1995). *Principles of Fermentation Technology*. Pergamon, UK, second edition.

Starov, V.; Petsev, D. and Ivanov, I. (1990). A Diffusion Model of Donnan Dialysis under Flow Conditions. *Journal of Membrane Science*, **53**, 45–57.

Stephanopoulos, G. (1983). Synthesis of Control Systems for Chemical Plants A challenge for creativity. *Computers & Chemical Engineering*, **7**(4), 331 – 365.

Stephanopoulos, G. (1989). *Chemical Process Control*. Prentice Hall.

Stephanopoulos, G.; Aristidou, A. and Nielsen, J. (1998). *Metabolic Engineering. Principles and Methodologies*. Academic Press.

Stiles, M. and Holzapfel, W. (1997). Lactic Acid Bacteria of Foods and Their Current Taxonomy. *International Journal of Food Microbiology*, **36**(1), 1 – 29.

Strathmann, H. (2004). *Ion-Exchange Membrane Separation Processes*. Membrane Science and Technology Series, 9. Elsevier.

Taylor, R. and Krishna, R. (1996). *Multicomponent Mass Transfer*. John Wiley and Sons.

Timmer, J.; Kromkap, J. and Robbertsen, T. (1994). Lactic Acid Separation from Fermentation Broths by Reverse Osmosis and Nanofiltration. *Journal of Membranes Science*, **92**, 185–197.

Toftegård, B. and Jørgensen, S. (1988). Stationary Profiles for Periodic Cycled Separation Columns: Linear Case. *Industrial & Engineering Chemistry Research*, **27**(3), 481–485.

van der Stegen, J.; Weerdenburg, H.; van der Veen, A. and Hogendoorn, J. (1999). Application of the Pitzer model for the estimation of activity coefficients of electrolytes in ion selective membranes. *Fluid Phase Equilibria*, **157**, 181–196.

Varadarajan, S. and Miller, D. (1999). Catalytic Upgrading of Fermentation-Derived Organic Acids. *Biotechnology Progress*, **15**(5), 845–854.

Wilhelm, F. (2001). *Bipolar Membrane Electrodialysis*. Ph.D. thesis, University of Twente. ISBN 9036515270.

Wilson, I.; Colin, P. and Cooke, M., editors (2000). *Encyclopedia of Separartion Science*, chapter Methods and Instrumentation. Academic Press.

Wódzki, R. and Nowaczyk, J. (1999). Membrane Transport of Organics. II. Permeation of Some Carboxylic Acids through Strongly Basic Polymer Membrane. *Journal of Applied Polymer Science*, **71**, 2179–2190.

Young-Jung, W.; Jin-Nam, K. and Hwa-Won, R. (2006). Biotechnological Production of Lactic Acid and Its Recent Applications. *Food Technology and Biotechnology*, **44**, 163–172.

Zhang, D. and Cheryan, M. (1994). Starch to Lactic Acid in a Continuous Membrane Bioreactor. *Process Biochemestry*, **29**, 145–150.

Zheleznov, A.; Windmöller, D.; Körner, S. and Böddeker, K. (1998). Dialytic Transport of Carboxylic Acids through an Anion Exchange Membrane. *Journal of Membrane Science*, **139**, 137–143.

This PhD-project was carried out at CAPEC, the Computer Aided Product-Process Engineering Center.
CAPEC is committed to research, to work in close collaboration with industry and to participate in educational activities. The research objectives of CAPEC are to develop computer-aided systems for product/process simulation, design, analysis and control/operation for chemical, petrochemical, pharmaceutical and biochemical industries. The dissemination of the research results of CAPEC is carried out in terms of computational tools, technology and application. Under computational tools, CAPEC is involved with mathematical models, numerical solvers, process/operation mathematical models, numerical solvers, process simulators, process/product synthesis/design toolbox, control toolbox, databases and many more. Under technology, CAPEC is involved with development of methodologies for synthesis/design of processes and products, analysis, control and operation of processes, strategies for modelling and simulation, solvent and chemical selection and design, pollution prevention and many more. Under application, CAPEC is actively involved with developing industrial case studies, tutorial case studies for education and training, technology transfer studies together with industrial companies, consulting and many more.

Further information about CAPEC can be found at www.capec.kt.dtu.dk.

Computer Aided Process Engineering Center
Department of Chemical and Biochemical Engineering
Technical University of Denmark
Søltofts Plads, Building 229
DK-2800 Kgs. Lyngby
Denmark

Phone: +45 4525 2800
Fax: +45 4525 2906
Web: www.capec.kt.dtu.dk

ISBN : 978-87-92481-37-5